BEHAVIOUR OF MACHINE FOUNDATIONS SUBJECTED TO
VERTICAL DYNAMIC LOADING

SILIPIUS JOSEPH MBAWALA

A Thesis submitted in partial fulfilment of the requirements for the degree

of

PHILOSOPHIAE DOCTOR (CIVIL ENGINEERING)

in the

FACULTY OF ENGINEERING, BUILT ENVIRONMENT AND
INFORMATION TECHNOLOGY

UNIVERSITY OF PRETORIA

OCTOBER 2015

THESIS SUMMARY

Supervisor: Professor G. Heymann

Co-supervisor: Professor C.P, Roth

Co-supervisor: Professor P.S, Heyns

Department: Civil Engineering

University: University of Pretoria

Degree: Philosophiae Doctor (Civil Engineering)

The vertical dynamic behaviour of machine foundations subjected to vertical dynamic loading was investigated for surface and embedded foundations. The responses of these machine foundations were determined using analytical and numerical solutions ranging from simple to complex. An accurate prediction of impedance functions for the foundation system is a key step in the design procedures. The prediction accuracy depends on how close the modelling procedures are to reality. The subject of soil dynamics is complex. At times, the choice of the analysis model is based on the experience of the engineer with the model. The chosen model may or may not result in an optimal, efficient, and accurate design.

The current advancement in manufacturing technology calls for machine foundation systems with high performance, availability and reliability. The analysis and design of such complex, large and sensitive machine foundations requires good understanding of their dynamic behaviour.

The aim of this thesis is to investigate and evaluate the most accurate analytical and numerical models for determining the dynamic behaviour of surface and embedded machine foundations.

Surface and embedded footings were cast at the experimental station at the University of Pretoria. The vertical dynamic behaviour of these foundations was determined by vertical harmonic loading. The measured impedance functions were compared with predicted responses obtained from analytical solution of the Winkler model, elastic half-space theory, simplified Lysmer (1965) model, Veletsos and Verbic (1973) models, the Dyna5 program and numerical solution of finite element method (Abaqus). The dynamic responses of the surface foundation predicted by the analytical solution proposed by Veletsos and Verbic (1973) soil with mass, compared reasonably well with the results obtained from field-measured data.

i

The measured impedance functions of the embedded foundation were compared with the predicted results ascertained using the analytical solution proposed by Novak and Beredugo (1972), Dyna5 program and numerical solution of the finite element method (Abaqus). It is shown that embedment increases stiffness, natural frequency, natural frequency ratio, and damping ratio. The embedment reduces resonant amplitude, resonant amplitude ratio and has an insignificant effect on resonant frequency and resonant frequency ratio. The measured dynamic responses compared favourably with the results predicted by the finite element method (Abaqus).

The conclusion is that the analytical model proposed by Veletsos and Verbic (1973) soil with mass, and the finite element method (Abaqus) can be used to accurately predict the dynamic response of surface and embedded machine foundations respectively.

ACKNOWLEDGEMENT

I wish to express my appreciation to the following organisations and individuals who have made this thesis possible:

TABLE OF CONTENTS

LIST OF TABLES

LIST OF FIGURES

xiv

xv

NOMENCLACTURE

Abbreviations:

DEGEBO	Deutsche Gesellschaft für Bodenforschung
FEM	Finite element method
MSD	Mass-spring-dashpot
SSI	Soil-structure interaction
SASSI	System for analysis of soil-structures interaction
CSW	Continuous surface wave
LVDT	Linear variable differential transducer
FFT	Fast Fourier transform
FRF	Frequency response function
CAE	Complete abaqus environment
M.F	Magnification factor

Symbols:

Roman letters

A	area of the foundation
a_o	dimensionless frequency
A_v	vibration amplitude
a_v	maximum acceleration amplitude
b_o	mass ratio
B_v	Lysmer's modified mass ratio
$c(\omega)$	Damping constant for embedded footing
C	viscous damping coefficient
C_1	half-space stiffness parameter
C_2	damping parameter
C_r	footing shape factor
C_v	vertical viscous damping coefficient
C_u	coefficient of elastic uniform compression
$[C]$	damping matrix
D	damping ratio
D_f	embedment depth
d	distance between two observation points
E	Young's modulus of elasticity
e	exponential function
F	Lysmer's displacement function
F_1	Lysmer's displacement function - stiffness
f_o	natural frequency of foundation system with zero embedment
f_d	natural frequency of foundation system with given embedment
F_2	Lysmer's displacement function - damping
f_1	displacement function - stiffness
f_2	displacement function - damping
$f_{\max}$	maximum frequency of applied load
f_{nv}	frequency of vibration
G	shear modulus of soil along embedment
g	mesh size
G_s	shear modulus of the side soil
$H(\omega)$	transfer function
i	$\sqrt{-1}$
K	stiffness of the system
$K^I(\omega)$	imaginary part - complex
$K^R(\omega)$	real part - complex
$[K_o]$	stiffness matrix
K_v	vertical static stiffness
$K_v(\omega)$	vertical complex dynamic stiffness

k_v	spring constant - Winkler model
$k(\omega)$	dynamic stiffness coefficient
$Im(z)$	imaginary part of the phase vector
M	mass of vibrating system
m	shear stiffness slope-gradient
M_f	mass of footing
Ms	equivalent mass of half-space medium
$[M]$	mass matrix
n	integer
N_f	natural frequency ratio
$N_v(t)$	time dependent vertical dynamic reaction force along the side of footing
P_o	force amplitude of the dynamic load
$P_v(t)$	vertical time dependent excitation force
$P_o(t)$	vertical harmonics force (complex)
$\{P_o\}$	applied vector force
R_a	resonant amplitude ratio
r_o	radius of contact area of footing/equivalent radius of footing
R_f	resonant frequency ratio
$R_v(t)$	vertical time dependent vertical dynamic reaction at the base of footing
S_1	function related to stiffness parameter
S_2	function related to damping parameter
t	time
V	absolute displacement of vibrating mass
V_o	complex amplitude displacement
V_v	vertical displacement
$\dot{V}$	velocity
$\ddot{V}$	acceleration
V_p	compression wave velocity
V_s	shear wave velocity
$u(t)$	vertical displacement in time domain
$\{U_{static}\}$	static displacement vector
U_{static}	back calculated static displacement
$U\,max$	maximum displacement amplitude at the given embedment
$U_o\,max$	maximum displacement amplitude for zero embedment
V_R	Rayleigh wave velocity
$\dot{w}$	normal to boundary velocity
$\dot{u}$	tangential to boundary velocities
$U(\omega)$	displacement response function

Greek letters

$X(\omega)$	compliance function
$X^R(\omega)$	real part of the compliance function
$X^I(\omega)$	imaginary part of the compliance function.
ω	circular frequency of dynamic load excitation
ω_o	natural frequency of foundation system for massless soil
ω_n	natural frequency of foundation system for footing with mass of soil
ρ_s	mass density of side soil layer along embedment
ϕ	phase angle
ρ	mass density of half-space medium - soil
β	Rayleigh damping coefficient which take stiffness proportional damping
α	Rayleigh damping coefficient which take mass proportional damping
δ	embedment ratio
σ	normal stress
τ	shear stress
λ	wavelength
ς	constant
λ_{min}	minimum wavelength
ω_d	damped natural frequency
ω_r	resonant frequency
$\Delta\phi$	phase change from one observation to another

CHAPTER 1

1   INTRODUCTION

1.1   Background

The primary goal in the design of machine foundations is to limit the response amplitude in all vibration modes to the specified tolerance. This is normally achieved by avoiding resonance by ensuring that the operating frequency is sufficiently remote from the natural frequencies of the foundations system. Excessive vibration can cause unsatisfactory performance of machine foundations, and in some cases, can reduce the in-service life of machines, foundations and neighbouring structures. The proper design of machine foundations ensures a satisfactory performance of machines and minimise disturbances for people working in the immediate vicinity.

Different methods are available for analysis of surface and embedded machine foundations. A scientific and sound engineering design model, taking into consideration the soil dynamics, was established in 1936 by Reissner. This modelling approach proposed by Reissner is known as elastic half-space theory. Over time, elastic half-space theory was simplified to empirical and semi-empirical analysis methods. These design methods can give reliable results when input parameters are properly chosen (Sung, 1953), however they are inefficient for modelling foundations with complex geometry and complicated loading. A more rigorous design method such as finite element methods may be appropriate for more complex problems.

The analysis and design of machine foundations are based on the prediction of dynamic behaviour of soil-structure interaction problems, which is governed by dynamic impedance functions (dynamic stiffness). These functions are used to describe an assumed linear relationship between forcing function and the resulting displacement responses (Gazetas, 1983 and Gazetas, 1991a). The solution for dynamic displacement is found using differential equations of motion.

Accurate impedance functions for foundation systems are important to the analysis and design of dynamically loaded machine foundations. The prediction accuracy will depend on the similarity of the modelling results to reality. The choice of the analysis model, depends to a large extent on the required accuracy, availability of computational power and required analytical efficiency. These factors are primarily governed by the importance of

1-1

the project. The subject of soil dynamics is complex and the choice of the analytical model may be based on the familiarity of the engineer with specific analytical models, which may, or may not, result in an efficient and accurate design.

The current advancement in manufacturing technology calls for machine foundation systems with higher performance, availability and reliability. For instance, the trend for the cement production industry and mining industry is to increase the size of the process plant (Meimaris et al., 2001 and Deolalikar, 2007). In the mining industry, the approach by mine owners is to increase the size of ore grinding mills in order to reduce the total life cycle costs of mine projects. The largest ore-grinding mill is about 12.8 m in diameter, with approximately 300 MN static loads (Orser et al., 2011). These developments have necessitated the re-evaluation of traditional techniques to analyse machine foundations.

These modern ore grinding mills are complex, and determination of dynamic behaviour is not an easy task, also new interdisciplinary phenomena increase the risk of using such mills (Reese, 2000, Meimaris and Cox, 2001 and Meimaris, 2002). The approach of having a single ore grinding mill has the disadvantage of causing a bottleneck when the unit goes out of service. Therefore, the reliability and availability of the ore grinding mill is of primary concern during the mine operation. Although, no major failure caused by poor design of the foundation systems has been reported, it is important that mine owners gain confidence in the dynamic behaviour of these larger and more complicated structures. A better understanding of the dynamic responses of these foundation systems is essential in order to avoid failure of these engineering structures.

The popular design approach by design engineers is to obtain impedance functions of the foundation systems using available simplified models (Hadjian et al., 1974; Gazetas, 1983 and Gazetas, 1991a). This method uses a lumped mass parameter whereby the foundation and all components of the superstructures are lumped together. This design approach is known as the two-stage design approach (decoupled) where a geotechnical engineer characterises the site to obtain soil parameters (shear modulus, Poisson's ratio, shear wave velocity and density of soil). From these soil parameters, the dynamic stiffness and damping of the foundation system is estimated using empirical, semi-empirical or numerical analysis. The estimated dynamic stiffness and damping of the foundation system are typically supplied to a structural engineer who uses these parameters to determine the dynamic behaviour of the superstructure.

Although, this design approach has been used for analysis and design of structures for decades, it is not clear if it is sufficiently accurate for analysis and design of machine foundations for large and sensitive machine foundations such as large ore mills. It is important to investigate whether this design approach is precise enough to model and analyse these complicated machine foundation systems.

Over the years, many methods have been developed to analyse the vibration of surface and embedded machine foundations. These methods can be classified as Mass-Spring Dashpot (MSD), Elastic half-space theory, Simplified half-space models and numerical methods. In this thesis, the dynamic response of surface foundations was determined using the analytical solution of mass-spring dashpot or Winkler model, elastic half-space theory, simplified half space of Lysmer (1965) model, Veletsos and Verbic (1973) models, Dyna5 program and the numerical solution of finite element method. For embedded foundations, the evaluation was based on the finite element method (Abaqus), the analytical solution proposed by Novak and Beredugo (1972) and the Dyna5 analysis program. The results were compared with data obtained from field measurements. The cone model presented by Wolf (1994) and Wolf and Deeks (2004) is not included in this investigation because it's development is based on the strength of materials not the rigorous theory of half-space. Also, the portion of half-space outside the cone is neglected and cone model cannot represent the influence of Rayleigh surface waves.

1.2 Hypothesis

Appropriate analytical and numerical models are required to accurately predict the vertical dynamic response of machine foundations subjected to vertical dynamic loads.

1.3 Objective

Analysis models that analyse the behaviour of machine foundations with the footing on the ground surface can be ranked from the least complex to the most complex as follows:

 i.   Mass-Spring Dashpot (MSD) or Winkler model;
 ii.   Elastic half-space theory (Sung 1953);
 iii. Simplified model of Veletsos and Verbic (1973) massless soil;
 iv.   Simplified model of Lysmer (1965);
 v.   Simplified model of Veletsos and Verbic (1973) soil with mass;
 vi.   Dyna5 program
 vii. Finite element method – isotropic soil, and
 viii. Finite element method – Gibson soil

Analysis models for embedded machine foundations can be ranked from the least complex to the most complex as:

  i. Novak and Beredugo (1972)
  ii. Dyna5 program
  iii. FEM – Isotropic soil
  iv. FEM – Gibson soil

The objective of this study is to investigate how complex the analytical and numerical models have to be in order to accurately model the vertical dynamic response of machine foundation systems.

1.4   Scope of the study

Surface and embedded footings were constructed at the University of Pretoria's experimental station and dynamically loaded in the vertical fashion to determine the vertical dynamic responses. The scope of the study is limited to machine foundations subjected to vertical loading only. Because the vertical response is easy to visualise. The research was based on field measurement, processing measured data and modelling foundation using the analytical and finite element methods.

The scope of the study included:

- The experimental tests to characterise the site in order to obtain elastic soil parameters. The shear wave velocity was determined from Continuous Surface Wave (CSW).tests
- Data analysis, which included translating acceleration responses to displacement amplitude.
- The back-calculation of the vertical dynamic responses obtained from field-measured data using forced vibration test carried out on a surface foundation system. These measured responses were compared with the results obtained from Winkler model, elastic half-space theory (Sung 1953), simplified models of Lysmer (1965), Veletsos and Verbic (1973) and the Dyna5 program, as well as the results obtained from the numerical solution by the finite element method (Abaqus).
- Back-calculation of the measured vertical dynamic responses of an embedded foundation. These measured results were compared with the analytical solution

1-4

proposed by Novak and Beredugo (1973) and the Dyna5 program as well as the results obtained from the finite element method (Abaqus).

• Evaluation of the effect of foundation embedment on the results obtained from the finite element method (Abaqus), the analytical solution proposed by Novak and Beredugo (1973), and the Dyna5 program.

1.5 Methodology

The methodology of the research project may be summarised as follows:

• Select suitable site for the experimental work.

• Carrying out Continuous Surface Wave test to determine shear modulus and shear wave velocity.

• Excavation of a trial pit to inspect soil profile.

• Cast concrete for surface and embedded footings.

• Calibration of accelerometers, LVDT and load cell.

• Conduct field tests to measure vibration of surface and embedded footings.

• Back-calculate the response of footings under forced vibration tests to obtain field-measured impedance functions (dynamic stiffness constant and damping constant).

• Prediction of dynamic response of surface foundation system using the Winkler model, elastic half-space theory (Sung 1953), simplified Lysmer (1965) model and simplified Veletsos and Verbic (1973) models, and finite element method.

• Prediction of the dynamic response of the embedded foundation system using the analytical solution proposed by Novak and Beredugo (1972), the Dyna5 program and the numerical solution of finite element method (Abaqus).

• Comparison of the predicted behaviour to the observed result for the analysis of all models to evaluate the accuracy of each method.

1.6 Organisation of thesis

Chapter 1 serves as the introduction to the thesis.

A review of the existing knowledge on the analysis and design of machine foundations is presented in Chapter 2. This includes a brief introduction to the historical background of the analysis and design of machine foundations. The literature focuses on determining the dynamic responses of machine foundations based on massless foundation systems, foundation systems with mass and numerical solutions of finite element method (Abaqus) and Dyna5 program.

Chapter 3 describes the experimental work.

Chapter 4 presents the results of the vertical dynamic responses of the surface and embedded footings obtained from the field measurements and includes measured and back-calculated data. The measured soil parameters, where the footings were constructed, are also presented in Chapter 4.

Chapter 5 discusses the vertical dynamic response of the footings described in Chapter 3 obtained from the Winkler model, elastic half-space theory (Sung 1953), simplified Lysmer (1965) model and simplified Veletsos and Verbic (1973) which consider the half-space with mass and without mass. In addition, Chapter 5, present the results of the surface foundation system predicted by the Dyna5 program.

For comparison purposes, the results from the analytical solutions are presented in parallel with the results obtained from field measurements. For the embedded foundation, the analytical solution is based on Novak and Beredugo (1972) and Dyna5 program.

Chapter 6 presents the results for the surface and embedded footings described in Chapter 3 obtained from the finite element method. The modelling for surface and embedded footings assumed that the footings are placed on a half-space (homogeneous linear elastic soil). The surface and embedded foundations were also modelled using a "Gibson soil", where the stiffness increases with depth. The results were compared with those for a homogeneous soil.

Chapter 7 discusses and compares the results for the surface and embedded foundations obtained from the field measurements to the responses predicted by each of the analytical methods.

Chapter 8 presents conclusions of this study.

CHAPTER 2

2 LITERATURE REVIEW

The primary goal in the design of machine foundations is to limit the amplitudes in all vibration modes to within the specified tolerances (Gazetas, 1983 and Gazetas, 1991b). This implies that the engineer is responsible for ensuring that the machine foundation is properly designed. Design methods, ranging from simple to complex, have been suggested to solve the problem of vibrating foundations. Selecting which method to be used for analysis and design of the machine foundations requires a good understanding of their dynamic behaviour.

This chapter discusses the existing knowledge concerning analysis and design of machine foundations. The literature review focuses on the use of the analytical and numerical methods. The analytical methods include the semi-empirical method of reduced natural frequency, mass-spring dashpot (MSD) or Winkler model, elastic half-space theory, and simplified half-space models. The elastic half-space theory includes Sung (1953) model. The simplified half-space models include simplified Lysmer (1965) model and simplified Veletsos and Verbic (1973) models which consider the half-space with mass and without mass. The numerical solution will focus on the analysis by finite element method (Abaqus) as well as Dyna5 program. These provide the basis for the understanding of the dynamic response of machine foundation systems. The literature review provides the basis for the knowledge of the field measurements as well as for data analysis. The existing information is reviewed, and the gap between existing knowledge is established. To clarify this, figures are listed at the end of the chapter.

2.1 Semi - empirical methods

The empirical methods were developed based on the observed behaviour of foundation subjected to vibration loads. The historical background of the design of machine foundations shows that the revolution of the design of foundation for machines began by using 'rules of thumb'. The main goal was to reduce resonant amplitude by increasing the mass of the footing. One of the first experimental studies to approximate the dynamic behaviour of foundation vibrations was carried out during the period of 1928 to 1939 by DEGEBO, an organisation in Germany, (Crockett and Hammond, 1949 and Richart et al., 1970). The aim of the DEGEBO study was to evaluate the dynamic soil properties in the

2-1

field by using a mechanical oscillator. From the field test results and analyses the method based on the "In-Phase Mass" was developed. The design approach considers that a mass of the soil beneath the footing moves with the footing.

2.1.1 "In-Phase" mass

The "In-Phase" mass design technique assumes that a finite mass of soil underneath a footing vibrates rigidly in phase with the footing. The natural frequency of the foundation system is determined using Equation 2.1.

$$f_n = \frac{1}{2\pi} \sqrt{\frac{k_v}{M + M_s}}$$
Equation 2.1

Where:

f_n is the natural frequency;

k_v is the spring constant;

M is the mass of footing and machine; and

M_s is the mass of the soil participating in vibration

The method aims at determining the resonant frequency of the undamped foundation systems. A method to estimate the mass of soil participating in vibration was suggested by Crockett and Hammond (1949). The method is intuitive because it is difficult to obtain reliable mass of soil in phase with footing. This is because the in phase mass depend on the mass of the footing and machine (dead load), exciting force, forcing frequency, base area of the footing, mode of vibration and soil type beneath the footing (Richart et al., 1970 and Rao, 1998). The "In-Phase" mass design technique was first introduced by Tschebotarioff and Ward (1948) and was modified by Tschebotarioff (1953). Tschebotarioff (1953) introduced a design method known as reduced natural frequency.

2.1.2 Reduced natural frequency

Reissner (1936) used the DEGEBO experimental test setup and test results to establish the theory of evaluating the dynamic response of vibrating footings as influenced by soil properties (Richart et al., 1970). Unfortunately, although the study by Reissner formed the basis of almost all studies on vibrating foundations, the theory did not receive immediate attention for different reasons. The main reason was that these results did not compare

favourably with the field-measured test results. The possible cause was the unrealistic assumed uniform contact pressure distribution, elastic soil medium and the shape of the contact area (Sung, 1953; Richart et al., 1970 and Rao, 1998). Other reasons included the permanent settlement developed during field measurements and an algebraic error of sign introduced in the calculation of the displacement function f_2 (Sung, 1953). This sign error was recognised by Sung (1953).

Because of these drawbacks during this time, the design of machine foundation had been based on the semi-empirical design approach. Tschebotarioff (1953) improved the "In-Phase" mass design method by considering different type of soil supporting the machine foundations. The method is known as reduced natural frequency because the natural frequency of machine system is reduced by considering the mass of soil vibrating with footing. Equation 2.1 becomes:

$$f_n = \frac{1}{2\pi} \sqrt{\frac{k'_v A}{M + M_s}}$$
Equation 2.2

Where:

f_n is the resonant frequency;

k'_v is the dynamic modulus of subgrade reaction;

A is a cross section area of footing in contact with soil;

M is the mass of footing and machine, and

M_s is the mass of the soil participating in vibration.

Tschebotarioff (1953) considered the static pressure caused by footing and rearranged Equation 2.2 to obtain Equation 2.3.

$$f_n = \sqrt{\frac{A}{F}} \frac{1}{2\pi} \sqrt{\frac{k'_v g}{1 + \frac{M_s}{M}}} = \frac{f_{nr}}{\sqrt{q_o}}$$
Equation 2.3

Where:

$f_{nr} = \frac{1}{2\pi} \sqrt{\frac{k'_v g}{1 + \frac{M_s}{M}}}$ is the reduced natural frequency;

$q_o = \dfrac{F}{A}$ is the average vertical pressure between the base of the footing and the soil;

k'_v is the vertical distributed spring constant which taken as the modulus of subgrade reaction;

M is the mass of footing and machine;

A is cross section area of footing in contact with soil;

M_s is the mass of the soil participating in vibration;

F is the force exerted by footing and machine, and

g is the acceleration due to gravity.

Tschebotarioff (1953) developed the design chart of which the relationship between the contact area of the footing and reduced natural frequency for the different type of soil is established (Richart et al., 1970 and Rao, 1998). The main design procedures involve assuming the natural frequency of the foundation using no resonant condition criteria. The next step is to determine the total weight of the footing to calculate the static bearing pressure between footing and soil. Equation 2.3 is used to obtain reduced natural frequency for a particular design bearing pressure. From the calculated reduced natural frequency, the Tschebotarioff design chart is used to estimate the required area for no resonant criteria (Richart et al., 1970 and Rao, 1998). The obtained required area is compared to the estimated area. The required area must be less than the estimated area. The design approach is concerned only with the resonant frequency without considering the vibration amplitudes and wave propagating in the ground and for these reasons its use was discredited and will not be discussed in this thesis.

The history of development of methods for analysing machine foundations subjected to dynamic loads has followed two main schools of thought. The first is the mass spring dashpot model or classical Winkler model, which replaces the effect of the underlying soil medium with closely spaced independent linear springs or a bed of springs. The second takes into account soil behaviour by considering wave propagation as introduced by Lamb (1904). The next section will discuss the analysis of machine foundation using the Winkler model.

2.2 Winkler model

The closed form solution to analyse compressible layer of stone as a static problem by linearising the behaviour of the soil was proposed by Winkler in eighteen century (Terzaghi, 1955). In 1888, Zimmermann used the Winkler model to compute the stresses in railroad ties which were resting on ballast over their full length (Terzaghi, 1955). Since then the model has become popular in geotechnical engineering for analysing static and dynamic problems. In static problems, the method is used to determine the response of relatively flexible foundations such as Mat or Raft foundations, foundations for waste treatment and water tanks, slabs on grade, rigid pavements and laterally loaded deep foundations.

The Winkler soil model describes the simplest representation of the soil response due to surface loads. The model replaces the soil medium with independent vertical springs, which represent stiffness of the soil, as illustrated in Figure 2.1. The main feature of the Winkler soil model is that the contact pressure between the footing and soil is directly proportional to the corresponding vertical displacement of the contact surface.

A major shortcoming of the Winkler model is that it cannot sustain shear stresses and hence cannot spread loads to the neighbouring parts, which are not directly loaded. Basically, the model suffers from a complete lack of continuity in the supporting medium as shown in Figure 2.1. This inherent deficiency of the Winkler model, in describing the continuum behaviour of the real soil mass for a static problem, has led to the development of many other simple soil response models. These include the Filonenko-Borodich model (1945), the Hetenyi model (1946), the Pasternak Model (1954) and the Kerr Foundation model (1964).

In dynamic analysis, the Winkler model ignores the damping of the medium due to the geometry and does not consider the dynamic interaction between the soil and the footing. In order to account for damping, viscous dampers are added to the system, parallel to the elastic springs, to simulate energy dissipation as shown in Figure 2.2. The addition of the dampers results in two model parameters, the spring and viscous damper or Mass-spring dashpot model (MSD model). This model is known as Winkler Kelvin-Voigt (Hetenyi, (1946), Terzaghi, (1955) and Barkan, (1962). The name is given to commemorate Kelvin and Voigt who used the viscous damping method for the first time.

Barkan (1962) carried out several field tests to determine soil elastic properties using plate load tests. Barkan used test results to establish charts from which design soil parameters are obtained and used in the dynamic Winkler model to estimate dynamic behaviour of the foundation system. The method by Barkan (1962) is known as the dynamic subgrade or dynamic Winkler model method as shown in Figure 2.1. This method is popular and is still used in India for design of machine foundations (Prakash and Puri, 2006).

For an undamped foundation system subjected to vertical harmonic load, the differential equation of motion is given by:

$$M\ddot{U}_v + k_v U_v = P_o sin(\omega t)$$ Equation 2.4

Where:

M is the lumped mass of the footing and oscillating mechanism;

t is the time;

ω is the forcing frequency;

k_v is a vertical distributed spring constant;

U_v is the vertical displacement, and

P_o is the force amplitude.

The general solution for Equation 2.4 is:

$$U_v = Asin(\omega_o t) + Bcos(\omega_o t) + \frac{(P_o/k_v)}{\left(1 - \frac{\omega^2}{\omega_0^2}\right)}(sin(\omega t))$$ Equation 2.5

Where:

A and B are constants;

ω is the forcing frequency;

t is time;

k_v is the vertical distributed spring constant;

ω_o is the natural frequency of the foundation system, and

P_o is the force amplitude.

For the steady state condition, the displacement amplitude is given by:

$$U_v = \frac{\left(P_o/k_v\right)}{\left(1 - \dfrac{\omega^2}{\omega_o{}^2}\right)}$$

Equation 2.6

Where:

ω_o is a natural frequency of the undamped foundation system.

The natural frequency of the foundation system is obtained from:

$$\omega_o = \sqrt{\frac{k_v}{M}}$$

Equation 2.7

2.3 Elastic half-space theory

Reissner (1936) established the solution to a foundation vibrating on a half-space. In developing the theory, Reissner used the solution developed by Lamb (1904) for a vibrating single vertical concentrated point load on a half-space, which is known as the Boussinesq dynamic problem, as shown in Figure 2.3. Reissner integrated Lamb's solution for a point load acting on an elastic half-space (Gong et al., 2006 and Chowdhury and Dasgupta, 2009). This solution forms the basis for the design of foundations vibrating on a half-space.

Reissner (1936) assumed that the soil medium on which the footing rests is a semi-infinite homogeneous, isotropic and elastic body subjected to vertical, uniformly distributed axis-symmetrical surface pressure. The soil properties required to describe the elastic body were shear modulus, Poisson's ratio and mass density of the soil (Sung, 1953; Bycroft, 1956 and Richart et al., 1970). Reissner suggested Equation 2.8 to calculate the vertical displacement at the centre of the uniformly loaded circular footing as illustrated in Figure 2.4.

$$U_v(t) = \frac{P_o e^{i\omega t}}{Gr_o}\left[f_1 + if_2\right]$$

Equation 2.8

Where:

U_v is the vertical displacement;

G is the shear modulus;

P_o is force amplitude of the dynamic load;

r_o is the radius of the footing;

2-7

ω is the frequency of excitation;

$i = \sqrt{-1}$, and

f_1 and f_2 are Reissner's frequency dependent displacement functions, which depend on the radius of the loaded area and the length of the shear wave propagated by the footing, and Poisson's ratio of the soil.

The influence of Poisson's ratio and shear wave velocity are contained in the Reissner's displacement functions f_1 and f_2. To address these complicated displacement functions in relationship to Poisson's ratio and the shear wave velocity, Reissner introduced the dimensionless frequency a_o which is given by:

$$a_o = \omega r_o \sqrt{\frac{\rho}{G}} = \frac{\omega r_o}{V_s} \qquad \text{Equation 2.9}$$

Where:

V_s is the velocity of shear wave propagating in the elastic body;

ω is the frequency of excitation;

r_o is the radius of the footing, and

ρ is the mass density of soil.

In addition, Reissner established a dimensionless term, known as the mass ratio, which is given by:

$$b_o = \frac{m}{\rho r_o^{\,3}} \qquad \text{Equation 2.10}$$

Where:

m is the total mass of the vibrating footing and exciting mechanism, which rests on the surface of the elastic half-space.

Equation 2.10 incorporates the influence of the soil mass underneath the vibrating footing. Using a mass-spring dashpot model with a single degree of freedom, Reissner's equation to calculate amplitude is expressed as:

$$U_v = \frac{P_o}{G r_o} \sqrt{\frac{f_1^{\,2} + f_2^{\,2}}{\left(1 + b_o a_o^{\,2} f_1\right)^2 + \left(b_o a_o^{\,2} f_2\right)^2}} \qquad \text{Equation 2.11}$$

The dimensionless amplitude is given by:

$$\frac{U_v G r_o}{P_o} = M.F = \sqrt{\frac{f_1^2 + f_2^2}{\left(1 + b_o a_o^2 f_1\right)^2 + \left(b_o a_o^2 f_2\right)^2}}$$ Equation 2.12

Where:

$M.F$ is the magnification factor

The phase angle (φ) between the external force $P = P_o e^{i\alpha t}$ and ground displacement U_v is expressed as:

$$\tan\varphi = \frac{f_2}{f_1 + b_o a_o^2 \left(f_1^2 + f_2^2\right)}$$ Equation 2.13

Essentially, these sets of equations use compliance functions, which assume the footing and half-space are massless as shown in Figure 2.2.

The phase angle (ϕ) between the external force $P = P_o e^{i\alpha t}$ and footing displacement U_v is:

$$\tan\phi = \frac{f_2}{f_1}$$ Equation 2.14

Sung (1953), Quinlan (1953) and Bycroft (1956) extended Reissner's solution to account for the effect of pressure distribution at the contact area between footing and the surface of the half-space. Sung (1953), Quinlan (1953) and Bycroft (1956) solutions assume that the contact pressure distribution between the footing and half-space medium is that produced by a rigid footing, a uniform loading and parabolic loading. It is obvious that the solution is an approximation as the assumptions for the soil medium and pressure distribution underneath the footing are crude. In the Reissner (1936), Bycroft (1956) and Sung (1953) solutions, the value of f_1 and f_2, which are functions of Poisson's ratio of the half-space medium, can be obtained from charts to determine the footing displacement.

Sung (1953) determined only the displacement at the centre of the loaded footing while Bycroft (1956) went further and calculated the displacement of the footing as a weighted average of the displacement over the loaded area. This implies that the Bycroft (1956) solution is based on more realistic assumptions than the Sung (1953) solution in solving Reissner (1936) equation. In this study, Sung (1953) displacement functions are used. This is because Sung (1953) generated displacement functions for f_1 and f_2 to solve Reissner (1936) equation in the form of power series functions for a rigid base, a uniform loading

2-9

and parabolic loading for Poisson's ratios of 0, 0.25, 0.333 and 0.5, which can be easily applied. Hsieh (1962) presented the same approach, where he established displacement functions F_1 and F_2 to solve Reissner (1936) equation.

The half-space theory provided the basis for analysis of the machine foundation subjected to dynamic loading. Because the half-space theory requires assumptions concerning the pressure distribution below the footing, Sung (1953) recommended the use of a ring-form load for more accurate estimation of axial symmetric load distribution underneath the footing. Since then, the half-space theory has been simplified ranging from simple to complex to determine the response of machine foundation system under dynamic loading. The simplified models which will be discussed in this thesis include those proposed by Lysmer (1965), Veletsos and Verbic (1973) with massless soil and footing as well as Veletsos and Verbic (1973) with mass of the soil and footing.

2.4   Simplified Lysmer (1965) model

Lysmer (1965) investigated a theoretical solution introduced by Reissner (1936) for a circular rigid footing resting on an elastic half-space which was subjected to steady state vertical oscillation. Lysmer (1965) used concentric rings of constant pressure and assumed the displacement of all rings to be the same, simulating constant pressure exerted beneath the footing.

Reissner's solution considers an estimation of displacement functions f_1 and f_2 which are obtained from charts to calculate the displacement response of machine foundations. To eliminate the influence of Poisson's ratio, Lysmer (1965) multiplied the term $(f_1 + if_2)$ in Equation 2.8 by a factor $4/(1-\nu)$ and defined a new compliance function as described in Equation 2.15.

$$F = \frac{4}{(1-\nu)}(f_1 + if_2) = F_1 + iF_2$$
<div align="right">Equation 2.15</div>

Where:

The functions F_1 and F_2 can be obtained from Equation 2.16.

$$F_1 = \frac{-f_1}{f_1^2 + f_2^2} \quad \text{and} \quad F_2 = \frac{f_2}{f_1^2 + f_2^2} \times \frac{1}{a_o}$$
<div align="right">Equation 2.16</div>

2-10

For a vertical vibrating rigid circular footing, the influence of the geometry of the footing is shown in the Reissner's dimensionless mass ratio (b_o) illustrated in Equation 2.10. Lysmer introduced a modified mass ratio given by Equation 2.17.

$$B_v = \left(\frac{1-v}{4} \right) \frac{m}{\rho r_o^3}$$
Equation 2.17

Where:

v is the Poisson's ratio.

This implies that in Lysmer (1965) model a chart is not required to extract different values of f_1 and f_2 because they are expressed in the single displacement function by specifying geometry of the footing, soil type and excitation frequency, (Richart et al., 1970 and Das, 2011). Using Lysmer (1965) model, the amplitude of vertical vibrations is given by:

$$U_v = \frac{(1-v)P_o}{4Gr_o} Z$$
Equation 2.18

Where:

Z is the magnification factor. The equation of motion for Lysmer (1965) model is given by:

$$M\ddot{U} + C\dot{U} + KU = P_O sin(\omega t)$$
Equation 2.19

Where:

M is the mass of the foundation system;

C is the viscous damping coefficient of the foundation system;

K is the stiffness of the system;

U is the absolute displacement of the mass;

ω is the forcing frequency;

t is the time, and

P_o is the force amplitude.

For vertical vibration, C in Equation 2.19 is equal C_v, therefore, the vertical viscous damping coefficient of the foundation sytem is given by:

$$C_v = \frac{3.4r_o^2}{1-v} \sqrt{\rho G}$$
Equation 2.20

2-11

Where:

r_o is an equivalent radius of the footing;

v is a Poisson's ratio of the soil;

G is the shear modulus of the soil, and

ρ is the mass density of the soil.

For vertical vibration, K in Equation 2.19 is equal to K_v which is the same constant used to calculate settlement for static loading:

$$K_v = \frac{4Gr_o}{1-v}$$ Equation 2.21

For vertical vibration, the damping ratio is given by:

$$D = \frac{C_v}{C_c} = \frac{0.425}{\sqrt{B_v}}$$ Equation 2.22

Where:

B_v is Lysmer's modified mass ratio obtained from Equation 2.17.

C_c = critical damping coefficient $= 2\sqrt{K_v M}$

The vertical dynamic displacement of a machine foundation system is determined using Equation 2.23.

$$U_v = \frac{(P_o/K_v)}{\sqrt{\left[1-\left(\frac{\omega^2}{\omega_o^2}\right)\right]^2 + 4D^2\left(\frac{\omega^2}{\omega_o^2}\right)}}$$ Equation 2.23

Where:

P_o is the amplitude of the forcing function;

ω_o is the natural frequency of the system;

ω is the frequency of excitation;

K_v is the stiffness of the system, and

D is the damping ratio.

Equation 2.23 can be used to evaluate the elastic dynamic response of rigid footings subjected to harmonic loads. The work by Lysmer resulted in 'Simplified Lysmer (1965)

2-12

model (Lumped parameter model) in which a mass, spring, and dashpot are used to simplify the analysis. The mass of the system is lumped together in one mass (M). All effects contributing to the stiffness are lumped together in one stiffness parameter (K_v) and represented by a spring. And all effects contributing to damping are lumped together in one parameter (D) and represented by a dashpot. K_v and D are frequency dependent parameters. For surface foundations other simplified models include Veletsos, and Verbic (1973) massless of soil and footing, Veletsos and Verbic (1973) with mass of footing and soil and Dyna5 program. The dynamic response of the embedded foundation system can be predicted using the model proposed by Novak and Beredugo (1972) and the Dyna5 program. These analytical methods use impedance functions to estimate machine foundation behaviour.

2.5   Impedance functions

Impedance functions represent the frequency dependent stiffness and damping characteristic of foundation-soil interaction. These can be obtained using available analytical solutions or can be measured in the field. The dynamic impedance functions obtained from the field measurements represent the actual dynamic behaviour of soil-structure interaction.

The prediction of dynamic behaviour of soil-structure interaction is governed by dynamic impedance functions. These functions are used to describe an assumed linear relationship between force and displacement at a particular frequency of a dynamically loaded machine foundation. The impedance function of the machine foundations is frequency dependent. The inverse of the impedance function is called compliance or frequency response function. The frequency response functions can be obtained from either measured data or analytical solutions and may be presented in terms of magnitude and phase.

Accurate impedance functions of a foundation system are a key requirement in analysis and design of dynamically loaded machine foundations. These impedance functions allow resonant amplitude, resonant frequency, natural frequency and dynamic stiffness of foundation systems to be predicted.

To date, few research studies have documented the responses of the vertical dynamic impedance functions of shallow foundations obtained from field measurements (Dunn et al., 2009; Dunn, 2010 and Tileylioglu, 2011). Veletsos and Verbic (1973) investigated the effect of material damping for a steady-state response of harmonically excited footings.

2-13

Gazetas (1991a) presented various formulas and charts of impedance functions for different modes of vibration for surface and embedded footings, which can readily be used by practicing engineers. In their study, they suggested the use of models with mass by taking the spring stiffness equal to the static stiffness of the system instead of the use of massless models. The use of massless models may result in the effective stiffness becoming negative over a large frequency range. Evaluation of impedance functions assumes that the footing is completely rigid and remains in contact with the soil at all times (Gazetas, 1991; Verruijt, 2003). Therefore, the displacement of the footing is assumed to be equal to the displacement of the soil surface beneath the footing.

Impedance functions can be determined from the frequency response functions measured in the field (Crouse et al., 1984; Wong and Trifunac, 1988; Crouse et al., 1990; Srinivasan et al., 1991; DeBarros and Luco, 1995; Tileylioglu, 2008; Dunn et al., 2009; Dunn, 2010 and Ahn, 2011). The comparison between impedance functions obtained from field data with those predicted from theoretical models shows that the general responses of the foundations are frequency dependent. This observation shows that it is important to consider footing inertia force in the analysis and design of machine foundations.

Nii (1987) carried out laboratory experimental tests to determine dynamic stiffness for surface and embedded footings on a half-space made from silicon rubber. The dynamic impedances were measured using mechanical impedance measurement techniques. The dynamic stiffness and damping coefficient obtained from the experimental test data indicated that dynamic stiffness and damping coefficients are frequency dependent.

Crouse et al (1990) carried out experimental work to determine impedance functions for a forced vibration test on surface and embedded footings. The results indicated that the use of static-stiffness and low-frequency values of damping would be inappropriate in soil-structure interaction models of high frequency machinery on small footings. The forced vibration tests performed by Crouse et al (1984) were designed to determine impedance functions of the accelerograph station. The results indicated that the theory underestimates the real part of the vertical impedance stiffness, but overestimates the imaginary part.

Although theoretical models assume a massless foundation, the experimental results showed satisfactory agreement between theoretical and experimental results. Srinivasan et al., (1991) compared theoretical results obtained from the Lysmer (1965) model and experimental results. This revealed that Lysmer (1965) model overestimates the natural frequency and damping coefficient.

The assumed massless foundation developed by Lysmer (1965) model was critically analysed by Verbic (1972) who has pointed out that this assumption has no significant effect on the frequency response function. Verbic (1972) then suggested that the single-degree of freedom (SDOF) model as proposed by Lysmer (1965,) shown in Equations 2.19 to 2.23, can be used without loss of information when compared to the actual soil-structure interaction system.

A summary outlining the development of soil-structure interaction methods for machine foundations can be found in Gazetas (1983) and Kausel (2010). In the review, Gazetas (1983) indicated that in the design and analysis of machine foundation it is important to evaluate impedance characteristics obtained at the frequencies of interest.

The review of available solutions for impedance functions is provided by Shah, 1968; Veletsos and Verbic, 1973; Veletsos and Verbic, 1974; Gazetas, 1991b; Nii, 1987. and Veletsos and Tang, 1987. The soil profile is assumed to be viscoelastic or elastic half-space, and simplified as a single degree of freedom system as shown in Figure 2.2. For each excitation frequency, the dynamic impedance is calculated using Equation 2.24, which is the ratio between the applied force (or moment) and resulting steady state displacement response (or rotation) at the centre of the base of a massless footing and soil. The obtained impedance functions are employed to describe a linear relationship between the forcing function and the displacement response (Gazetas, 1991b). This assumed relationship allows for the solution of dynamic displacement using the differential equation of motion. The response of the system is described in Equation 2.24 and is known as complex dynamic stiffness.

$$K_o(\omega) = \frac{P_o(t)}{U_o(t)}$$ Equation 2.24

Where:

$P_o(t)$ is the harmonic force, and

$U_o(t)$ is the harmonic displacement.

For the assumed applied vertical harmonic force, a particular solution of displacement in the time domain is given by $u_p(t) = U_v e^{i\omega t}$. Substituting this expression in Equation 2.19, the vertical displacement is obtained by:

$$U_v = \frac{P_o}{K_o - M\omega^2 + iC\omega}$$

Equation 2.25

Where:

ω is a frequency of excitation;

K_o is equivalent to static stiffness $\left(K_o = K_{static}\right)$;

M is the lumped mass of footing and machine

C is the radiation damping coefficient of the soil-foundation system, and

P_o is the vertical force amplitude.

The vertical displacement amplitude is given by:

$$\left|U_v\right| = \frac{P_o}{\sqrt{\left(K_o - M\omega^2\right)^2 + \left(C\omega\right)^2}}$$

Equation 2.26

while the static displacement is obtained by:

$$U_{static} = \frac{P_o}{K_o}$$

Equation 2.27

and

$$\frac{P_o}{U_v} = \left(K_o - M\omega^2 + iC\omega\right)$$

Equation 2.28

Equation 2.28 can also be expressed as:

$$K_v(\omega) = \left(K_o - M\omega^2 + iC\omega\right)$$

Equation 2.29

Where:

$K_v(\omega)$ is the complex dynamic stiffness.

For a very low frequency ω, K_o has a dimension of force per length. The typical values of K_o for foundation systems depend on the footing characteristics, such as width of footing and underlying soil properties. The complex dynamic stiffness shown in Equation 2.29 can be written in the general form as:

$$K_v(\omega) = K^R(\omega) + iK^I(\omega)$$

Equation 2.30

where,

$$K^R(\omega) = K_o - M\omega^2$$

Equation 2.31

and

$$K^I(\omega) = C\omega$$

Equation 2.32

Where:

$K^R(\omega)$ is the real part known as effective dynamic stiffness which reflects the stiffness and inertia of the supporting soil. The dependence of the real part on frequency is attributed solely to the influence of frequency on inertia, because at small strains, soil properties are essentially frequency independent (Gazetas, 1983 and Gazetas, 1991b).

$K^I(\omega)$ is the imaginary part which reflects the radiation and material damping of the foundation systems. Radiation damping is the result of energy dissipation by waves propagating away from foundation systems and is frequency dependent, while material damping is mainly due to hysteretic cyclic behaviour of soil, which is practically frequency independent (Gazetas, 1983 and Gazetas, 1991b).

If Equation 2.31 is normalized by K_o, which is K_{static} for low frequency, then, the equation will reduce to:

$$\frac{K^R(\omega)}{K_o} = k(\omega) = \left(1 - \frac{M}{K_o}\omega^2 \right)$$

Equation 2.33

Where:

$k(\omega)$ is a dynamic stiffness coefficient of the foundation (Veletsos and Verbic, 1973; Veletsos and Verbic, 1974 and Gazetas, 1991) and is simplified as:

$$k(\omega) = \left(1 - \frac{\omega^2}{\omega_n^2} \right)$$

Equation 2.34

The analysis of field data involves carrying out a fast Fourier transform (FFT) of displacement and FFT of the input force. P_o and U_o are complex functions. Equation 2.29 describes the impedance functions and it is necessary to mention that, this equation is the

2-17

result of the division of complex values. As an example, assume that the foundation is excited by a vertical forcing function with frequency of 20 Hz, and the displacement response is recorded, then the complex dynamic stiffness is given by:

$$K_{v(20Hz)} = \frac{-1591618.45 + 183337.83i}{-3.0779 + 1.4008i} = 74904.40 + 3153.54i$$

The numerator is the FFT of the input data (forcing function) while the denominator is the FFT of the output (displacement response) obtained from the field-measured data. The results take the form of Equation 2.31 and Equation 2.32, where:

$$K^R(\omega) = K_o - M\omega^2 = 74904.40 \text{ and } K^I(\omega) = C\omega = 3153.54 \qquad \text{Equation 2.35}$$

The complex dynamic stiffness is the magnitude of the real and the imaginary part as shown in Figure 2.5. Therefore, the presentation of responses of a foundation system using impedance functions is obtained by back-calculation. The directly measured dynamic responses may be presented in terms of displacement velocity and acceleration depending on which response has been measured in the field.

2.5.1 Veletsos and Verbic 1973 massless soil

The simplified analysis methods determine dynamic response of machine foundation system by force vibration tests assume that the footing and soil are massless as shown in Figure 2.2 (Sung, 1953; Lysmer, 1965; and Veletsos and Verbic, 1973). The behaviour of a foundation system may be modelled more realistically by assuming that the footing is placed on the surface of a column of soil, which possesses mass distributed along its length, as shown in Figure 2.6. If this column of soil mass is loaded by vertical harmonic load, the column will vibrate with the mass of soil, which is distributed along the width and length as shown in Figure 2.6. For an approximate analysis at the low frequency $(a_o \leq 1.5)$ the column may be assumed to be massless and, the distributed mass can be lumped and placed on the top of a spring and dashpot as shown in Figures 2.7 and 2.8 (Verbic 1972 and Veletsos and Verbic 1973).

The complex dynamic stiffness or impedance function of footing on massless system can be approximated by the following equation:

$$K(\omega) = K_o(k(\omega)(a_o, v) + ia_o c(\omega)(a_o, v)) \qquad \text{Equation 2.36}$$

Where:

K_o represents static stiffness;

$c(\omega)$ is the damping coefficient;

$k(\omega)$ is the dynamic stiffness coefficient;

ν is Poisson's ratio of the half-space medium, and

a_o is the dimensionless frequency $(a_o \leq 1.5)$ given by Equation 2.9.

For an equivalent mass spring-dashpot representation of the half-space supporting medium, $k(\omega)$ is a measure of the dynamic stiffness coefficient of the spring and c_ω is a measure of damping coefficient of the dashpot (Shah, 1968 and Verbic, 1972). The analysis procedures take into account only geometric radiation damping (Veletsos and Verbic, 1973). For high frequencies, an approximate semi-empirical expression for dynamic stiffness coefficients and damping coefficient of the dashpot of a vertically vibrating rigid footing is presented in Table 2.1 (Veletsos and Verbic, 1973 and Veletsos, 1974).

Table 2-1: Coefficients for the vertical dynamic stiffness (Veletsos and Verbic, 1973)

Poisson ratio - ν	0	0.33	0.5
Coefficients			
b_1	0.25	0.35	0
b_2	1	0.8	0
b_3	0	0	0.17
b_4	0.85	0.75	0.85

Where:

b_1, b_2, b_3 and b_4 are numerical coefficients, which depend on the Poisson's ratio.

Using the numerical coefficients given in Table 2.1, dynamic stiffness coefficient is:

$$k(\omega) = 1 - b_1 \frac{(b_2 a_o)^2}{1 + (b2a_o)^2} - b_3 a_o^{\ 2}$$

Equation 2.37

while the damping coefficient is given by:

$$c(\omega) = b_4 + b_1 b_2 \frac{(b_2 a_o)^2}{1 + (b2a_o)^2}$$

Equation 2.38

All the models described up to this point assume that the foundation soil is massless, however it is known that some of the soil below the footing also vibrates as a result of the vibration of the footing itself (Verbic 1972 and Veletsos and Verbic 1973). Veletsos and

2-19

Verbic (1973) developed an analytical model which includes mass of the soil below the footing. This model will be described in the next section.

2.5.2 Veletsos and Verbic 1973 soil with mass

Veletsos and Verbic (1973) suggested a model, which can take into account the mass of the supporting medium and footing. Equation 2.26 gives the displacement steady state motion of the foundation due to harmonic excitation. Equation 2.29 gives the complex dynamic stiffness. If Equation 2.29 is compared with Equation 2.36 at a specified frequency and equating the imaginary part, the dashpot coefficient (C) can be expressed by:

$$C = c(\omega)\frac{K_o r_o}{V_s}$$

Equation 2.39

From Equation 2.36, it can be observed that a desirable representation can be achieved by assuming that the real part from the massless solution is equal to the static stiffness $\left(K^R(\omega) = k(\omega)K_o\right)$. Therefore, if the real part of Equation 2.29 is equated to the real part of Equation 2.36 and equating $M = M_s$, the term M_s is assumed to be the mass of the half-space medium as shown in Figure 2.8, then M_s takes the form:

$$M_s = \left(1 - k(\omega)\right)\frac{K_o}{\omega^2}$$

Equation 2.40

The frequency ω^2 can be eliminated by introducing a dimensionless frequency a_o and a dimensionless parameter B_v. This can be achieved by substitution of Equations 2.9, 2.10, 2.17 and Equation 2.34 into Equation 2.40, then Equation 2.40 becomes:

$$M_s = B_v \frac{K_o r_o^2}{V_S^2}$$

Equation 2.41

If K_o in Equation 2.40 is taken as a static stiffness obtained from Equation 2.21 and substituting V_s obtained from elastic theory $\left(V_s = \sqrt{G_o/\rho_s}\right)$ in Equation 2.41, then:

$$M_s = \frac{4B_v}{1-v}\rho_s r_o^3$$

Equation 2.42

The effect of mass of the footing vibrating in the vertical direction can be described by adding the inertia of footing M_f to the inertia of an equivalent oscillator with mass M_s as

2-20

shown in Figure 2.9. The dynamic behaviour of the machine foundation can be conveniently specified by the natural frequency ω_n and damping ratio D (Veletsos and Verbic 1973). The natural frequency (ω_n) of a foundation system that includes half-space mass is determined by:

$$\omega_n = \left(\sqrt{\frac{K_o}{M_s + M_f}} \right) \times \omega_o \qquad \text{Equation 2.43}$$

Where:

ω_o is the natural frequency of the system assuming that the half-space is massless as shown in Equation 2.7 and (M_s) is obtained from Equation 2.42.

The damping ratio (D) of the foundation system is obtained from Equation 2.44.

$$D = \frac{C}{2\sqrt{K_o \left(M_s + M_f \right)}} \qquad \text{Equation 2.44}$$

The displacement amplitude of the foundation system as suggested by Veletsos and Verbic (1973) is given by:

$$U_v = \frac{P_o \Big/ K_o}{\sqrt{\left(1 - \left(\frac{\omega}{\omega_n} \right)^2 \right)^2 + 4D^2 \left(\frac{\omega}{\omega_n} \right)^2}} \qquad \text{Equation 2.45}$$

2.5.3   Impedance methods using Dyna 5 program

The real part, damping coefficient and phase angle of shallow and deep foundations can be determined using the Dyna5 program. The obtained real and the imaginary part can be used to determine complex dynamic stiffness using Equation 2.36. In the Dyna5 program, the effective dynamic stiffness and the damping coefficient are considered to be frequency dependent. The calculation of effective dynamic stiffness and damping coefficient for shallow foundations is based on the theory described by Veletsos and Verbic (1973). For embedded foundations, the solution is based on the method proposed by Novak and Beredugo (1972). If the layer below footing is five times the equivalent footing radius, the program considers the soil profile as a half-space. The soil material properties of the layer are introduced in the program by specifying shear wave velocity, unit weight, and

Poisson's ratio. In Dyna5 program, the harmonic force input can be of constant amplitude (non-quadratic) or the frequency dependent (quadratic) excitation.

The numerical method of the Dyna5 program is useful for calculating dynamic impedance function. These values can be used in the finite element method to determine dynamic response behaviour of the structure in time domain. The proposed analytical models assume that the footing is a rigid body placed on the surface of an elastic half-space. However, in practice, machine foundations are partially embedded at a certain depth below ground level. In this next section, the effect of foundation embedment will be discussed.

2.5.4   Embedded foundation

Although most machine foundations are partially or fully embedded, there is little information about analysis and design of embedded machine foundations. The most used analytical solution method for approximating the dynamic response of embedded foundation system is the one proposed by Baranov (1967), and this was extended by Novak and Beredugo (1972). Other analytical solutions are those proposed by Gazetas et al., 1985; Gazetas, 1991a; and Gazetas, 1991b. These analytical approaches assume that the soil is divided at the horizontal plane at the foundation base. The base area is treated as an elastic half-space. The embedment soil medium is approximated as a series of independent infinitesimally thin elastic layers (Novak and Beredugo, 1972; Novak, 1972; Novak et al., 1978).

Numerous researchers studied the effects of embedment on the dynamic responses of embedded foundation. The studies suggest that embedment increases stiffness and reduces the resonant displacement amplitude (Lysmer and Kuhlemeyer, 1969; Novak, 1970; Chae, 1971; Novak and Beredugo, 1972; Gupta, 1972; Novak, 1974; Novak et al., 1978; Lin and Jennings, 1984; Gazetas and Stokoe, 1991; Inukai and Imazawa, 1992). The studies further suggest that the increase in stiffness of the foundation systems causes an increase in the resonant frequencies of the foundation systems (Novak and Beredugo 1972; Gupta, 1972; El Naggar, 2001). However, some studies reported that increasing embedment caused little or no increase in resonant frequency (Chae, 1971; Gazetas and Stokoe 1991 and Inukai and Imazawa, 1992). Chae (1971) argues that the resonant frequency would not change because the effective stress at the foundation level will increase because of the surcharge, which balances the increase of stiffness due to embedment.

The contradiction between researchers about the increase of the resonant frequency, with an increase of depth of embedment could be due to the quality of the modelling of the side contact between the foundation and the soil. Novak (1970) noted that the response of embedded foundation could be substantially affected by the nature of the contact between the footing and the surrounding soil. Novak realised that the description of embedment effect is complicated. It depends on the time which can affect the quality of side contact. In the recognition of the effect of time on the dynamic response of embedded foundations, for this study, the embedded foundation was left for 12 months to allow improvement of contact between the soil and the side of the footing. From the literature review, it is clear that uncertainty still exist regarding the effect of embedment on the resonant frequency and natural frequency of machine foundations.

Chae (1971) introduced dimensionless quantities, known as amplitude reduction coefficient (R_f) and embedment factor (N_f), to express the response of embedded footing. Novak and Beredugo (1972) used resonant amplitude ratio to describe the response of embedded footings under dynamic loading. The geometry of the footing is described by embedment ratio (δ) as shown in Equation 2.46 (Novak and Beredugo, 1972 and Gazetas and Stokoe, 1991):

$$\delta = \frac{D_f}{r_o}$$
Equation 2.46

Where:

D_f is the embedment depth as shown in Figure 2.10, and

r_o is a radius or equivalent radius of the footing.

The resonant amplitude ratio as suggested by Novak and Beredugo (1972) is given by:

$$R_a = \frac{Umax}{U_0max}$$
Equation 2.47

Where:
$U\,max$ is the maximum displacement amplitude at the given embedment, and
$U_0\,max$ is the maximum displacement amplitude for zero embedment (surface footing).

For a square footing, r_o is half the width of the footing, while for a circular footing r_o is the radius of the footing as shown in Figure 2.10. The relationship between embedment

2-23

depth and resonant frequency is expressed in terms of resonant frequency ratio, which is defined by:

$$R_f = \frac{f_d}{f_o}$$ Equation 2.48

Where:

R_f is the resonant frequency ratio

f_o is the resonant frequency of foundation system with zero embedment.

f_d is the resonant frequency of the foundation system at a given embedment D_f.

Novak and Beredugo (1972) presented the solution for determining the dynamic response of embedded foundation systems. Their solution is based on the determination of stiffness and damping coefficients (impedance functions) of the embedded machine foundation systems. The solution uses the concepts proposed by Reissner (1936) for solving the problem of vibration on the half-space medium as shown in Figure 2.10. The basic differential equation for the problem shown in Figure 2.10 is given by:

$$M\ddot{U}(t) = P_v(t) - R_v(t) - N_v(t)$$ Equation 2.49

Where:

M is the mass of foundation system;

$\ddot{U}$ is the acceleration;

$P_v(t)$ is a time dependent vertical excitation force;

$R_v(t)$ is a vertical dynamic reaction at the base of footing, and

$N_v(t)$ is the total vertical dynamic reaction force along the sides of the footing

The total reaction force $N_v(t)$ depends on the quality of the contact between the footing and soil. The following assumptions were made to solve Equation 2.49.

- the footing is a rigid, cylindrical body with radius r_o;
- the response is a linear elastic;
- the vertical dynamic reaction $R_v(t)$ is independent of the embedment depth;
- there is perfect bond between sides of the footing and the soil, and
- the excitation force is harmonic and acts along the vertical axis of the footing.

Because it is assumed that the footing is placed on the surface of an elastic half-space soil medium and the reaction at the base is independent of soil reaction along the surface of footing sides, the relationship between displacement $U(t)$ and elastic half-space reaction $R_v(t)$ is given by Equation 2.50, as was suggested by Reissner (1936).

$$\frac{R_v(t)}{U_v(t)} = Gr_o(C_1 + iC_2)$$ Equation 2.50

where,

$$C_1 = \frac{-f_1}{f_1^2 + f_2^2} \text{ and } C_2 = \frac{f_2}{f_1^2 + f_2^2}$$ Equation 2.51

In Equation 2.51, f_1 and f_2 are Reissner's frequency dependent displacement functions, which depend on the radius of the loaded area, and the length of the shear wave propagated by the footing, as well as on Poisson's ratio of the soil. The displacement functions f_1 and f_2 can be separated into real and imaginary parts. This implies that C_1 is related to the stiffness and C_2 is related to damping of the embedded foundation system. Equation 2.50 shows that the complex dynamic stiffness of the foundation system has real and imaginary parts $(C_1 + iC_2)$.

The vertical dynamic reaction force $N_v(t)$ is a complex function acting along the sides of the surface of the footing. The complex function $N_v(t)$ depends on the embedment depth (D_f), the shear modulus of the adjacent soil (G_S), and the density (ρ_s) of the adjacent soil. The reactions along the sides of the footing are obtained by considering the dynamic reaction per unit depth of embedment (Novak and Beredugo, 1972; Novak, 1990). The vertical dynamic reaction force is given by:

$$N_v(t) = \int_0^{D_f} s(z,t)dz$$ Equation 2.52

in which $s = s(z,t)$ is the Baranov solution for a unit reaction (independent of z) of which the mathematical expression is described by Novak (1970), Novak and Beredugo (1972), and Novak and Han (1990). Therefore, the vertical dynamic reaction force is given by:

$$S(t) = G_s(S_1 + iS_2)U_v(t)$$ Equation 2.53

Where:

$U_v(t)$ is the vertical displacement response of the footing,

S_1 is a function related to stiffness parameters,

S_2 is a function related to damping of the foundation system (Novak and Beredugo 1972).

The total vertical dynamic reaction force along the sides of footing takes the form:

$$\frac{N_v(t)}{U_v(t)} = G_s D_f (S_1 + iS_2)$$

Equation 2.54

Equation 2.49, 2.50 and 2.54 indicate that embedment increases the vertical reaction (friction) along the sides of the footing, which results in an increase of stiffness of the foundation system. To account for this increase in stiffness of the foundation system, the displacement functions proposed by Reissner given in Equation 2.49 and 2.51 need to be modified. This can be done by substituting Equation 2.54 into Equation 2.49, which is the equation of motion. The equation of motion for an embedded footing then takes the form:

$$M\ddot{U}(t) + Gr_o \left[C_1 + iC_2 + \frac{G_s}{G} \frac{D_f}{r_o} (S_1 + iS_2) \right] U(t) = P(t)$$

Equation 2.55

With the complex forcing function $P(t) = P_o e^{i\omega t}$ and steady state response of $u(t) = U_o e^{i\omega t}$, the solution for the vertical frequency dependent dynamic stiffness is given by:

$$k(\omega) = Gr_o \left(C_1 + \frac{G_s}{G} \frac{D_f}{r_o} S_1 \right)$$

Equation 2.56

while the frequency dependent damping coefficient is:

$$c(\omega) = \frac{Gr_o}{\omega} \left(C2 + \frac{G_s}{G} \frac{D_f}{r_o} S_2 \right)$$

Equation 2.57

In Equations 2.56 and 2.57, C_1 and S_1 are stiffness parameters, and C_2 and S_2 are damping parameters obtained from a polynomial functions shown in Table 2-2 (Novak and Beredugo 1972). In Equation 2.56 and 2.57, G is the small strain shear modulus of the half-space shown in Figure 2.10. The value of G_S is obtained from the density ratio:

$$G_s = \left(\frac{\rho_s}{\rho} \right)^3 G$$

Equation 2.58

Where:

ρ_s is the density of embedment soil layer.

ρ is the density of the half-space soil.

The amplitude of vibration for the embedded footing is obtained by using the values of the stiffness and damping coefficient determined from Equation 2.56 and 2.57 respectively. Equation 2.59 gives the vertical amplitude of vibration:

$$U_v = \frac{P_v/k}{\sqrt{\left(1 - \left(\frac{\omega}{\omega_o}\right)^2\right)^2 + 4D^2\left(\frac{\omega}{\omega_o}\right)^2}}$$ Equation 2.59

Where:

P_o is the force amplitude;

k is the dynamic stiffness shown in Equation 2.56;

ω is the forcing frequency;

ω_o is the natural frequency of the foundation system, and

D is the damping ratio.

Table 2-2: Stiffness and damping parameters for half-space and side layers (Novak and Beredugo, 1972)

Poisson's ratio (ν)	Values	Validity range
(a) Half-space		
0.25	$C_1 = 5.37 + 0.364a_o - 1.41a_o{}^2$ $C_2 = 5.06a_o$	$0 \le a_o \le 1.5$
(b) Side Layer		
any value	$S_1 = 0.2153a_o + 2.760a_o/a_o + 0.0608$ $S_2 = 6.059a_o + 0.7022a_o/a_o + 0.01616$	$0 \le a_o \le 2.0$

2.6 The finite element method

The literature shows that the analysis and design of vibrating foundations can be carried out using Mass spring dashpot or Winkler model, half-space theory and simplified half-space models. It is understood that simplified models often cannot handle modelling complex geometry foundation systems (Hadjin et al., 1974; Hall and Kissenpfennig, 1976 and Dutta and Roy, 2002). The modelling of complex foundation systems requires the use of the finite element method; this has been popular in civil engineering since 1960 (Chowdhury and Dasgupta 2009). There are various finite element methods, which are used to analyse and design foundations subjected to dynamic loadings. Therefore, the designer must choose a suitable finite element program for analysis according to the subject in question. The following sections will discuss the finite element method.

2.7 Wave propagation by finite element method

Modelling wave propagation with finite element techniques for soil-structure interaction problems has received increased interest in recent years. This is because the vibrating machine, the footing and the soil can be analysed together. In addition, the propagation of the mechanical waves radiating away from the footing can also be analysed.

Different soil-structure interaction (SSI) finite element methods have been introduced to analyse the dynamic behaviour of machine foundation systems (SHAKE2000, LUSH, SASSI and FLUSH). Numerious research studies have been carried out to compare the dynamic responses of machine foundations obtained using finite element methods and simplified models (Hadjian et al., 1974; Hall and Kissenpfennig, 1976). The results indicate that both procedures will yield the same results if they have been appropriately used to solve the same problem (Hall and Kissenpfennig, 1976). However, few studies have been carried out to compare the results obtained from field measurements and the finite element method.

There are a considerable number of commercial general-purpose finite element software packages capable of analysing soil-structure interaction problems such as Plaxis, Abaqus, Adina, Ansys PAFEC, SAP2000, GTSTRUCTDL and STAAD PRO (Chowdhury and Dasgupta 2009; Bhatia 2009). The capabilities of these commercial finite element software packages differ from one to another, especially when the problem of modelling wave propagation at the boundaries is considered. Therefore, it is important for the user to select reliable general finite element programs, which can analyse wave propagation problems.

Numerous researchers have used Abaqus software to model Rayleigh waves propagating along the surface of a soil medium. The results indicate an acceptable agreement between the numerical simulation and the field measurements, with judicious choices of the appropriate domain scale, mesh size and boundary conditions (Hall and Bodare, 2000; Zerwer et al., 2002; Zerwer et al., 2003; Inci, 2008; Motamed et al., 2009; Mbawala et al., 2011). Different research studies reported using Abaqus to solve wave propagation problems by force vibration methods to determine the frequency response functions of mechanical systems (Zhang and Yuchuan, 2007 and Zhao, 2009). Abaqus was used in this study to investigate the vertical dynamic response of surface and embedded machine foundation systems due to vertical harmonic excitation force.

A critical aspect, when dealing with dynamic analysis of soil-structure interaction using the finite element technique, is the modelling of unbounded media. The technique becomes difficult when a forcing function with a large range of frequencies is used (Mbawala et al., 2011). The finite element model must be terminated at some finite boundary. The simple solution to this problem is to define a large domain so that waves reflected from the boundary do not have time to return to the region of interest during the analysis. However, for wave propagation problems which involve soil with high wave velocity, this is not often a practical option. The practical option is to introduce boundaries which absorb these waves.

Different solutions have been proposed on the subject of non-reflecting boundaries (Lysmer and Kuhlmeyer, 1969; Liu and Achenbach, 1994; Liu and Jerry, 2003; and Nielsen, 2006). Lysmer and Kuhlmeyer (1969) introduced local non-reflection boundaries by viscous dampers attached to the boundaries to absorb waves. Abaqus implements the same principles for non-reflecting boundaries (Abaqus Theory Manual, 2011). In developing non-reflecting boundaries, it is assumed that the dynamic response of the medium near the boundary is linear elastic. The distribution of damping to the wave energy in the longitudinal direction is given by $\sigma_{xx} = -d_p \dot{V}_x$, of which $-d_p$ is chosen as damping constants to avoid reflection of wave energy back to the model in the longitudinal direction. The distribution of damping for shear wave energy back to the medium at the boundary is given by $\sigma_{xy} = -d_s \dot{V}_y$ and $\sigma_{xz} = -d_s \dot{V}_z$. The damping constant $-d_s$ is chosen to avoid the reflection of shear wave energy back to the model. Therefore, the viscous boundary proposed by Lysmer and Kuhlemeyer (1969) is defined by:

$$\sigma = a\rho V_p \dot{w}$$ <div style="float:right">Equation 2.60</div>

$$\tau = b\rho V_s \dot{u}$$ <div style="float:right">Equation 2.61</div>

Where:

σ and τ are normal stress and shear stress respectively;

a and b are dimensionless quantities

ρ is the mass density of the soil medium;

$\dot{w}$ and $\dot{u}$ are normal and tangential velocities respectively, and

V_p and V_s are the velocities of P-wave and S-wave respectively.

The solution by Lysmer and Kuhlmeyer (1969) suggests that the infinite elements are only efficient for body waves propagating normally to the boundary (P-waves and S-waves). However, the infinite elements can also absorb surface wave (Rayleigh and Love) if boundaries are arranged so that the dominant direction of wave propagation is orthogonal to the boundaries and are placed at a reasonable distance from the region of main interest.

Mbawala et al, (2011) described modelling procedures to analyse wave propagation problems using the Abaqus. The results indicate that the proper choice of domain size, element sizes, and use of infinite element at the boundaries minimises the vertical displacement caused by spurious reflections. In the analysis, Abaqus/Explicit was used to simulate the wave propagation in the ground by simulating Continuous Surface Wave (CSW) tests. Abaqus/Explicit is a special-purpose analysis technique which uses an explicit dynamic finite formulation (Abaqus Theory Manual, 2011).

2.7.1   Mesh size

The dimension of the finite elements must be selected while taking into consideration the wavelength of the propagating perturbation. The finite element mesh size limits the highest frequency that can be analysed (Alheid, 1994) and acts as a low–pass filter. Therefore, large elements filter short wavelengths (Zerwer et al., 2003). On the other hand, employing very small elements can cause numerical instability. The element size must be chosen according to the frequency content of the applied load. Differences in the element sizes should be as small as possible to avoid false reflections.

Equation 2.62 is used to estimate mesh element size (g) as proposed by Cook et al., (2002). In Equation 2.62, if f_{max} is the maximum frequency of the applied load, and V_i is

the propagation velocity of a wave which can be a P-wave, S-wave, or Rayleigh wave in the material, then the mesh element size should satisfy the relationship in Equation 2.62:

$$g \leq \varsigma\lambda_{min} = \varsigma\frac{V_i}{f_{max}}$$ Equation 2.62

Where:

g is the mesh size, and λ_{min} is a minimum wavelength, which is estimated using the maximum frequency of the wave f_{max}.

The constant ς depends on whether the mass matrices are consistent or lumped. For consistent mass matrices, the constant is $\varsigma = 0.25$ and for lumped mass is $\varsigma = 0.2$ (Cook et al., 2002). In a lumped mass, the mass of an element is represented by the particle masses which are lumped at the node. For consistent mass matrix, the mass of an element is linearly formulated and uses the same shape function used to formulate the stiffness matrix (Cook, 2002 and Zerwer et al., 2002).

2.8   Finite element method - steady state response analysis

The finite element method solution focuses on a continuum medium where the continuum is divided into a finite set of elements. The basic principle of solution is based on developing the solution for a static problem and extending this to a dynamic solution. In the analysis of geotechnical engineering structures, regardless whether the loading is static or dynamic, engineers are usually interested in displacement due to an action acting on the structure. Therefore, for a static action force, the relationship between force, static displacement and stiffness matrix shown in Equation 2.27, can be presented in the form of:

$$[K_o]\{U_{static}\} = \{P_o\}$$ Equation 2.63

Where:

$[K_o]$ is the global stiffness matrix;

$\{P_o\}$ is an applied vector force, and

$\{U_{static}\}$ is unknown displacement vector which is determined using the inverse of the static stiffness matrix as shown in Equation 2.64:

$$\{U_{static}\} = [K_o]^{-1}\{P_o\}$$ Equation 2.64

In the dynamic analysis, Equation 2.63 contains two more matrices, the mass matrix $[M]$ and proportional damping matrix $[C]$. The equation of motion is expressed as:

$$[M]\{\ddot{U}\}+[C]\{\dot{U}\}+[K]\{U\}=\{P\}$$

Equation 2.65

The solution of the steady state problem may be solved using the complex method. For this, in the equation of motion, the force and displacement vectors are given by:

$$\{P\}=\{P_o\}e^{i\omega t}$$

Equation 2.66

$$\{u(t)\}=\{U\}e^{i\omega t}$$

Equation 2.67

Where:

P_o is the force amplitude.

Therefore, the displacement response is given by:

$$\{u\}=\{U_o\}e^{i\omega t}$$

Equation 2.68

$$\{\dot{u}\}=i\omega\{U_o\}e^{i\omega t}$$

Equation 2.69

$$\{\ddot{u}\}=-\omega^2\{U_o\}e^{i\omega t}$$

Equation 2.70

Where:

$\{U_o\}$ is a constant complex displacement vector.

$\{u\}$ is the displacement response

$\{\dot{u}\}$ is the velocity response

$\{\ddot{u}\}$ is the acceleration response

Substituting Equations 2.68, 2.69 and 2.70 in Equation 2.65, the equation of motion becomes time independent and takes the form of Equation 2.25.

The task is to solve the linear differential equation by the numerical finite element method. Abaqus uses the Newmark method to solve steady state response problems. This method calculates the response of the system directly in terms of the physical degrees of freedom of the model using mass, damping, and stiffness matrices of the machine foundation system, which are depending on frequency (Abaqus Theory Manual, 2011). Steady-state dynamic analysis provides the steady-state amplitude and phase of the response of the

2-32

system due to harmonic excitation at a given frequency. Usually such analysis is done as a frequency sweep by applying the loading at a series of different frequencies and recording the response.

2.9 Damping

In numerical calculations, two types of damping exist; numerical damping, due to finite element formulation and physical damping which includes materials damping (hysteresis) , viscous damping and friction damping (Chowdhury and Dasgupta, 1998; Cook et al., 2002; Zerwer et al., 2002; Di Mino et al., 2009; Chowdhury and Dasgupta, 2009).

The frequency response of the system subjected to dynamic load depends on the amount of damping specified in the model. Due to the limitations of knowledge about damping, the viscous damping is represented in the system by using the equivalent Rayleigh damping or proportional damping and modal damping. Rayleigh damping is a simplified way of approximating physical damping. Rayleigh damping defines the global damping matrix $[C]$ as a linear combination of the global mass and stiffness matrices which is given by:

$$[C] = \alpha[M] + \beta[K]$$

Equation 2.71

Where:

$[M]$ is the mass matrix of the physical system;

$[K]$ is the stiffness matrix of the system, and

α and β are the pre-defined coefficients, which depend on the damping ratio and natural frequencies of the vibrating system.

Equation 2.71 expresses frequency dependence of damping. In finite element analysis, the coefficient α and β are often determined by choosing the fraction of damping D_1 and D_2 at two different natural frequencies ω_1 and ω_2 of the system (Chowdhury and Dasgupta 2009; Ju and Ni 2007; Di Mino et al 2009). The coefficient α is given by:

$$\alpha = \frac{2\omega_1\omega_2(D_1\omega_2 - D_2\omega_1)}{\left(\omega_2{}^2 - \omega_1{}^2\right)}$$

Equation 2.72

The coefficient β is:

2-33

$$\beta = \frac{2(D_2\omega_2 - D_1\omega_1)}{(\omega_2^{\,2} - \omega_1^{\,2})}$$

Equation 2.73

Where:

β is a coefficient related to the effect of stiffness on the system damping.

The relationship between the fraction of critical damping, frequency, and coefficients α and β demonstrating the effect of stiffness and mass is illustrated in Figure 2-11 (Chowdhury and Dasgupta 2009; Cook et al., 2002 and Zerwer et al., 2002)

2.10 Three-dimensional finite element models

As physical problems are in three dimensions, using two dimensional analysis can lead to dynamic response, which do not represent the three-dimensional problem (Hadjian et al,. 1974; Luco and Hadjian, 1974). Luco and Hidjian (1975) showed that for better results, finite element modelling should consider three-dimension modelling to maintain the correct radiation damping characteristic.

In many cases, for three dimensional analysis, two planes of symmetry exist, in which case only one quarter of the problem is considered in the analysis, as shown in Figure 2.12. The finite element model is shown in Figure 2.12. For vertical displacement, the symmetry boundary condition is applied to the xy (i.e., z = 0) and plane of zy (i.e. x=0).

2.11 Gibson soil half space

In the analysis of machine foundations, it is common to assume that the soil underneath the footing is a homogeneous or layered half-space. These assumptions may not be realistic in practice as the soil usually progressively become stiffer with depth even for uniform deposits. The effective stress in the soil increases with depth. This type of soil is known as Gibson soil. Gibson soil is defined as being an incompressible, isotropic, elastic half-space in which the shear modulus G increases linearly with depth. Gibson (1967) suggested the model of an inhomogeneous soil profile with increasing shear stiffness with depth in the form of:

$$G = G_o(1 + mz)$$

Equation 2.74

Where:

G is the shear stiffness at the depth of z;

G_o is the shear stiffness at the surface;

2-34

m is the rate of increase of shear stiffness per meter depth, and

z is the depth as shown in Figure 2.13. The relationship assumes that the soil density, Poisson's ratio and damping are constant with depth.

2.12 Compliance function

For a single degree of freedom system, the frequency response function or compliance function is the inverse of the impedance function. The results of the steady-state direct analysis in the Abaqus software is presented using the compliance functions. It is important to establish the relationship between impedance and compliance functions. Recalling Equation 2.30 the compliance function is given by:

$$X(\omega) = \frac{1}{K^R(\omega) + iK^I(\omega)}$$ Equation 2.75

Where:

$K^R(\omega)$ is the real part of the complex dynamic stiffness, and

$K^I(\omega)$ is the imaginary part of the complex dynamic stiffness.

The compliance function can be expressed in a more general form as:

$$X(\omega) = X^R(\omega) + iX^I(\omega)$$ Equation 2.76

Where:

$X^R(\omega)$ is the real part of the compliance function, and

$X^I(\omega)$ is the imaginary part of the compliance function.

Because compliance is the inverse of impedance, there exists a relationship which links the two impedance functions $K^R(\omega)$ and $K^I(\omega)$ to the compliance function $X^R(\omega)$ and $X^I(\omega)$. For a single degree of freedom, the relationships are shown in Equations 2.77 and 2.78.

$$K^R = \frac{X^R}{(X^R)^2 + (X^I)^2}$$ Equation 2.77

$$K^I = \frac{-X^I}{(X^R)^2 + (X^I)^2}$$ Equation 2.78

2-35

2.13 Summary

This chapter provided a review of the methods used to analyse machine foundations subjected to vertical dynamic loadings. The historical background shows that the evolution of the design of machine foundations started by using 'rules of thumb'. The main goal was to reduce the resonant amplitude by increasing the mass of the footing. The "In-phase" mass and reduced natural frequency mass were regarded as empirical methods, these came after the 'rule of thumb' design approach. Another early method used to design machine foundations was mass spring dashpot or the Winkler model.

The elastic half-space theory design method takes into consideration the effect of wave propagation caused by the vibrating footings. The method is regarded as a more scientific design method, which superseded the empirical design methods. The development of the elastic half-space theory used the concept introduced by Lamb (1904).

The elastic half-space theory can be simplified to the damped-single degree of freedom systems, which is frequency independent or frequency dependent. These methods sometime are known as lumped parameter models or simplified elastic half-space models.

For complex soil-structure interaction problems, it is appropriate to use the finite element method to determine the dynamic response of machine foundations. Therefore, machine foundations can be designed using the following methods:

- Mass-spring dashpot or Winkler model;
- Elastic half-space method;
- Simplified elastic half-space method or lumped parameter method, and
- Numerical methods such as the finite element method.

Foundation embedment increases the stiffness of the foundation systems and reduces the amplitude at resonance. From the literature, it appears that embedment has little influence on the resonant frequency. However, some researchers pointed out that with a perfect bond between soil and surface of the embedded footing, the resonant frequency increases as the embedment increases.

The literature remains silent on the effect of embedment on the natural frequency of the foundation systems. However, for undamped systems the condition of resonance is described as occurring when the forcing frequency coincides with the natural frequency of the foundation system. For a damped system, which undergoes forced vibration, the

2-36

resonant frequency occurs at a frequency which is less than the undamped natural frequency. Therefore, it is important to investigate the effect of the embedment on the natural frequency of the foundation systems. It is also noted that some workers use the terms resonant frequency and natural frequency interchangeably.

The advancement in the technology of the mining and manufacturing industries has resulted in the construction of sensitive and complex vibrating structures, for example, large ore grinding mills. These structures are not only sensitive but also have complex interdisciplinary loading and complex geometry. The investment in these kinds of structures demands a high level of reliability. The current common design method of machine foundations is the two-stage approach where geotechnical engineers determine the dynamic stiffness and damping constant of the machine foundation systems. These parameters are given to the structural engineer to calculate dynamic behaviour of the super-structure. This approach uses the Winkler model or simplified analytical models, which may not be suitable when dealing with the design of sensitive and complex engineering structures.

Numerical methods such as the finite element method may be a better tool for design of the engineering structures with complex interdisciplinary loading and complex geometry. The finite element method has some limitations, such as analysis time and cost, and requires a properly-trained analyst to deal with waves propagating in the ground, especially at the boundaries. The aim of this project is to investigate the complexity of the analytical and numerical solutions required to accurately predict the vertical dynamic behaviour of machine foundations.

Figure 2.1: Winkler subgrade foundation

Figure 2.2: Equivalent mass spring-dashpot

Figure 2.3: Point load on elastic body

Figure 2.4: Footing resting on the surface of elastic half-space
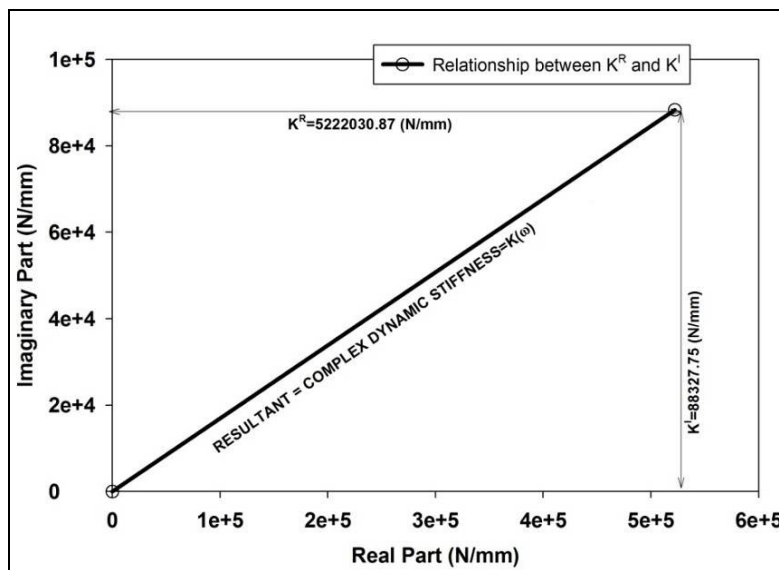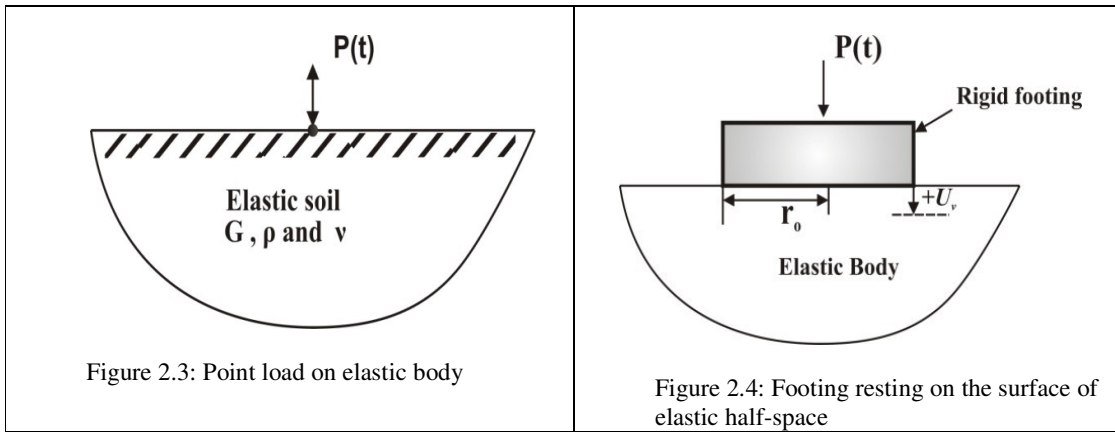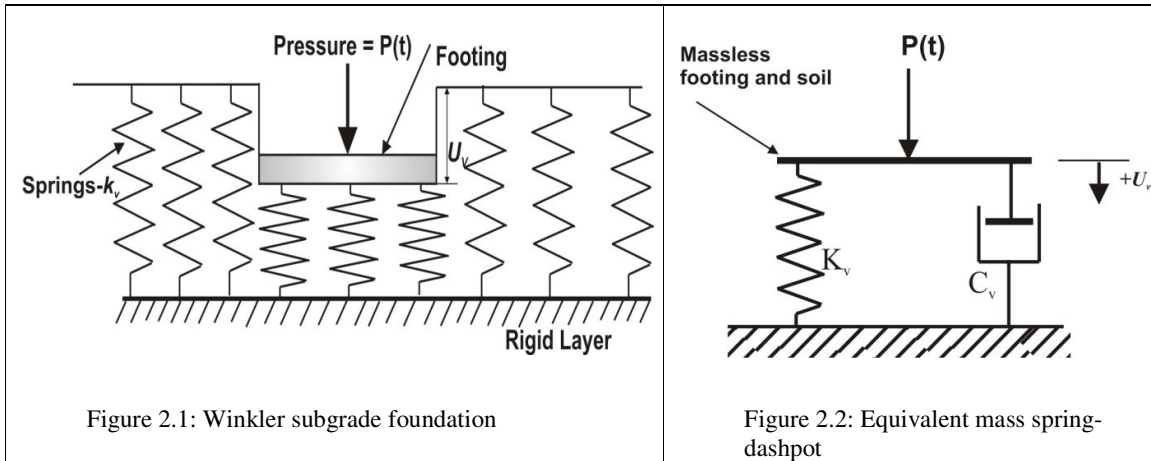
Figure 2.5: Relationship between Real part and Imaginary Part

2-38

Figure 2.6: Soil column with mass distributed along its length

Figure 2.7: Lumped mass of soil with massless column

Figure 2.8: Equivalent mass spring-dashpot with mass of soil.

Figure 2.9: Equivalent mass spring-dashpot with mass of soil and footing.

2-39
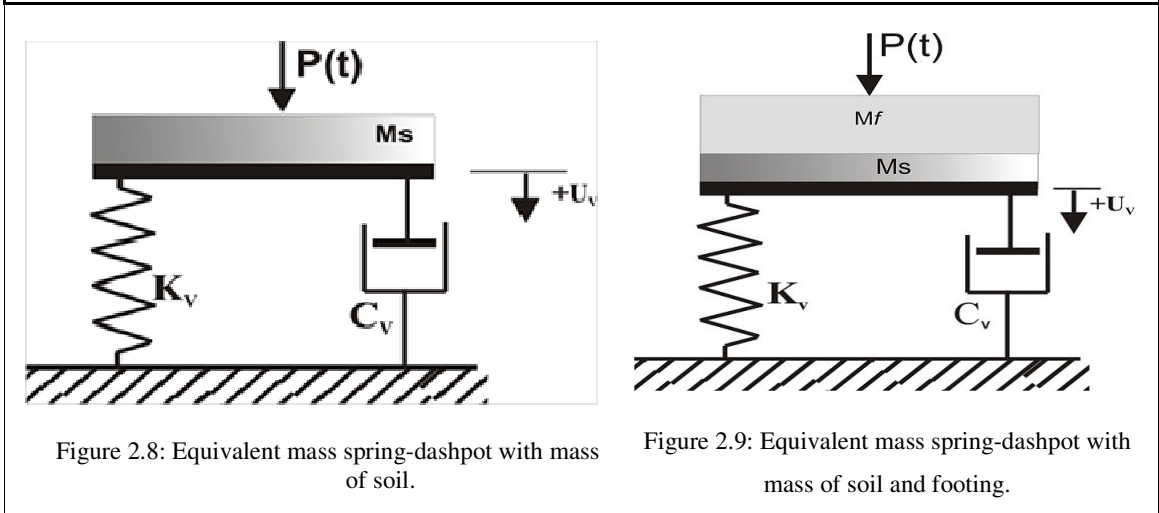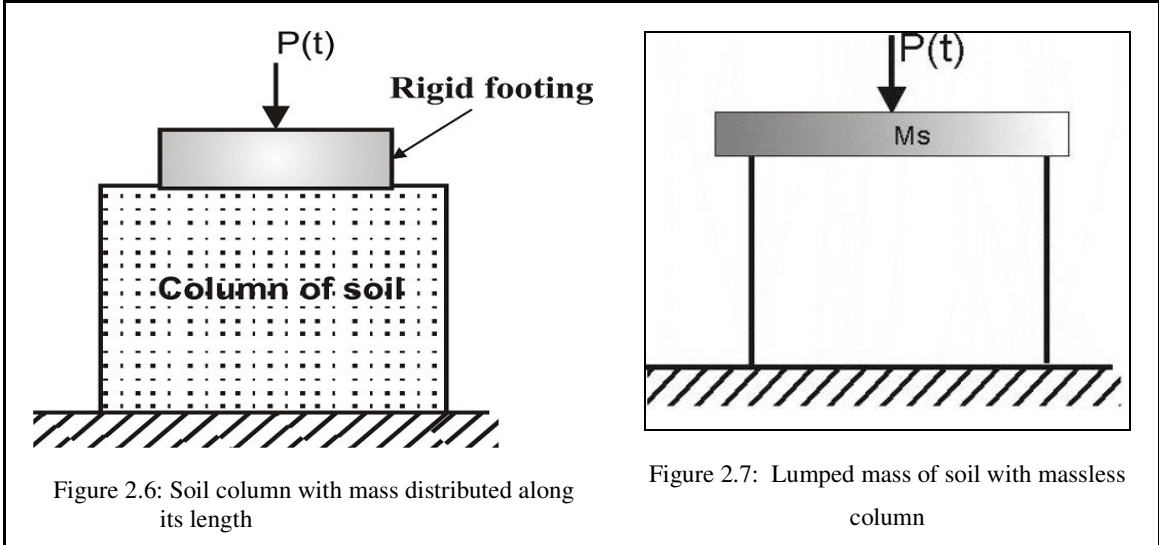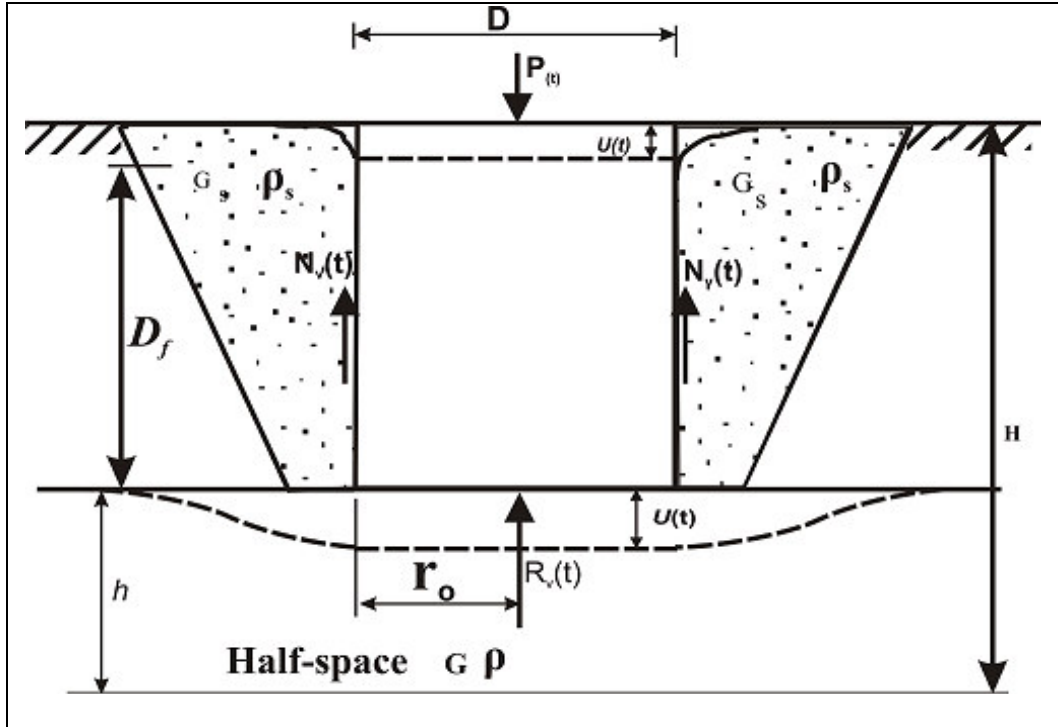
Figure 2.10: Embedment footing
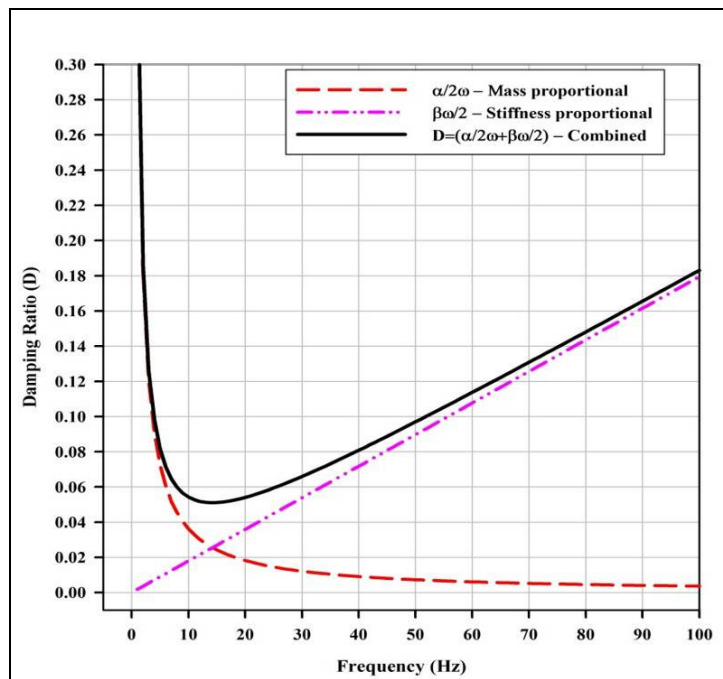
Figure 2.11: Proportional damping scheme of vibrating system
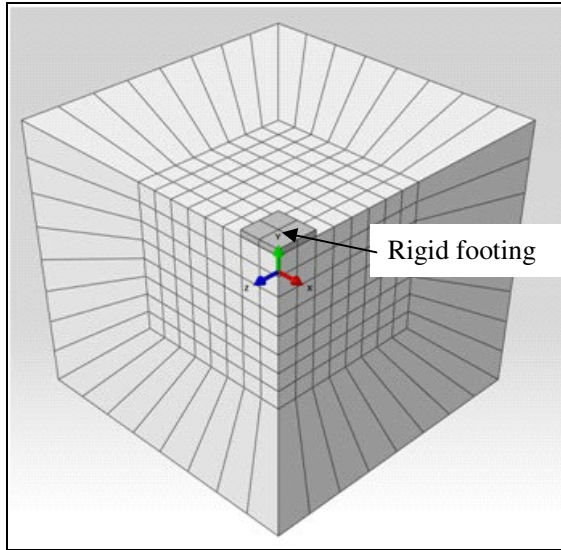
Figure 2.12: Three-dimensional model in finite element method (Abaqus)
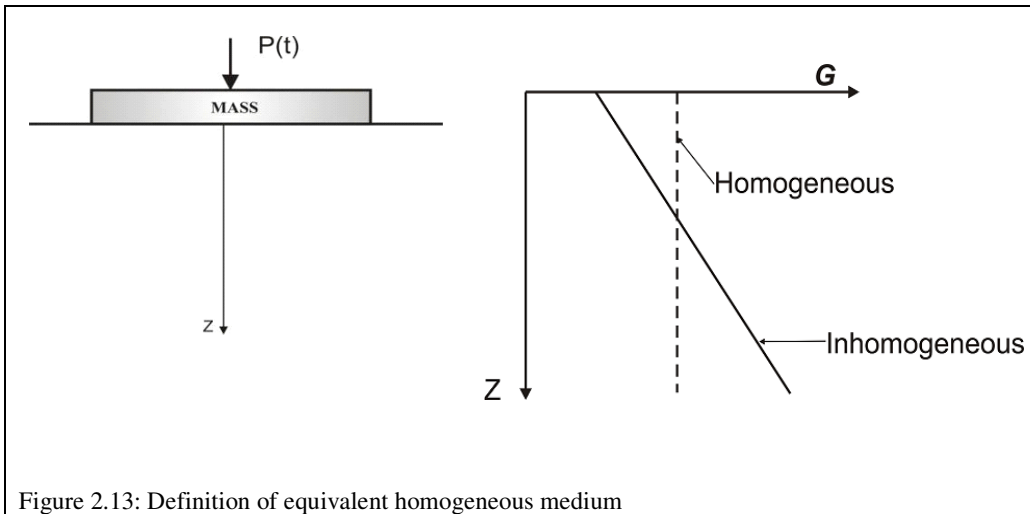
Figure 2.13: Definition of equivalent homogeneous medium

CHAPTER 3

3 EXPERIMENTAL WORK

3.1 Introduction

Correct evaluation of the soil parameters for machine foundation design is important. The basic soil parameters required for an analysis of machine foundation are shear modulus, Poisson's ratio and mass density. The shear modulus of the soil is a difficult parameter to obtain both in the laboratory and in the field (Whitman and Richart, 1967; Nayfeh and Serhan, 1989; Matthews et al., 1996 and El Naggar, 2003).

Laboratory tests require undisturbed soil samples. This may be difficult for materials such as sand and gravels and sometimes impossible for materials such as rock masses. Field seismic techniques are popular for determining ground stiffness by measuring the velocity of Rayleigh waves propagating along the ground surface. These techniques allow elastic soil properties to be determined on a representative volume of a ground at the in situ stress state (Matthews et al., 1995; Kramer, 1996; Matthews et al., 1996; Heymann, 2007 and Clayton et al., 2012). In this study the field seismic techniques of continuous surface waves (CSW) were used to determine the shear modulus of a soil profile. The fieldwork was carried out at the University of Pretoria experimental station where footings installed. The study was conducted on two footings; the first footing was placed on the surface, and the second was embedded. It was necessary to characterise the site before embarking on the actual measurements of dynamic behaviour of the surface and embedded foundations. The measured soil elastic properties were used to analyse the vertical dynamic response of the surface and embedded foundations.

3.2 Site investigation

The site is located at the University of Pretoria experiment station close to the University of Pretoria sports centre with approximately GPS coordinates of easting 626474 and northing 7151305. The site investigation involved excavation of the trial pit and determination of the shear modulus using the seismic technique of Continuous Surface Wave testing (Heymann, 2007). The trial pit of 2000 mm x 1500 mm in the plan was excavated to 1500 mm depth.

3.2.1 Soil profile

The soil profile was established from the excavated trial pit to the depth of 1500 mm as shown in Figure 3.1. The log of the soil profile is shown in Figure 3.2. The general soil profile of the site is residual andesite which consisted of silty clay with gravels.

3.2.2 Continuous surface wave test

Continuous Surface Wave testing was carried out at the experimental station to determine ground stiffness. This was carried out by exciting the ground with a vertical harmonic load with frequency ranging from 6 Hz to about 85 Hz as illustrated in Figures 3.3 and 3.4. The shaker used to generate sinusoidal seismic force with a known frequency which generates seismic energy at the surface of the ground. Figure 3.3 shows the shaker weighing 20.0 kg, which generates higher frequencies and produces short Rayleigh waves to characterise soil at shallow depths. Figure 3.4 shows the shaker weighing 71.4 kg, which generates low frequencies, with long Rayleigh waves which penetrate to the greater depth. The use of both shakers allowed the profile of the soil to be established from shallow depth to the greater depths (Heymann, 2007).

The vertical responses in the time domain were observed at distances of 500 mm, 1000 mm, 1500 mm, 2000 mm and 2500 mm starting from the edge of the shaker as shown in Figure 3.3. The Rayleigh wave propagating along the ground surface was detected by an array of geophones placed in line as shown in Figures 3.3 and 3.4. Geophones measure the ground velocity responses. The test was carried out close to where the footings were to be installed. The obtained velocity data were analysed to determine phase velocity, which was then used to calculate the shear modulus of the soil profile.

3.3 Calibration

The main components used for the field measurements were hydraulic power packs, actuator (hydraulic shaker-zonic ES362-1 inertia excitation system) and servo controller. Other components were data acquisition system, amplifier and accelerometers. It was important to check the accuracy of the measuring instruments before carrying out field measurements. The load cell was calibrated against a dead weight standard Budenberg calibration system shown Figure 3.5. The calibrated value was 2.0 kN/mV. The vertical response of the foundation system was measured using 1 g accelerometers. The calibration certificates are shown in Appendix A and B. The calibration factors for accelerometer one

and two are presented in Table 3-1. The 1 g accelerometers used for measurements are shown in Figures 3.6 and 3.7.

Table 3-1. Calibration values for 1 g accelerometers

S/No	Accelerometer serial number	Calibration Factor
1	SN.22590	1048 mV/g
2	SN.24742	1104 mV/g

3.4   Construction and instrumentation of surface footing

The surface footing was constructed from unreinforced concrete with a dimension of 2500 mm x 2000 mm in plan and 400 mm depth as shown in Figure 3.8 and 3.9. The hydraulic shaker with mass of 361.4 kg was used to subject the foundation to dynamics loading. The shaker and other instruments were transported from the University of Pretoria to the experiment station. During the casting of the concrete, the fixing bolts were inserted into the concrete at the centre of the footing. The shaker was bolted at the centre of the surface of footing to ensure that the shaker excite only vertical 'rigid body' mode as illustrated in Figures 3.10 and 3.11. The positioning of the shaker aimed at avoiding rocking modes of foundation and exciting the elastic modes of the concrete block. Figure 3.11 illustrates the schematic field instrumentation setup.

The instrumentation setup is divided into two parts; the first part entails the system which was used to excite the foundation, and the second part is the system that recorded the foundation response due to dynamic loading. Figure 3.12 shows the hydraulic power packs used to pump hydraulic oil to actuate the internal mass of the shaker and Figure 3.13 shows the servo controller used to control the movement of the internal mass. The harmonic loads depended on the setup actuator stroke and frequency of excitation. The internal mass of the shaker is capable of moving the actuator stroke to 50.0 mm which mean that the mass can move ± 25.0 mm from its mid position. The movement of internal mass with specified frequency creates the load at the bottom of the shaker. The internal mass of the shaker is shown in Figure 3.14.

The foundation response of the surface foundation was determined by applying a vertical harmonic load using the shaker. The vertical response of the foundation system was obtained from two 1 g accelerometers placed 200 mm from the edge of shaker to measure the response as illustrated in Figures 3.10 and 3.11. Two additional 4g accelerometers were

3-3

placed 300 mm from the edge of the shaker as a backup. The results obtained from the 4g accelerometers are not presented in this report.

The measured data was stored using a Nicolet data acquisition system, which is shown in Figures 3.15 and 3.16. The data logger is capable of storing data from eight channels. The vertical acceleration of the footing was measured using 1 g accelerometers at the sampling frequency of 800Hz. The force exerted by the shaker was measured by the load cell placed at the bottom of the shaker as shown in Figure 3.14. A Linear Variable Differential Transducer (LVDT) measured the vertical displacement of the internal mass of the shaker.

3.5 Field experimental measurements for surface foundation

The measurements involved measuring the following: the vertical response of foundation systems, the displacement of the internal mass of the shaker and the loads exerted by the shaker on the foundation. The first step was to identify the actuator stroke, which allowed the internal mass of the shaker to excite the foundation up to 100 Hz without exceeding the set maximum load of 12 kN. Zero readings for the accelerometers, LVDT and load cell were also recorded without excitation. Three data sets were recorded and the average of the three readings was used as the zero reading.

The foundation system was excited by the hydraulic shaker with the forcing frequencies presented in Table 3.2. The forces produced by the shaker for different forcing frequencies are shown in Figure 3.17. From Figure 3.17, it is evident that the forces produced by the shaker are not constant. The plot of force versus frequency shows that the maximum force produced by the shaker was 11.4 kN at a frequency of 65.0 Hz. By exciting the foundation system for a few seconds at each forcing frequency, it was ensured that steady state conditions were reached before recording the output. This was done for all frequencies shown in Table 3.2. If the forcing function is harmonic, the response should also be harmonic. To check if the set forcing frequency produces the harmonic output with the same frequency, a fast Fourier transform (FFT) was carried out for all-measured data. As an example, Figure 3.18 shows the displacement spectrum amplitude at 40.0 Hz excitation, which indicates that the output response was at 40.0 Hz.

Table 3-2: Forcing frequencies

S/No	Frequency (Hz)	S/No	Frequency (Hz)	S/No	Frequency (Hz)	S/No	Frequency (Hz)	S/No	Frequency Hz
1	10	14	41	27	50.6	40	62	53	76
2	15	15	42	28	51	41	63.1	54	77
3	20	16	43	29	51.6	42	64	55	78
4	25	17	44	30	52	43	65.1	56	79
5	30	18	44.9	31	53	44	66	57	80
6	32	19	46.1	32	54.1	45	67	58	83
7	34	20	47	33	55.1	46	69	59	85
8	35	21	47.5	34	56.1	47	69.9	60	87.1
9	35.9	22	48	35	57	48	71.1	61	90
10	36.9	23	48.4	36	58	49	72	62	92
11	38.1	24	49	37	59	50	73	63	95.1
12	39.1	25	49.4	38	60	51	74	64	100
13	40	26	50	39	61	52			

3.6 Determination of coefficient of elastic uniform compression

The coefficient of elastic uniform compression is required for the Winkler model and was determined using a block vibration test. As a part of the experimental test procedures described in Section 3.5, a discrete harmonic vertical force was applied to the surface footing using the hydraulic shaker as illustrated in Figure 3.10. The Indian standard procedures for determination of the coefficient of elastic uniform compression stipulate that the size of the block should be 1500 mm x 750 mm x 700 mm (Prakash, 1981). In this study, the available experimental set up was used to determine the coefficient of elastic uniform compression. Therefore, the maximum acceleration amplitudes obtained in Section 3.5 were used to determine the coefficient of elastic uniform compression of the soil (see section 4.5).

3.7 Embedded footing

The embedded footing was constructed by excavating the pit to the depth of 1240 mm. The concrete formwork was constructed as shown in Figure 3.19. The block with the dimension of 1200 mm x 1200 mm in the plan and 1240 mm was cast in place as shown in Figure 3.20.

The footing was backfilled using the excavated soil in layers of 310 mm and compacted using a handheld compactor. The full-embedded footing is shown in Figure 3.21 and this

3-5

was left for 12 months to improve the quality of contact between soil and footing . After 12 months, the vibration tests were carried out to determine the dynamic behaviour of the full embedded foundation as shown in Figure 3.22. The schematic diagram for full embedment is shown in Figure 3.23. The density of each soil layer was measured using the nuclear density method as shown in Figure 3.24. The same instrumentation setup and test procedures deployed for the surface foundation was used for the embedded foundation. Except for the embedded foundation, the full based PC Spider-8 data acquisition system control was used to record the output response as shown in Figure 3.25.

After carrying out measurements on the full-embedded footing as shown in Figure 3.22, the compacted material was excavated to a depth of 310 mm. The foundation response was therefore measured on the foundation with an embedment of 930 mm as shown in Figure 3.26. Another measurement was carried out with embedments of 620 mm as shown in Figure 3.27 and the schematic diagram for embedments of 620 mm is shown in Figure 3.28. Other measurements were carried out with embedments of 310 mm and zero embedment as shown in Figures 3.29 and 3.30 respectively. The forces excited the foundation system for each embedment was measured using load cell. Figure 3.31 shows the plot of measured force produced by shaker versus frequency of excitation from different embedments.

3-6

Figure 3.1: Excavated trial pit
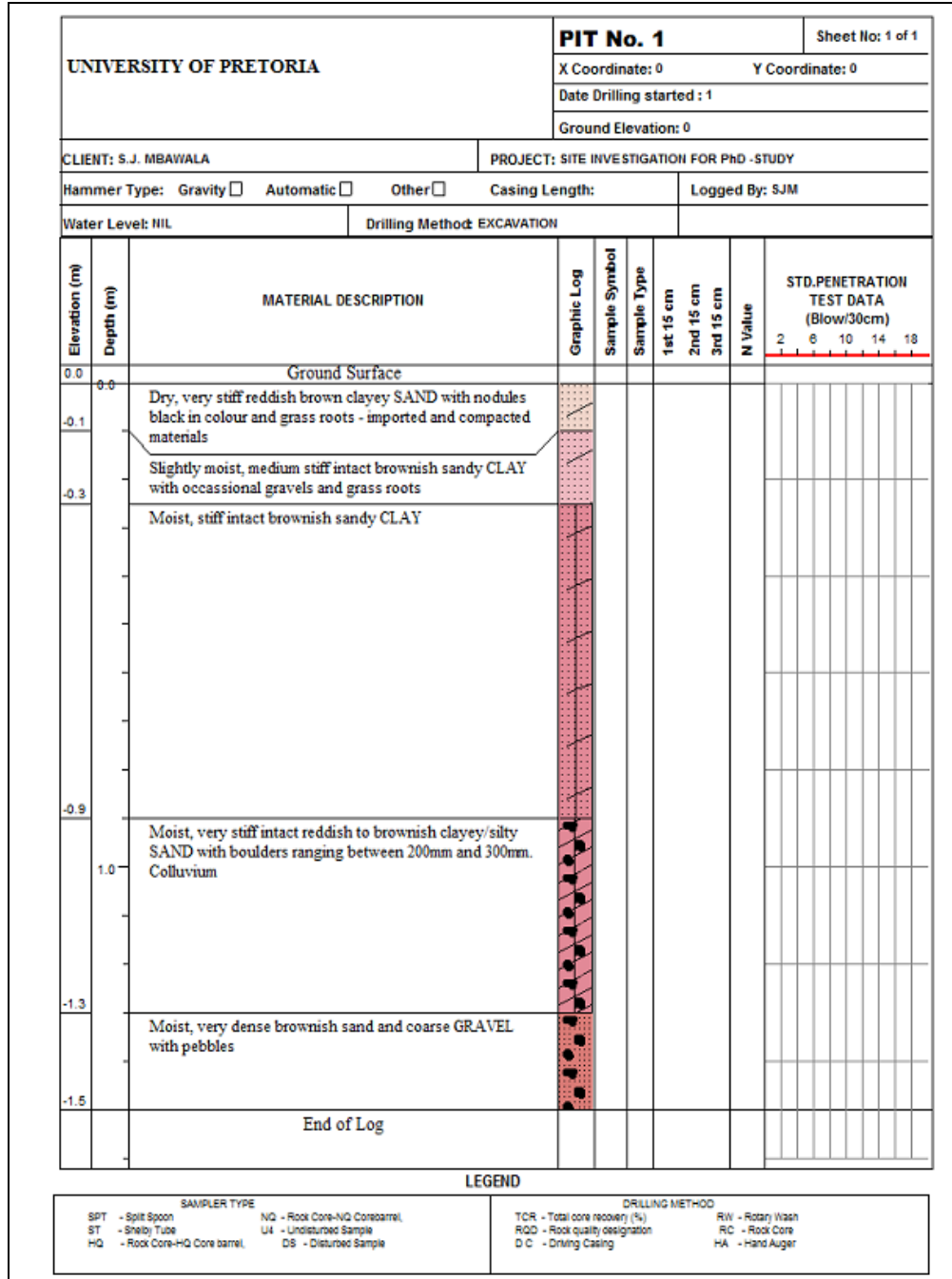
Figure 3.2: Trial Pit log

Figure 3.3: Shaker for measuring shallow depths

Figure 3.4: Shaker for measuring greater depths

Figure 3.5: Dead weight standard Budenberg calibration system

Figure 3.6: Accelerometer 1 fixed on surface of footing using an aluminium block.

Figure 3.7: Accelerometer 2 fixed on surface of footing using an aluminium block
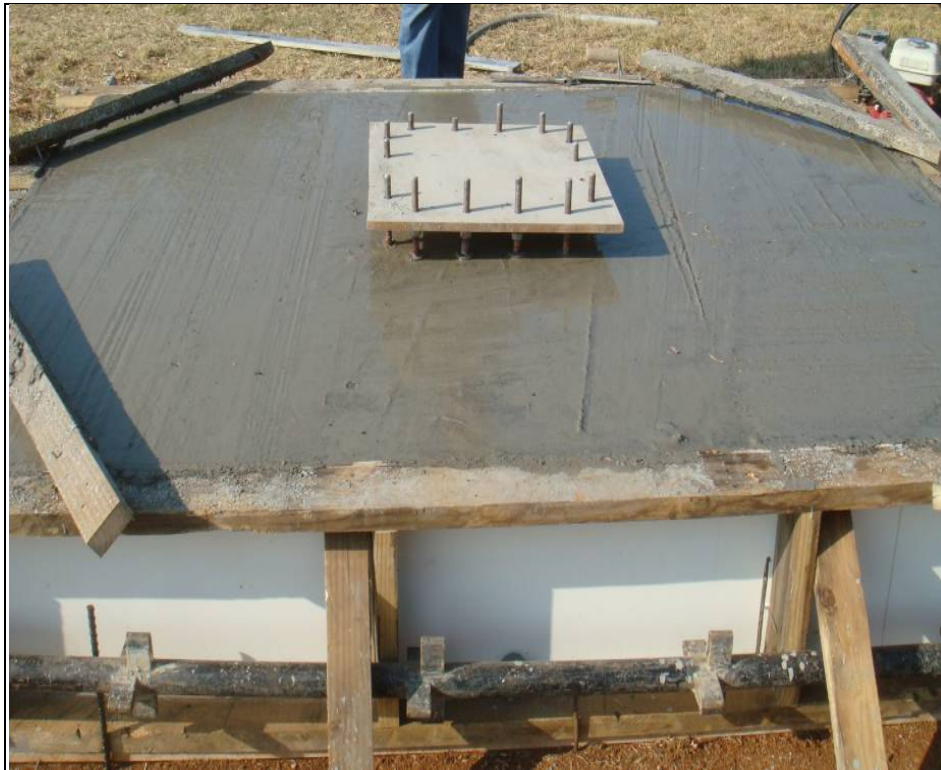
Figure 3.8: Surface footing during construction
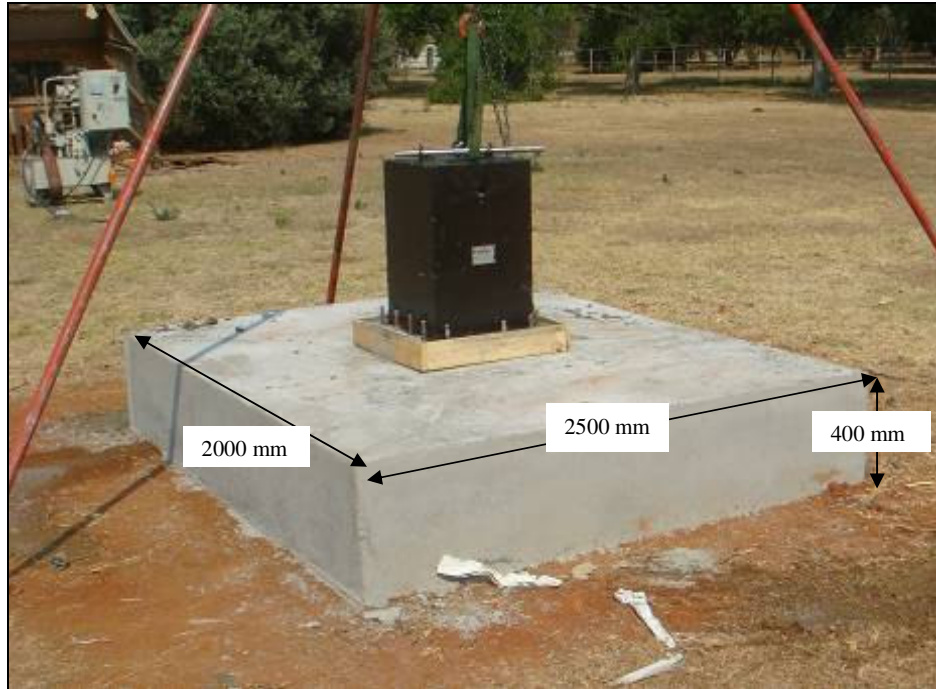
Figure 3.9: Surface footing mounted with hydraulic shaker
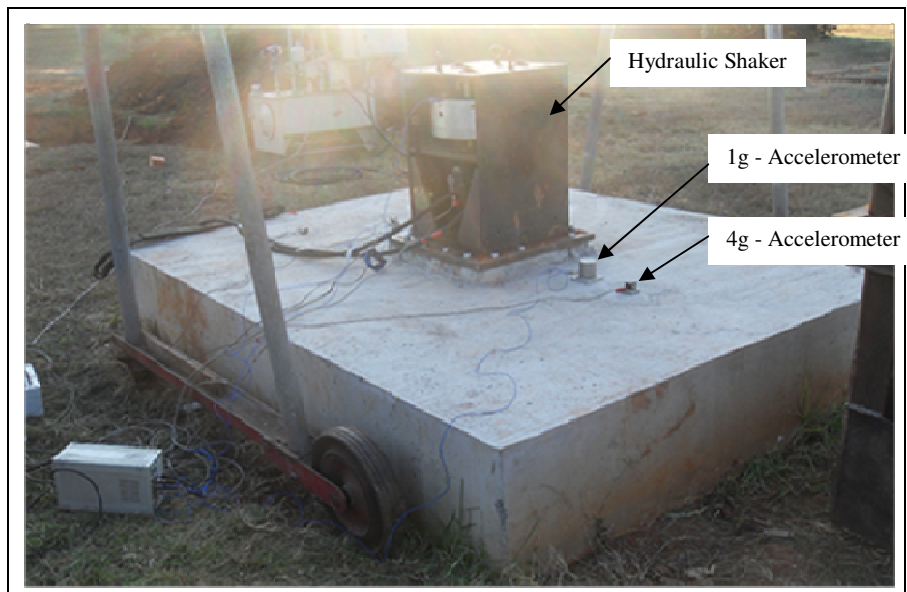
Figure 3.10: Surface footing test set up.
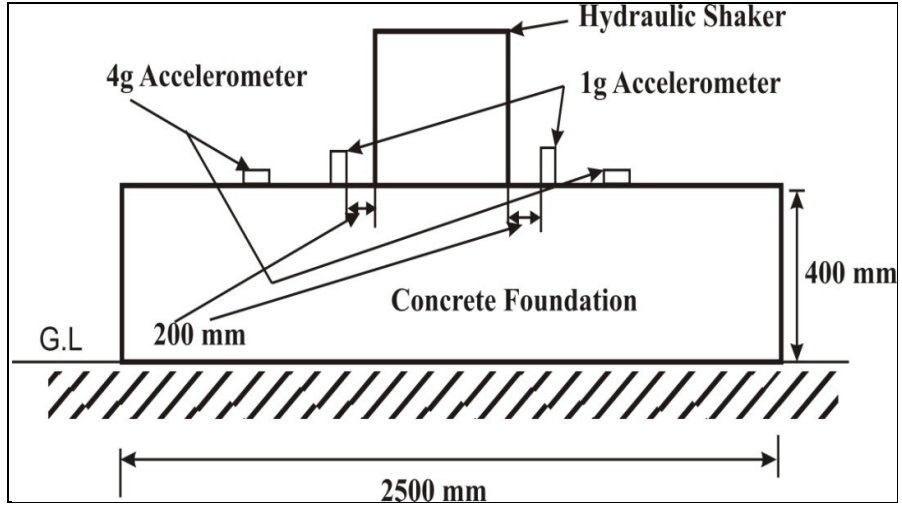
Figure 3.11: Surface footing schematic test set up

Figure 3.12: Hydraulic Powerpacks

Figure 3.13: Servo controller
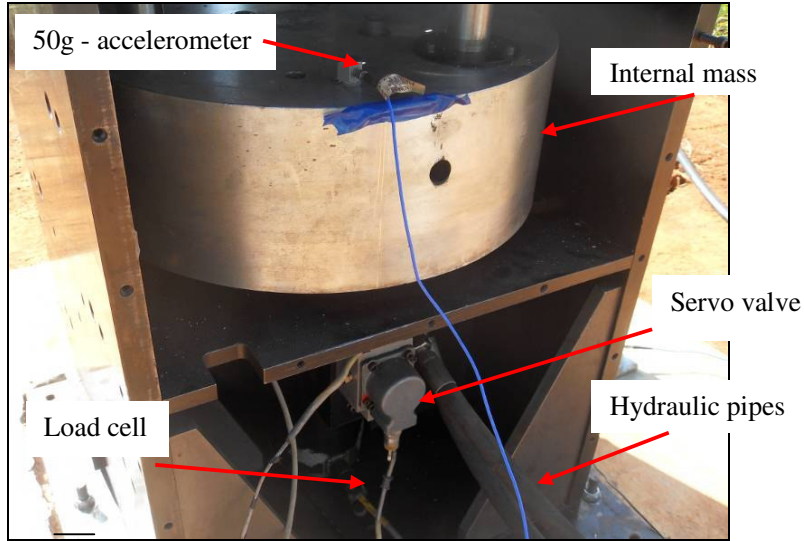
Figure 3.14: Internal mass of shaker

Figure 3.15: Nicolet data acquisition system
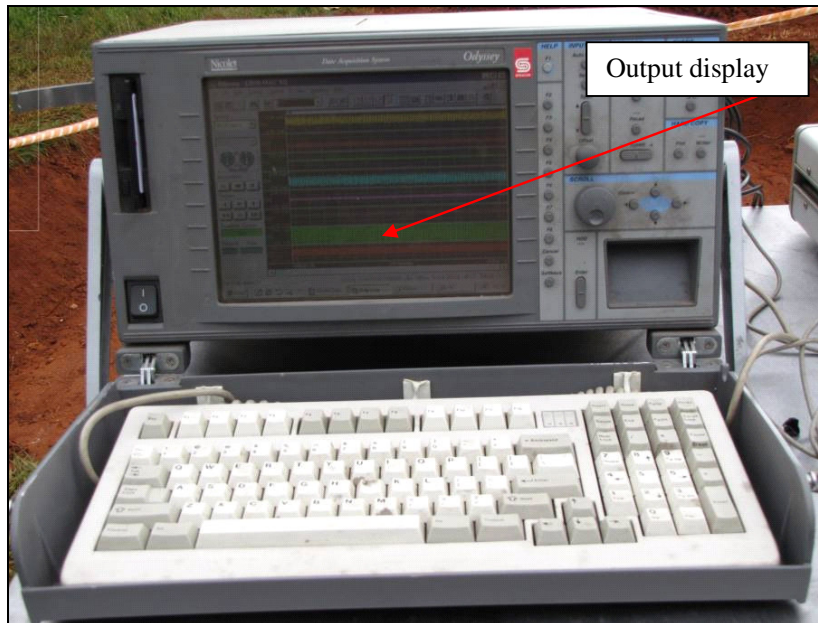
Figure 3.16: Output - Nicolet data acquisition system
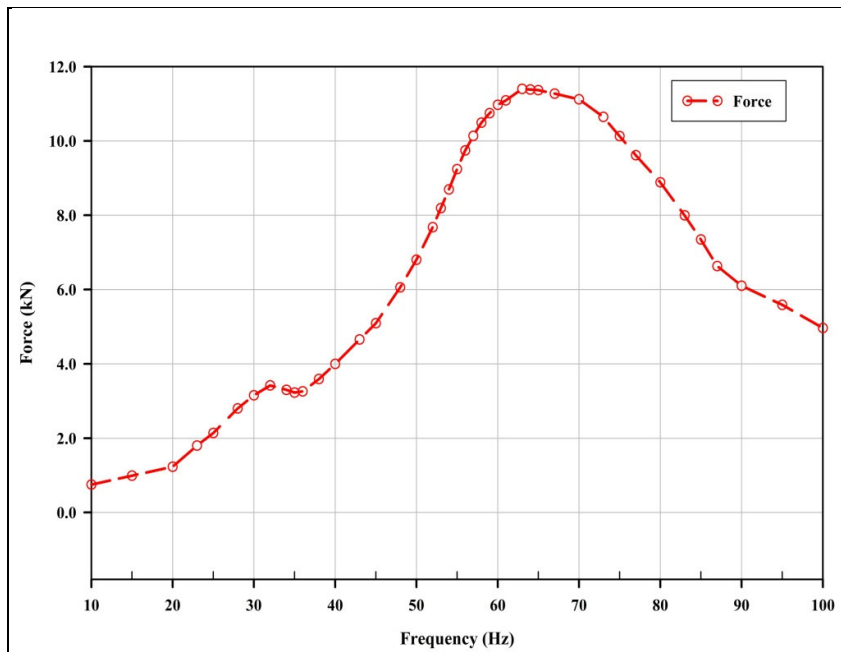
Figure 3.17: Force produced by Shaker for surface foundation
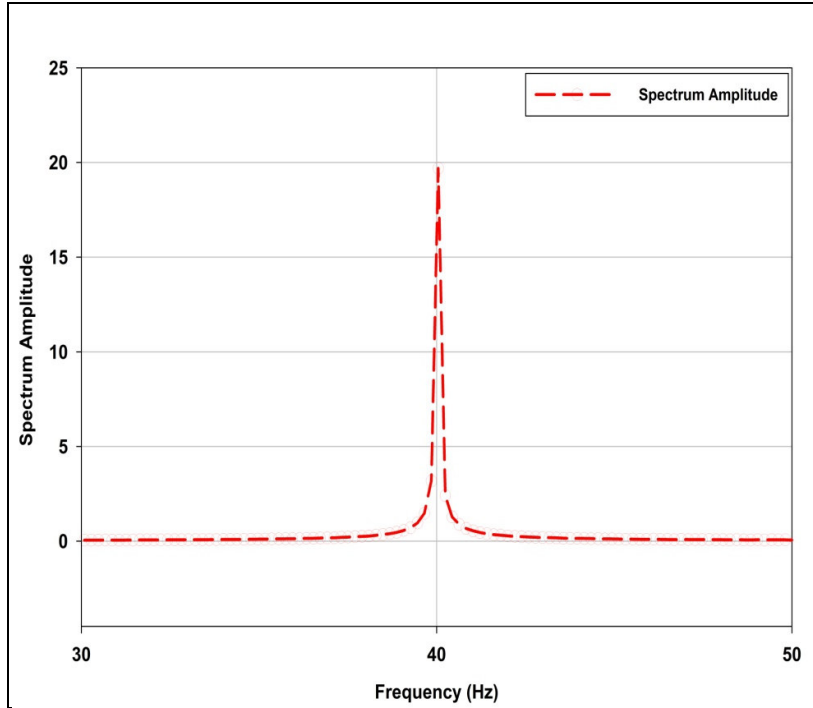
Figure 3.18: Accelerometer 1acceleration spectrum amplitude

Figure 3.19: Excavated pit with formwork

3-17
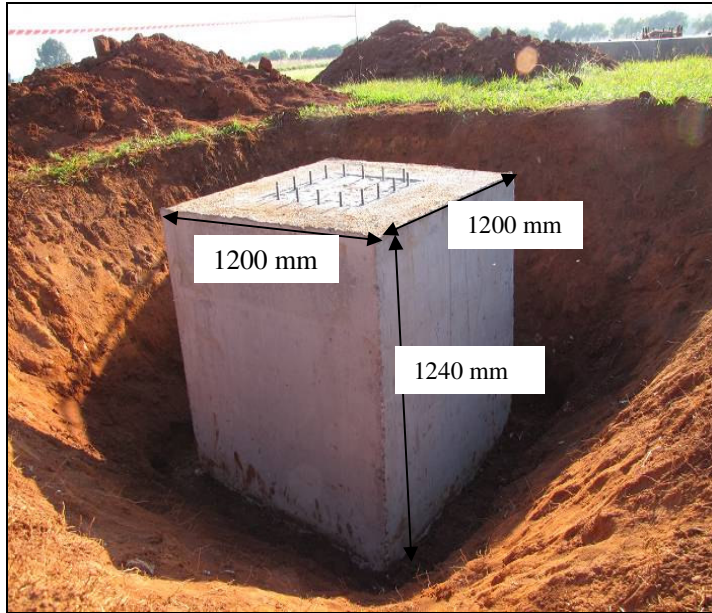
Figure 3.20: Cast footing ready to be embedded

Figure 3.21: Full embedded footing
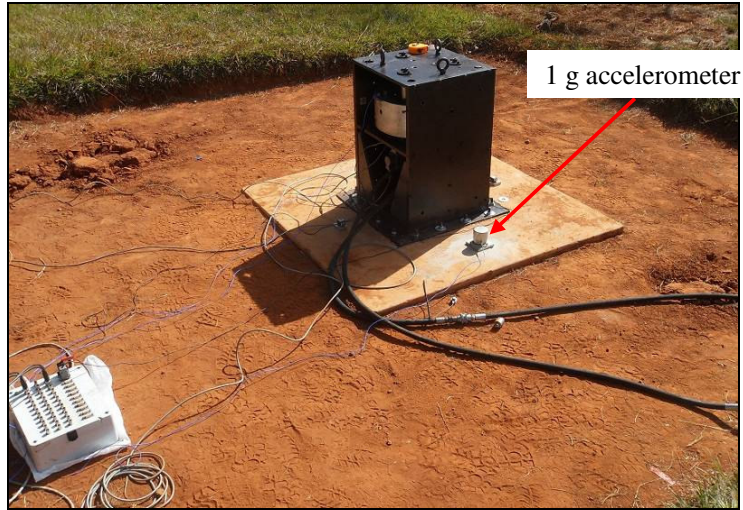
Figure 3.22: Test setup for full-embedded footing – 1240 mm
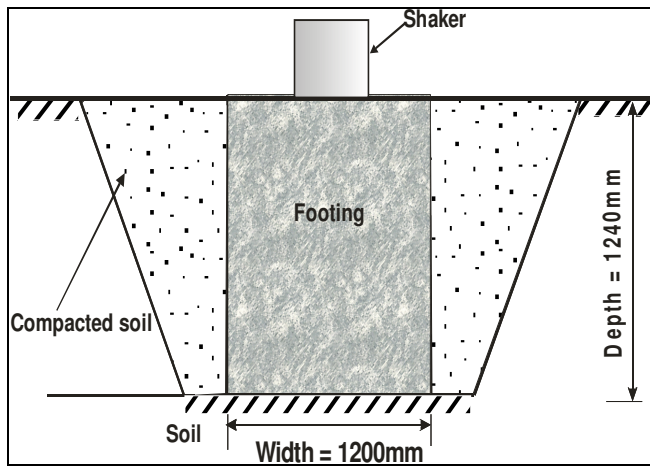
Figure 3.23: Schematic test setup for full-embedded footing

3-19

Figure 3.24: Density determination

Spider-8 data acquisition system
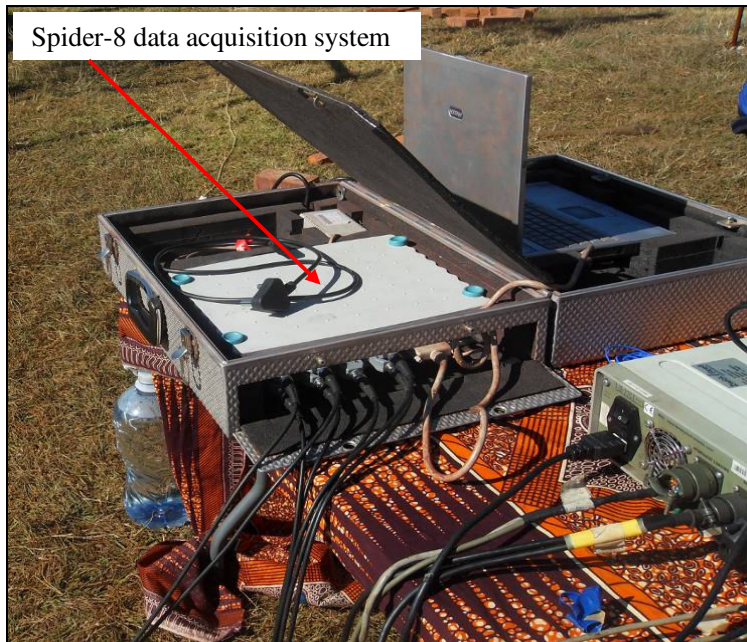
Figure 3.25: Spider-8 – Data Acquisition system
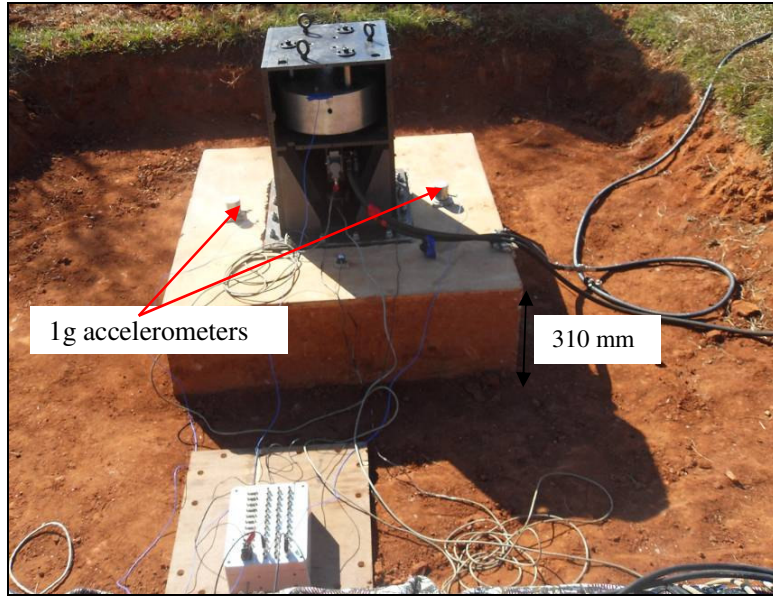
Figure 3.26: Embedded footing - 930 mm
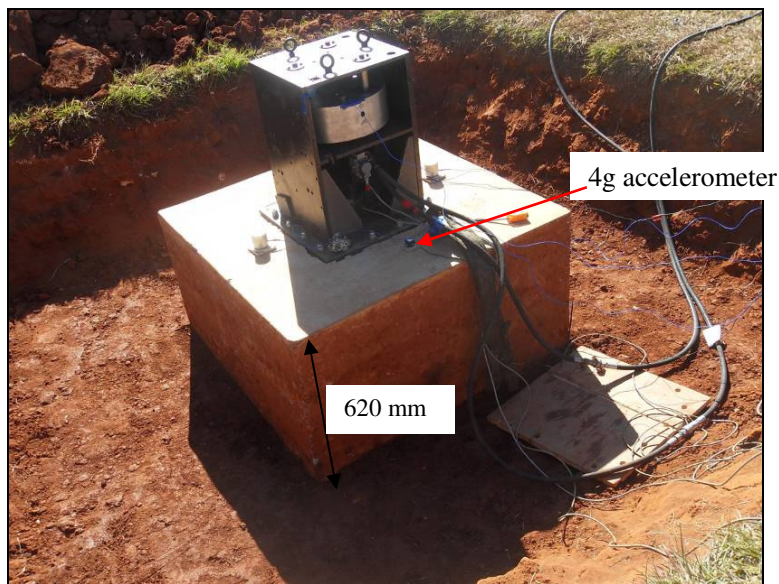
Figure 3.27: Embedded footing - 620 mm

3-21
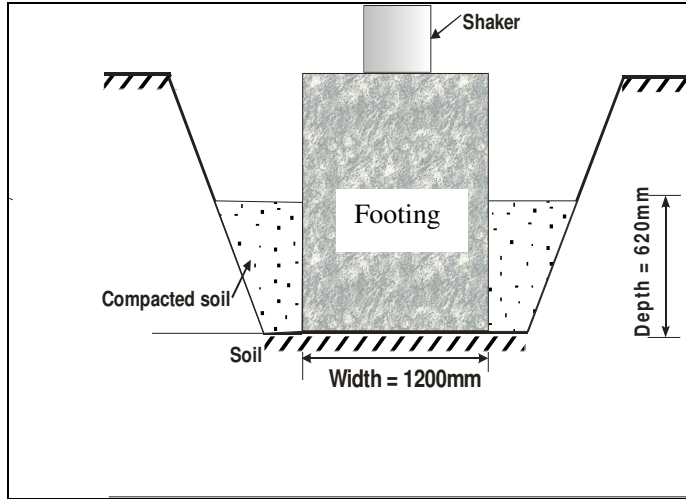
Figure 3.28: Schematic setup for 620mm Embedment
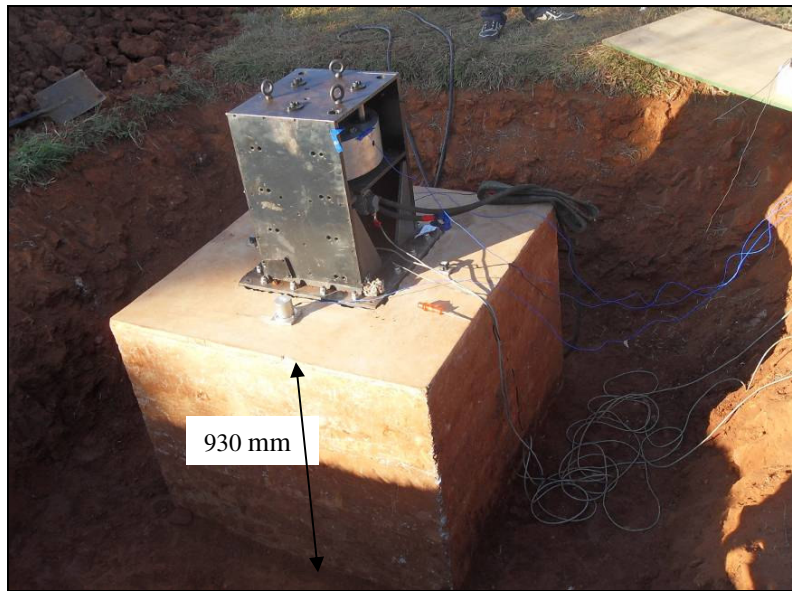
Figure 3.29: Embedded footing – 310 mm

3-22
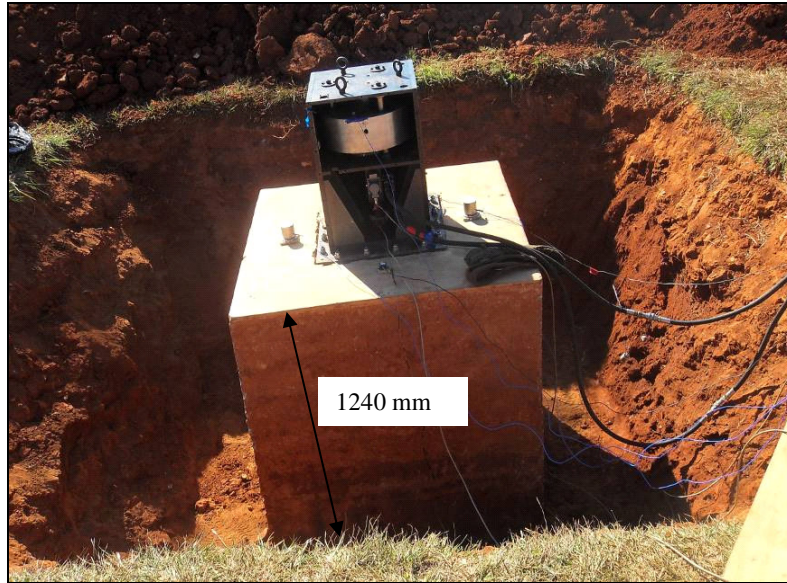
Figure 3.30: Zero embedded footing – 0 mm
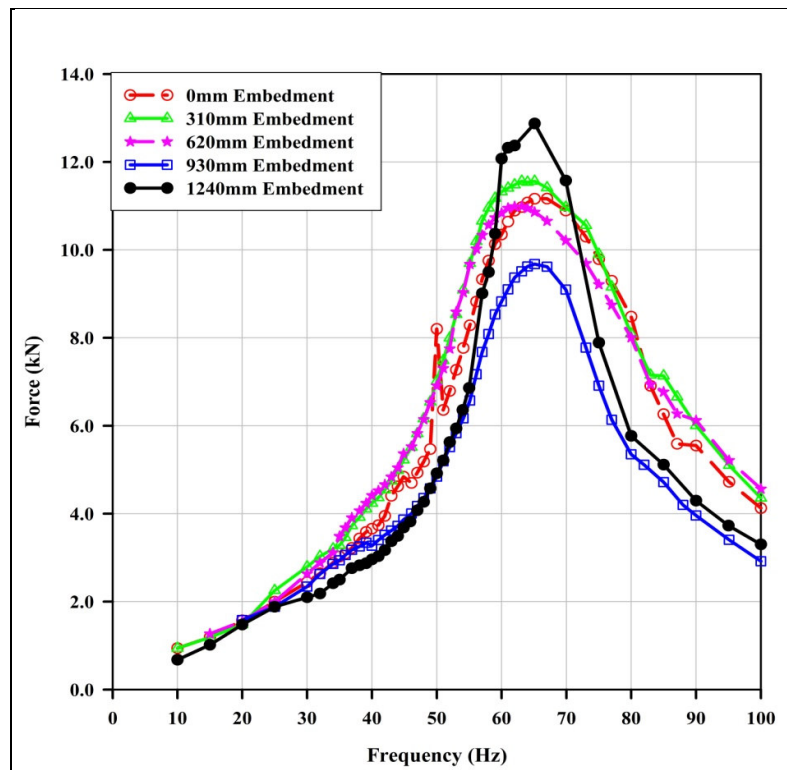
Figure 3.31: Measured forces produced by shaker for different embedment

3-23

CHAPTER 4

4 EXPERIMENTAL RESULTS

4.1 Introduction

The field work involved site characterisation using the seismic method of Continuous Surface Wave (CSW) test. The small shear stiffness of the soil profile was determined and presented. In addition, the dynamic behaviour of the foundation systems were determined using force vibration tests on the surface and embedded footings. The vertical dynamic responses of the footings were back-calculated using the field-measured data. The responses are presented in terms of impedance, compliance (receptance) and accelerance functions. In addition, results presented in this chapter include foundation displacement amplitude, the complex dynamic stiffness, loss angles, and acceleration responses of the footings.

From the field measurements, the natural frequency and the resonant frequency of the surface and embedded foundations were also determined. For the embedded foundation, the effect of the embedment is described using resonant amplitude ratio and resonant frequency ratio. In additional, a new dimensionless quantity known as the natural frequency ratio is introduced to express the effect of embedment on the natural frequency of the foundation system.

4.2 Continuous surface wave test

The small strain shear modulus was determined using the Continuous Surface Wave tests as described in Section 3.4. From the measured data, the dominating frequency and phase angle at each observation point was determined by calculating the Fourier transform of the geophone output by means of the fast Fourier transform (FFT) algorithm. Typical results of geophone frequency spectrum depicted at 73.4 Hz are shown in Figure 4.1. From this, the existence of the dominating frequency of 73.4 Hz is clearly indicated. The phase angle at the dominating frequency was determined from the real [Re (z)] and imaginary [Im (z)] part of the phase vector using Equation 4.1. From the response at each geophone, the phase different were determined.

$$\phi = tan^{-1}\left(\frac{Im(z)}{Re(z)}\right)$$
Equation 4.1

The phase difference was used to estimate the phase velocity between points. The wavelength (λ) for each vibrating frequency was determined using Equation 4.2.

$$\lambda = \frac{d}{n + \frac{\Delta\phi}{2\pi}}$$
Equation 4.2

Where:

d is the distance between two geophones,

$\Delta\phi$ is the phase difference between two geophones, and

n is an integer, which depends on the number of wavelengths between the geophones.

The Rayleigh wave velocity (V_R) is given by:

$$V_R = f\lambda$$
Equation 4.3

Where:

f is the frequency of excitation.

The velocity of a Rayleigh wave in an elastic half-space is slower than the shear wave velocity. For a Poisson's ratio of 0.25, the Rayleigh wave travels at a velocity of approximately 0.9226 of the shear wave (Janghai et al., 2002). The relationship between Rayleigh wave velocity (V_R) and shear wave velocity (V_S) as a function of the Poisson's ratio is expressed as:

$$\frac{V_R}{V_S} = \frac{0.874 + 1.117\nu}{1 + \nu}$$
Equation 4.4

Where:

ν is the Poisson's ratio.

4-2

Figure 4.2 shows the field measured phase velocity plotted against excitation frequency. The shear wave velocity was determined by conducting an inversion analysis using the algorithm proposed by Wathelet et al., (2004). The profile of shear wave velocity is shown in Figure 4.3. The small strain shear modulus of the soil profile (G_o) was determined using the theory of elasticity:

$$G_o = \rho_s V_s^2$$
   Equation 4.5

Where:

ρ_s is a mass density of soil, and

V_s is the shear wave velocity.

The soil profile of shear modulus is shown in Figure 4.4. The properties of the soil and concrete used for analysis for both, the surface and embedded foundations are shown in Table 4-1.

Table 4-1: Material properties

Soil properties of the ground			Concrete properties		
Soil mass density (kg/m³)	Young's Modulus(E) MPa	Poisson's ratio	Concrete mass density (kg/m³)	Young's Modulus (E) MPa	Poisson's ratio
2000	250	0.25	2400	35000	0.2

4.3   Surface foundation

As described in Section 3.5, the acceleration responses of the foundation systems in the field were measured using accelerometers. However, determination of displacement is important in the analysis and design of machine foundations, because it allows for the determination of impedance functions. Therefore, the field-measured acceleration data was translated into displacement amplitudes by double integration of the acceleration data. The double integration of acceleration response to displacement response carried out by dividing acceleration with forcing frequency $\left(\omega^2\right)$ (Chopra 2007 and Crouse et al., 1984).

For a constant forcing function with amplitude P_o, the displacement is given by $u = U_o e^{i\omega t}$, the velocity is given by $\dot{u} = -i\omega U_o e^{i\omega t}$ while acceleration takes the form of $\ddot{u} = -\omega^2 U_o e^{i\omega t}$. The displacement amplitude is given by:

4-3

$$U_o = \frac{\ddot{u}}{-\omega^2}$$

Equation 4.6

For a given acceleration and forcing frequency the displacement can be calculated as:

$$U(f) = \frac{\ddot{U}(f)}{-\omega^2}$$

Equation 4.7

However, these equations are applicable only for the sine wave responses. At low frequencies, the response were not sinusoidal and hence physical integration was performed.

The vertical foundation response in the field was determined by measuring acceleration. The measured maximum acceleration amplitudes for each forcing frequency are shown in Table 4-2 and the force amplitude produced by the shaker is shown in Figure 4.5. From Figure 4.5, it is evident that the force produced by the shaker was not constant. The force versus frequency plot shows that the maximum force produced by the shaker was 11.4 kN at a frequency of 65.0 Hz.

4.3.1 Acceleration and displacement

The maximum acceleration at each forcing frequency measured by accelerometers 1 and 2 was calculated from the data. The plot of the acceleration amplitude at each forcing frequency measured by accelerometers 1 and 2 against frequency is shown in Figure 4.6. The plot of an average acceleration versus frequency is shown in Figure 4.7. The maximum measured acceleration amplitude is 2.5 m/sec^2. The displacements in the time domain due to forcing frequencies of 40 Hz, 59 Hz and 80 Hz are illustrated in Figure 4.8 which shows the sinusoidal responses. The displacement due to a forcing frequency of 59 Hz is higher compared to the forcing frequencies of 40 Hz and 80 Hz. The measured displacements amplitudes are shown in Table 4-3.

The plots of highest vertical displacement measured by accelerometers 1 and 2 versus frequency are shown in Figure 4.9. The plot of average vertical

4-4

displacement is shown in Figure 4.10. The similarity of the plots of displacement amplitude versus frequency from the two accelerometers indicates that the foundation movement was vertical and that very little rocking accured. The response shows two peaks, the first peak occurred at about 33 Hz and the second peak occurred at about 57.0 Hz. The maximum displacement of 0.0188 mm occured at the frequency of 57.0 Hz.

Table 4-2: Measured highest acceleration amplitude for each forcing frequency

S/No	Frequency (Hz)	Acceleration (m/sec^2)	S/No	Frequency (Hz)	Acceleration (m/sec^2)	S/No	Frequency Hz	Acceleration (m/sec^2)
1	10	0.11285022	24	49	1.48007231	47	69.9	2.31534404
2	15	0.11462739	25	49.4	1.57724152	48	71.1	2.28690926
3	20	0.14483935	26	50	1.60389913	49	72	2.2300397
4	25	0.24315926	27	50.6	1.70728878	50	73	2.18027883
5	30	0.39599622	28	51	1.66134404	51	74	2.11274622
6	32	0.44282987	29	51.6	1.75495956	52	75	2.01442631
7	34	0.52337804	30	52	1.78992769	53	76	1.96111109
8	35	0.4315397	31	53	1.92023609	54	77	1.91490457
9	35.9	0.48840926	32	54.1	2.02508935	55	78	1.87225239
10	36.9	0.55949622	33	55.1	2.19805057	56	79	1.81005131
11	38.1	0.57669261	34	56.1	2.32600709	57	80	1.7425187
12	39.1	0.64777957	35	57	2.33254044	58	83	1.58670274
13	40	0.7206437	36	58	2.42139913	59	85	1.40663283
14	41	0.79706218	37	59	2.50492631	60	87.1	1.28813752
15	42	0.914931	38	60	2.54224696	61	90	1.17084404
16	43	1.01445274	39	61	2.54224696	62	92	1.11042013
17	44	1.11042013	40	62	2.55322357	63	95.1	0.99966
18	44.9	1.18213422	41	63.1	2.52923204	64	100	0.85748609
19	46.1	1.26979109	42	64	2.51559	-	-	-
20	47	1.32875074	43	65.1	2.48746813	-	-	-
21	47.5	1.35211578	44	66	2.45370183	-	-	-
22	48	1.40898535	45	67	2.43326465	-	-	-
23	48.4	1.43449291	46	69	2.32187739	-	-	-

Table 4-3: Measured displacement amplitude for each forcing frequency

S/No	Frequency (Hz)	Displacement (mm)	S/No	Frequency (Hz)	Displacement (mm)	S/No	Frequency Hz	Displacement (mm)
1	5	0.00041	24	51	0.017058	47	75	0.008914
2	10	0.001151	25	52	0.017298	48	76	0.008367
3	15	0.001611	26	53	0.01754	49	77	0.007986
4	20	0.002552	27	54	0.017704	50	78	0.007552
5	25	0.004045	28	55	0.017951	51	79	0.007198
6	30	0.005918	29	56	0.018003	52	80	0.006762
7	32	0.006962	30	57	0.018024	53	83	0.00567
8	34	0.008099	31	58	0.01791	54	85	0.004994
9	35	0.007789	32	59	0.017657	55	87	0.0042

4-6

10	36	0.008329	33	60	0.017237	56	90	0.003649
11	37	0.008882	34	61	0.016776	57	92	0.003254
12	38	0.009378	35	62	0.016492	58	95	0.002854
13	39	0.009941	36	63	0.015811	59	100	0.002256
14	40	0.010454	37	64	0.015195			
15	41	0.011064	38	65	0.014525			
16	42	0.012015	39	66	0.013507			
17	43	0.013117	40	67	0.01329			
18	44	0.014054	41	69	0.012185			
19	45	0.014811	42	70	0.011609			
20	47	0.015306	43	71	0.010998	-		
21	48	0.015773	44	72	0.010408	-		
22	49	0.016315	45	73	0.009923	-		
23	50	0.016689	46	74	0.009425	-		

4.3.2 Impedance functions

The impedance functions of the foundation system were determined at the interface between the vibrating surface footing and the soil. In this study, it was assumed that the displacement amplitude of the footing was sufficiently small so that the characteristics of the soil-foundation system could be characterized in the frequency domain in terms of frequency response functions (FRF). Essentially, the procedure entails measuring the dynamic response of the foundation of known characteristics (e.g. mass and geometry) by subjecting it to measurable dynamic loading over a range of frequencies. The resulting foundation responses, loading and foundation characteristics, are then used to back-calculate impedance functions using an appropriate dynamic equation of motion. The impedance function is the complex dynamic stiffness as a function of frequency.

For each excitation, complex dynamic stiffness was calculated using Equation 2.24, which is the ratio of the force amplitude and the displacement amplitude at a given frequency. Information that may be extracted from the impedance function includes foundation displacement amplitude, resonant amplitude, resonant frequency, the complex dynamic stiffness, the real part of the

complex dynamic stiffness, the imaginary part of the complex dynamic stiffness, phase angle and loss angles.

4.3.3 Complex dynamic stiffness

The complex dynamic stiffness obtained from the field measurements using Equation 2.24 is shown in Figure 4.11. The average complex dynamic impedance function obtained from accelerometers 1 and 2 is indicated in Figure 4.12. The complex dynamic stiffness is nearly constant at low frequencies up to about 20.0 Hz, and as the frequency increases, the complex dynamic stiffness decreases up to approximately 45.0 Hz and after 45.0 Hz it increases up to approximately 80 Hz as shown in Figure 4.12.

4.3.4 Real part of complex dynamic stiffness (effective dynamic stiffness)

The relationship between the real part of the complex dynamic stiffness and the frequency of excitation for accelerometers 1 and 2 is shown in Figure 4.13 and Figure 4.14 shows the average for the two accelerometers. The real part of the complex dynamic stiffness decreases as the frequency of excitation increases and is similar in form to the theoretical curve as described by numerous authors (Gazetas, 1983; Nii, 1987; He and Fu, 2001). It passes through zero at 49.0 Hz which according to Equation 2.31 is the natural frequency of the foundation system.

4.3.5 Imaginary part of complex dynamic stiffness

The plots of the imaginary part obtained from the field-measured data for accelerometer 1 and 2 versus frequency of excitation are shown in Figure 4.15 and the average for the two accelerometers in Figure 4.16. From Figure 4.16 it is clear that as the forcing frequency increases the imaginary part increases. The experimental damping coefficient `C` estimated from Equation 2.32 for accelerometers 1 and 2, which is the ratio of the imaginary part of the complex dynamic stiffness and frequency of excitation is illustrated in Figure 4.17 and the average plot is shown in Figure 4.18. The response described in Figure 4.18 indicates that at lower frequency, on average the damping coefficient is constant until it reaches the forcing frequency of 45 Hz. For forcing frequencies higher than 45 Hz, the damping coefficient increases as the frequencies increase.

4.3.6 Phase and loss angles

The natural frequency of the foundation system can be determined from the plot of phase angles between the phase of footing and the phase of shaker versus excitation frequency. Figure 4.19 illustrates the relationship between phase angles obtained from field measurements with frequency of excitation for accelerometers 1 and 2. The plot of average phase angle versus forcing frequency is shown in Figure 4.20. At low frequency, the foundation vibrates in phase with the forcing function. As the frequency increases, the foundation changes from vibrating in phase with forcing function to out of phase at 124°. At the point when the phase angle is 90°, the forcing frequency coincides with natural frequency of the system. The estimated natural frequency of the foundation is 49.0 Hz.

The natural frequency of the system can also be determined from the ratio of imaginary part and real part of the dynamic stiffness. Tileylioglu (2008) and Tileylioglu et al., (2011) examined impedance functions for horizontal and rocking of a foundation due to a harmonic force exerted on the roof of a structure. They observed that the imaginary part (Equation 2.32) and real part (Equation 2.31) are related through the loss angle obtained from Equation 4.8.

$$Loss\,angle = \frac{C\omega}{K_o - M\omega^2} = \frac{K^I}{K^R}$$

Equation 4.8

Where:

ω is a frequency of the excitation;

K_o is equivalent to static stiffness $\left(K_o = K_{static}\right)$;

M is a lumped mass of footing and machine;

C is the radiation damping coefficient of the soil-foundation system;

$K^R(\omega)$ is the real part of complex dynamic stiffness, and

$K^I(\omega)$ is the imaginary part of complex dynamic stiffness.

Figure 4.21, illustrates the plot of the absolute values of the ratio of the imaginary part and the real part in radians obtained from the field-measured data for accelerometers 1 and 2. The plot of average loss angles versus forcing frequency is shown in Figure 4.22. In addition, Figure 4.22 shows the response of the system

4-9

when the forcing function is in phase (at frequencies below the peak) and out of phase (at frequencies above the peak) with displacement. The estimated natural frequency of the foundation system is 49.4 Hz.

4.4   Foundation frequency response functions (FRF)

The frequency response function expresses the foundation system response to the applied forces as a function of frequency. For a linear system with single degrees of freedom, the frequency response function can be modelled as shown in Figure 4.23. Where, $F(\omega)$ is the input force, which is a function of the angular frequency (ω), $H(\omega)$ is the transfer function (frequency response function), and $U(\omega)$ is the displacement response function. Each of the functions is a complex function. The relationship shown in Figure 4.23 uses displacement as the response and can be represented using Equation 4.9 and is known as the receptance function.

$$H(\omega) = \frac{U(\omega)}{F(\omega)}$$
Equation 4.9

Similar transfer functions can be developed for velocity and acceleration system response. If the response is the velocity, the frequency response function is referred to as mobility while for acceleration response, the frequency response function is referred to as accelerance. In this study, receptance and accelerance will be discussed.

4.4.1   Receptance

Receptance frequency response function is a ratio between the displacement and applied force as a function of frequency. Sometimes these are referred to as compliance functions (dynamic flexibility). Compliance functions are the inverse of impedance functions. The receptance frequency responses function (FRF) from the field-measured data for accelerometers 1 and 2 is illustrated in Figure 4.24. The plot of the average frequency response function is shown in Figure 4.25. The resonant amplitude and resonant frequency can be obtained from the frequency response function. A resonant frequency is defined as the forcing frequency at which a maximum occurs in the response amplitude (Chopra, 2007; Doebelin,

1998). From the plot, in Figure 4.25 it is evident that the resonant amplitude and resonant frequency is 2.94 x 10^{-6} mm - N^{-1} and 44 Hz respectively.

Real part - Receptance

The real part of the receptance function obtained from the experimental data is shown in Figure 4.26. The average response of the real part obtained from accelerometers 1 and 2 is shown in Figure 4.27. The natural frequency can be estimated by observing the frequency when it crosses zero. The real part is zero at a frequency of 49.5 Hz indicating that the estimated natural frequency of the foundation system is 49.5 Hz.

Imaginary part - Receptance

The plot of the imaginary part against the forcing frequency for accelerometers 1 and 2 is shown in Figure 4.28. This average obtained from accelerometers 1 and 2 is plotted versus forcing frequency in Figure 4.29. The resonant frequency of the foundation system can also be estimated when the plot of the imaginary part of the frequency response is a minimum as shown in Figure 4.29; here the imaginary part of the frequency response is a minimum at a frequency of 45.0 Hz

Phase and loss angles - Receptance

The plot of phase angles versus frequency that was derived from the receptance function is shown in Figure 4.30. The natural frequency of the foundation system can be estimated when the response lags behind the input by 90° phase. Figure 4.30 indicates the plots of phase angles against frequency obtained from accelerometers 1 and 2, while Figure 4.31 shows the plot of an average phase angles against frequency. The response lags behind the input by 90° at 49.5 Hz.

Loss angles derived from receptance for accelerometers 1 and 2 are shown in Figure 4.32. The plot of average loss angles is shown in Figure 4.33, which estimates the natural frequency of the foundation as 49.5 Hz.

4.4.2   Accelerance

The field measurements taken to obtain the vertical acceleration of the foundation system due to harmonic loads were measured using accelerometers. The frequency response function is represented as accelerance, which is the ratio of the measured acceleration to the input force. The frequency response function of the foundation

4-11

© University of Pretoria

obtained from accelerometers 1 and 2 is shown in Figure 4.34 while Figure 4.35 illustrates an average value of accelerance frequency response function. The frequency at maximum acceleration amplitude from accelerance is 50.0 Hz.

Real part - Accelerance

Figure 4.36 illustrates the plot of the real part of frequency response (accelerance) for accelerometers 1 and 2, while Figure 4.37 show the average plot of the real part of accelerance. The average plot indicates that at low frequencies, the real part increases as the frequency increases. The increase reaches a maximum accelerance of 0.10 mm/sec^2/N at the frequency of 37.0 Hz. The accelerance response starts decreasing as the forcing frequency increases until it reaches a minimum -0.10 mm/sec^2/N; it then remains constant as the frequency increases. The natural frequency of the foundation system can be estimated when the plot of the real part versus forcing frequency of the accelerance crosses zero (Ewins, 1991, and He and Fu, 2001). From the plot, the estimated natural frequency is 49.0 Hz.

Imaginary part - Accelerance

Figure 4.38 illustrated the imaginary part of frequency response (accelerance) plotted against frequencies for accelerometers 1 and 2. Figure 4.39 shows a plot of average values of the imaginary part of frequency response (accelerance). From Figure 4.39, it is shown that the imaginary part decreases as the frequency increases until it reaches a minimum at 50 Hz and then starts to increase as the frequency increases.

Phase and loss angles - Accelerance

The plot of phase angles versus frequency derived from the accelerance response function is shown in Figure 4.40. The natural frequency of the foundation system can be estimated when the response lag behind the input by 90° phase. Figure 4.41 show the plot of an average phase angle versus forcing frequency and the natural frequency of 49.0 Hz.

The plot of loss angle from accelerometer 1 and 2 is shown in Figure 4.42 while the average values are plotted in Figure 4.43. The natural frequency of the foundation systems estimated from the loss angle is 49.0 Hz.

The accelerance estimates the natural frequency of the surface foundation between 49.0 Hz and 50.0 Hz. This compares well with the receptance results which estimated the natural frequency between 49.0 Hz and 49.5 Hz. This indicates that the translation of acceleration response to displacement response using Equation 4.6 did not cause significant inaccuracy.

4.5 Vertical block vibration

The coefficient of elastic uniform compression of soil is the ratio of pressure (vertical pressure causing compression) to the corresponding elastic vertical deformation. The coefficient of elastic uniform compression subjected to dynamic loads, such as machine foundation, can be obtained from vertical block vibration tests (block resonance tests), wave propagation tests (Continuous Surface Wave tests), and from the empirical method proposed by Barkan (1962). All three methods will be evaluated and compared. The footing block shown in Figure 3.10 was subject to vertical harmonic load. Equation 4.10 is used to calculate the amplitude of vibration A_v at the given frequency (Barkan 1962; Rao, 2011 and Prakash, 1981).

$$A_v = \frac{a_v}{4\pi^2 f^2}$$

Equation 4.10

Where:

A_v is the displacement amplitude;

a_v is acceleration amplitude (given in Table 4.2) and

f is the frequency of vibration.

For the surface foundation, the displacement amplitude A_v at each frequency is plotted against frequency as shown in Figure 4.44. The frequency at peak response is taken as the resonant frequency of the vibrating block system, which is the same as natural frequency for undampled system. From Figure 4.44, the estimated frequency of the vibrating block system at the peak amplitude is 59.0 Hz.

The coefficient of elastic uniform compression (C_u) was calculated using the following relationship:

4-13

$$Cu = \frac{4\pi^2 f_n^2 M}{A}$$
Equation 4.11

Where:

f_n is the natural frequency of the block system in vertical vibration;

M is lumped mass of oscillating system (footing and shaker), and

A is the contact area of the block with soil.

The contact area of the surface footing as shown in Figure 3.10 is 5.0 m². Using Equation 4.11, the estimated coefficient of elastic uniform compression is 141,860,430 N/m³.

Observing Equation 4.11, the coefficient of elastic uniform compression (C_u) is inversely proportional to the contact area with a constant of proportionality of $4\pi^2 f_n^2 M$ which is a spring constant. This shows that if the natural frequency and mass of the vibrating block system is known, the spring constant (k_s) can be obtained from:

$$k_s = 4\pi^2 f_n^2 M$$
Equation 4.12

The coefficient of elastic uniform compression (C_u) of soil was also estimated from the theory of elasticity using the relationship established by Barkan (1962) shown in Equation 4-13:

$$C_u = C_r \frac{E}{(1-v^2)\sqrt{A}}$$
Equation 4.13

Where:

A is the footing contact area with soil;

v is Poisson's ratio;

E is the Young modulus of soil, and

C_r is the footing shape factor.

The value of C_r can be obtained from Figure 4.45, as was suggested by Barkan (1962).

4-14

The shear stiffness of the soil on site was determined using the Continuous Surface Wave test. From the Continuous Surface Wave test, the soil profile shows that on average the small strain shear stiffness of the soil (G_o) from the ground surface to about 8 m is 100 MPa. For isotropic material, the Young modulus (E) is estimated using the following equation:

$$E = 2G_o(1+v)$$
    Equation 4.14

Where:

v is Poisson's ratio, which is assumed to be 0.25.

From Equation 4.14, the estimated Young modulus of the soil is 250 MPa. Using Equation 4.13 and C_r of 1.067 obtained from Figure 4.45, the coefficient of elastic uniform compression of the soil is 127, 247,175 N/m^3.

The coefficient of elastic uniform compression was estimated using a method proposed by Barkan (1962). According to Barkan, the site being studied is characterized as silty clay soil and the coefficient of elastic uniform compression is 98.1 x 10^6 N/m^3 for a base area of 10 m^2. Inspecting Equation 4.13 this indicates that the coefficient of elastic uniform compression (C_u) is inversely proportional to the square root of the contact area. Barkan (1962) suggested that if the spring constant, or coefficient of elastic uniform compression of one plate (footing) is known, the spring constant or coefficient of elastic uniform compression of the second plate (footing) could be obtained using the following relationship:

$$\frac{C_{u-s1}}{C_{u-s2}} = \sqrt{\frac{A_2}{A_1}}$$
    Equation 4.15

Where:

C_{u-s1} is a coefficient of elastic uniform compression of known soil;

C_{u-s2} is the coefficient of elastic uniform compression of soil to be determined, and

A_1 and A_2 are the known areas.

4-15

Using Equation 4.15, the coefficient of elastic uniform compression of soil for the footing with a base area of 5.0 m^2 is 138,734,500 kN/m^3. The vertical spring constant of the footing is obtained using Equation 4.16.

$$k_v = C_u A$$
Equation 4.16

Where:

A is the contact area between footing and soil. The spring constant for each method is tabulated in Table 4-4.

Table 4-4: Estimated spring constants.

Method	C_u (N/m^3)	Spring constant k_s (N/m)
Wave propagation (CSW)	127,247,175	636,235,876
Vertical block vibration	141,860,430	709,302,152
Estimated using Barkan (1962)	138, 734,350	693,671,752
Average Value	**135,934,200**	**679,736,594**

All three methods gave a value of coefficient of elastic uniform compression within 6% of the average value.

4.6   Embedded footing

Footings for vibrating machines are usually constructed partially or fully embedded. The analysis of embedded machine foundations requires determination of the impedance functions. As for surface foundations, these impedance functions can be obtained using available analytical solutions or can be measured in the field.

The vertical response of the foundation system was measured using accelerometers as described in Section 3.7. The field-measured acceleration data was translated to displacement amplitudes using Equation 4.6. The vertical dynamic frequency response function of the foundation with different embedments was obtained by conducting FFT calculations of the input and output data.

4.6.1 Displacement amplitude

The field-measured displacement amplitudes were obtained using Equation 2.26 for embedment of 0, 310, 620, 930, and 1240 mm. Figure 4.46 shows the plot of displacement amplitude versus frequency of excitation due to exerted forces. The maximum displacement amplitudes due to exerted forces for different embedment are presented in Table 4-5. The plot of maximum displacement amplitude versus embedment depth is shown in Figure 4.47 and from this it is evident that the displacement decreases as embedment increases. However, the displacement amplitude at embedment of 930 mm is inconsistency in comparison to the displacement amplitude at the embedment of 620 mm and 1240 mm which might have been caused by insufficient excitation force.

4.6.2 Displacement amplitude at resonant

The field-measured displacement amplitudes were obtained using Equation 2.26 for embedment of 0, 310, 620, 930, and 1240 mm. The displacement amplitudes were divided by exerted force to obtain frequency response function. Figure 4.48 show the plot of displacement amplitude due to unit load versus frequency of excitation. The maximum displacement amplitudes due to unit load for different embedment are presented in Table 4-6. The plots show that there are three peaks. The first peak is observed at the frequency of about 25Hz and the maximum peak at the frequency of 38.1 Hz. The third peak is observed between forcing frequency of 50 Hz and 65 Hz. The plot of maximum displacement amplitude versus embedment depth at resonant is shown in Figure 4.49 and from this it is evident that the resonant amplitude decreases as embedment increases.

4.6.3 Resonant amplitude ratio

The resonant amplitude ratio is the ratio of the peak amplitude for an embedded footing to the peak amplitude for zero embedment. The resonant amplitude ratio is determined using Equation 2.47 and these ratios from different embedments are shown in Table 4-6. The resonant amplitude ratios obtained from the field-measured data are plotted against embedment ratios (Equation 2.46) as shown in Figure 4.50. Here it can be seen that the resonant amplitude ratio decreases as embedment increases.

Table 4-5: The maximum displacement amplitude and amplitude ratio

Embedment (mm)	Displacement amplitude (mm)	Embedment ratio	Amplitude ratio	Frequency at maximum displacement
0	0.0206	0.000	1	58.0
310	0.0185	0.5167	0.64	57.0
620	0.0145	1.033	0.45	57.0
930	0.0132	1.550	0.35	65.1
1240	0.0079	2.067	0.18	61.0

Table 4-6: The resonant amplitude and resonant amplitude ratio

Embedment (mm)	Displacement (mm/N)	Embedment ratio	Resonant amplitude ratio
0	5.9926×10^{-6}	0.000	1
310	3.4514×10^{-6}	0.5167	0.5759
620	2.2808×10^{-6}	1.033	0.3806
930	2.0849×10^{-6}	1.550	0.3479
1240	1.2874×10^{-6}	2.067	0.2148

4.6.4 Resonant frequency

A resonant frequency is defined as the forcing frequency at which the largest response amplitude occurs (Chopra 2007; Doebelin 1998). For undamped systems, the resonant frequency is equal to the natural frequency of the systems. For a damped system, the damped natural frequency occurs at slightly less than the undamped natural frequency of the system. The damped natural frequency is calculated using Equation 4.17:

$$\omega_d = \omega_o \sqrt{1 - D^2}$$
    Equation 4.17

Where:

ω_d is damped natural frequency

ω_o is the undamped natural frequency of the foundation system, and

D is the damping ratio of the system.

4-18

For a damping ratio (D) less than 0.7071 and a harmonic excitation force, the resonant frequency (ω_r) of the vibrating system is obtained from Equation 4.18 (Das, 2011; Kameswara, 1998; Kameswara, 2011; and Richart et al., 1970):

$$\omega_r = \omega_o \sqrt{1 - 2D^2}$$
Equation 4.18

Experimental results in Figure 4.51 show that embedment does not have a significant effect on the resonant frequency. The resonant frequency varied between 35.9 Hz and 39.1 Hz for all embedment levels.

Equation 4.18 establishes that the damping ratios for different embedments may be determined by using resonant frequency and natural frequency. The estimated damping ratios for foundation systems with different embedments are presented in Table 4-7. Figure 4.52 show the plots of damping ratio against embedment depth. From the plots, it is clear that damping ratio increases as the embedment increases.

Table 4-7: The field-measured natural and resonant frequency of the foundation system

Embedment depth (mm)	Experimental results			
	Natural frequency	Resonant frequency	Resonant frequency ratio	Estimated Damping ratio
0	41.0	38.1	1	0.2612
310	46.1	39.1	1.0262	0.3725
620	51.0	36.9	0.9685	0.4881
930	47.0	35.9	0.9423	0.4564
1240	55.0	36.9	0.9685	0.5243

4.6.5 Resonant frequency ratio

The observed resonant frequency ratios are determined by using Equation 2.48, and plotted against embedment ratio as shown in Figure 4.53. Similar from Figure 4.51 and Figure 4.53 shows that embedment does not have a significant effect on resonant frequency ratio.

4.6.6 Complex dynamic stiffness

Figure 4.54 shows the plot of the complex dynamic stiffness versus the forcing frequency for the footing embedded at 0, 310, 620, 930, and 1240 mm. From here, it is observed that the complex dynamic stiffness is nearly constant at low frequencies up to about 20 Hz. Beyond 20 Hz the complex dynamic stiffness

decreased as the embedment increases up to about 38 Hz. Thereafter, the complex dynamic stiffness increases as the frequency increases. At low frequencies, the effect of embedment is insignificant; however, as the frequency of excitation increases, the effect of embedment on the complex dynamic stiffness is significant.

4.6.7 Real part of complex dynamic stiffness

The plot of the real part for different embedment is shown in Figure 4.55 and it is observed that at low frequencies the real part increases as the embedment increases. However, the effect of embedment is insignificant at low frequency of excitation. It is common to estimate the natural frequency of the foundation from the plot of the real part against the forcing frequency. The natural frequency of the foundation system obtained increased as the embedment increased.

4.6.8 Imaginary part of complex dynamic stiffness

The plot of the imaginary part versus forcing frequency for embedded foundation is shown in Figure 4.56. The plots indicate that the imaginary part increases as the embedment increases.

4.6.9 Phase and loss angles

The plot of phase angles versus forcing frequency for 0, 310, 620, 930, and 1240 mm embedment is shown in Figure 4.57. This indicates that the natural frequency of foundation systems increases as the embedment increases. The natural frequency of the foundation system can be obtained from the plot of the loss angle versus frequency of excitation. The plots of loss angle versus forcing frequency for 0, 310, 620, 930, and 1240 mm embedment are shown in Figures 4.58. The plot shows clear peaks at the natural frequency which increases as the embedment increases.

From the plot of the loss angle versus frequency, it is possible to establish the natural frequency for a heavily damped system because the plot clearly shows a peak at the natural frequency. The natural frequencies measured in the field are presented in Table 4.8. The effect of embedment of the foundation on the natural frequency of the foundation system is shown Figure 4.59 and here it can be observed that the natural frequency of the foundation system increases significantly as the embedment increases.

Table 4-8: The field-measured natural frequency of the foundation system.

Embedment (m)	Measured Natural frequency (Hz)	Natural frequency ratio	Embedment ratio
0.00	41.0	1.000	0
310	46.1	1.1244	0.5167
620	51.0	1.2439	1.0333
930	47.0	1.1463	1.55
1240	55.0	1.3414	2.0667

4.6.10 Natural frequency of foundation system

The experimental results show that the natural frequency of the foundation system increases as the embedment increases. The natural frequency increased from 41.0 Hz at zero embedment to 55.0 Hz at a full embedment. Figure 4.59 show the plot of the natural frequency versus embedment depth.

A new dimensionless quantity knows as Natural Frequency ratio (N_f) is introduced to express the effect of embedment on the natural frequency of foundation systems. The Natural Frequency ratio is the ratio of the natural frequency for an embedded footing to the natural frequency for zero embedment. The Natural Frequency ratio is determined using the following equation:

$$N_f = \frac{\omega_D}{\omega_{Do}}$$

Equation 4.18

Where:

N_f is the natural frequency ratio;

ω_D is the natural frequency of the foundation system with an embedment, and

ω_{Do} is the natural frequency of the foundation system with zero embedment.

The natural frequency ratio calculated using Equation 4.18 is shown in Table 4.8. The plot of natural frequency ratio versus embedment ratios obtained from the field-measured data is shown in Figure 4.60. This shows that as the embedment increases, the natural frequency ratio increases significantly. The natural frequency

increased by 34% from zero embedment to full embedment where as the resonant frequency descreased slightly by 6% from zero to full embedment.

4.7 Summary

In this chapter, the shear modulus and shear wave velocity of the soil profile where the footings were constructed was determined. The small strains shear modulus will be used in Chapter 5 to determine the theoretical dynamic behaviour of the surface and embedded foundations. In addition, the same small strains shear modulus will be used in Chapter 6 to determine the dynamic behaviour of surface and embedded foundation using numerical analysis. In additional, the dynamic behaviour of the surface and embedded foundation were determined.

4.7.1 Surface foundation

The observed dynamic behaviour of the surface foundation was the displacement amplitude, resonant amplitude, resonant frequency, dynamic stiffness and natural frequency. The experimental results show that the resonant frequency obtained from the frequency response function is 45.5 Hz. It is also reveals that the resonant frequency can be estimated from the plot of complex dynamic stiffness against forcing frequency, as well as from the plot of the imaginary part versus forcing frequency of the frequency response function (receptance). The natural frequency of the surface foundation was determined from the plot of phase angle versus forcing frequency, as well as from loss angle versus forcing frequency.

4.7.2 Embedded foundation

The dynamic behaviour of the embedded foundation determined experimentally was the the displacement amplitude, resonant amplitude, resonant frequency, natural frequency and dynamic stiffness. The effect of embedment is described by dimensionless quantities known as resonant amplitude ratio, resonant frequency ratio and the newly introduced quantity known as natural frequency ratio. The observed dynamic responses of the surface and embedded foundation will be compared with analytical solutions and numerical solutions discussed in Chapter 5 and 6 respectively.
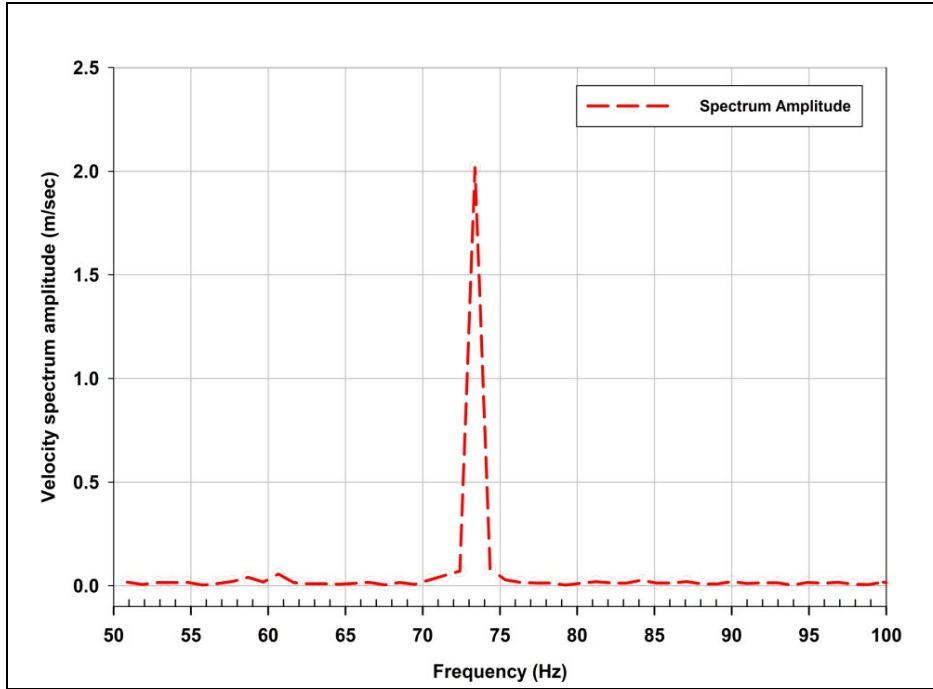
Figure 4.1: Geophone spectrum amplitude for 73.4 Hz
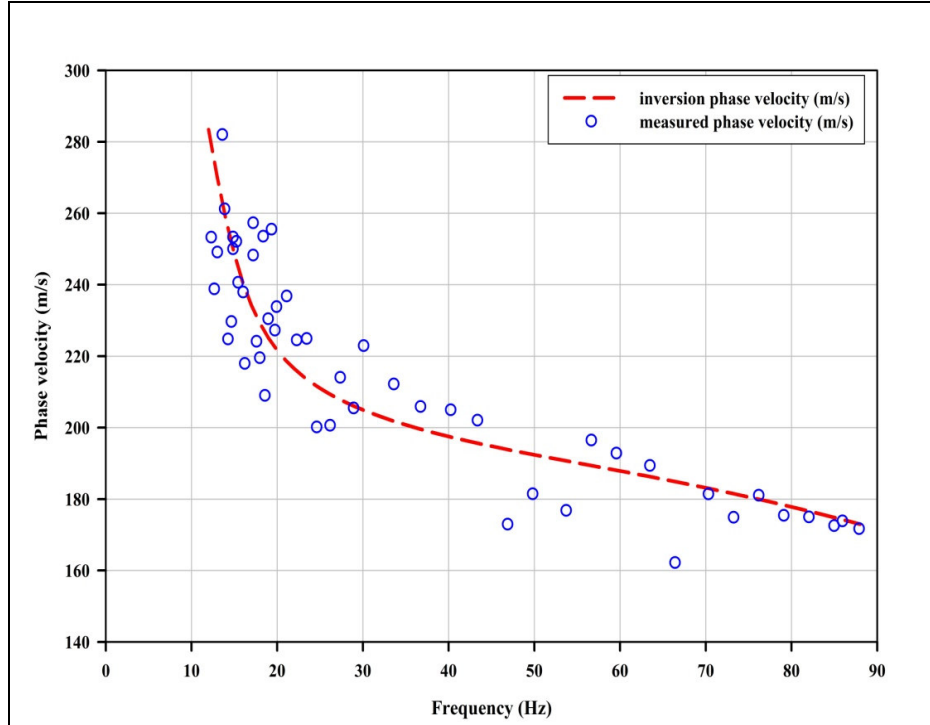
Figure 4.2: Field-measured phase velocity
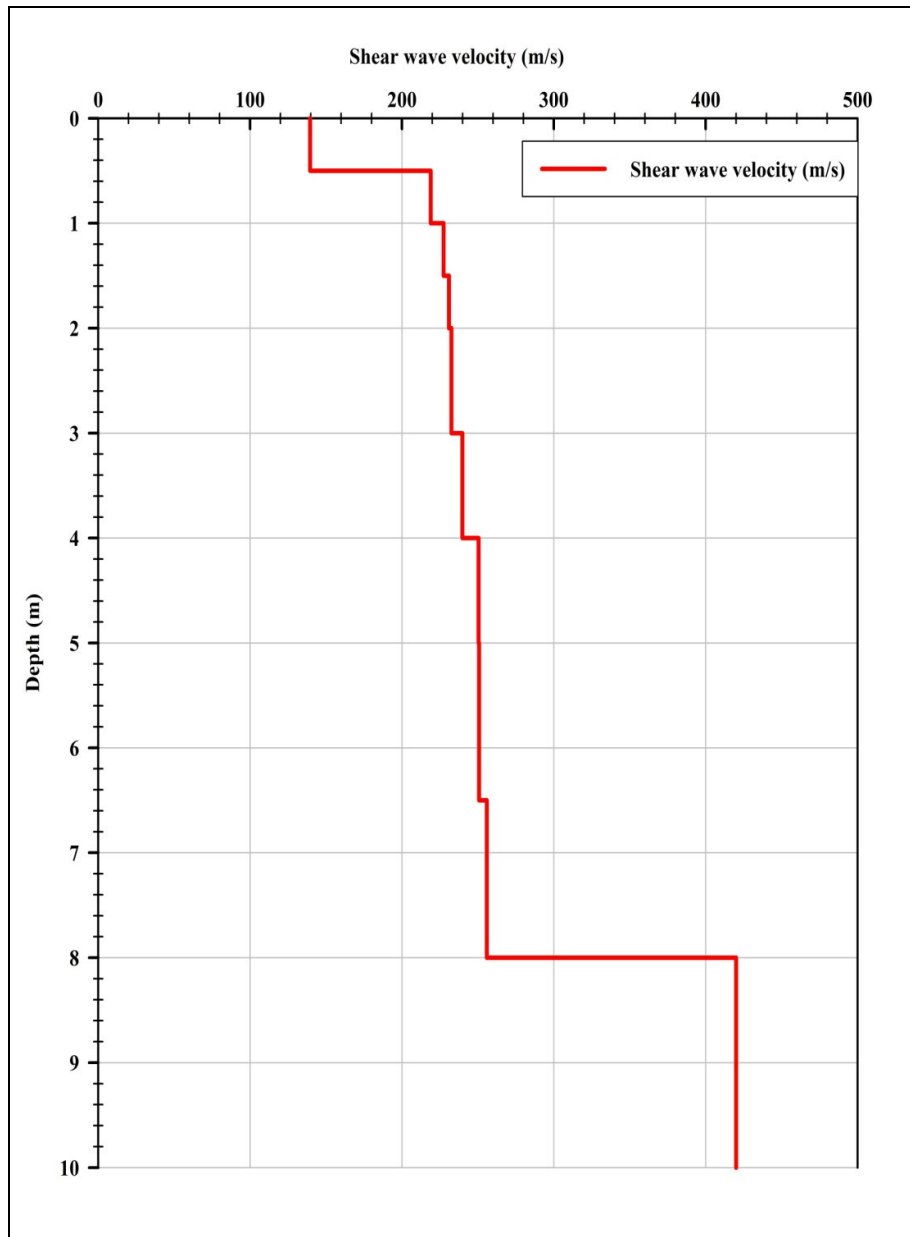
Figure 4.3: Field-measured shear wave velocity
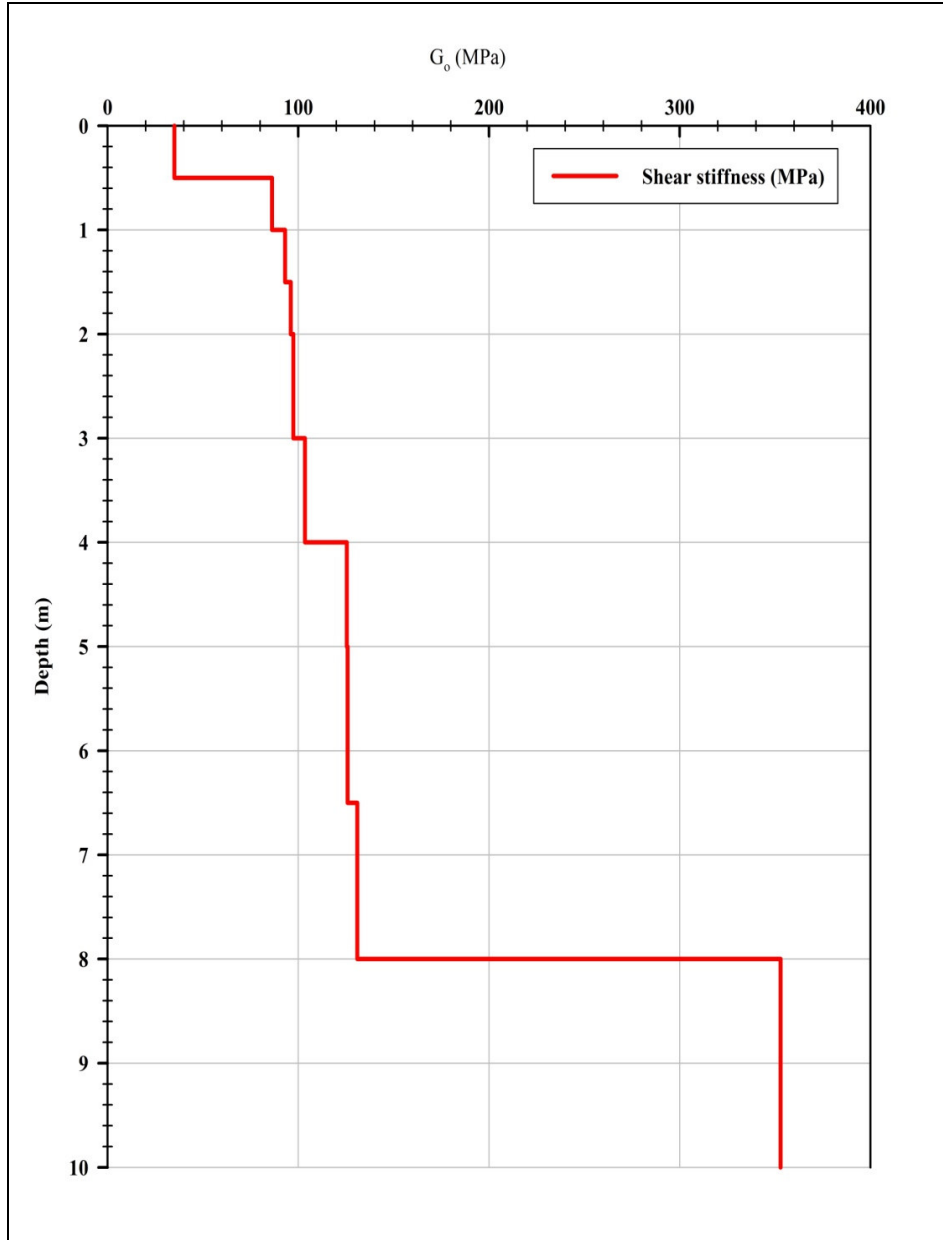
Figure 4.4: Field-measured stiffness
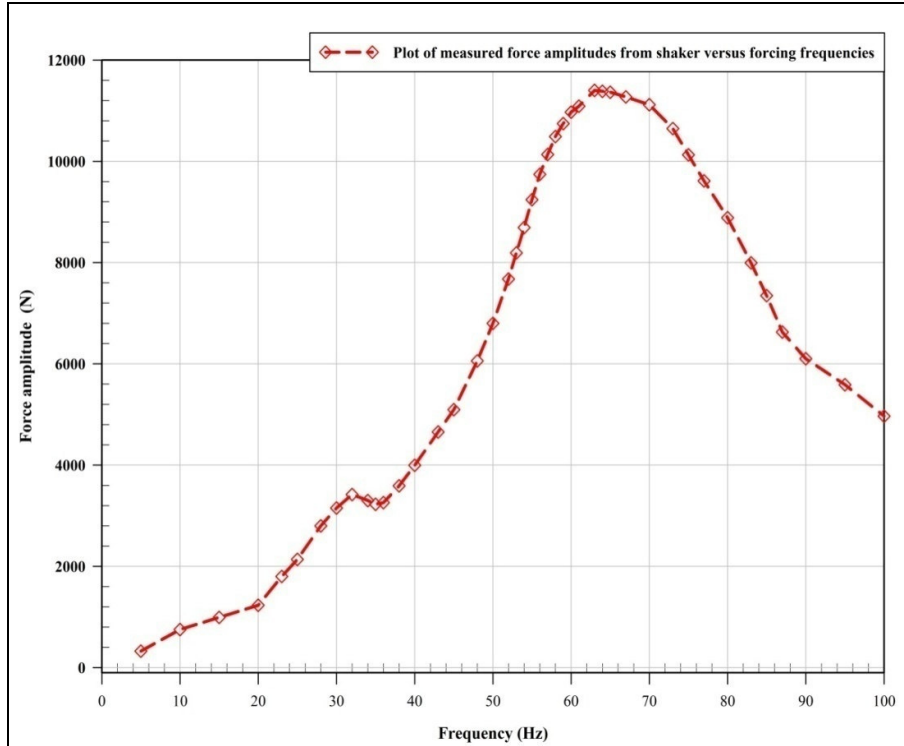
Figure 4.5: Measured force from shaker
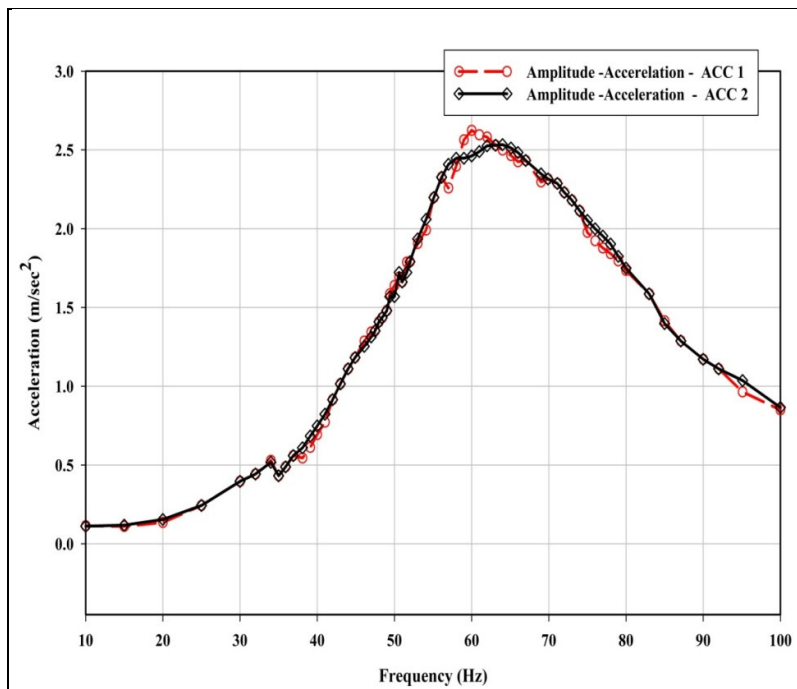
Figure 4.6: Measured acceleration from accelerometer 1 and 2

4-26
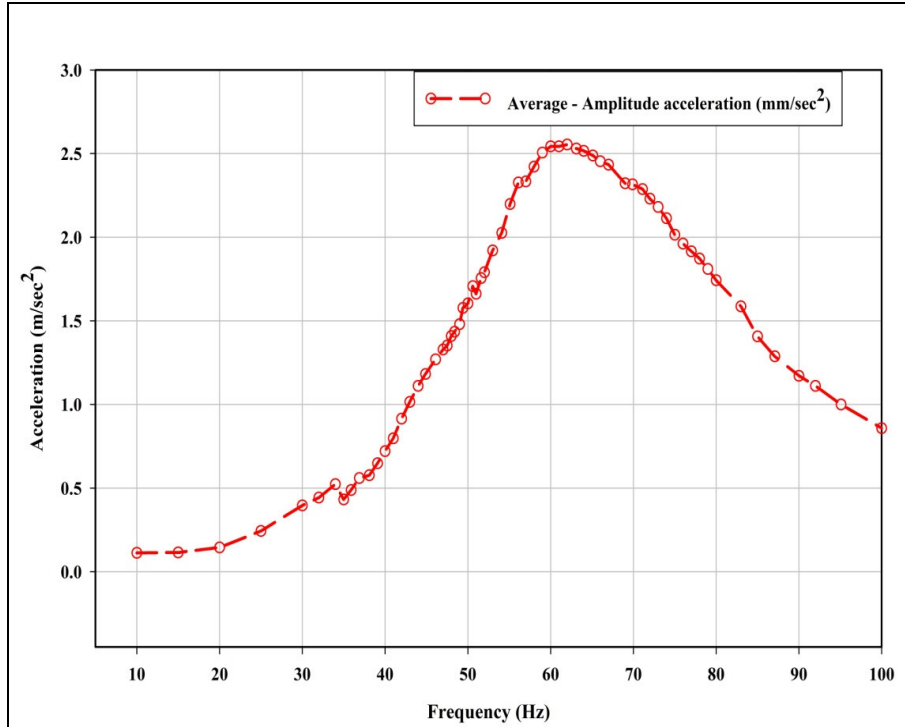
Figure 4.7: Average measured acceleration.
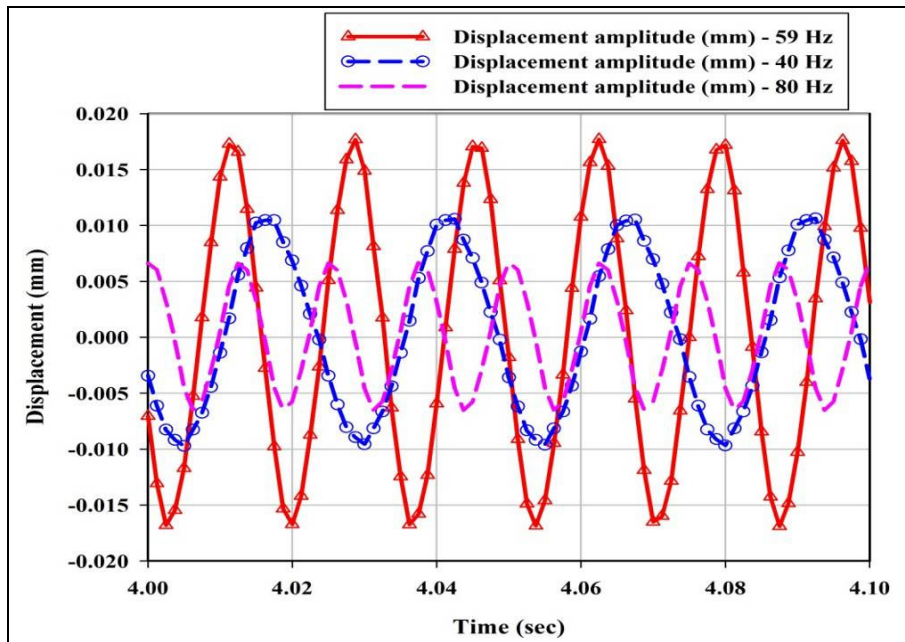
Figure 4.8: Vertical displacement in time domain

4-27
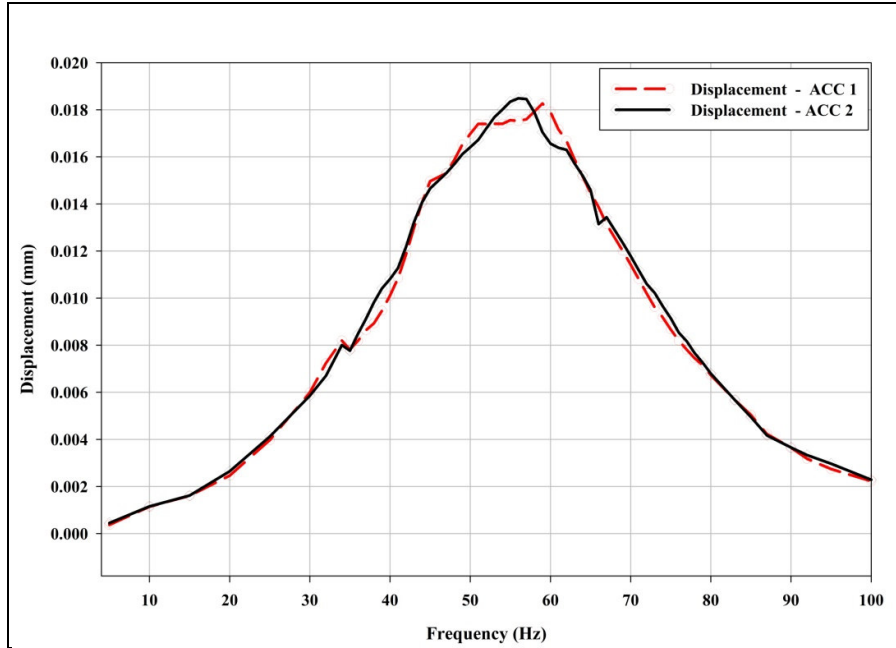
Figure 4.9: Footing vertical displacement response from accelerometer 1 and 2.
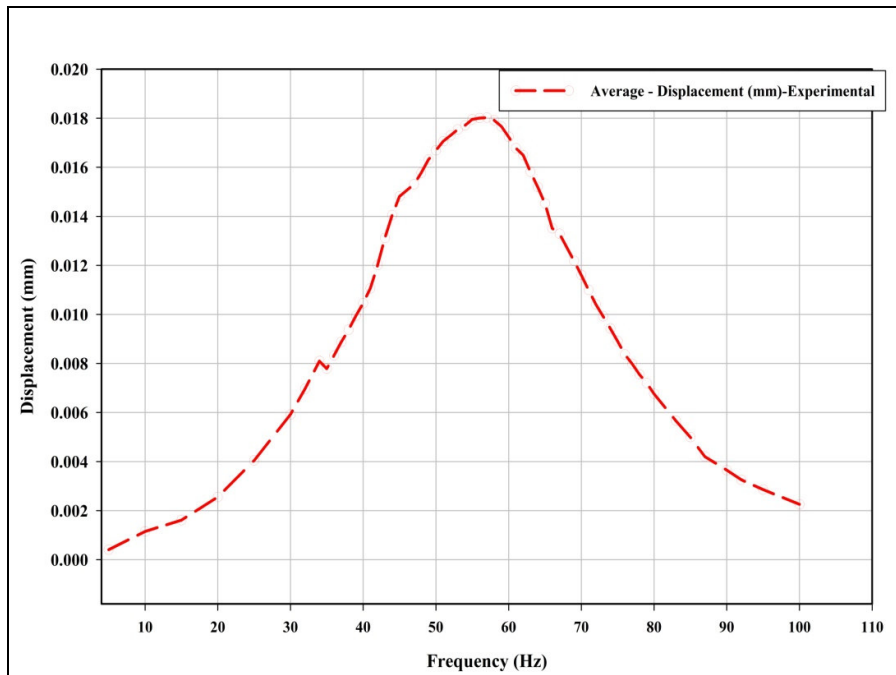
Figure 4.10: Average measured footing displacement response.

4-28
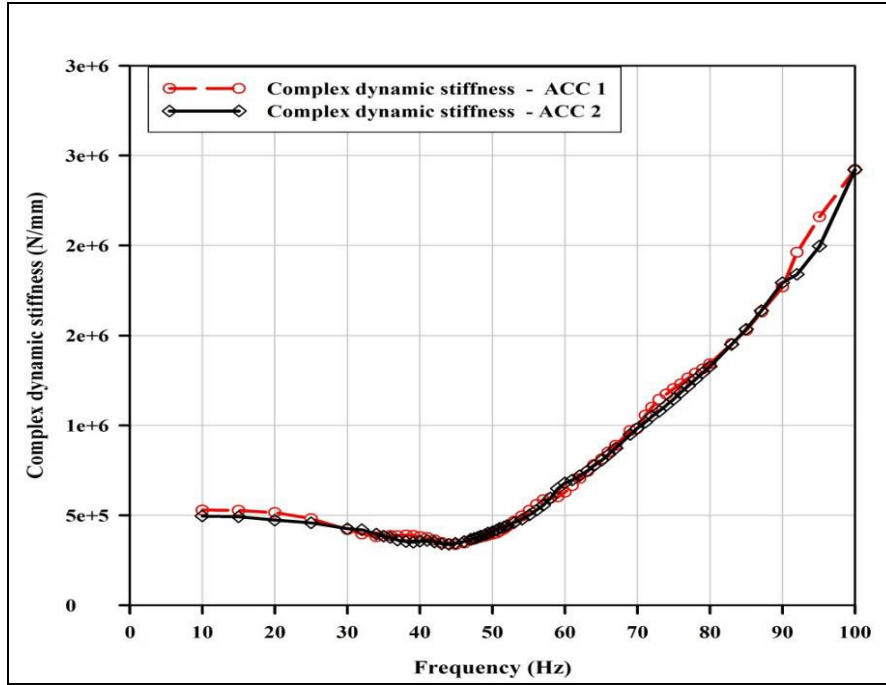
Figure 4.11: Complex dynamic stiffness from accelerometer 1 and 2.
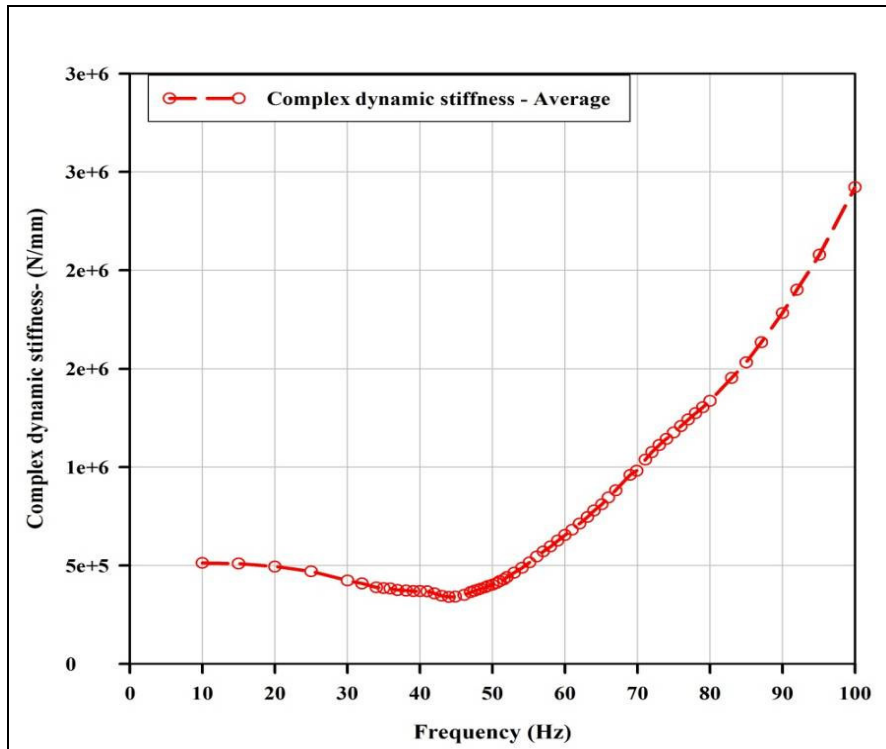
Figure 4.12: Measured foundation Complex dynamic stiffness – Average

4-29
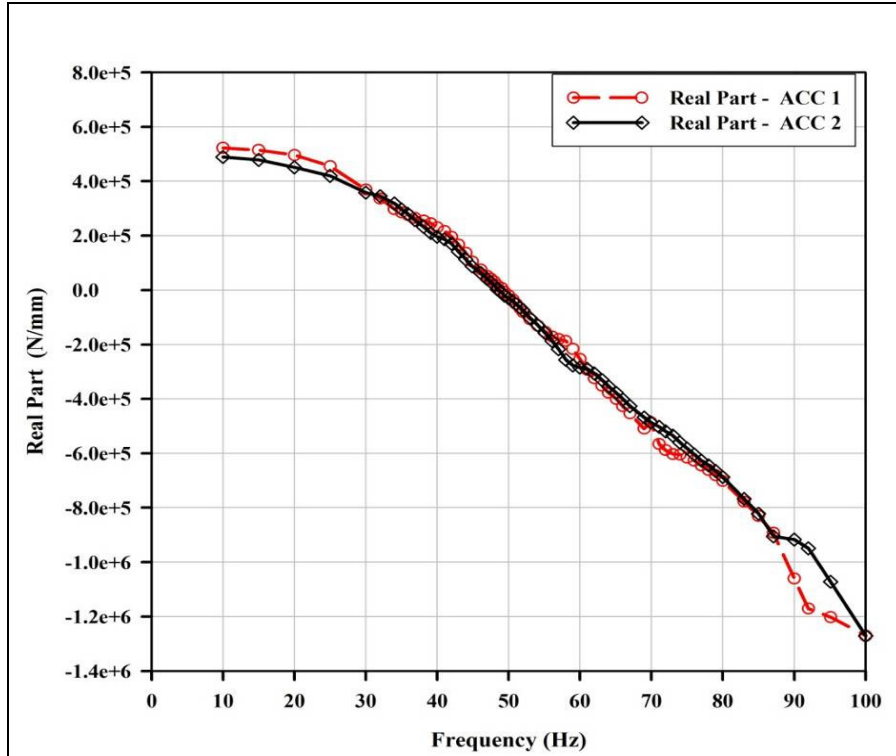
Figure 4.13: The real part of complex dynamic stiffness from accelerometer 1 and 2
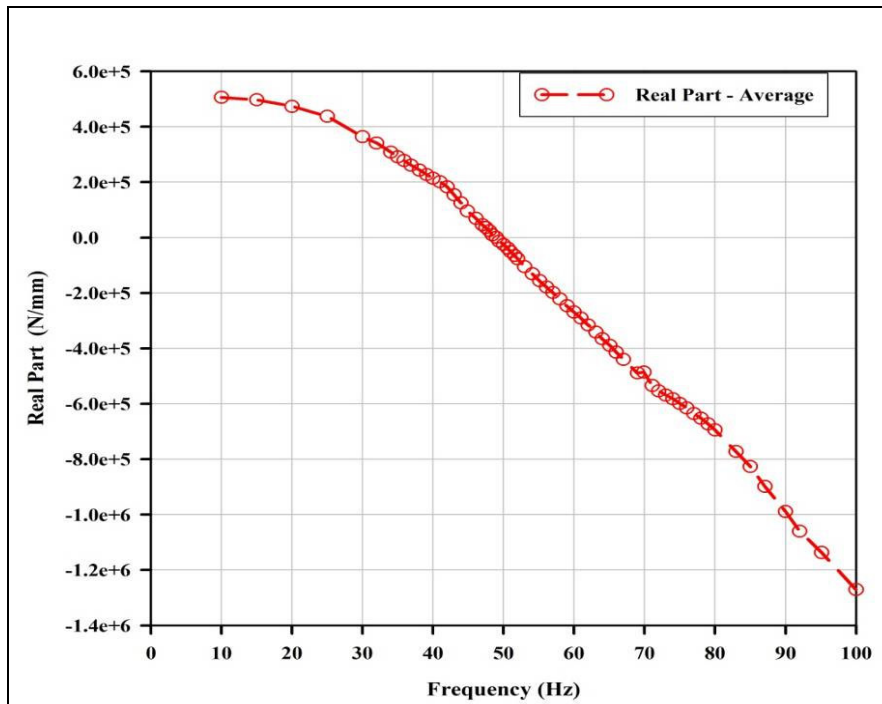
Figure 4.14: Average real part of complex dynamic stiffness.

4-30
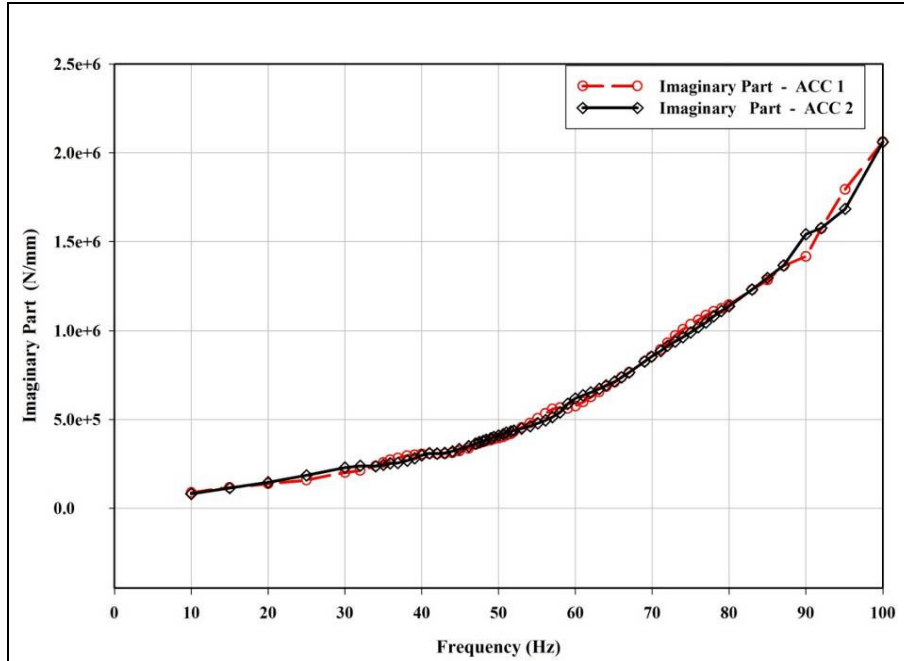
Figure 4.15: The imaginary part of complex dynamic stiffness - from accelerometer 1 and 2
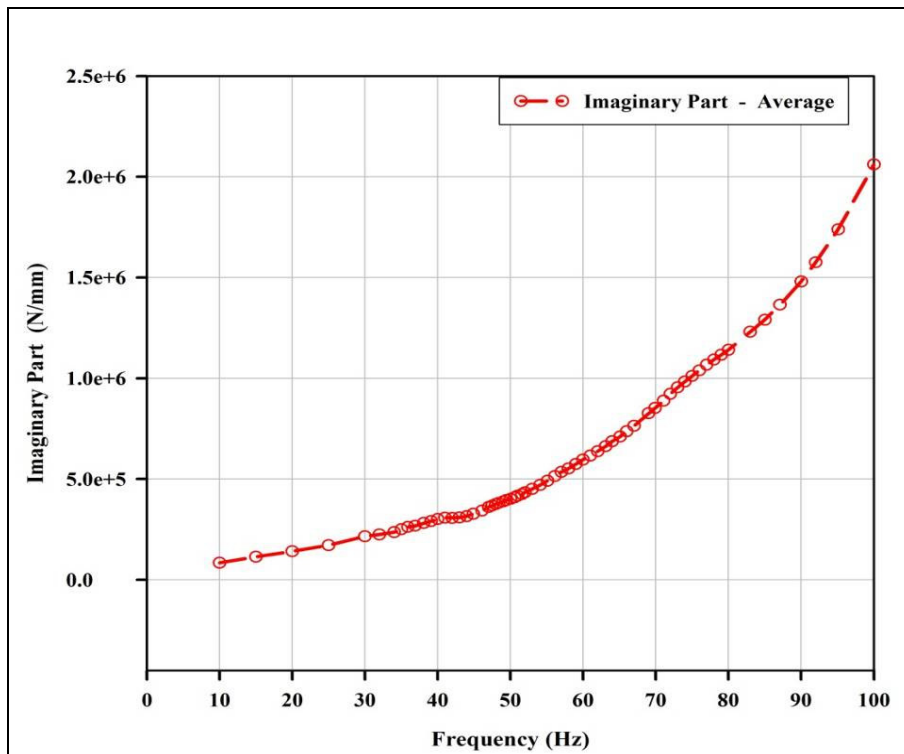
Figure 4.16: Average imaginary part of complex dynamic stiffness

4-31
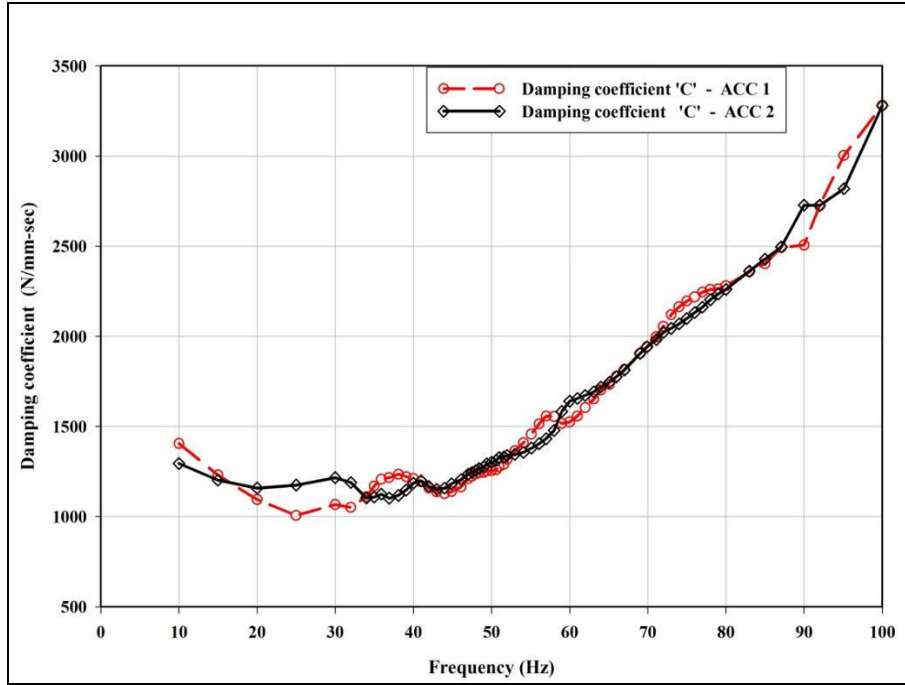
Figure 4.17: Damping coefficients from accelerometers 1 and 2
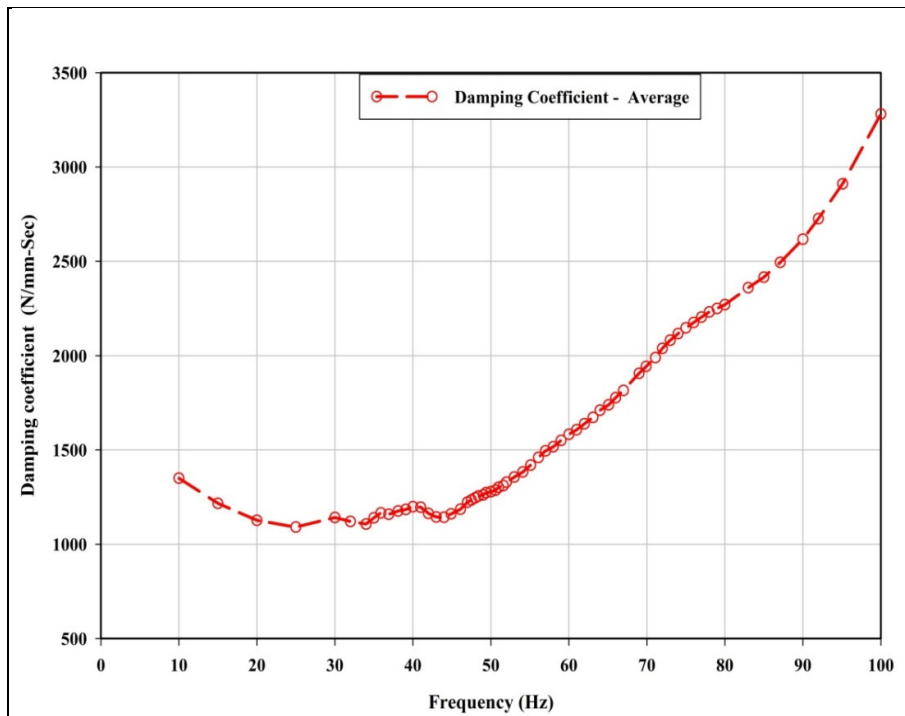
Figure 4.18: Average of damping coefficient
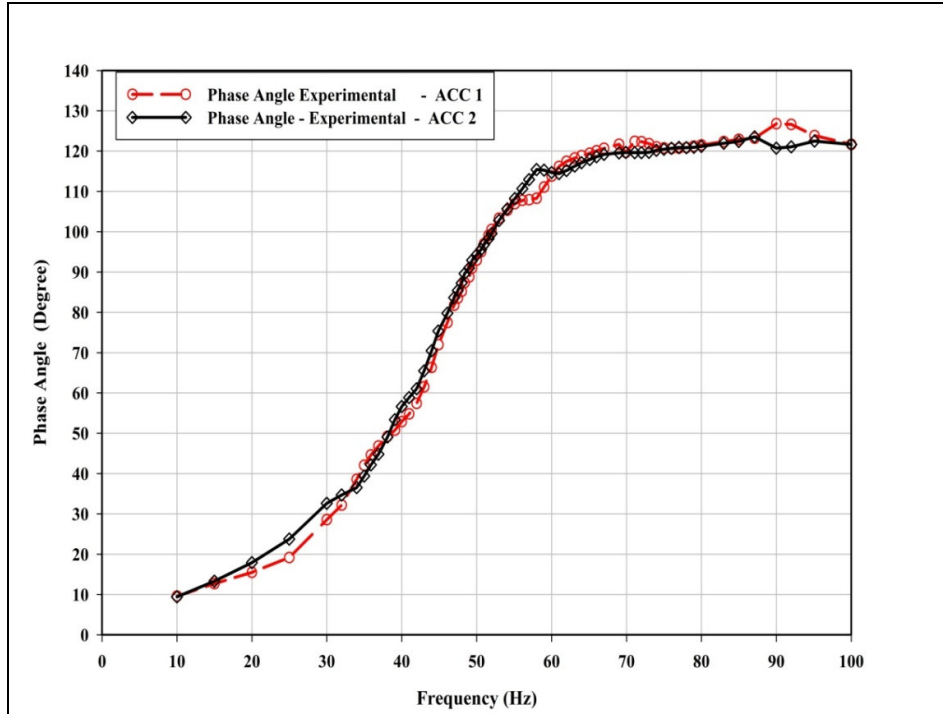
Figure 4.19: Phase angle between forcing function and harmonic vertical displacement for accelerometer 1 and 2
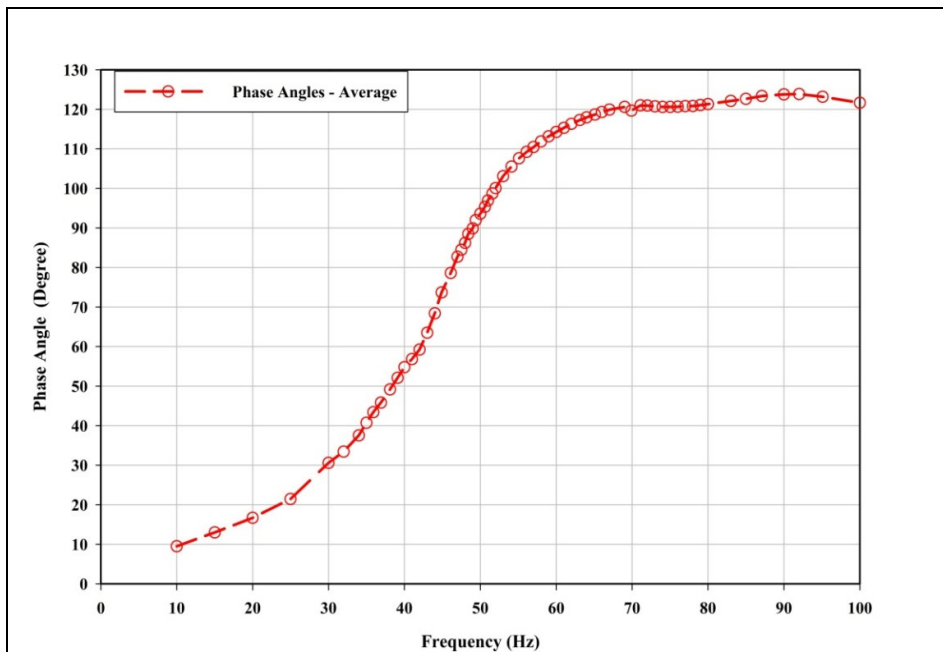
Figure 4.20: Phase angle between forcing function and harmonic vertical displacement
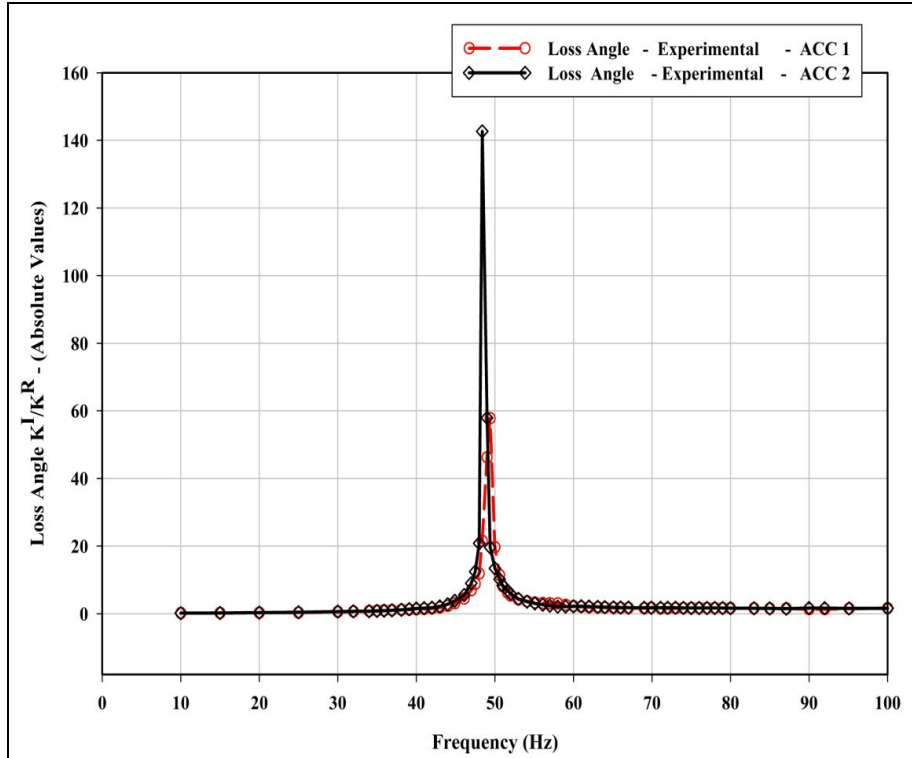
Figure 4.21: Loss angle or damping factor of the foundation system
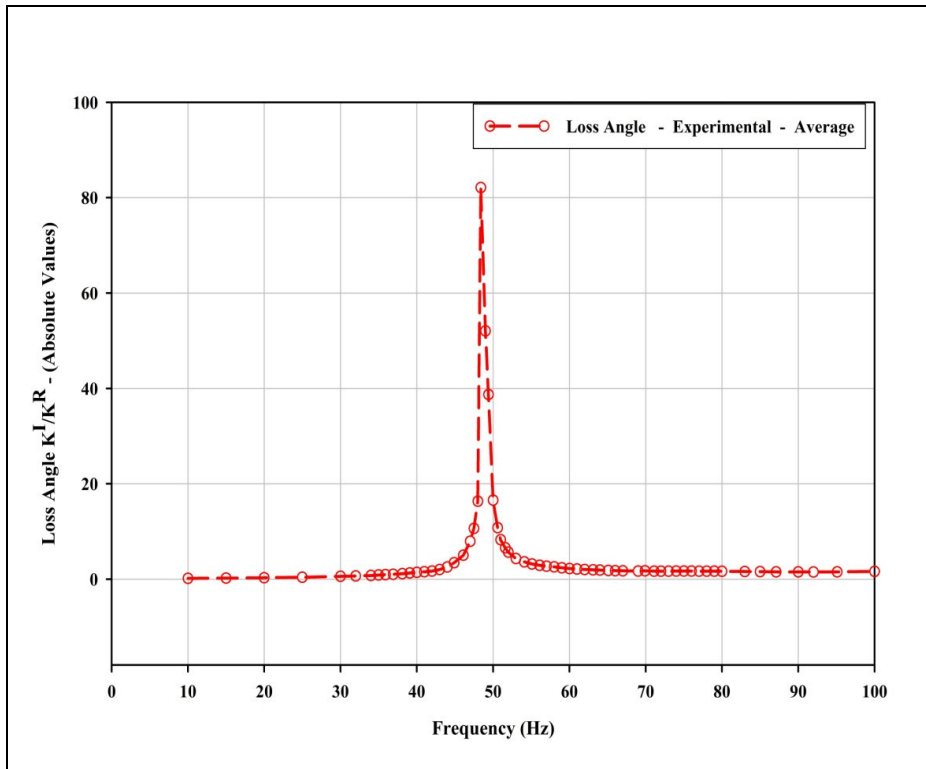
Figure 4.22: Average loss angle or damping factor of the foundation system

4-34
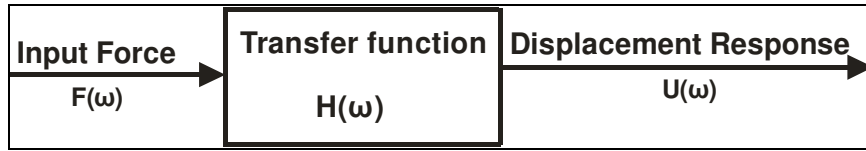
Figure 4.23: Frequency response model
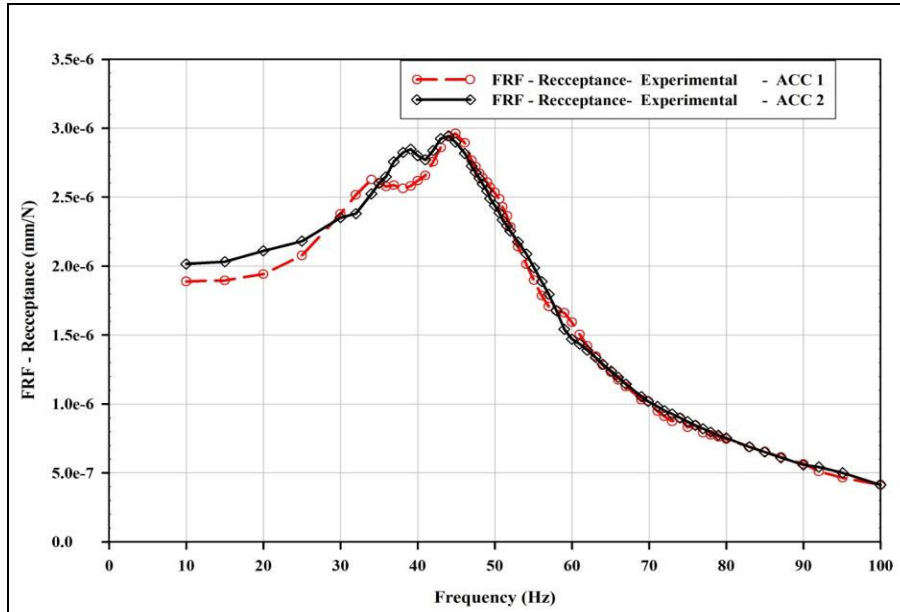
Figure 4.24: Foundation FRF – Receptance for accelerometer 1 and 2
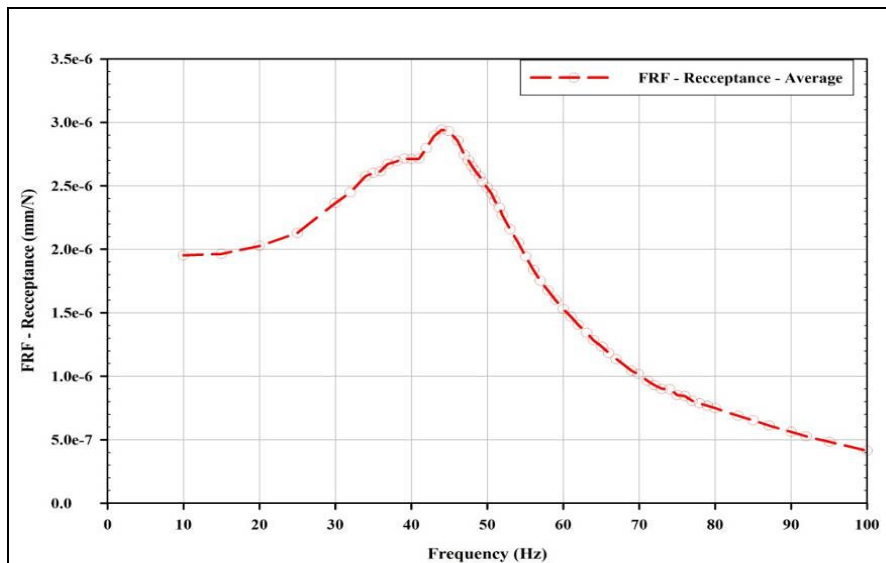
Figure 4.25: Average foundation frequency response function – Receptance

4-35
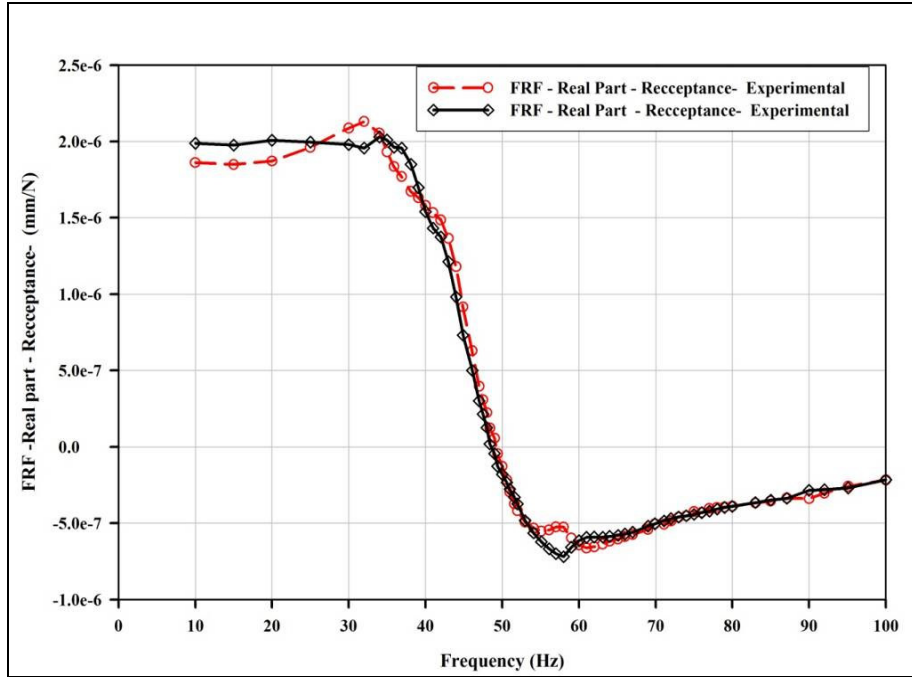
Figure 4.26: Real part from frequency response function – Receptance from accelerometer 1 and 2
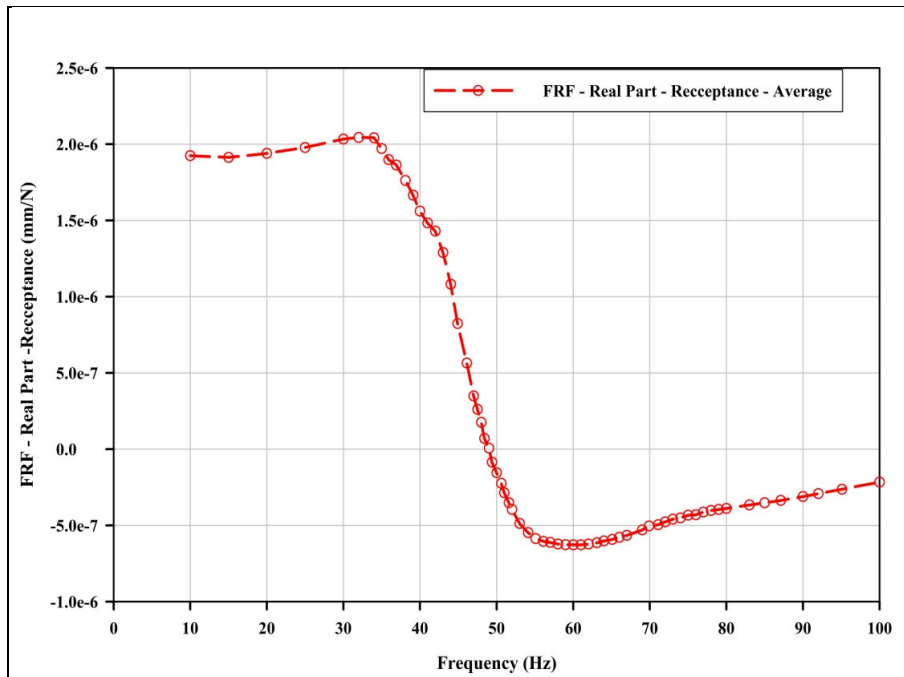
Figure 4.27: Average real part of frequency response function – Receptance.

4-36
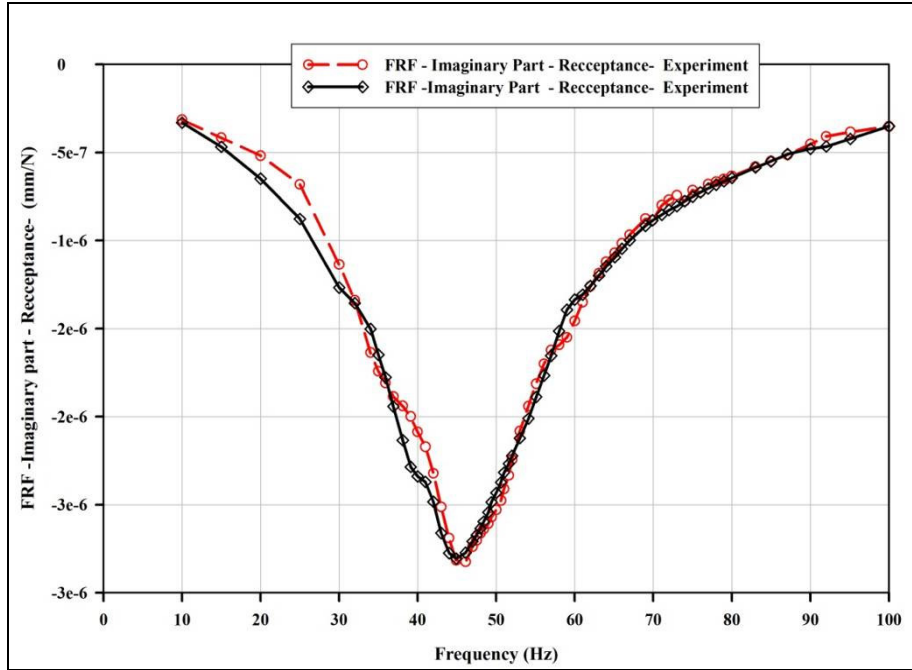
Figure 4.28: Imaginary part of frequency response function – Receptance from accelerometer 1 and 2
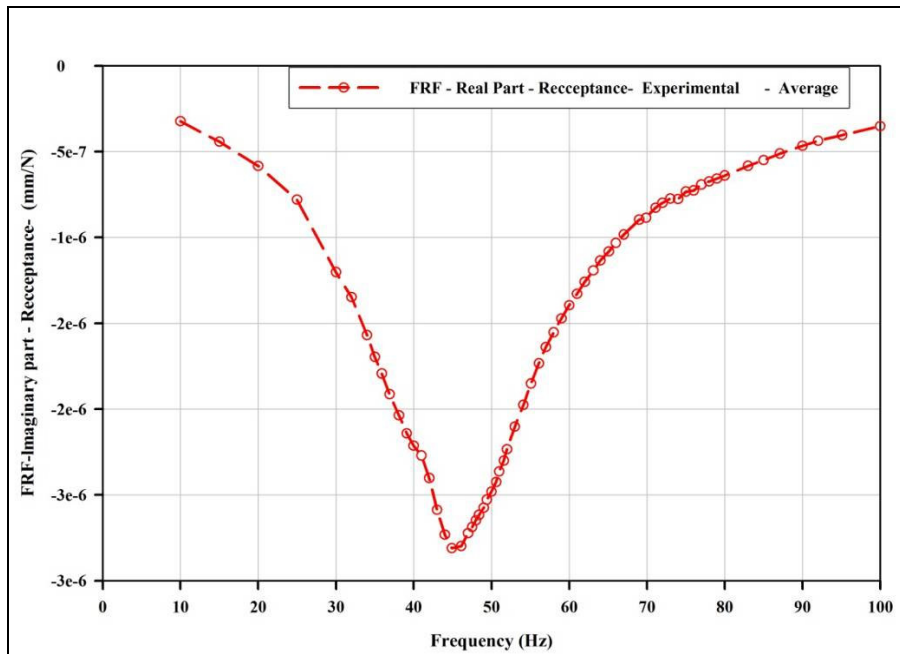
Figure 4.29: Average imaginary part of frequency response function – Receptance Average

4-37
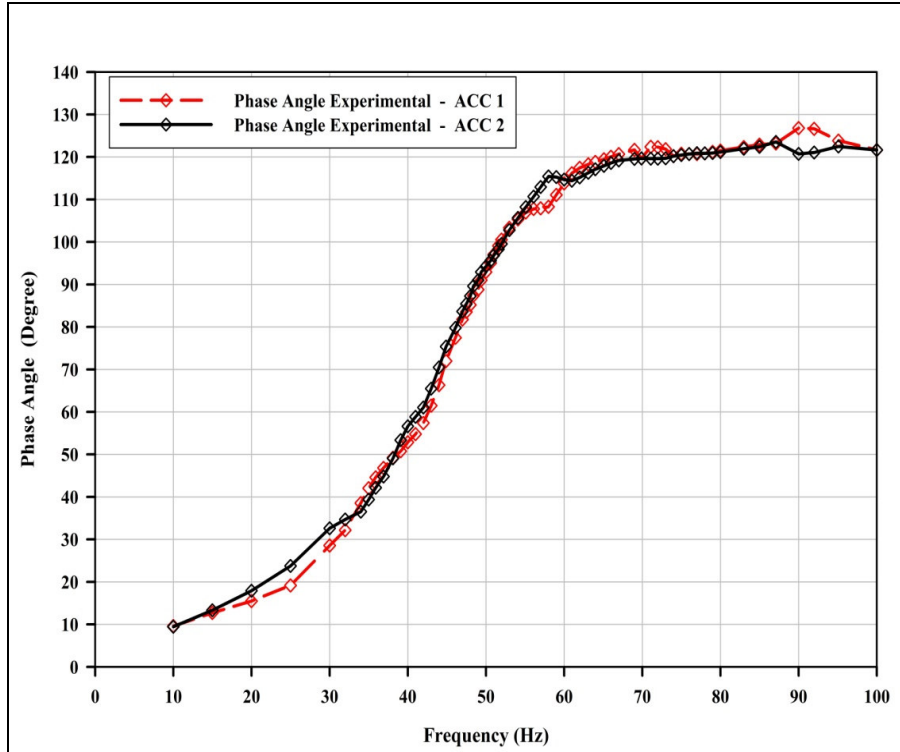
Figure 4.30: Phase angle between forcing function and displacement – Receptance from accelerometer 1 and 2
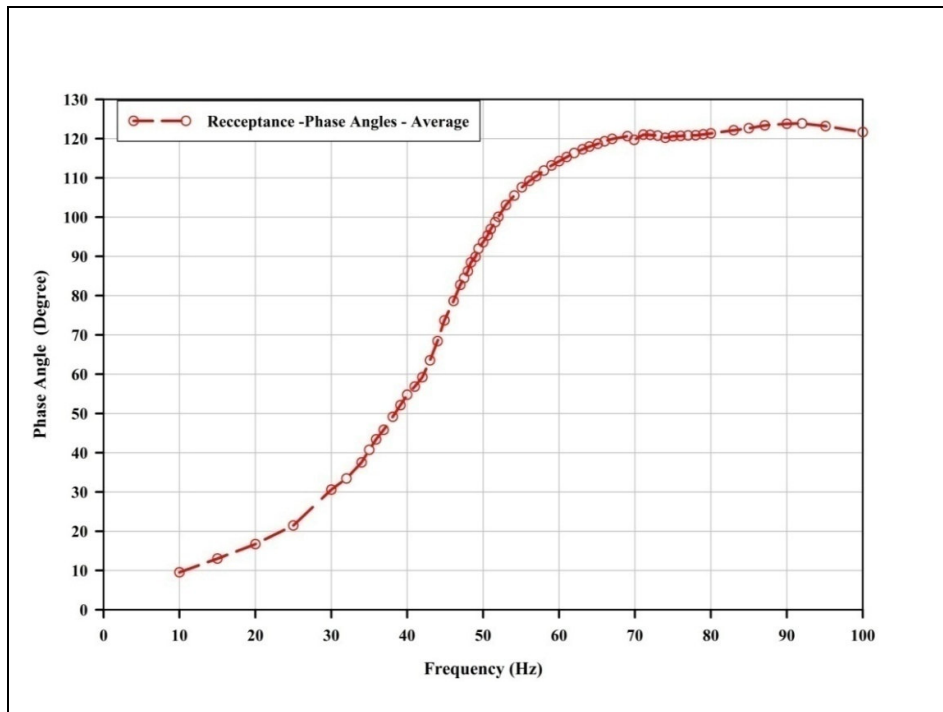
Figure 4.31: Phase angle between forcing function and displacement – Receptance
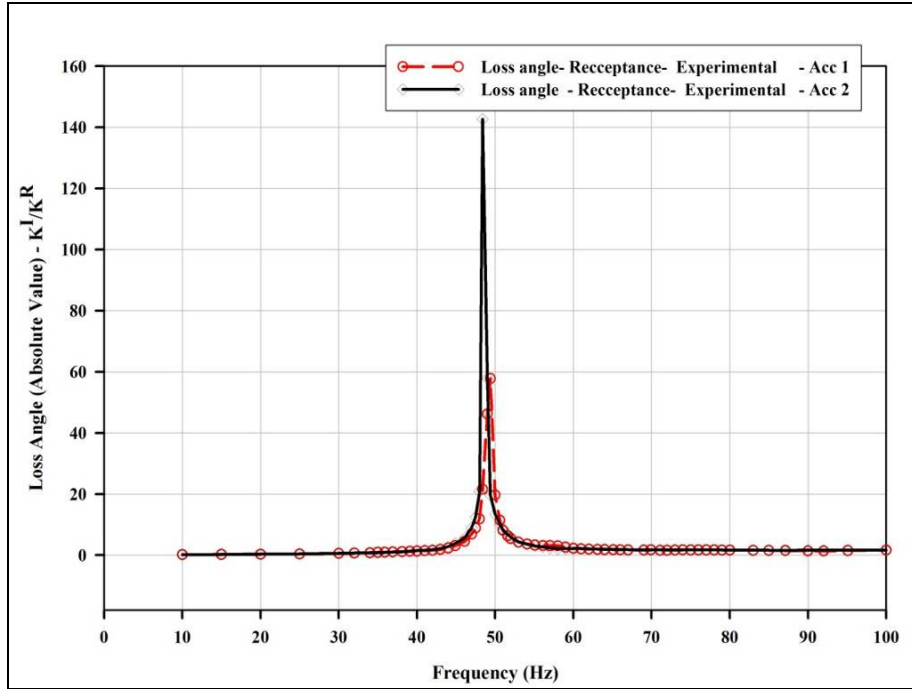
Figure 4.32: Loss angle – Receptance from accelerometer 1 and 2.
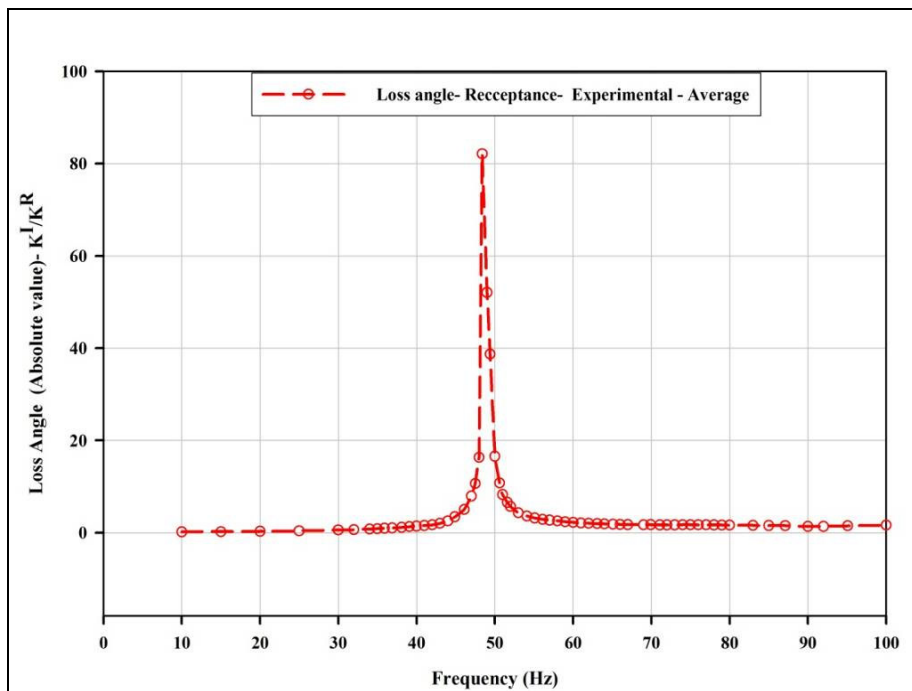
Figure 4.33: Loss angle or damping factor – Receptance

4-39
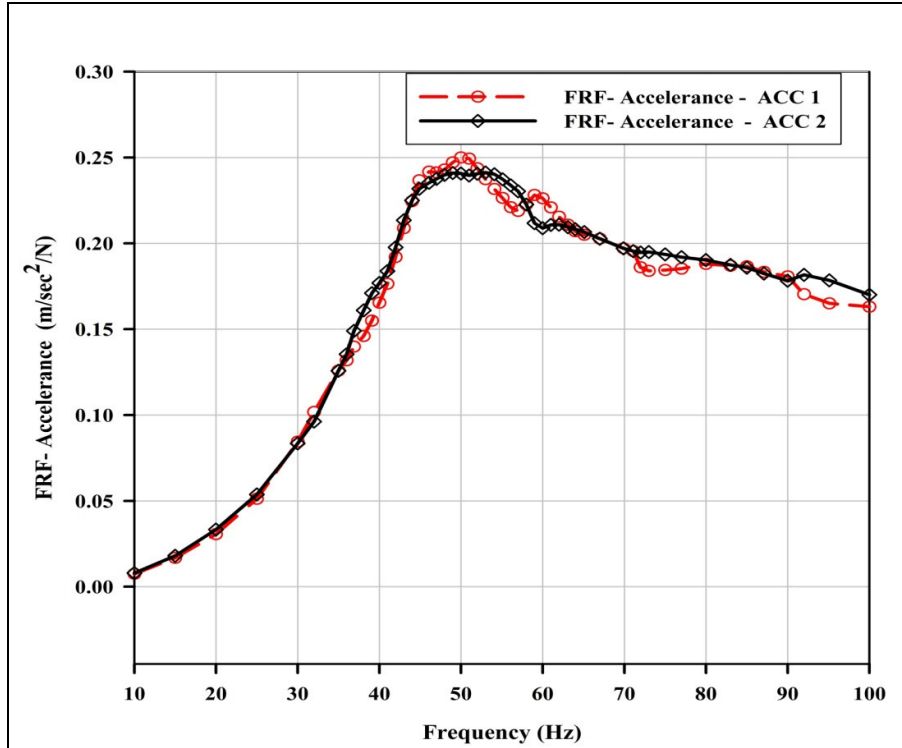
Figure 4.34: Foundation frequency response function – Accelerance
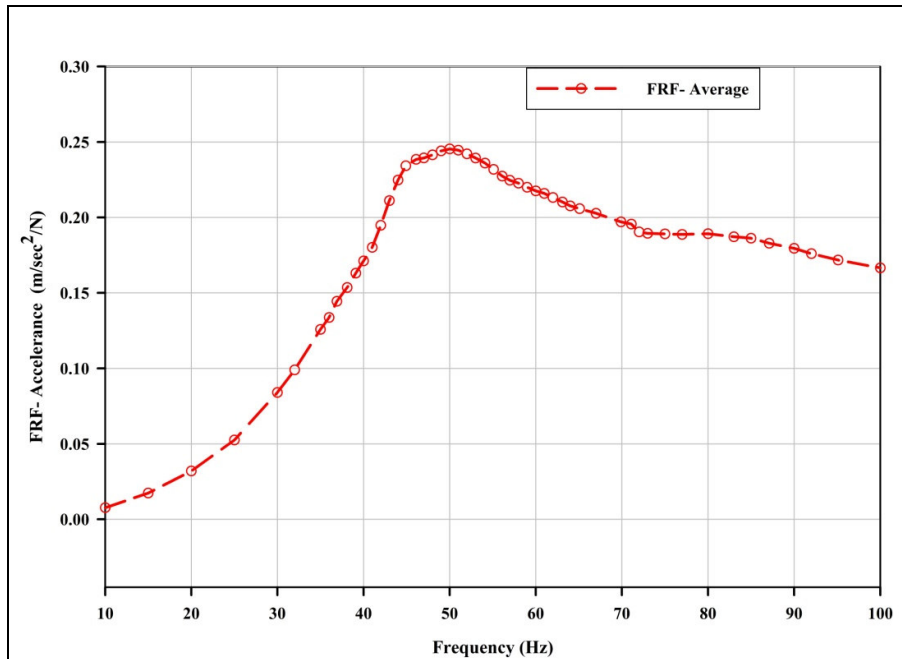
Figure 4.35: Average foundation frequency response function – Accelerance

4-40
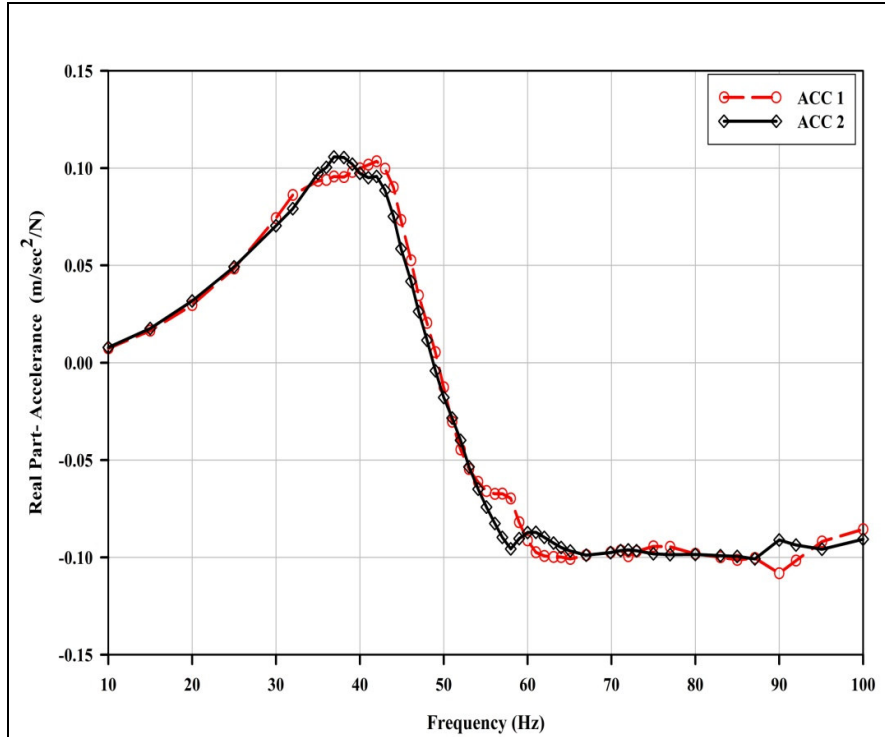
Figure 4.36: Real part from frequency response function – Accelerance from accelerometer 1 and 2
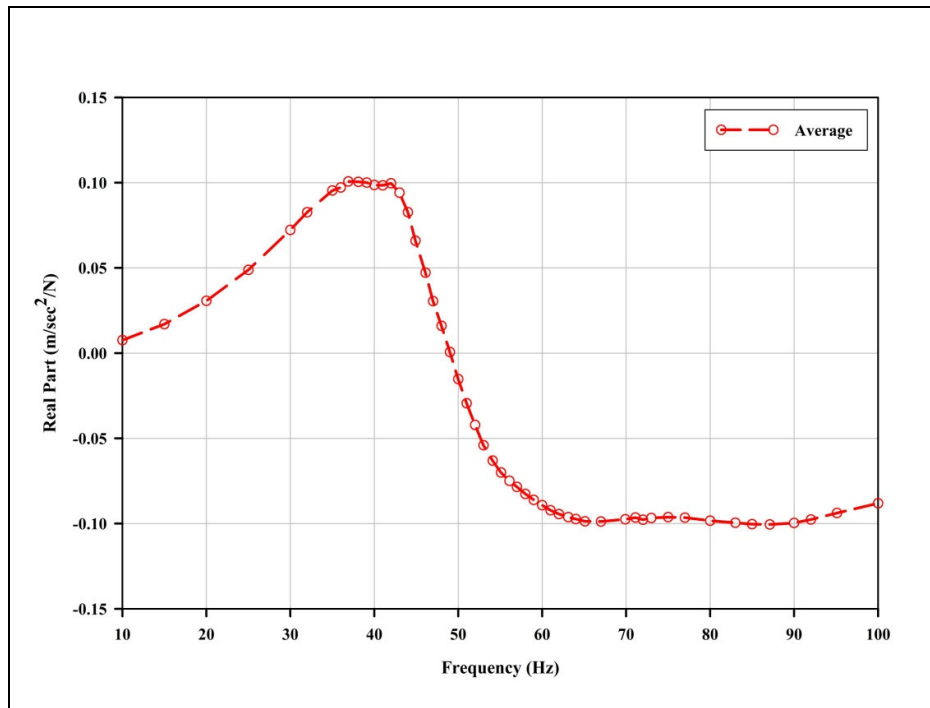
Figure 4.37: Average real part from frequency response function – Accelerance
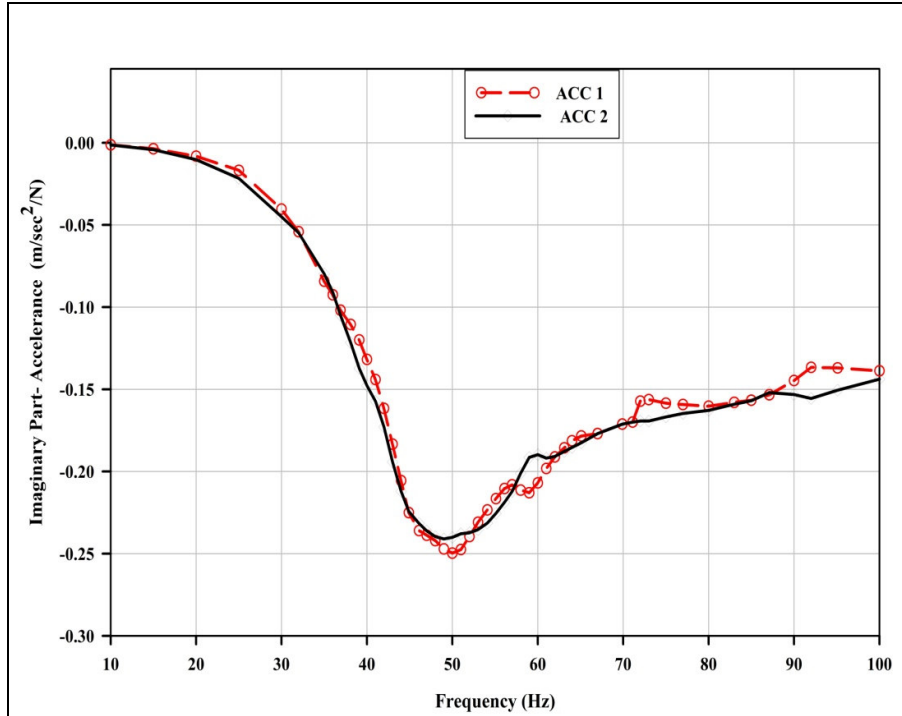
Figure 4.38: Imaginary part of frequency response function – Accelerance from accelerometer 1 and 2
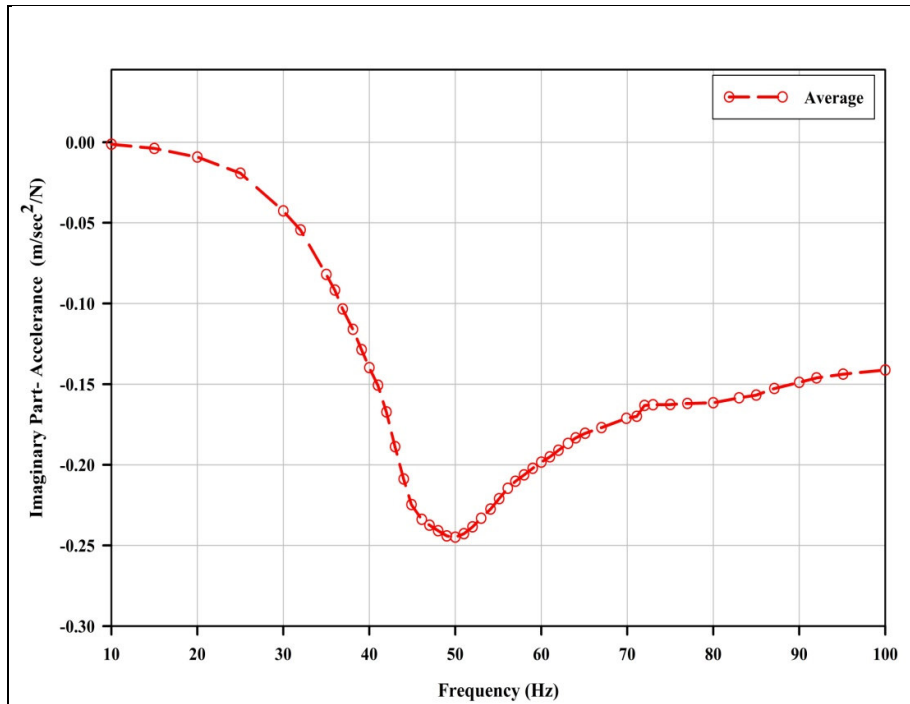
Figure 4.39: Imaginary part of frequency response function – Accelerance

4-42
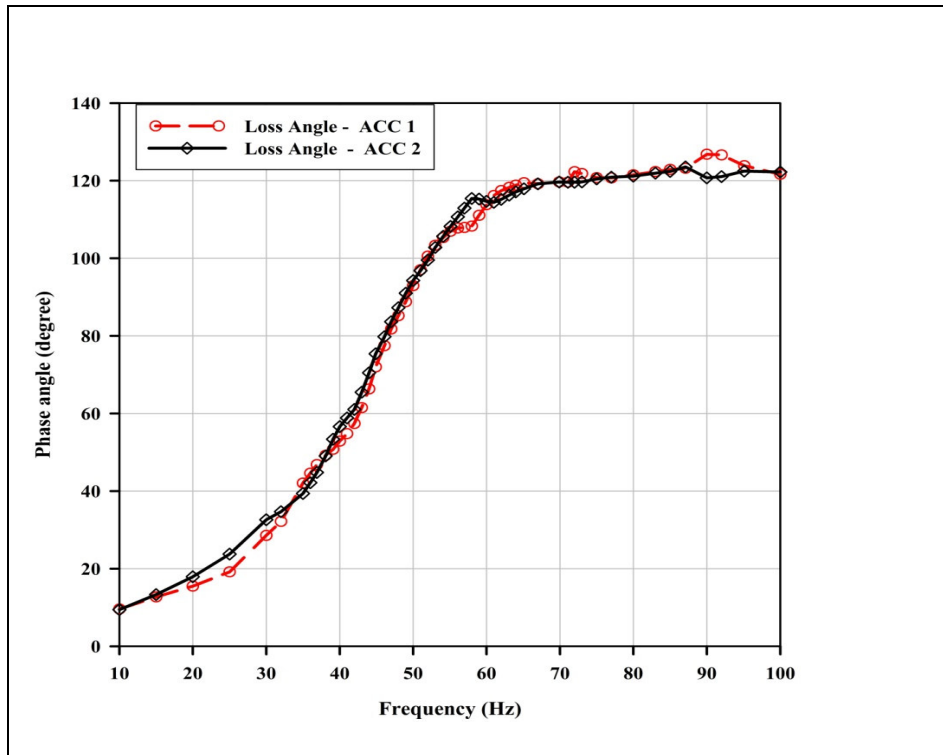
Figure 4.40: Phase angle between forcing function and acceleration – Accelerance from accelerometer 1 and 2
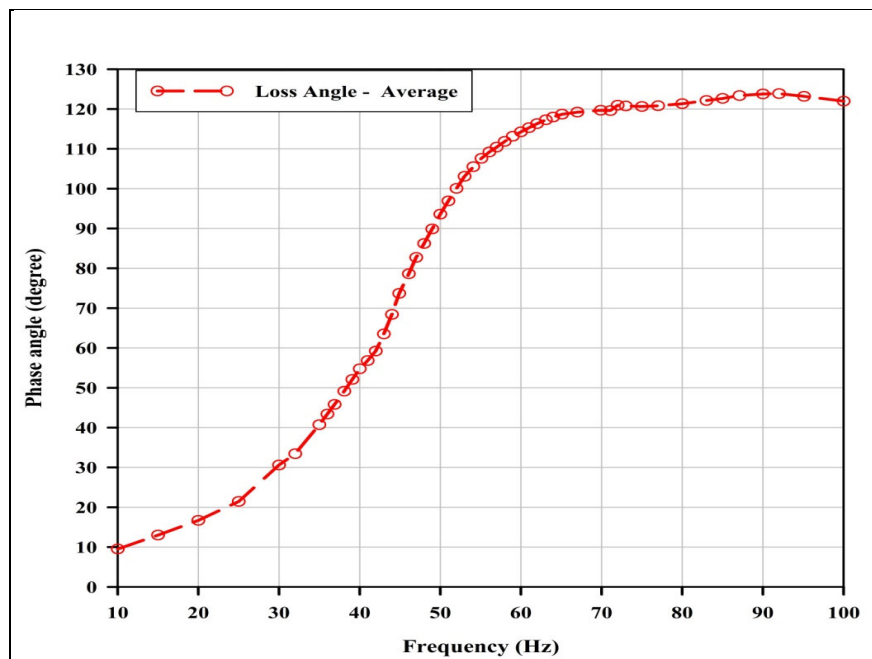
Figure 4.41: Average phase angle between forcing function and acceleration – Accelerance

4-43
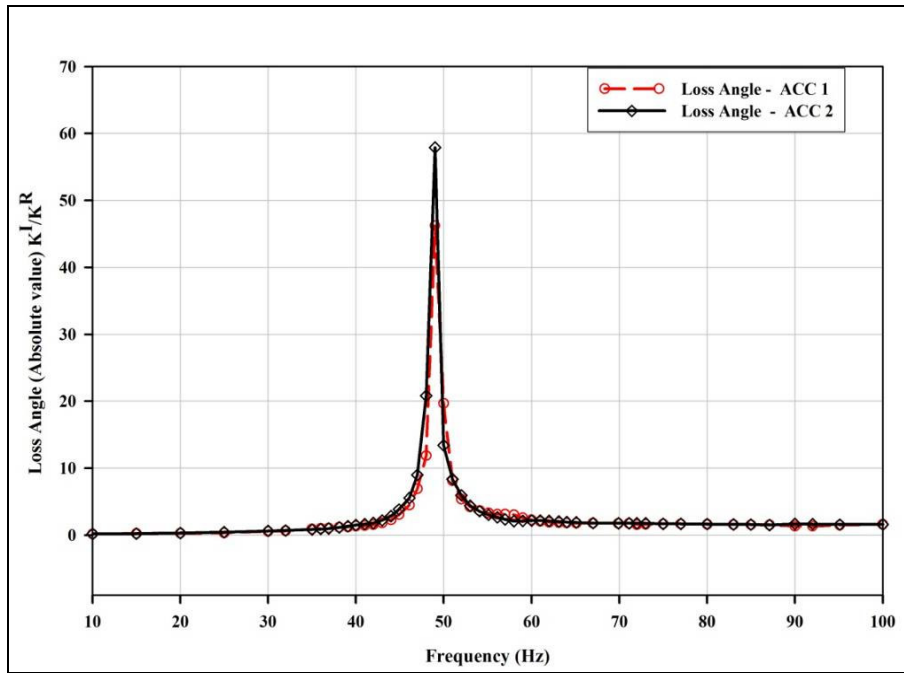
Figure 4.42: Loss angle – Accelerance from accelerometer 1 and 2
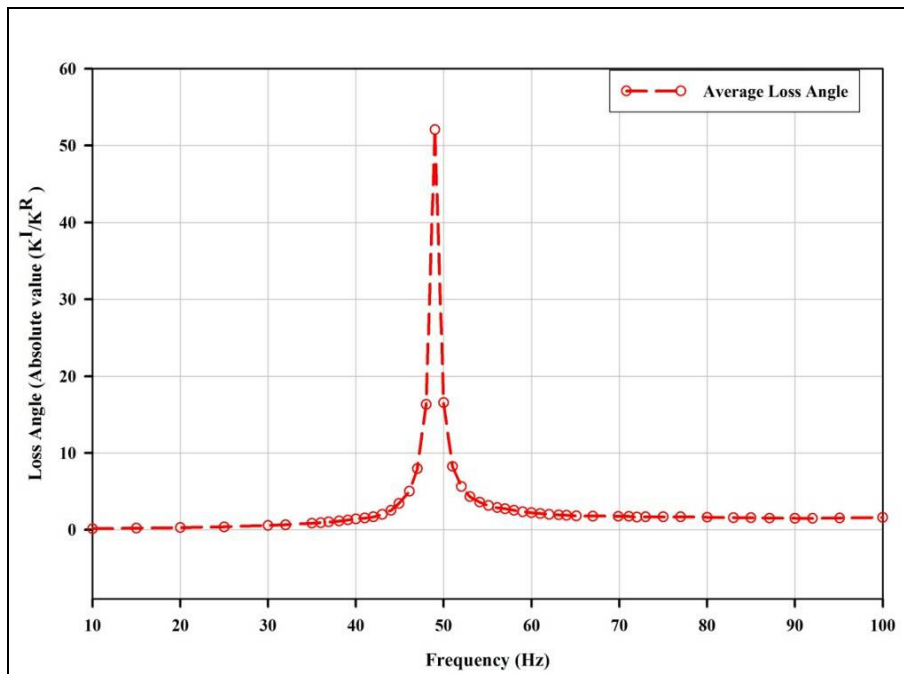
Figure 4.43: Average loss angle – Accelerance from accelerometer 1 and 2

4-44
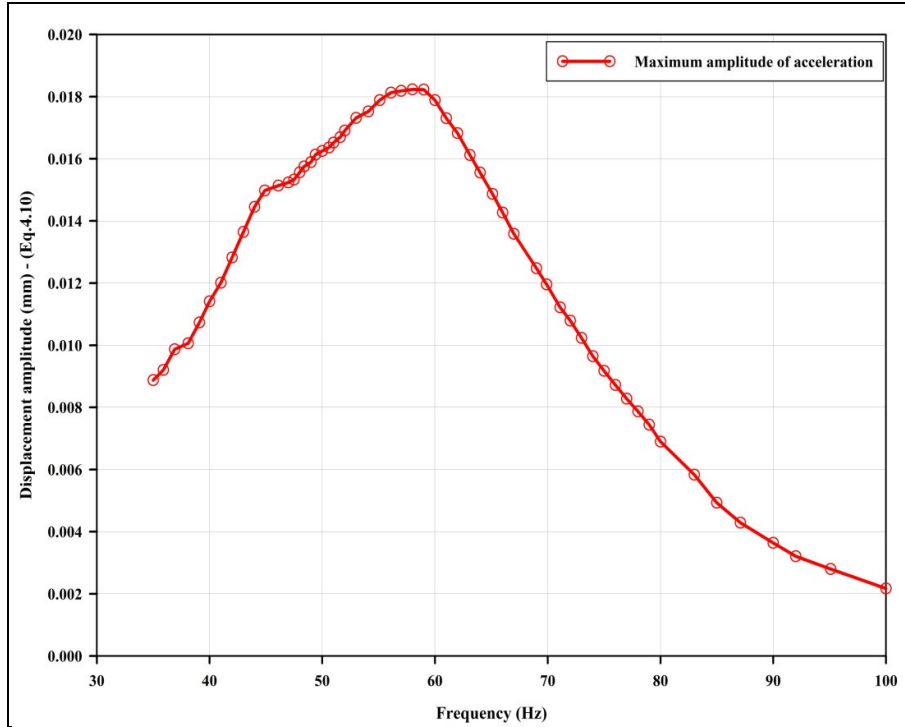
Figure 4.44: Determination of natural frequency of block system (Undamped system)
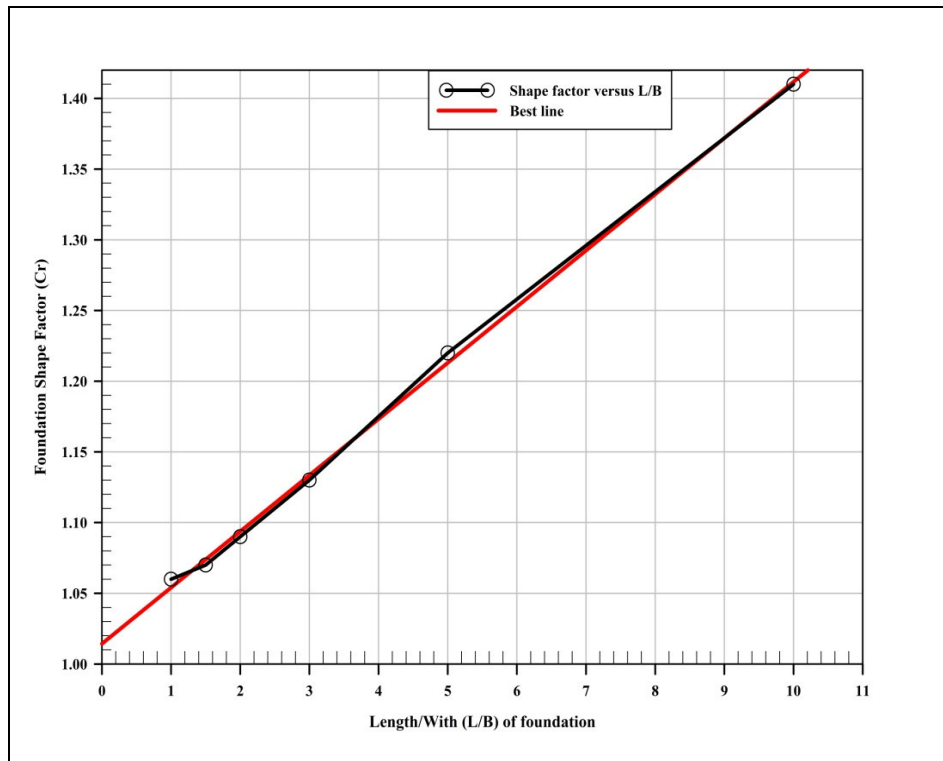
Figure 4.45: Estimation of shape factor (Barkan 1962)

4-45
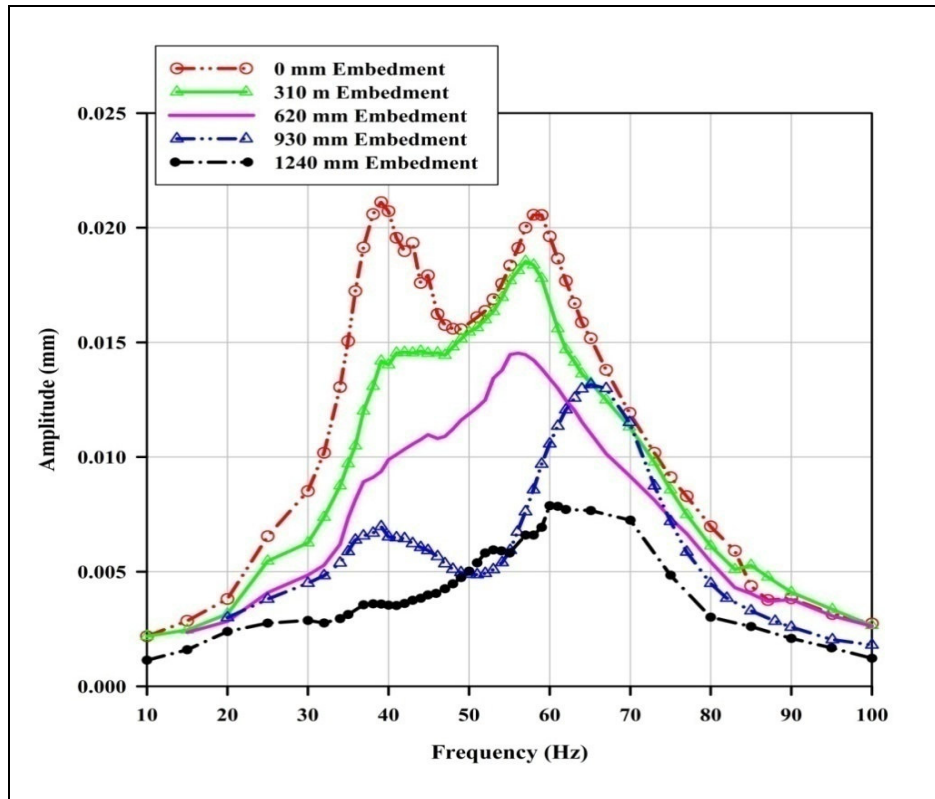
Figure 4.46: Displacement due to exerted loads
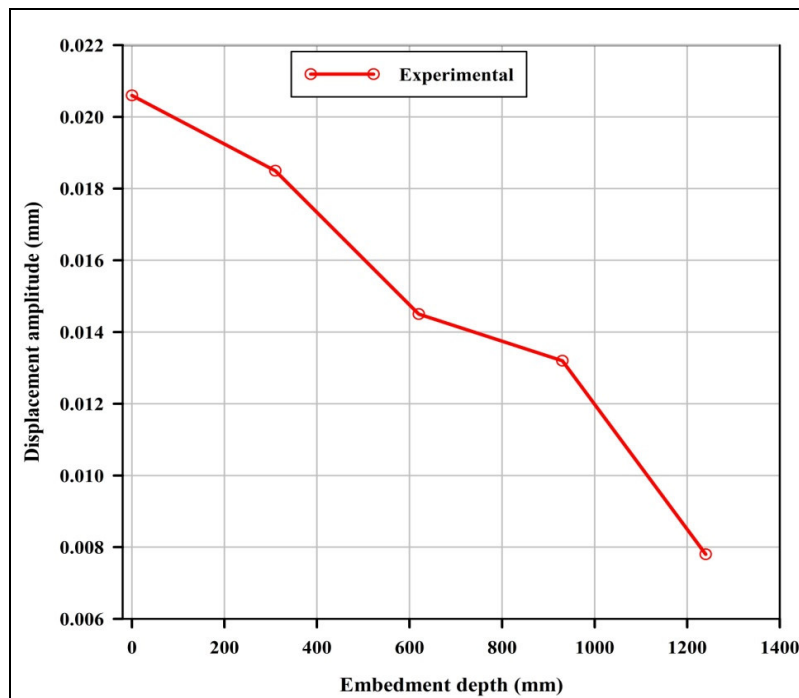
Figure 4.47: Displacement due to loads with increase in embedment depth

4-46
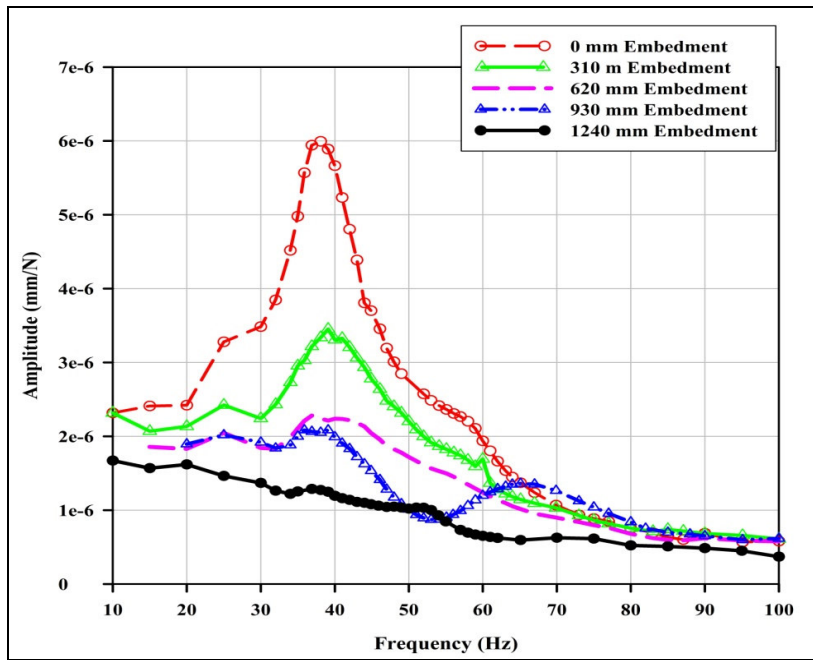
Figure 4.48: Displacement due to unit load
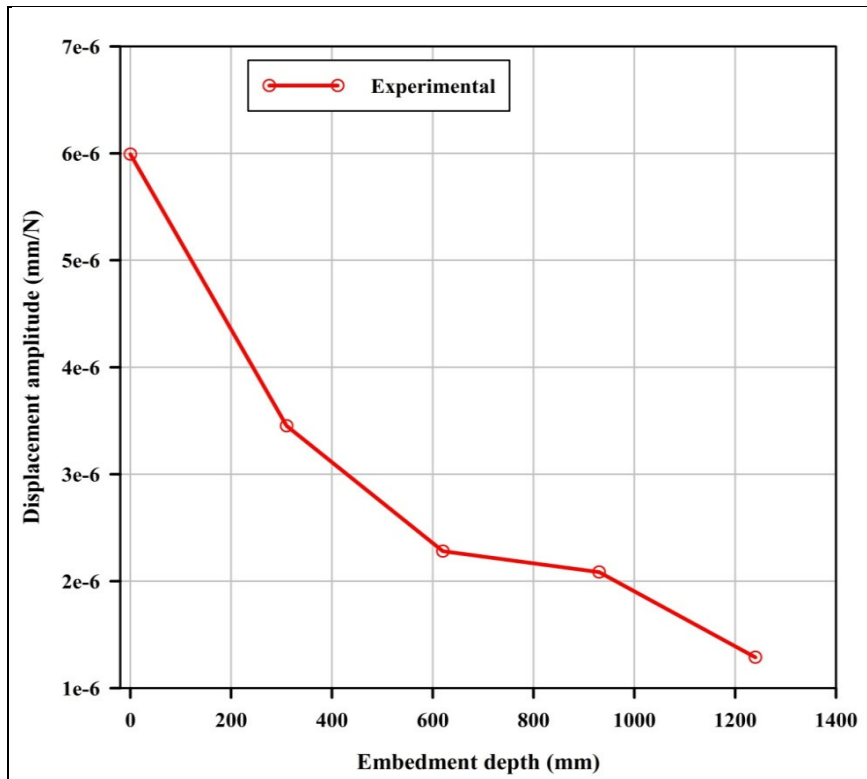
Figure 4.49: Displacement with increase in embedment depth

4-47
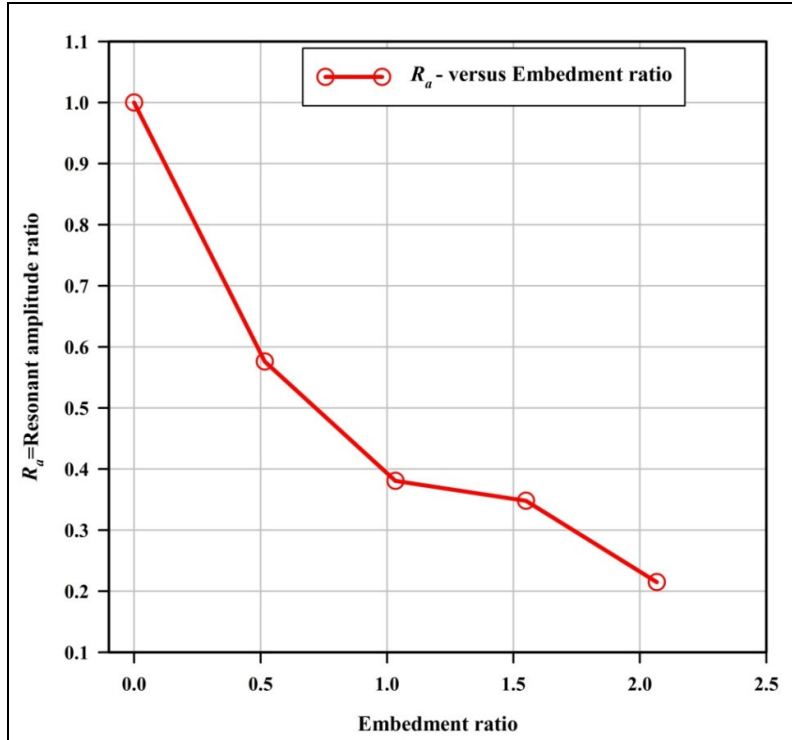
Figure 4.50: Effect of embedment on resonant amplitude ratio
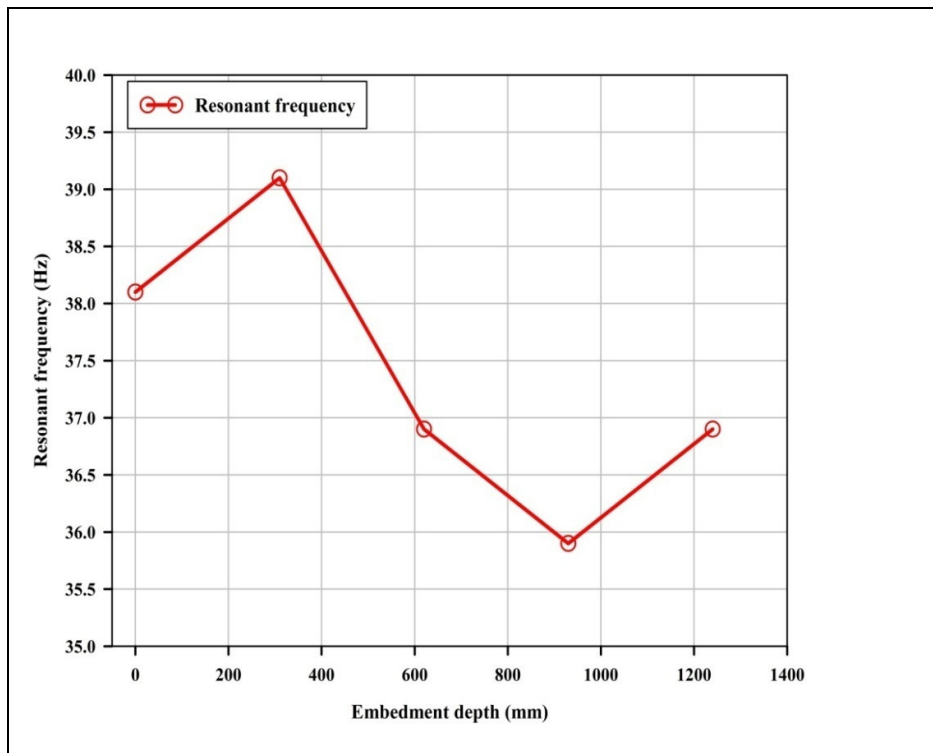
Figure 4.51: Effect of embedment on resonant frequency

4-48
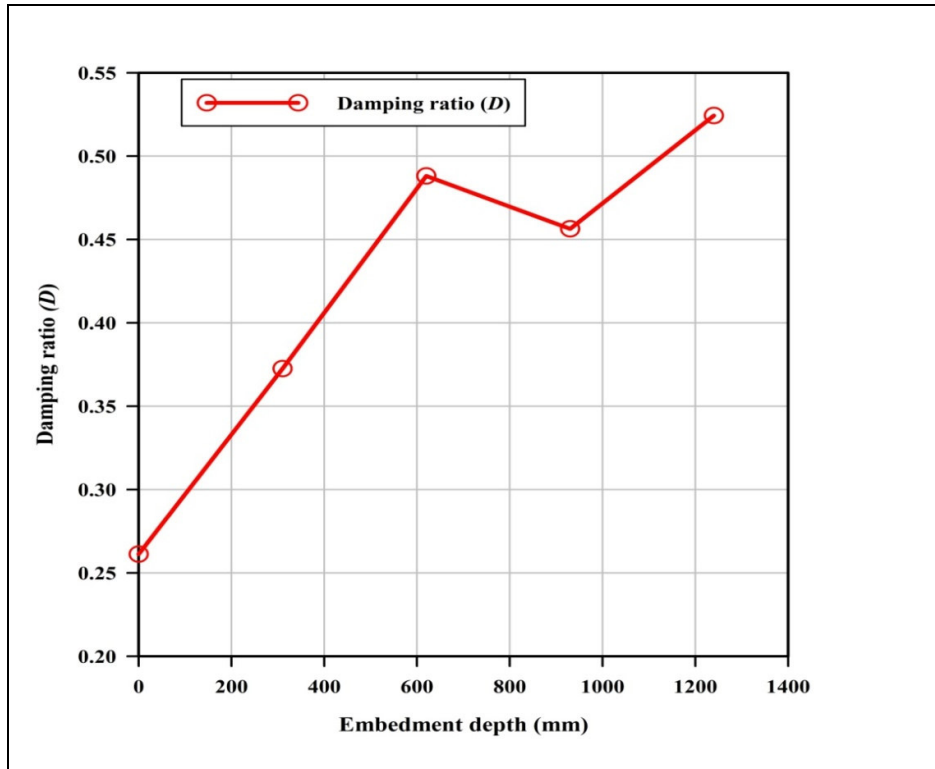
Figure 4.52: Effect of embedment depth on damping ratio
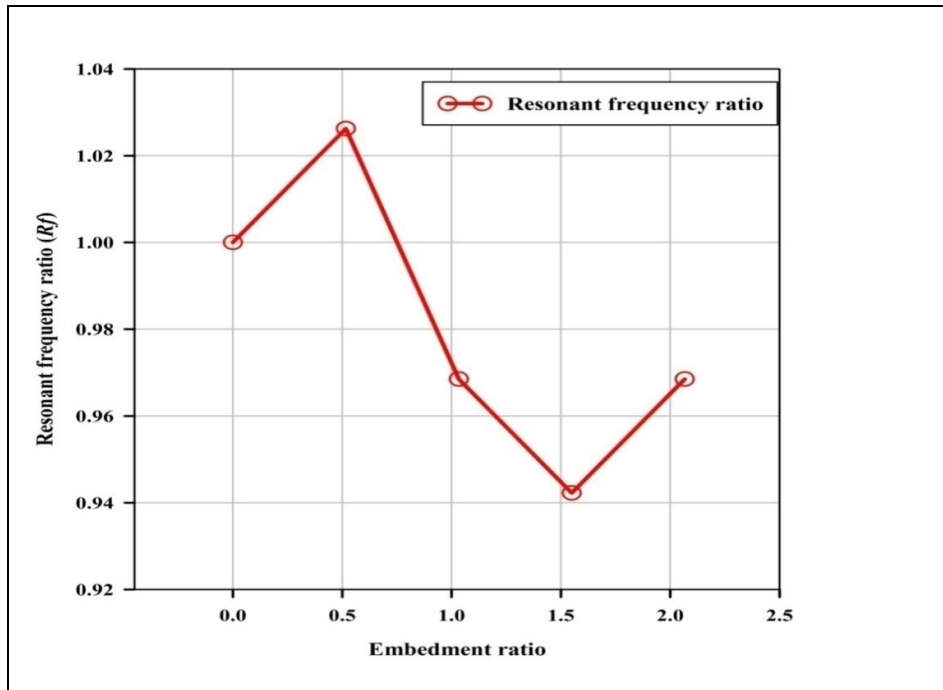
Figure 4.53: Effect of embedment depth on resonant frequency ratio

4-49
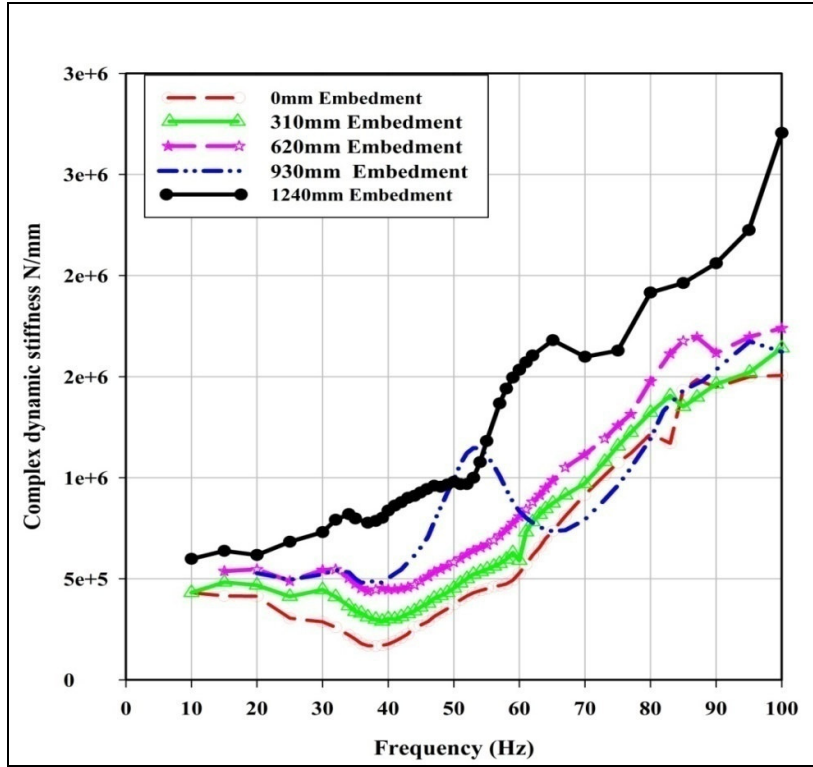
Figure 4.54: Complex dynamic stiffness for different embedment depths
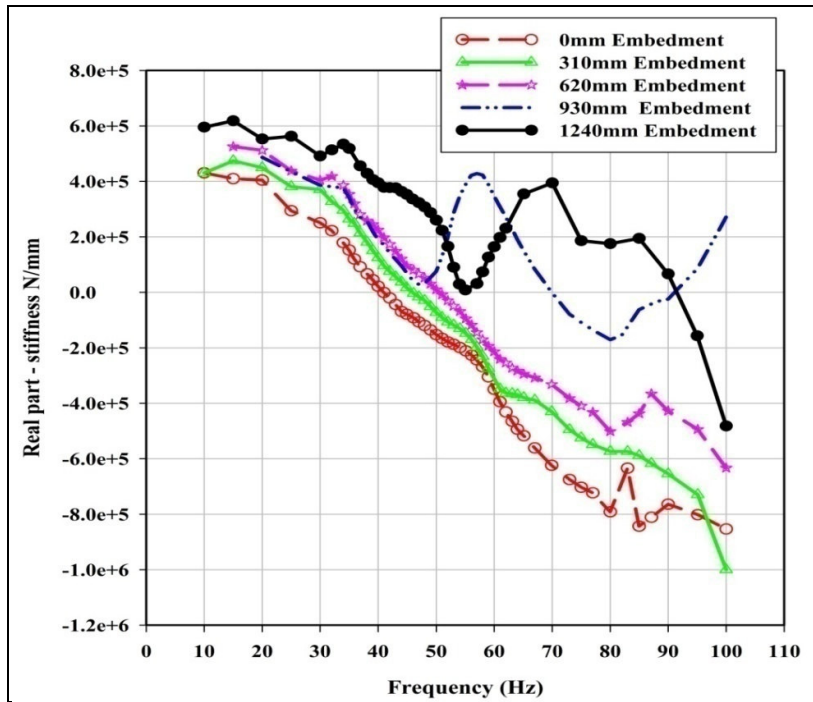
Figure 4.55: Plot of the real part versus frequency

4-50
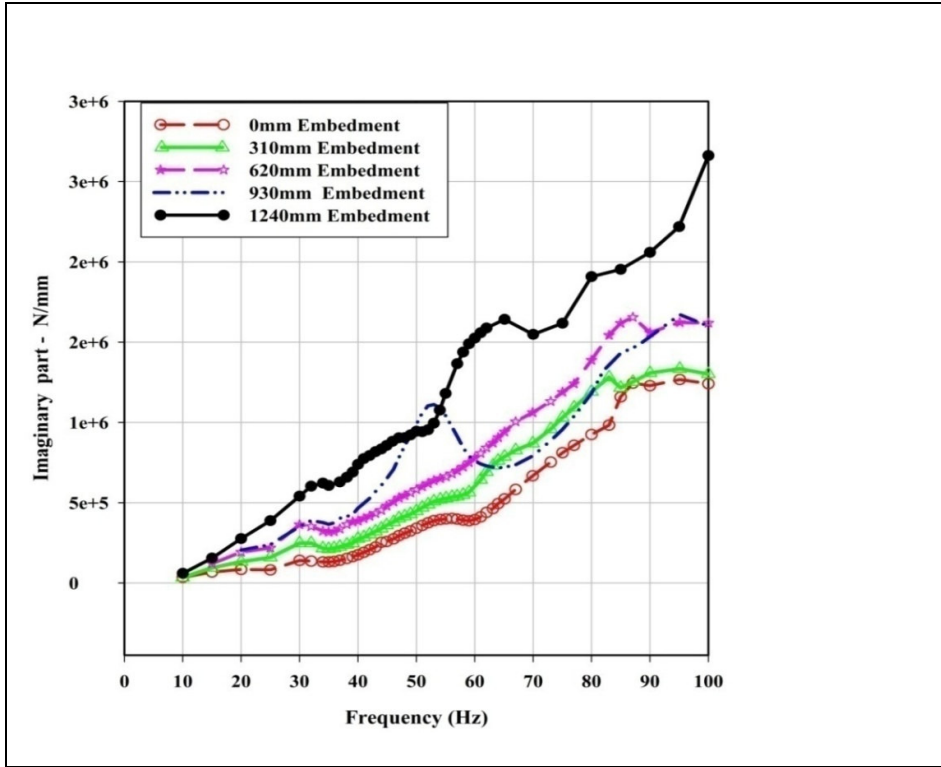
Figure 4.56: Imaginary part
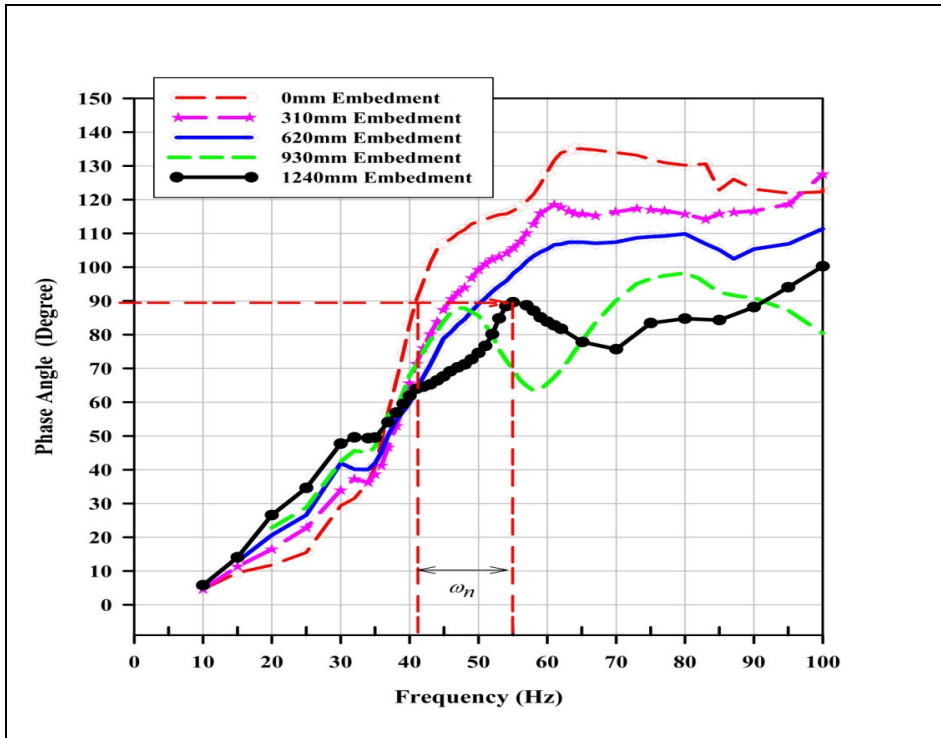
Figure 4.57: Phase angles for different embedment depths

4-51
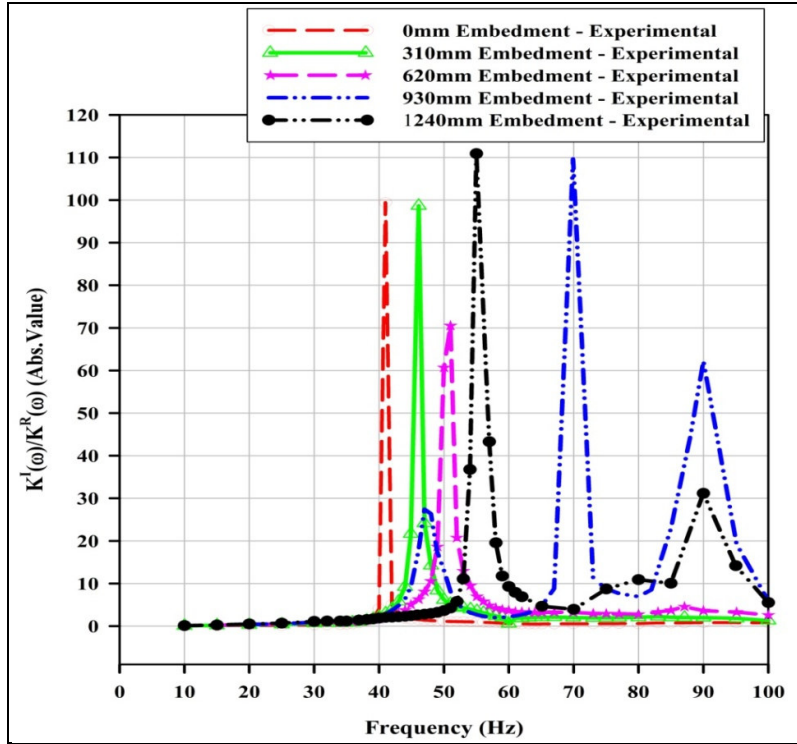
Figure 4.58: Loss angles against frequency for different embedment depths
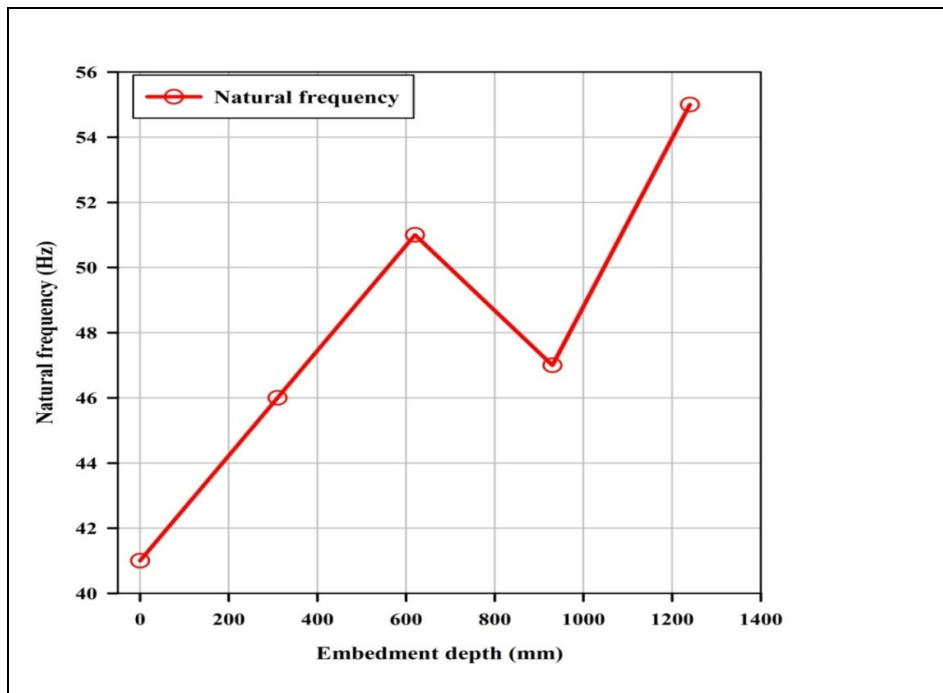
Figure 4.59: Natural frequency for 0, 310, 620 and 1240 mm embedment depths

4-52
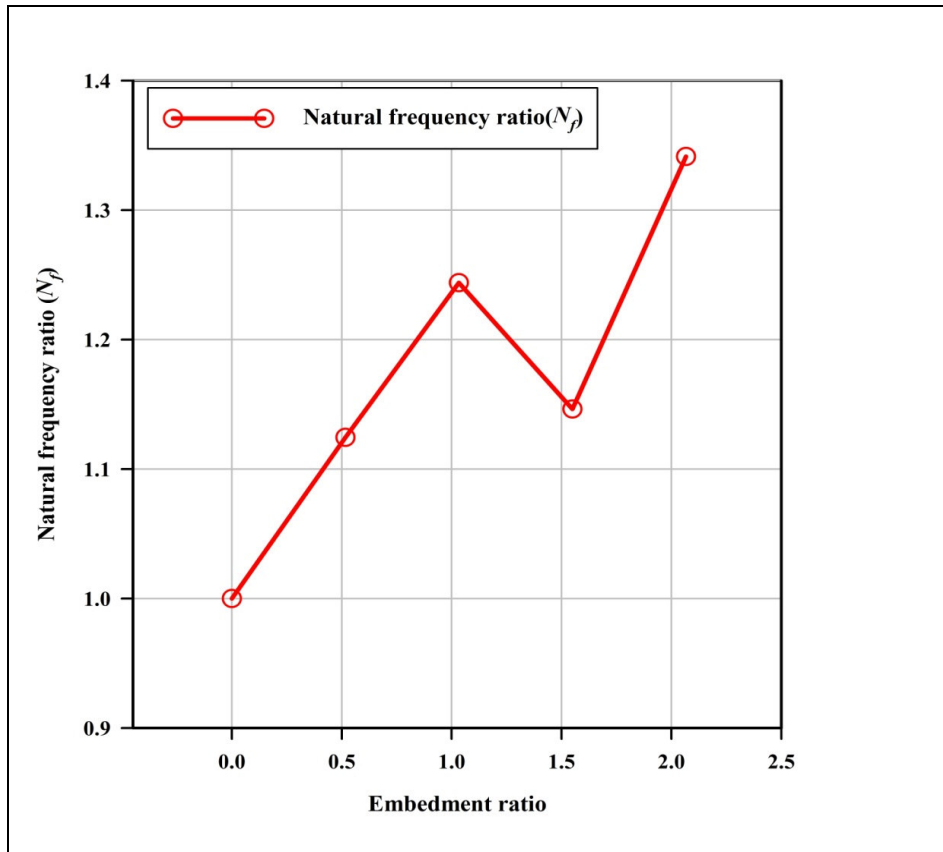
Figure 4.60: The effect of embedment on resonant frequency ratio

CHAPTER 5

5 SIMPLIFIED MODELS

5.1 Introduction

The objective of this chapter is to evaluate the accuracy of the simplified models in determining dynamic responses of the surface and embedded foundation systems. The vertical dynamic responses of the surface and embedded foundation systems, due to the vertical harmonic load, are determined using simplified models (analytical solution). The vertical dynamic responses of the foundation systems obtained using these solutions are compared with the responses obtained from field measurements. From this comparison, the the following analytical models were selected, and in order of increasing complexity are: Mass Spring Dashpot (MSD) or Winkler model, elastic half-space theory using Sung's (1953) displacement functions, Veletsos and Verbic (1973) massless soil, Lysmer (1965) model, Veletsos and Verbic (1973) soil with mass and Dyna5 program. The evaluation of embedded foundations is based on the analytical solutions suggested by Novak and Beredugo (1972) and the Dyna5 program.

5.2 Winkler model

The response of a footing resting on a semi-infinite medium (half-space) subjected to vertical dynamic loads can be modelled by using the Winkler model. The equilibrium of forces in the vertical direction including the inertia forces determine the dynamic response of the footing. The main parameter for the analysis using the Winkler model is the coefficient of elastic uniform compression of the soil (C_u). The spring constant (k_v) is obtained by multiplying the known base area of the footing and the coefficient of elastic uniform compression of the soil (C_u). The spring constant (k_v) is not a soil property as it depends on the contact area between the footing surface and the soil.

Although the Winkler model has inherent shortcomings, engineers widely use the model for analysis and design of machine foundations. The attractiveness of the model is due its simplicity and low computational effort. In principle, the Winkler model does not consider geometric and material damping of the vibrating system. In designing machine foundations, it is common to use the Winkler model with damping by introducing a

dashpot, which represents viscous damping of the system. The viscous damping used in the analysis is usually obtained from empirical formulae or charts.

5.2.1 Winkler model

The response of the surface foundation presented in Section 3.6 (Figure 3.12) was determined by using the Winkler model. The analysis using the Winkler model requires a spring constant. This was determined using three methods. The coefficient of elastic uniform compression obtained from field measurement using the Continuous Surface Wave test as well as vertical block vibration test. In addition, the coefficient of elastic uniform compression was taken from empirical values proposed by Barkan (1962). The theoretical dynamic response of the footing, with a dimension of 2500 mm x 2000 mm and 400 mm depth was determined using the spring constants tabulated in Table 4-4. The problem was reduced to an undamped single degree of freedom problem. In the analysis, it was assumed that the foundation system is subjected to loads with varying forcing frequency from 10.0 Hz to 100.0 Hz. The vertical harmonic forces of $P_v(t) = P_o sin(\omega t)$ excited the foundation system at the centre. The amplitude forces P_o used for analysis are presented in Figure 4.5.

The undamped natural frequency of the foundation system predicted by the linear elastic Winkler model is presented in Table 5-1 and Figure 5.1 shows the displacement amplitude. As expected for an undamped model, Figure 5.1 shows that the displacement at resonance becomes infinite. This indicates that the undamped Winkler model cannot predict the displacement of machine foundations at resonance.

The natural frequency of the foundation system obtained using Equation 2.7, which assumed that the half-space medium is massless. In the analysis the soil is replaced by an equivalent spring k_v. The undamped natural frequencies of the foundation system obtained from three different methods using Equation 2.7 are listed in Table 5-1. The plot of vertical displacement against forcing frequency is shown in Figure 5.1. For an undamped system, the resonant frequency is equal to the natural frequency of the foundation system. The natural frequency estimated using spring constants obtained from Continuous Surface Wave test, vertical block vibration, and empirical value proposed by Barkan (1962) ranges between 55.9 Hz and 59.0 Hz with an average of 57.8 Hz.

Table 5-1: Spring constant and Predicted natural frequency

Method	Spring constant k_s (N/m)	Predicted Natural frequency (Hz)
Wave propagation (CSW)	636,235,876.0	55.9
Vertical block vibration	709,302,152.0	59.0
Estimated using Barkan (1962)	693,671,752.3	58.5
Average Value	**679,736,593.5**	**57.8**

5.2.2 Damped Winkler model – Irish and Walker (1969)

Damping was introduced in the Winkler model to determine the vertical displacement amplitude of the foundation system. The damping ratio D was estimated using a method suggested by Irish and Walker (1969), they developed a chart to estimate the damping ratio of cohesive soil shown in Figure 5.2. The damping ratio for granular materials is 50 percent of the cohesive soil ($D_{granular\ soil} = 0.5 D_{cohesive\ soil}$). For the surface foundation $b = m / \rho R^3 = 1.3$ from which the damping ratio (D) can be estimated as 0.343 for Poisson's ratio of 0.25 as shown in Figure 5.2. This estimated damping ratio was used to analyse the dynamic response of the foundation systems using the damped Winkler model. The displacement amplitudes obtained from CSW test, vibration block test and empirical method suggested by Barkan (1962) are shown in Table 5-2. The plots of vertical displacement of the foundation system against frequency of excitation obtained from the damped Winkler model as well as the field measurements are shown in Figure 5.3. The plot shows that the Winkler model for the chosen damping ratio overestimates the vertical displacement. The error ranges between 23.3% and 27.8%. It may be seen that the predicted amplitude at any given frequency from the three damped Winkler models are similar. This is to be expected given that the same damping ratio and spring constants that differed only slightly were used as input parameters.

Table 5-2: Predicted displacement for damped Winkler model

Method	Maximum displacement (mm)	Frequency (Hz) at maximum displacement	% Error
Experimental results	0.0180	57.0	
Wave propagation (CSW)	0.0230	58.6	27.8
Vertical block vibration	0.0222	59.8	23.3
Estimated using Barkan (1962)	0.0223	59.8	23.9

The displacements were divided by force in order to establish the frequency response function for the Winkler model with damping. The resonant frequencies were determined as the peak of the frequency response function. These frequency response functions using spring constant obtained from Continuous Surface Wave test, vertical block vibration and empirical value proposed by Barkan (1962) are shown in Figure 5.4; the estimated resonant frequencies are 49.0 Hz, 51.5 Hz and 52.1 Hz respectively. The resonant frequency of the surface foundation system obtained from the field-measured data is 45 Hz. The percentage of error with reference to the resonant frequency obtained from field-measured data is presented in Table 5-3. It is shows that the spring constant obtained from the seismic test (CSW) resulted in the most accurate prediction of resonant frequency compared to the vertical block vibration and empirical value proposed by Barkan (1962).

Table 5-3: Predicted resonant frequency for damped Winkler model

Method	Predicted resonant frequency (Hz)	% Error
Wave propagation (CSW)	49.0	+8.9
Vertical block vibration	51.5	+14.4
Estimated using Barkan (1962)	52.1	+15.8

5.3   Models based on Elastic half–space theory

Reissner (1936) established the theoretical basis for studying the response of dynamic loaded footing which is supported by an elastic half-space. Reissner assumed the soil is a semi-infinite, homogeneous, elastic and isotropic body. In the analysis, the soil is defined by small strain shear modulus (G), Poisson`s ratio (ν) and mass density (ρ). In the following sections the vertical dynamic responses of the surface foundation described in Figure 3.12 (Section 3.6), will be analysed using elastic half-space theory applying Sung's (1953) displacement functions, Lysmer (1965) model and Veletsos and Verbic (1973) simplified models.

5.3.1   Sung (1953)

Sung (1953) extended Reissner's solution and developed equations for three cases of contact pressure distribution on a circular loaded area and reported the solution in series form for various Poisson's ratios from which f_1 and f_2 is calculated. Sung's

5-4

displacement functions for a rigid footing were used to solve Equation 2.1 using the soil parameters shown in Table 4-1.

Displacement amplitude

The surface footing presented in Section 3.5 (Figure 3.10) was simulated using the analytical solution by exerting the vertical loads measured in the field. The response of the foundation systems was determined using Sung's displacement functions. The vertical displacement of the foundation system is shown in Figure 5.5.

In addition, the displacement for the analytical solution at the frequency of $1.25 \times fmax$ and $0.75 \times fmax$ is compared with the one obtained experimentally as shown in Table 5.4, where $fmax$ is the frequency at the maximum displacement amplitude.

The displacement percentage error in comparison to the experimental results at maximum displacement is 45.6%. The percentage error for displacement at 0.75fmax and 1.25fmax is 38.5% and 55.5% respectively.

Complex dynamic stiffness

The complex dynamic stiffness, obtained using Sung's solution, is shown in Figure 5.6. From these results, it is indicated that at low frequencies the complex dynamic stiffness decreases as the frequency increases. For the analytical solution, as the frequency increases the stiffness decreases down to approximately 59.0 Hz, and then increases. The complex dynamic stiffness measured in the field decreases to about 45.0 Hz, then increases as the frequency increases. The results reflect that at low frequencies the complex dynamic stiffness obtained from Sung's solution are similar compared with the complex dynamic stiffness obtained experimentally. At frequencies between 10Hz and 45Hz the complex dynamic stiffness determined using Sung (1953) displacement function differs from the experimental value by approximately between 27 % and 31.6% respectively.

Table 5-4: Predicted displacement for Sung (1953) solution to field-measured data

Method	Displacement (mm)			Estimated frequency (Hz)	% Error		
	0.75*fmax*	*fmax*	+1.25*fmax*	*fmax*	0.75*fmax*	*fmax*	+1.25*fmax*
Experimental results	0.013	0.018	0.011	56.1	62.9	45.6	55.5
Analytical–Sung (1953)	0.00483	0.0098	0.004894	55			

5-5

Real part of complex dynamic stiffness

A comparison between the real parts, which are referred as the effective dynamic stiffness, taken from the field-measured data with the effective dynamic stiffness obtained from Sung's solution, is shown in Figure 5.7. The responses show that at the low frequency, the effective dynamic stiffness from the field-measured data is lower than the effective dynamic stiffness stated in Sung's solution. At a frequency of 10.0 Hz, effective dynamic stiffness from Sung's solution is higher than effective dynamic stiffness obtained from field-measured data by about 28.8 %; this difference is maintained to about 50.0 Hz. At frequency above 50.0 Hz, the difference increased.

The natural frequency of the foundation system can be obtained from the plot of the real part versus the forcing frequency when the effective dynamic stiffness (real part) crosses zero. From Figure 5.7, the curve plotted from Sung's solution crosses zero at 57.9 Hz while the curve plotted from field-measured data crosses zero at 49.0 Hz. Therefore, Sung's solution overestimates natural frequency by about 20.4 %.

Imaginary part of complex dynamic stiffness

Figure 5.8 illustrates the relationship between the imaginary part and the frequency of excitation for Sung's solution, and the one measured in the field. From Figure 5.8, it is shown that the imaginary part determined analytically increases as the frequency increases up to a forcing frequency of about 79.0 Hz and there after it decreases. The imaginary part measured in the field increases as the forcing frequency increases.

Phase and loss angle

The plot of phase angle versus frequency of excitation obtained experimentally and Sung's solution is shown in Figure 5.9. Phase angles between forcing function and footing displacement are given in Equation 2.14. Figure 5.9 shows the plot of phase angle between forcing function and footing displacement. The vertical displacement of footing becomes out of phase with the forcing function at the frequency of 58 Hz which is taken to be the natural frequency of the foundation system, the one measured in the field is 49.0 Hz. Sung (1953) solutions over estimates the natural frequency by about 17.3 % compared to the field-measured natural frequency.

The loss angles estimated from results collected from the field-measured data and those obtained from the analytical solution by Sung's solution are shown in Figure 5.10. The

natural frequency obtained from Sung's solution is 59.4 Hz while field-measured data estimates natural frequency of 49.4 Hz. From the results, Sung's solution overestimates natural frequency by about 20.2 %.

5.3.2 Lysmer (1965) model

The response of the surface foundation presented in Section 3.5 (Figure 3.10) was analysed by using Lysmer (1965) model discussed in section 2.4 and the results compared to the field measurements. This section will discuss the displacement amplitude, complex dynamic stiffness, the real part, the imaginary part, phase angle and loss angels of the surface foundation system.

Displacement amplitude

The measured vertical displacement response of the foundation system due to vertical excitation is shown in Figure 5.11 and compared to the analytical solution proposed by Lysmer (1965) model.

The error in comparison to the experimental results at maximum displacement is 31.9 %. The percentage errors for 0.75*fmax* and 1.25*fmax* are shown in Table 5.5.

Complex dynamic stiffness

Figure 5.12 shows that the complex dynamic stiffness obtained from Lysmer (1965) model increases as the frequency of excitation increases. The trends from observed and predicted curves are similar. The complex dynamic stiffness determined using Lysmer (1965) model at low frequency is higher than the complex dynamic stiffness obtained from field-measured data. As the frequency increases, the different between the predicted and measured complex stiffness increases up to the measured resonant frequency. At the frequency of 100 Hz the predicted and measured complex stiffness is almost the same.

Table 5-5: Predicted displacement for by Lysmer (1965) model

Method	Displacement (mm)			Estimated frequency (Hz	% Error		
	0.75*fmax*	*fmax*	+1.25*fmax*	*fmax*	0.75*fmax*	*fmax*	+1.25*fmax*
Experimental results	0.013	0.018	0.011	56.1	56.2	31.9	1.8
Lysmer (1965) model	0.00569	0.01226	0.0112	63.0			

Real part of complex dynamic stiffness

A comparison between the measured and predicted real parts by Lysmer (1965) model is shown in Figure 5.13. The plot indicates that Lysmer (1965) model predicts high effective dynamic stiffness at the low frequencies compared to the field-measured effective dynamic stiffness. The response show that from the frequency of 10.0 Hz to about 70 Hz the effective dynamic stiffness obtained from Lysmer (1965) model solution is higher by about 29% compared to the effective dynamic stiffness obtained from field-measured data. Lysmer (1965) model predicts the natural frequency of the foundation system as 57.5 Hz. From the plot of the real part against forcing frequency, it is shown that Lysmer (1965) model solution overestimates natural frequency by about 17.3 %.

Imaginary part of complex dynamic stiffness

Figure 5.14 present the measured imaginary part, and imaginary part obtained from analytical solution using Lysmer (1965) model. From Figure 5.14, it is shown that measured and predicted imaginary part of complex dynamic stiffness increases as the forcing frequency increases. The imaginary part determined using Lysmer (1965) model at low frequency is higher than the imaginary part obtained from field-measured data. As the frequency increases the different between the predicted and measured imaginary part increased up to about 45 Hz. Thereafter, the different is small and at the frequency of 100 Hz the predicted and measured imaginary part is almost the same.

Phase and loss angles

The plot of phase angles versus frequency of excitation obtained from field-measured data and from Lysmer (1965) model is shown in Figure 5.15. From Figure 5.15, the natural frequency of the foundation system estimated using Lysmer (1965) model solution is 57.5 Hz. Lysmer (1965) model overestimated the natural frequencies by about 17.3 %.

Figure 5.16 shows the measured and predicted loss angles. Lysmer (1965) model solution estimates natural frequency of 57.4 Hz. This predicted model overestimates natural frequency by 17.1 %.

5.3.3 Veletsos and Verbic (1973) – massless soil

The vertical dynamic responses of the surface foundation system described in Section 3.5, (Figure 3.10) were determined using the analytical solution proposed by Veletsos and Verbic (1973) massless soil as discussed in section 2.5.1. This solution assumes that the mass of the footing and the supporting medium is zero as shown in Figure 2.2. In Figure 5.17, the response from analytical solution by Veletsos and Verbic (1973) is plotted together with the vertical displacement response of the foundation system obtained from the field-measured data.

The error between predicted and measured maximum displacement is 38.4 %. The percentage errors for displacement at 0.75*fmax* and 1.25*fmax* are shown in Table 5.6.

Complex dynamic stiffness

The complex dynamic stiffness of the foundation system obtained using Veletsos and Verbic (1973) assuming that soil medium is massless is shown in Figure 5.18. The complex dynamic stiffness for analytical solution decreases as the frequency excitation increases as shown in Figure 5.18. The difference is almost constant at the low frequencies and at about 55.0 Hz the measured and predicted complex dynamic stiffness is the same, there after as the frequency increases the different between two becomes large.

Table 5-6: Predicted displacement for Veletsos and Verbic (1973) massless soil

Method	Displacement (mm)			Estimated frequency (Hz)	% Error		
	0.75*fmax*	*fmax*	+1.25*fmax*	*fmax*	0.75*fmax*	*fmax*	+1.25*fmax*
Experimental results	0.013	0.018	0.011	56.1	54.6	38.4	13.5
Veletsos and Verbic (1973)	0.0059	0.01108	0.00951	60.0			

Real part of complex dynamic stiffness

A comparison between the plots for the real parts obtained experimentally and that from the analytical solution proposed by Veletsos and Verbic (1973) massless soil is shown in Figure 5.19. At low frequencies, the real part obtained from the field-measured data is lower than the effective dynamic stiffness obtained from Veletsos and Verbic (1973) solution. The difference between the two increases as the frequency increases. At

5-9

10.0 Hz, the difference is about 29.6 % with a maximum difference of 260% at 100.0 Hz.

The natural frequency of the foundation system can be obtained at the point where the plot of the real part versus frequency crosses a zero line. From Figure 5.19, it shows that the plot of the real part against frequency by Veletsos and Verbic (1973) massless soil does not cross zero due to the absence of inertia forces.

Imaginary part of complex dynamic stiffness

Figure 5.20 illustrates the relationship between the imaginary part versus the frequency of excitation for the field-measured data and the solution obtained using Veletsos and Verbic (1973) massless soil. The plot of the imaginary part obtained from the analytical solution is a straight line indicating that the imaginary part is proportional to excitation frequency. At the low frequency, the imaginary part obtained from Veletsos and Verbic (1973) solution is higher compared to measured imaginary part. As the frequency of excitation increases the difference increases and attained the maximum at about 60 Hz.

Phase and loss angles

The plot of phase angle between force and displacement versus frequency of excitation measured experimentally and the one obtained from the analytical solution by Veletsos and Verbic (1973) massless soil is shown in Figure 5.21. The estimated natural frequency of the foundation system using Veletsos and Verbic (1973) solution is 57.5 Hz. Veletsos and Verbic (1973) solution overestimates the natural frequency by about 17.3 %.

5.3.4   Veletsos and Verbic (1973) – Soil with mass

The foundation displacement response obtained using the analytical solution assuming that the elastic half-space and footing has masses, as proposed by Veletsos and Verbic (1973), is compared with the vertical displacement response obtained from field-measured data as is shown in Figure 5.22.

The displacement error when comparing results at maximum displacement is 56.2 %. The percentage errors for displacement at 0.75*fmax* and 1.25*fmax* are shown in Table 5.7.

Complex dynamic stiffness

The complex dynamic stiffness obtained using the solution proposed by Veletsos and Verbic (1973) soil with mass is shown in Figure 5.23. The complex dynamic stiffness obtained from the analytical solution is constant from 10 up to about 20 Hz. The maximum and minimum difference occurs at the frequence of 45 Hz and 100 Hz respectively. As the frequency of excitation increases, the complex dynamic stiffness increases. The trend of the plotted curves of the complex dynamic stiffness obtained from field measurements and the analytical solution by Veletsos and Verbic (1973) are similar.

Table 5-7: Predicted displacement for Veletsos and Verbic (1973) soil with mass

Method	Displacement (mm)			Estimated frequency (Hz)	% Error		
	0.75$fmax$	$fmax$	+1.25$fmax$	$fmax$	0.75$fmax$	$fmax$	+1.25$fmax$
Experimental results	0.013	0.018	0.011	56.1	63.5	56.2	40.5
Veletsos and Verbic (1973)	0.00475	0.00789	0.00655	59.0			

Real part of complex dynamic stiffness

A comparison between the real part obtained from the field measurements and the solution proposed by Veletsos and Verbic (1973) soil with mass is shown in Figure 5.24. The response shows that at the low frequencies, the effective dynamic stiffness obtained from the field-measured data is lower than the effective dynamic stiffness using the analytical solution proposed by Veletsos and Verbic (1973). The plots show that in the frequency range of about 30.0 Hz to 70.0 Hz, the predicted real part is very similar to the measured data. The plot of real part against frequency by Veletsos and Verbic (1973) crosses zero at 50.3 Hz. The solution by Veletsos and Verbic (1973) with mass closely predicts the measured natural frequency, overestimating it by about 2.7 %.

Imaginary part of complex dynamic stiffness

The plot of imaginary part against frequency obtained from field-measured data, and the one from the analytical solution proposed by Veletsos and Verbic (1973) are reflected in Figure 5.25. The plot of the imaginary part obtained from the analytical solution is a straight line indicating that the imaginary part is proportional to excitation frequency. The imaginary part from the field-measured data, show that as the frequency increases

the imaginary part increases. At 10.0 Hz the difference is about 116.7% with maximum difference of 204% at about 43.0 Hz above 43.0 Hz the difference decreased to about 15.6 % at 100.0 Hz.

Phase and loss angles

The plot of phase angle between force and displacement versus frequency of excitation measured in the field and that obtained from analytical solution by Veletsos and Verbic (1973) soil with mass is shown in Figure 5.26. Here the natural frequency of the foundation system estimated by using Veletsos and Verbic (1973) solution is 50.0 Hz. The natural frequency of the foundation system obtained from field-measured data is 49.0 Hz. Veletsos and Verbic (1973) solution overestimates the natural frequency by about 2.0%.

The loss angles obtained from field-measured data and analytical solution by Veletsos and Verbic (1973) soil with mass is shown in Figure 5.27. From the plot of the loss angle against forcing frequency the estimated natural frequency is 50 Hz. The natural frequency estimated from loss angle overestimates the natural frequency by 2% compared to the natural frequency obtained from field-measurements.

Estimation of damping ratio

The undamped natural frequency of the foundation system can be obtained at the intersection between the curve of dynamic stiffness coefficient (real part) and the curve of Equation 5.1 as illustrated in Figure 5.28 (Ahn 2007 and Ahn et al., 2011).

$$k(\omega) = \frac{m\omega^2}{K_o}$$
Equation 5.1

Using Veletsos and Verbic (1973) the undamped natural frequency of the foundation system is 50.0 Hz. This undamped natural frequency can be used to measure damping ratio using damping constants estimated from Figure 5.29. The damping ratio (D) is calculated using Equation 5.2.

$$D = \frac{c}{2M\omega_o}$$
Equation 5.2

Where:

c is the damping constant, and

M is the mass of the footing.

5.3.5 Numerical method using Dyna 5 program

The response of the surface foundation systems described in Section 3.5 (Figure 3.10) was determined using the Dyna5 analysis program. Dyna5 program is a popular computer program which is widely used in industry and therefore it was important to include it in this study. Dyna5 program is based on Veletsos and Verbic (1973) massless soil model.

The forces exerted on the surface foundation in the field with their respective forcing frequencies as shown in Figure 4.5 were used as input in the Dyna5 program. The response of the foundation system for each frequency was calculated to obtain the displacement, dynamic stiffness coefficient, and damping coefficient, phase shift and magnification factor.

For comparison purposes, the vertical response obtained from the Dyna5 program is plotted together with the vertical displacement response of the foundation system obtained from field-measurements as shown in Figure 5.30. The plots show that Dyna5 program underestimates the maximum vertical displacement amplitude by about 56.2 %. The percentage errors for displacement at 0.75$fmax$ and 1.25$fmax$ are shown in Table 5-8.

Complex dynamic stiffness

The complex dynamic stiffness obtained from the Dyna5 program is shown in Figure 5.31 and this stiffness from Dyna5 program increases as the frequencies increase, as shown in Figure 5.31. The plot shows that complex dynamic stiffness determined from Dyna5 program is higher than the complex dynamic stiffness obtained from field-measured data.

Table 5-8: Predicted displacement for Dyna5 program

Method	Displacement (mm)			Estimated frequency (Hz)	% Error		
	0.75$fmax$	$fmax$	+1.25$fmax$	$fmax$	0.75$fmax$	$fmax$	+1.25$fmax$
Experimental results	0.013	0.018	0.011	56.1	65.5	56.2	37.6
Dyna5 program	0.00449	0.00789	0.006867	59.0			

Real part of complex dynamic stiffness

The plots of the real part taken from the field-measured data and the one from Dyna5 program are shown in Figure 5.32. The real part obtained from the field-measured data is lower than the effective dynamic stiffness obtained from Dyna5 program. As the frequency increases, the differences between predicted and measured real part increases. The differences increased from 29.6 % to 136.5% for the frequency of 10.0 Hz and 100 Hz respectively.

Imaginary part of complex dynamic stiffness

The plot of imaginary part against forcing frequency obtained from field-measured data, and the one obtained from Dyna5 is shown in Figure 5.33. The plot of the imaginary part obtained from Dyna5 program is a straight line which indicates that the imaginary part is proportional to excitation frequency.

Phase angles

The plots of phase angle between force and displacement versus frequency of excitation for field-measured data and from the Dyna5 program are shown in Figure 5.34. From this, the natural frequency of the foundation system estimated from Dyna5 program is 50.3 Hz, while the natural frequency of the foundation system obtained from field-measured data is 49.0 Hz. Hence, Dyna5 program overestimates natural frequency by 2.6 %.

5.3.6   Embedded foundation by Novak and Beredugo (1972)

The vertical dynamic behaviour of the embedded footing as described in Chapter 3 (Section 3.7) was determined by using the analytical solution proposed by Novak and Beredugo (1972). The forces exciting the foundation system were measured in the field and used to model the vertical excitation. However, in this section, the responses due to a unit load are also reported. The mathematical models illustrating the embedment depth are shown in Figures 5.35(a) to 5.35(e).

The responses of the foundation system for different embedment were determined using parameters shown in Table 5-9. An assumed Poisson's ratio of 0.25 was used to analyse the responses of all embedment layers. Because it was assumed that the displacement of the foundation is within the linear elastic range, material damping was not considered in this analysis. The shear modulus of the elastic half-space was taken as 100 MPa base on

the CSW test results. The shear modulus of the side soil layers was calculated using Equation 2.58. The vertical dynamic responses that will be presented in this section are displacement amplitude, resonant amplitude, resonant frequency, complex dynamic stiffness, the real part of the complex dynamic stiffness, the imaginary part of complex dynamic stiffness and the phase angle between the force and the displacement. The dimensionless quantities used to describe the effects of the foundation embedment are the resonant amplitude ratio, resonant frequency ratio and natural frequency ratio.

Table 5-9: Input parameters for Novak and Beredugo (1972) and Dyna5 program

Embedment depth (m)	Density of soil - side layer ρ_s (kg/m^3)	Unit weight of soil - side layer γ_s (kN/m^3)	Shear modulus of soil - side layer -G_s (MPa)	Shear wave velocity – side layer V_s (m/s)
0	2028	19.895	100	222.1
310	2040	20.042	102	224.0
620	2078	20.385	108	228.0
930	2095	20.552	110	229.0
1240	2043	20.042	102	224.0

Displacement amplitude

The vertical displacement response of the embedded foundation systems was determined using the analytical solution proposed by Novak and Beredugo (1972) for embedment of 0 mm, 310 mm, 620 mm, 930 mm and 1240 mm. The vertical displacement amplitude of the foundation system is shown in Figure 5.36. From the plots, it is shown that as the embedment increases, the displacement amplitudes decreases.

In addition, the displacement of the analytical solution at the frequency of $1.25 \times fmax$ and $0.75 \times fmax$ for embedment of 0 mm, 310 mm, 620 mm, 930 mm and 1240 mm is compared with the one obtained experimentally as shown in Table 5.10 to Table 5.14, where *fmax* is the frequency at the maximum displacement amplitude.

The displacement percentage error in comparison to the experimental results at maximum displacement at 0 mm, 310 mm and 620 mm embedment is 2 %, 3.8 % and 2 % respectively. At embedment of 930 mm and 1240 mm the error is 33.3% and 30.4 % respectively. The prediction models overestimated displacement amplitude at 0 mm, 310 mm and 1240 mm embedment and underestimated displacement amplitude at embedment of 620 mm and 930 mm.

5-15

Table 5-10: Predicted displacement for 0mm Embedment - Novak and Beredugo (1972)

Method	Displacement (mm)			Estimated frequency (Hz)	% Error		
	0.75f_{max}	f_{max}	+1.25f_{max}	f_{max}	0.75f_{max}	f_{max}	+1.25f_{max}
Experimental results	0.0177	0.0206	0.0101	58.8	+11.3	2.0	25.7
Novak and Beredugo (1972)	0.0197	0.021	0.0127	57.6			

Table 5-11: Predicted displacement for 310mm Embedment - Novak and Beredugo (1972)

Method	Displacement (mm)			Estimated frequency (Hz)	% Error		
	0.75f_{max}	f_{max}	+1.25f_{max}	f_{max}	0.75f_{max}	f_{max}	+1.25f_{max}
Experimental results	0.0146	0.0185	0.0106	57.6	-15.1	+3.8	+16.0
Novak and Beredugo (1972)	0.0124	0.0192	0.0123	57.6			

Table 5-12: Predicted displacement for 620mm Embedment - Novak and Beredugo (1972)

Method	Displacement (mm)			Estimated frequency (Hz)	% Error		
	0.75f_{max}	f_{max}	+1.25f_{max}	f_{max}	0.75f_{max}	f_{max}	+1.25f_{max}
Experimental results	0.0103	0.0145	0.0093	56.0	21.4	2.0	0
Novak and Beredugo (1972)	0.0081	0.0139	0.0093	57.3			

Table 5-13: Predicted displacement for 930mm Embedment - Novak and Beredugo (1972)

Method	Displacement (mm)			Estimated frequency (Hz)	% Error		
	0.75f_{max}	f_{max}	+1.25f_{max}	f_{max}	0.75f_{max}	f_{max}	+1.25f_{max}
Experimental results	0.0051	0.0132	0.0039	65.8	-7.8	33.3	12.8
Novak and Beredugo (1972)	0.0055	0.0088	0.0034	62.4			

Table 5-14: Predicted displacement for 1240mm Embedment - Novak and Beredugo (1972)

Method	Displacement (mm)			Estimated frequency (Hz)	% Error		
	0.75f_{max}	f_{max}	+1.25f_{max}	f_{max}	0.75f_{max}	f_{max}	+1.25f_{max}
Experimental results	0.0040	0.0079	0.0050	58.8	+2.5	30.4	0
Novak and Beredugo (1972)	0.0039	0.0103	0.0050	57.6			

Resonant amplitude

The resonant amplitudes due to the vertical unit load using the analytical solution proposed by Novak and Beredugo (1972) are presented in Table 5-15. The plot of the displacement versus the frequency of excitation due to a unit load for different embedment depth is shown in Figure 5.37. This reflects that as the embedment increases, the resonant amplitudes decreases. The model predicts that at an embedment depth of more than approximately 600mm, the displacement versus frequency plot no longer exhibits a peak.

Resonant amplitude ratio

The resonant amplitude ratio is calculated using Equation 2.47. The predicted resonant amplitude ratios from different embedment are shown in Table 5 -15. From Table 5 -15, it can be seen that the resonant amplitude ratio decreases significantly as the embedment increases. At full embedment, the resonant amplitude is only 23.2% of the amplitude at zero embedment.

Table 5-15: Predicted resonant amplitude and resonant amplitude ratios for Novak and Beredugo (1972)

Embedment depth (m)	Embedment ratio	Resonant amplitude (mm/N)	Resonant amplitude ratio -
0	0	0.000005068	1
310	0.52	0.000002770	0.547
620	1.03	0.000001856	0.366
930	1.55	0.000001384	0.273
1240	2.07	0.000001178	0.232

Resonant frequency

The predicted resonant frequencies of the embedded foundation systems can be determined from Figure 5.37 and from the plot of the magnification factor versus the forcing frequency. Figure 5.38 illustrates the magnification factor for different embedments obtained using Novak and Beredugo (1972) analytical solution. For each plot the resonant frequency was taken as the one which corresponds to peak value. For embedment between 600mm and 1240mm no peak value is clear as the plot has no peak. Because there is an insignificant change between the resonant frequency between 310mm and 620mm embedment, the resonant frequencies for 620mm, 930 and 1240mm were taken as the same value of resonant frequency for embedment of 620mm. The resonant frequencies obtained from Figures 5.37 and 5.38 are presented in Table 5-16.

5-17

Table 5-16: Predicted resonant frequency and resonant frequency ratio for Novak and Beredugo (1972)

Embedment depth (m)	Embedment ratio	Resonant frequency (Hz)	Resonant frequency ratio
0	0	36.1	1
310	0.52	33.5	0.928
620	1.03	33.5	0.928
930	1.55	33.5	0.928
1240	2.07	33.5	0.928

Resonant frequency ratio

The effect of embedment on the resonant frequency of the foundation system can be explained using a dimensionless parameter known as the resonant frequency ratio. The resonant frequency ratios predicted, using the analytical solution as suggested by Novak and Beredugo (1972), are presented in Table 5-16. It shows that the resonant frequency ratio decreases as the embedment increases up to an embedment ratio of 0.5, and then, remains constant as the embedment ratio increases.

Complex dynamic stiffness

Figure 5.39 shows the vertical complex dynamic stiffness for different embedments obtained from Novak and Beredugo (1972). From the plot is shown that as the embedment increases the complex dynamic stiffness increases.

Real part of complex dynamic stiffness

The real part determined by using Novak and Beredugo (1972) analytical solution obtained from different embedments is shown in Figure 5.40. From the plot is shown that as the embedment increases the real part of complex dynamic stiffness increases.

Imaginary part of complex dynamic stiffness

The imaginary part obtained using Novak and Beredugo (1972) analytical solution for different embedment is shown in Figure 5.41 and this describes that as the embedment increases, the imaginary part of complex dynamic stiffness increases.

Phase angles

The plots of phase angle between force and displacement versus frequency obtained from the analytical solution by Novak and Beredugo (1972) for different embedments

are shown in Figure 5.42. The plots of phase angles versus frequencies are used to estimate the natural frequencies of embedded foundation systems. From these, it is predicted that as embedment increases the natural frequency will increase. The natural frequencies of the embedded foundation for different embedments obtained from analytical solutions are shown in Table 5-17.

Natural frequency ratio

The effect of foundation embedment can be described by the dimensionless quantity known as the natural frequency ratio (N_f) calculated by equation 4.18. The natural frequency ratio predicted by Novak and Beredugo (1972) solution are presented in Table 5-17 which illustrates that the natural frequency ratio increases as the embedment increases.

Table 5-17: Predicted natural frequency and Natural frequency ratio for Novak and Beredugo (1972)

Embedment depth (m)	Embedment ratio	Natural frequency (Hz)	Natural frequency ratio
0	0	40.3	1
310	0.52	45.7	1.134
620	1.03	51.0	1.266
930	1.55	56.0	1.390
1240	2.07	59.0	1.464

5.3.7 Embedded foundation numerical analysis - Dyna5 program

The vertical dynamic behaviour of the embedded footing as described in Chapter 3 (Section 3.7) was determined using the Dyna5 program. The forces measured in the field used to excite the foundation system in the vertical direction. Also, a unit force was used to excite the foundation system to obtain frequency response function. The models illustrating the embedment depth are shown in Figure 5.35(a) to 5.35(e). The responses of the foundation system for different embedment were determined by using the parameters shown in Table 5-9. The analysis assumed that the Poisson's ratio for all layers is 0.25. The material damping was not considered in the analysis. A small strain shear modulus of the elastic half-space of 100 MPa was used in the analysis. The shear modulus of the side soil layers was calculated using Equation 2.58.

5-19

Displacement amplitude

The vertical displacement response of the embedded foundation systems was determined using dyna5 program for embedment of 0 mm, 310 mm, 620 mm, 930 mm and 1240 mm. The vertical displacement amplitude of the foundation system is shown in Figure 5.43. From the plots, it is indicated that as the embedment increases, the displacement amplitudes decreases.

In addition, the displacement of the analytical solution at the frequency of $1.25 \times fmax$ and $0.75 \times fmax$ for embedment of 0 mm, 310 mm, 620 mm, 930 mm and 1240 mm is compared with the one obtained experimentally as shown in Table 5.18 to Table 5.22, where $fmax$ is the frequency at the maximum displacement amplitude.

The displacement percentage error in comparison to the experimental results at maximum displacement for 0 mm, 310 mm and 620 mm embedment is 1 %, 4.9 % and 11.7% respectively. At embedment of 930 mm and 1240 mm the error is 39.4% and 15.1 % respectively. The prediction models overestimated displacement amplitude at 0 mm and 1240 mm embedment and underestimated displacement at embedment of 310 mm, 620 mm and 930 mm.

Table 5-18: Predicted displacement for 0mm Embedment - Dyna5 program

Method	Displacement (mm)			Estimated frequency (Hz)	% Error		
	0.75*fmax*	*fmax*	+1.25*fmax*	*fmax*	0.75*fmax*	*fmax*	+1.25*fmax*
Experimental results	0.0177	0.0206	0.0101	58.8	1.7	1.0	22.8
Dyna5 program	0.0180	0.0208	0.0124	57.6			

Table 5-19: Predicted displacement for 310mm Embedment - Dyna5 program

Method	Displacement (mm)			Estimated frequency (Hz)	% Error		
	0.75*fmax*	*fmax*	+1.25*fmax*	*fmax*	0.75*fmax*	*fmax*	+1.25*fmax*
Experimental results	0.0146	0.0185	0.0106	57.6	24.7	4.9	8.5
Dyna5 program	0.0110	0.0176	0.0115	57.6			

Table 5-20: Predicted displacement for 620mm Embedment - Dyna5 program

Method	Displacement (mm)			Estimated frequency (Hz)	% Error		
	0.75*fmax*	*fmax*	+1.25*fmax*	*fmax*	0.75*fmax*	*fmax*	+1.25*fmax*
Experimental results	0.0103	0.0145	0.0093	56.0	26.2	11.7	7.5
Dyna5 program	0.0076	0.0128	0.0086	57.0			

Table 5-21: Predicted displacement for 930mm Embedment - Dyna5 program

Method	Displacement (mm)			Estimated frequency (Hz)	% Error		
	0.75*fmax*	*fmax*	+1.25*fmax*	*fmax*	0.75*fmax*	*fmax*	+1.25*fmax*
Experimental results	0.0051	0.0132	0.0039	65.8	2.0	39.4	33.3
Dyna5 program	0.0050	0.0080	0.0052	62.4			

Table 5-22: Predicted displacement for 1240mm Embedment - Dyna5 program

Method	Displacement (mm)			Estimated frequency (Hz)	% Error		
	0.75*fmax*	*fmax*	+1.25*fmax*	*fmax*	0.75*fmax*	*fmax*	+1.25*fmax*
Experimental results	0.0040	0.0079	0.0050	60.0	+17.5	15.2	10.0
Dyna5 program	0.0033	0.0091	0.0045	60.0			

Resonant amplitude

Figure 5.44 shows the resonant amplitudes of the embedded foundation systems due to a unit load for different embedment. From the plot, it is shown that as the embedment increases the vertical resonant amplitude decreases. The resonant amplitudes obtained from Dyna5 program presented in Table 5-23. Figure 5.45 illustrates the magnification factor for different embedment obtained from Dyna5 program.

Resonant amplitude ratio

The resonant amplitude ratio was determined using Equation 2.44. The predicted resonant amplitude ratios from different embedment are shown in Table 5-23 and here it can be seen that the resonant amplitude ratio decreases significantly as embedment increases.

Table 5-23: Predicted resonant amplitude and resonant amplitude ratio for Dyna5 program

Embedment depth (mm)	Embedment ratio	Resonant amplitude (mm/N)	Resonant amplitude ratio
0	0	4.4666×10^{-6}	1
310	0.52	2.5529×10^{-6}	0.5716
620	1.03	1.7718×10^{-6}	0.3967
930	1.55	1.3611×10^{-6}	0.3047
1240	2.07	1.1569×10^{-6}	0.2590

5-21

Resonant frequency

The resonant frequencies of the embedded foundation systems are determined from Figure 5.44. In addition, the resonant frequency can be obtained from the plot of magnification factor versus forcing frequency. Figure 5.45 illustrate the magnification factor for different embedment obtained using the Dyna5 program. The resonant frequencies obtained from Figures 5.44 and 5.45 are presented in Table 5-24.

Resonant frequency ratio

The resonant frequency ratios predicted by Dyna5 program are presented in Table 5-14. From Table 5-24, it is shown that the resonant frequency ratio decreases as the embedment increases up to an embedment ratio of 0.5, and then, remains constant as the embedment ratio increases.

Table 5-24: Predicted resonant frequency and resonant frequency ratio for Dyna5 program

Embedment depth (mm)	Embedment ratio	Resonant frequency (Hz)	Resonant frequency ratio
0	0	36.4	1
310	0.52	31.0	0.852
620	1.03	31.0	0.852
930	1.55	31.0	0.852
1240	2.07	31.0	0.852

Complex dynamic stiffness

Figure 5.46 shows the vertical complex dynamic stiffness obtained from Dyna5 program. From the plot it is seen that as the embedment increases, the complex dynamic stiffness increases. The rate of increase is small at the low frequencies, as the frequency increases the rate of increase is higher.

Real part of complex dynamic stiffness

The real part obtained from Dyna5 program for different embedments is shown in Figure 5.47. This indicates that at the lower frequencies of up to about 40 Hz for higher embedment, the stiffness increases as the forcing frequency increases. Beyond 40 Hz, the real part decreases as the frequency increases. For lower embedments, the real part decreases as the forcing frequency increases.

Complex dynamic stiffness of the imaginary part

The imaginary part obtained from Dyna5 program for different embedment is shown in Figure 5.48. From Figure 5.48, it is shown that the imaginary part increases as the embedment increases. The rate of increase is constant as the forcing frequency increases.

Phase angles

The plots of phase angle between force and displacement versus forcing frequency predicted by the Dyna5 program for different embedment are shown in Figure 5.49. The natural frequencies of the embedded foundation for different embedments obtained from Dyna5 program are shown in Table 5-25. The natural frequency of the foundation system increases as the embedment increases as shown in Table 5-25.

Natural frequency ratio

The natural frequency ratio obtained using Dyna5 program are presented in Table 5-25. The natural frequency ratio increases as the embedment increases.

Table 5-25: Predicted natural frequency and natural frequency ratio for Dyna5 program

Embedment depth (m)	Embedment ratio	Natural frequency (Hz)	Natural frequency ratio
0	0	42	1
310	0.52	47.1	1.121
620	1.03	52.3	1.245
930	1.55	57.2	1.362
1240	2.07	60.4	1.438

5.3.8 Comparison between predicted and observed responses

In this section the behaviour of the embeded foundation obtained analytically, as suggested by Novak and Beredugo (1972) and Dyna5 program are compared with the experimental results. The compared responses are the displacement amplitude, amplitude at resonant, resonant amplitude ratio, resonant frequency, resonant frequency ratio, natural frequency and the natural frequency ratio. To allow direct comparison, the field results are normalised with respsect to the applied load.

Displacement amplitude

Figure 5-50 shows the plot of measured displacement amplitude for 0 mm embedment compared to the analytical solution by Novak and Beredugo (1972) and Dyna5 program.

5-23

From the plot, it is illustrated that Novak and Beredugo (1972) and Dyna5 program predicted similar response as the one measured experimentally. The comparison of the responses for embedment of 310 mm and 620 mm are shown in Figure 5-51 and 5-52 respectively. From the plot, it is shown that prediction models predicted response close to what measured experimentally. The responses for embedment of 930 mm and 1240 mm are shown in Figure 5-53 and 5-54 respectively. From the plot, it is shown that prediction models overestimated displacement at maximum amplitude compared to what measured experimentally.

The displacements at maximum for different embedment was determined and plotted versus embedment depth as shown in Figure 5-55. From the plot, it is shown that as embedment increases the displacement amplitude decreases. The prediction models predicted similar values as the one measured experimentally with embedment of 0 mm.

Resonant amplitude

Figure 5.56 shows the plot of the resonant amplitude for different embedments taken from the analytical solution as suggested by Novak and Beredugo (1972), Dyna5 program and the one measured experimentally. The plot shows that the prediction underestimated the resonant amplitude compared to the measured displacement amplitude. From Figure 5.56, it is shown that resonant amplitude decreases as the embedment increases. At zero embedment, Novak and Beredugo (1972) and Dyna5 program under estimated the resonant amplitude for about 15.4% and 25.3% respectively compared to the resonant amplitude measured experimentally. The plot shows that, the response predicted from the analytical solution by Novak and Beredugo (1972) from embedment of 930 mm is similar to the one predicted by the Dyna5 program.

Resonant amplitude ratio

The resonant amplitude ratio obtained from field-measured data is compared with the predicted resonant amplitude ratios for different embedment ratios as illustrated in Figure 5.57. From the plot, it is observed that in all cases the resonant amplitude ratio decreases as the embedment ratio increases. The results show that the analytical solution by Novak and Beredugo (1972) underestimates the resonant amplitude ratio compared to that from the field measurements. Dyna5 program predicted resonant amplitude ratio similar to the one measured in the field up to 1.0 embedment ratio. Beyond 1.0 embedment ratio Dyna5 program underestimated resonant amplitude ratio. The trend of plotted curves is the same in all three cases showing that the resonant amplitude ratio

decreases as embedment increases. It also shows that the rate of reduction of the resonant amplitude ratio is higher at low values of embedment ratio. This suggests that even small levels of embedment can significantly reduce the maximum vibration amplitude.

Resonant frequency

In Figure 5.58, the resonant frequencies obtained from field measurements are compared to the predicted resonant frequencies. From the plot, it is shown that, both the analytical solution and Dyna5 program underestimate resonant frequency compared to measured resonant frequency. The resonant frequency obtained from analytical and Dyna5 program decreases as the embedment depth increases up to the embedment depth of 310 mm, then remains constant as the forcing frequency increases.

Resonant frequency ratio

The resonant frequency ratio obtained from the field-measured data was compared with resonant frequency ratio determined using Dyna5 program and the analytical solution by Novak and Beredugo (1972) as shown in Figure 5.59. The plot indicates that the predicted resonant frequency ratio decreased up to the embedment ratio of about 0.52 and then remains almost constant as embedment ratio increases. The prediction model under estimated resonant frequency ratios compared to the observed resonant frequency ratios. The observed and predicted resonant frequency ratios remained in a narrow range for different embedments, indicating that embedment has an insignificant effect on resonant frequency ratio.

Natural frequency

The natural frequencies obtained experimentally are plotted together with the predicted natural frequency. From the plot, it is shown that the natural frequency increases as the embedment increases. Figure 5.60 show that Dyna5 program slightly overestimates the natural frequency for all embedment depths. The natural frequencies from the analytical solution suggested by Novak and Beredugo (1972) are very close to the measured natural frequency up to embedment depth of about 600 mm. At more than 600 mm embedment, the natural frequencies obtained from the analytical solution by Novak and Beredugo (1972) are higher than the measured natural frequencies.

Natural frequency ratio

The natural frequency ratio obtained from the analytical solution by Novak and Beredugo (1973), Dyna5 program and measured data are shown in Figure 5.61. The plots show that as the embedment increases the natural frequency ratio increases. From Figure 5.61, it is illustrated that up to an embedment ratio of 1.0, there is a good agreement between the predicted natural frequency ratio and the field-measured data. Above an embedment ratio of 1.0, the natural frequency ratio is overpredicted by approximately 10%.

5.4 Summary

Different methods were used to predict the dynamic behaviour of machine foundations. This chapter presented the most popular analytical methods used in the industry for the design of machine foundations. These are the Mass–Spring Dashpot or Winkler model, elastic half-space theory and simplified models. In addition, the Dyna5 program was used to predict the dynamic behaviour of the surface and embedded foundations. The aim of this chapter was to evaluate the accuracy of the analytical methods to predict the dynamic behaviour of the surface and embedded foundations.

5.4.1 Surface foundation

Table 5-26 presents the summary of the measured vertical dynamic responses of surface foundation. Tables 5-27 to 5-34 summarises the vertical dynamic behaviours predicted by the Winkler model, elastic half-space theory, and simplified models. The simplified models include Lysmer (1965) model, Veletsos and Verbic (1973) massless soil and Veletsos and Verbic (1973) soil with mass analytical methods. For damped Winkler model, only the results for CSW test is compared and ranked. Tables 5-27 to 5-34 demonstrate the ranking of each method, which was established by comparing the observed and predicted vertical dynamic behaviour of the foundation system.

Table 5-26: Experiment results from surface foundation - Impedance functions

S/No	Analysis method	Parameter
1	Vertical dynamic displacement (mm)	0.0188
2	Vertical complex dynamic stiffness (N/mm)	512,885.0
3	Real part of complex dynamic stiffness(N/mm)	505,819.8
4	Imaginary part of complex dynamic stiffness(N/mm)	84,832.9
5	Natural frequency from phase angle (Hz)	49.0

6	Natural frequency from real part (Hz)	49.0
7	Natural frequency loss angle (Hz)	49.4
8	Resonant frequency (Hz)	44.0
9	Resonant amplitude (mm/N)	2.9421×10^{-6}

Table 5-27: Comparison of resonant frequency for different analysis methods

S/No	Analysis method	Resonant frequency (Hz)	Error (%)	Ranking
1	Winkler model – no damping	N/A		
2	Damped Winkler model (CSW test)	49	8.9	1
3	Elastic half-space theory – Sung (1953)	N/A	N/A	
4	Lysmer (1965) model	N/A	N/A	
5	Veletsos and Verbic (1973) massless	N/A	N/A	
6	Veletsos and Verbic (1973) soil with mass	15	65.9	2
7	Numerical method – Dyna5 program	15	65.9	2

Table 5-28: Comparison of vertical displacement at the peak for different analysis methods

S/No	Analysis method	Displacement (mm)	Error (%)	Ranking
1	Winkler model – no damping	N/A	N/A	-
2	Damped Winkler model (CSW test)	0.0230	27.8	1
3	Elastic half-space theory – Sung (1953)	0.0098	45.6	4
4	Lysmer (1965) model	0.01226	31.9	2
5	Veletsos and Verbic (1973) massless soil	0.01108	38.4	3
6	Veletsos and Verbic (1973) soil with mass	0.00789	56.2	5
7	Numerical method – Dyna5 program	0.00789	56.2	5

Table 5-29: Comparison of complex dynamic stiffness at 10 Hz - different analysis methods

S/No	Analysis method	Complex dynamic stiffness (N/mm) at 10 Hz	Error (%)	Ranking
1	Winkler model – no damping	N/A	N/A	-
2	Damped Winkler model (CSW test)	-	-	-
3	Elastic half-space theory – Sung (1953)	651,419.6	27.0	1
4	Lysmer (1965) model	683,231.2	33.2	5
6	Veletsos and Verbic (1973) massless soil	655,311.9	27.8	2
7	Veletsos and Verbic (1973) soil with mass	661,013.3	28.9	3
8	Numerical method – Dyna5 program	680,600.8	32.7	4

Table 5-30: Comparison of real part of complex dynamic stiffness at 10 Hz from different
nalysis methods

S/No	Analysis method	Real part (N/mm) at 10 Hz	Error (%)	Ranking
1	Winkler model – no damping	N/A	N/A	-
2	Damped Winkler model (CSW test)	-	-	-
3	Elastic half-space theory – Sung (1953)	651,412.8	28.8	2
4	Lysmer (1965) model	652,458.9	29.0	3
5	Veletsos and Verbic (1973) massless soil	655,305.7	29.6	4
6	Veletsos and Verbic (1973) soil with mass	634,929.3	25.5	1
7	Numerical method – Dyna5 program	655,300.0	29.6	4

Table 5-31: Comparison of imaginary part of complex dynamic stiffness at 10 Hz for different
analysis methods

S/No	Analysis method	Imaginary part (N/mm) at 10 Hz	Error (%)	Ranking
1	Winkler model	N/A	N/A	N/A
2	Damped Winkler model (CSW test)	-	-	-
3	Elastic half-space theory – Sung (1953)	-	-	-
4	Lysmer (1965) model	202736.8	139.0	4
5	Veletsos and Verbic (1973) massless soil	183779.8	116.6	1
6	Veletsos and Verbic (1973) soil with mass	183856.7	116.7	2
7	Numerical method – Dyna5 program	183,846.0	116.8	3

Table 5-32: Comparison of natural frequency for different analysis methods

S/No	Analysis method	Natural frequency (Hz)	Error (%)	Ranking
1	Winkler model – no damping	57.7	17.8	4
2	Damped Winkler model (CSW test)	56	17.8	4
3	Elastic half-space theory – Sung (1953)	58	18.4	5
4	Lysmer (1965) model	57.5	17.3	3
5	Veletsos and Verbic (1973) massless soil	57.5	17.3	3
6	Veletsos and Verbic (1973) soil with mass	50.0	2.0	1
7	Numerical method – Dyna5 program	50.3	2.6	2

Table 5-33: Comparison of natural frequency from real part for different analysis methods

S/No	Analysis method	Natural frequency (Hz)	Error (%)	Ranking
1	Winkler model	N/A	N/A	-
2	Damped Winkler model (CSW test)	N/A	N/A	-

3	Elastic half-space theory – Sung (1953)	57.9	20.4	3
4	Lysmer (1965) model	57.5	17.3	2
5	Veletsos and Verbic (1973) massless soil	N/A	N/A	-
6	Veletsos and Verbic (1973) soil with mass	50.3	2.7	1
7	Numerical method – Dyna5 program	N/A	N/A	-

Table 5-34: Comparison of natural frequency obtained from loss angle for different analysis methods

S/No	Analysis method	Natural frequency (Hz)	Error (%)	Ranking
1	Winkler model	N/A	N/A	-
2	Damped Winkler model (CSW test)	N/A	N/A	-
3	Elastic half-space theory – Sung (1953)	59.4	20.2	3
4	Lysmer (1965) model	57.4	17.1	2
5	Veletsos and Verbic (1973) massless soil	N/A	N/A	-
6	Veletsos and Verbic (1973) soil with mass	50.0	2.0	1
7	Numerical method – Dyna5 program	N/A	N/A	-

This concluded the most accurate simplified model on predicting dynamic behaviour of the foundation systems and the comparison deduced the following:

- The Winkler model is useful only for predicting natural frequency of the foundation systems. Even though the model ranked number four it was able to predict the natural frequency within 18% of the observed natural frequency. The method cannot be used to predict displacement and resonant amplitudes of the machine foundations;

- From the study, it is shown that, if the damping constant is properly chosen, the damped Winkler model can be used at the preliminary design stage to predict the resonant frequency of the machine foundations;

- It is illustrated that the spring constant obtained from Continuous Surface Wave test is more accurately on estimating the resonant frequency compared to the vertical block vibration and empirical value proposed by Barkan (1962). Therefore, the small strain shear stiffness obtained from Continuous Surface Wave test, with properly chosen damping constant, can be used at the preliminary design stage to predict resonant frequency of the machine foundation systems;

5-29

- The analytical solutions at the low frequency of about 10 Hz predicted complex dynamic stiffness of the real part and imaginary part which were higher than the measured values;

- The analytical models and the Dyna5 program underestimated displacement in the range of 31.9 % and 56.2 % compared to measured value;

- The analytical models and the Dyna5 program also overestimated the complex dynamic stiffness. The error for real part of the complex dynamic stiffness ranges between 25.5 % and 29.6 %. The imaginary part of complex dynamic stiffness was overestimated in the range of 116 % and 139 %, and

- The analytical solutions and Dyna5 program overestimated the natural frequency in the range of 2 % and 20.4 %.

The analytical model proposed by Veletsos and Verbic (1973) soil with mass is rated as the most accurate analytical model among the evaluated analytical models. The model predicts the vertical dynamic responses of vibrating footing close to measured responses because the modelling consider the effect of the soil half space beneath the footing.

5.4.2   Embedded foundation

The vertical dynamic behaviour of the embedded foundation was studied using the analytical methods proposed by Novak and Beredugo (1972) and Dyna5 program. The dynamic behaviours determined from the embedded foundation were resonant amplitude, resonant frequency, natural frequency, and dynamic stiffness. The effect of the embedment was evaluated using the dimensionless quantities referred to as the resonant amplitude ratio, resonant frequency ratio, and natural frequency ratio. The predicted response of displacement amplitude, resonant frequency and natural frequency will be compared to the observed responses.

Table 5-35 presents the summary of the measured vertical dynamic responses of embedded foundation. Tables 5-36 to 5-50 summarises the vertical dynamic behaviours predicted by Novak and Beredugo (1972) and Dyna5 program. Tables 5-36 to 5-50 also show the ranking of each method, which was established by comparing the observed and predicted vertical dynamic behaviour of the foundation system.

Table 5-35: Experiment results from embedded foundation - Impedance functions

Embedment (mm)	Displacement amplitude (mm)	Resonant amplitude (mm/N)	Resonant frequency (Hz)	Natural frequency (Hz)
0	0.0206	5.9926×10^{-6}	38.1	41.0
310	0.0185	3.4514×10^{-6}	39.1	46.1
620	0.0145	2.2808×10^{-6}	36.9	51.0
930	0.0132	2.0849×10^{-6}	35.9	47.0
1240	0.0079	1.2874×10^{-6}	36.9	55.0

Table 5-36: Comparison of displacement amplitude - 0 mm embedment

S/No	Analysis method	Displacement amplitude (mm)	Error (%)	Ranking
1	Novak and Beredugo (1972)	0.021	2.0	2
2	Dyna5 program	0.0208	1.0	1

Table 5-37: Comparison of displacement amplitude - 310 mm embedment

S/No	Analysis method	Displacement amplitude (mm)	Error (%)	Ranking
1	Novak and Beredugo (1972)	0.0192	3.8	1
2	Dyna5 program	0.0176	4.9	2

Table 5-38: Comparison of displacement amplitude - 620 mm embedment

S/No	Analysis method	Displacement amplitude (mm)	Error (%)	Ranking
1	Novak and Beredugo (1972)	0.0139	2.0	1
2	Dyna5 program	0.0128	11.7	2

Table 5-39: Comparison of displacement amplitude - 930 mm embedment

S/No	Analysis method	Displacement amplitude (mm)	Error (%)	Ranking
1	Novak and Beredugo (1972)	0.0132	33.3	1
2	Dyna5 program	0.0088	39.4	2

Table 5-40: Comparison of displacement amplitude - 1240 mm embedment

S/No	Analysis method	Displacement amplitude (mm)	Error (%)	Ranking
1	Novak and Beredugo (1972)	0.0103	30.4	2
2	Dyna5 program	0.0091	15.2	1

Table 5-41: Comparison of resonant frequency - 0 mm embedment

S/No	Analysis method	Resonant frequency (Hz)	Error (%)	Ranking
1	Novak and Beredugo (1972)	36.1	5.3	2
2	Dyna5 program	36.4	4.5	1

Table 5-42: Comparison of resonant frequency - 310 mm embedment

S/No	Analysis method	Resonant frequency (Hz)	Error (%)	Ranking
1	Novak and Beredugo (1972)	33.5	14.3	1
2	Dyna5 program	31.0	20.7	2

Table 5-43: Comparison of resonant frequency - 620 mm embedment

S/No	Analysis method	Resonant frequency (Hz)	Error (%)	Ranking
1	Novak and Beredugo (1972)	33.5	9.2	1
2	Dyna5 program	31.0	16.0	2

Table 5-44: Comparison of resonant frequency - 930 mm embedment

S/No	Analysis method	Resonant frequency (Hz)	Error (%)	Ranking
1	Novak and Beredugo (1972)	33.5	6.7	1
2	Dyna5 program	31.0	13.6	2

Table 5-45: Comparison of resonant frequency - 1240 mm embedment

S/No	Analysis method	Resonant frequency (Hz)	Error (%)	Ranking
1	Novak and Beredugo (1972)	33.5	9.2	1
2	Dyna5 program	31.0	16.0	2

Table 5-46: Comparison of natural frequency - 0 mm embedment

S/No	Analysis method	Natural frequency (Hz)	Error (%)	Ranking
1	Novak and Beredugo (1972)	40.3	1.7	1
2	Dyna5 program	42.0	2.4	2

Table 5-47: Comparison of natural frequency - 310 mm embedment

S/No	Analysis method	Natural frequency (Hz)	Error (%)	Ranking
1	Novak and Beredugo (1972)	45.7	1.0	1
2	Dyna5 program	47.1	2.2	2

Table 5-48: Comparison natural frequency - 620 mm embedment

S/No	Analysis method	Natural frequency (Hz)	Error (%)	Ranking
1	Novak and Beredugo (1972)	51.0	0	1
2	Dyna5 program	52.3	2.6	2

Table 5-49: Comparison of natural frequency - 930 mm embedment

S/No	Analysis method	Natural frequency (Hz)	Error (%)	Ranking
1	Novak and Beredugo (1972)	56.0	19	1
2	Dyna5 program	57.2	21.7	2

Table 5-50: Comparison of natural frequency - 1240 mm embedment

S/No	Analysis method	Natural frequency (Hz)	Error (%)	Ranking
1	Novak and Beredugo (1972)	59.0	7.0	1
2	Dyna5 program	60.4	9.8	2

The results by Novak and Beredugo (1972) and Dyna5 program are compared with the results obtained from field measurements. The responses predicted by Novak and Beredugo (1972) analytical solution shows reasonable conformity with the results obtained experimentally.
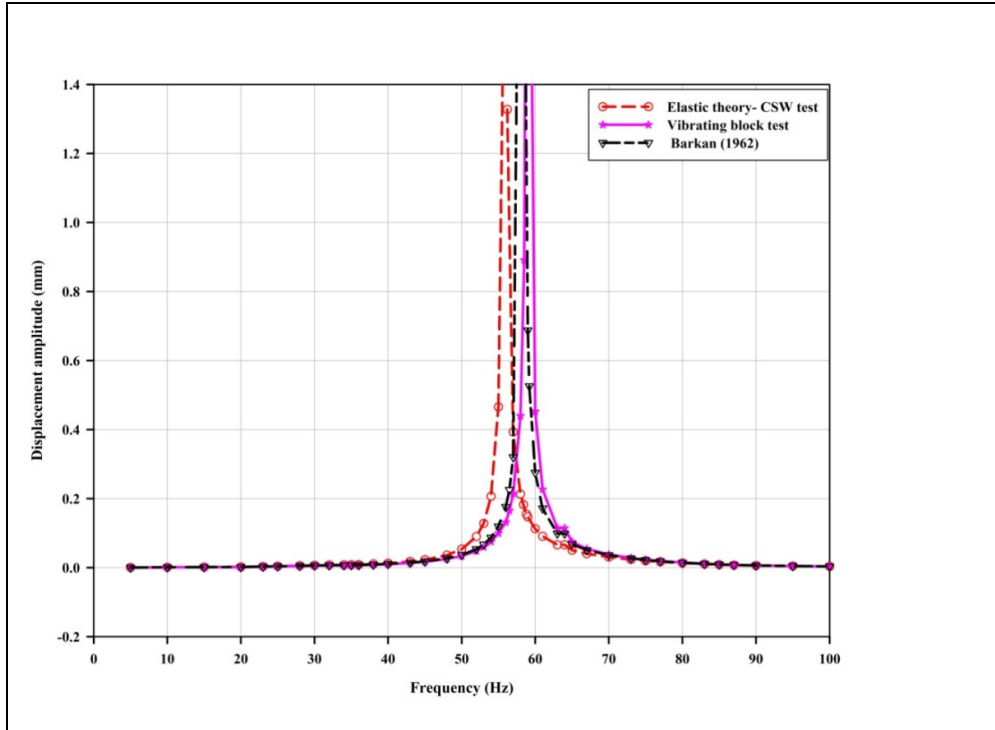
Figure 5.1: Displacement responses – Winkler model – No damping
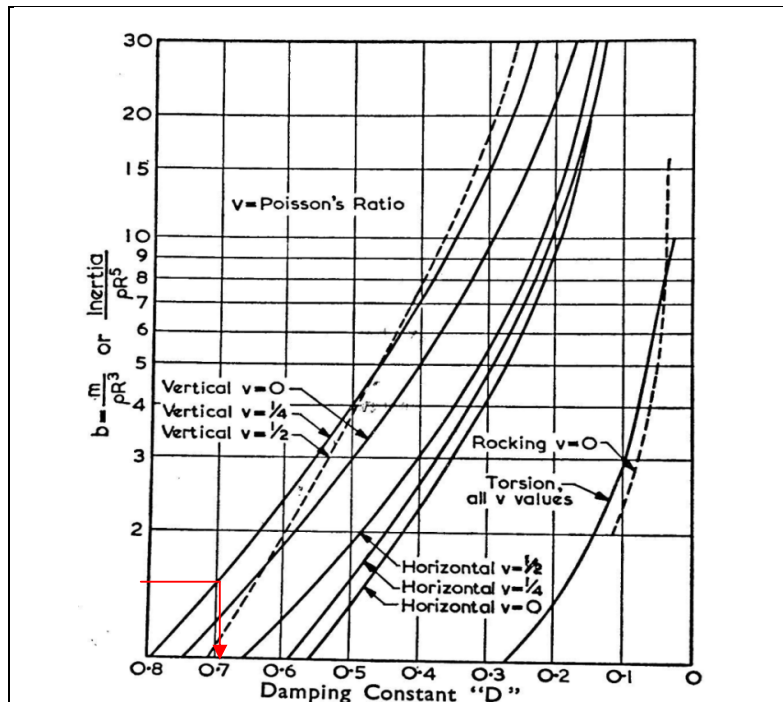
Figure 5.2 : Damping constant by Irish and Walker (1969)

5-34
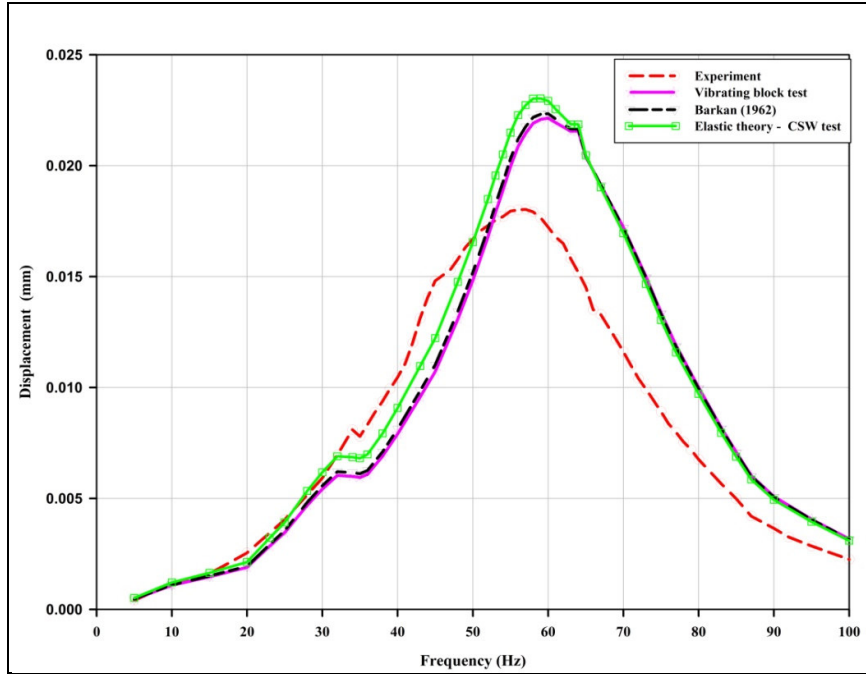
Figure 5.3: Displacement – Winkler model with damping
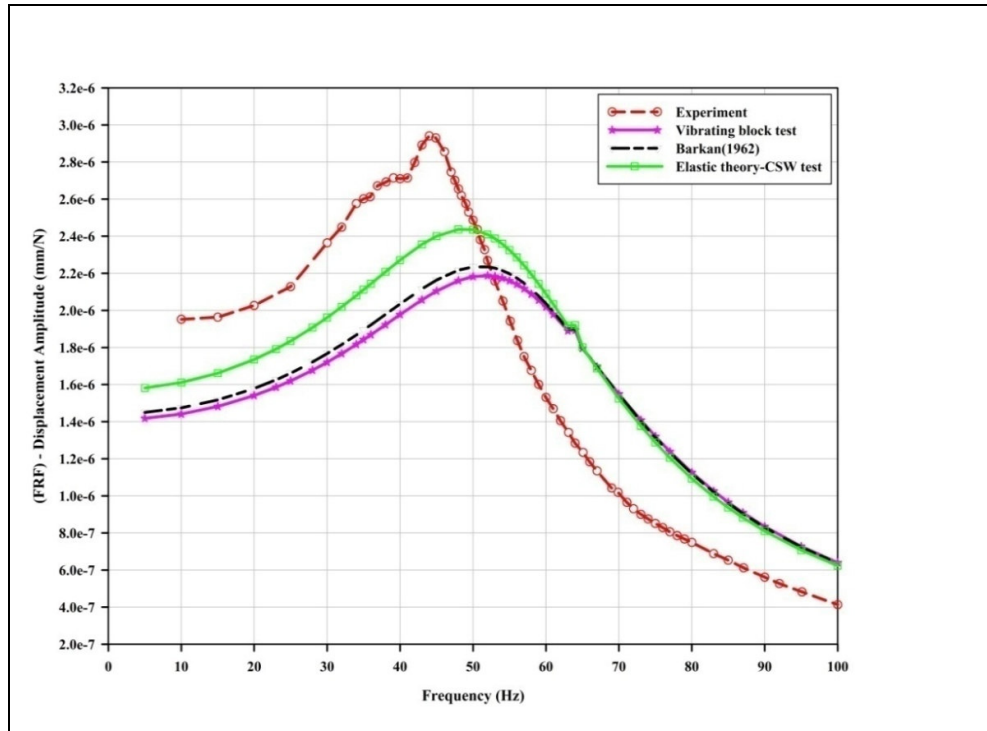
Figure 5.4: Frequency response function -Winkler model with damping
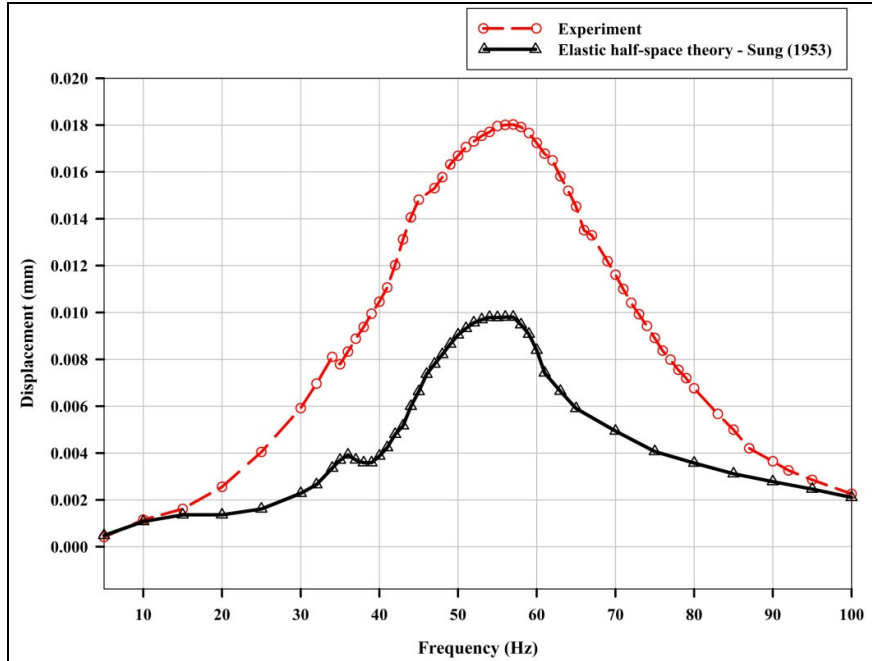
Figure 5.5: Vertical displacement response of foundation from field-measured data and Sung (1953)
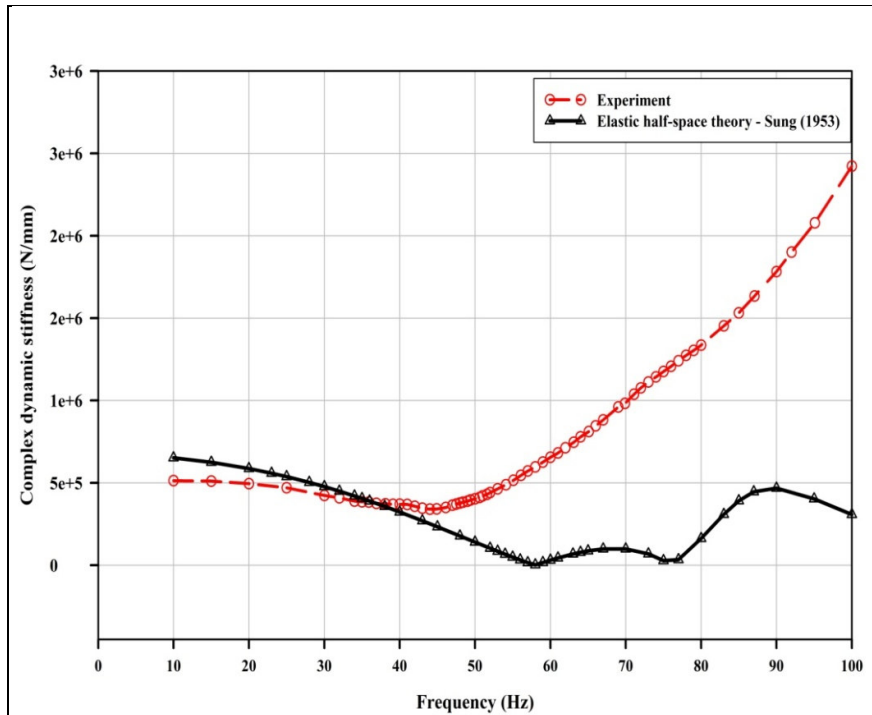
Figure 5.6: Vertical complex dynamic stiffness obtained experimentally and from Sung (1953).

5-36
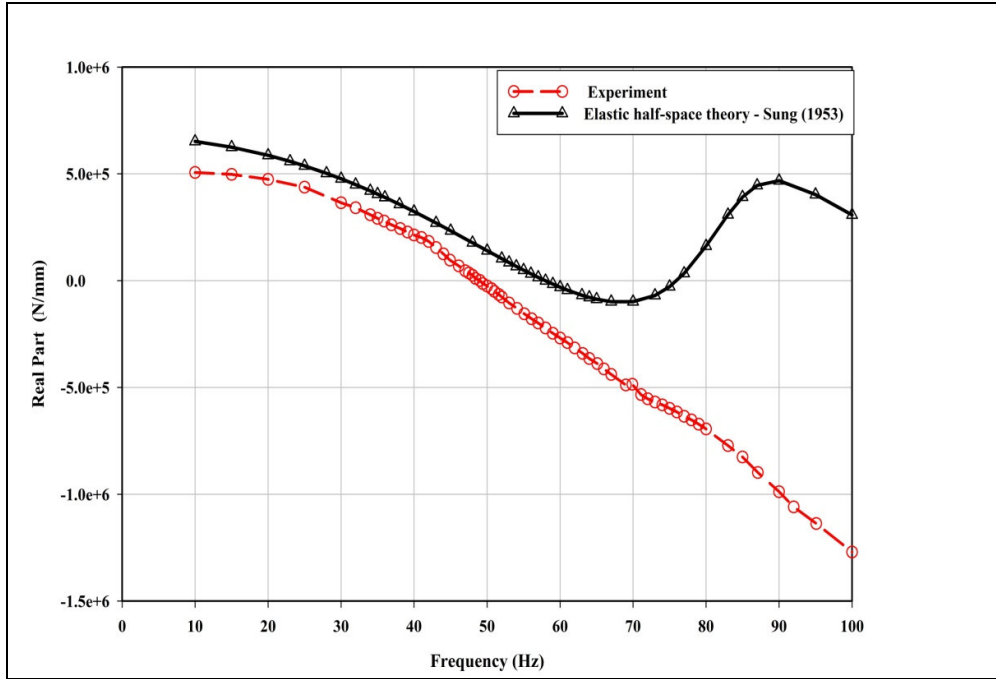
Figure 5.7: Effective dynamic stiffness (real part) from field-measured data and Sung (1953)
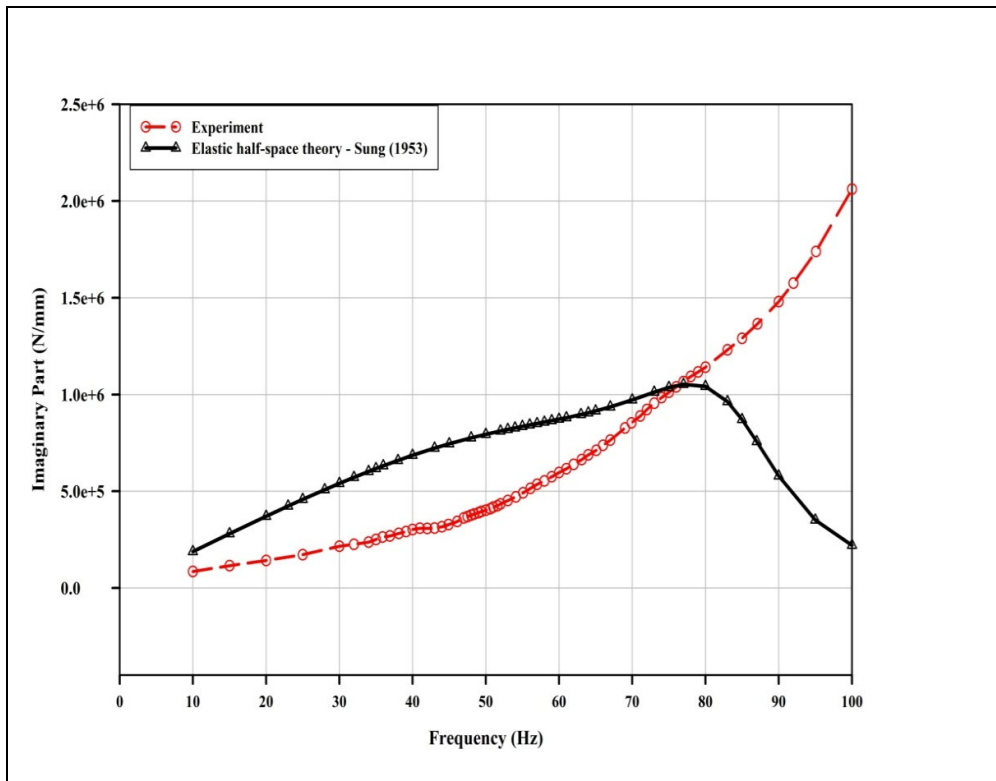
Figure 5.8: Imaginary part from field-measured data and Sung (1953)

5-37
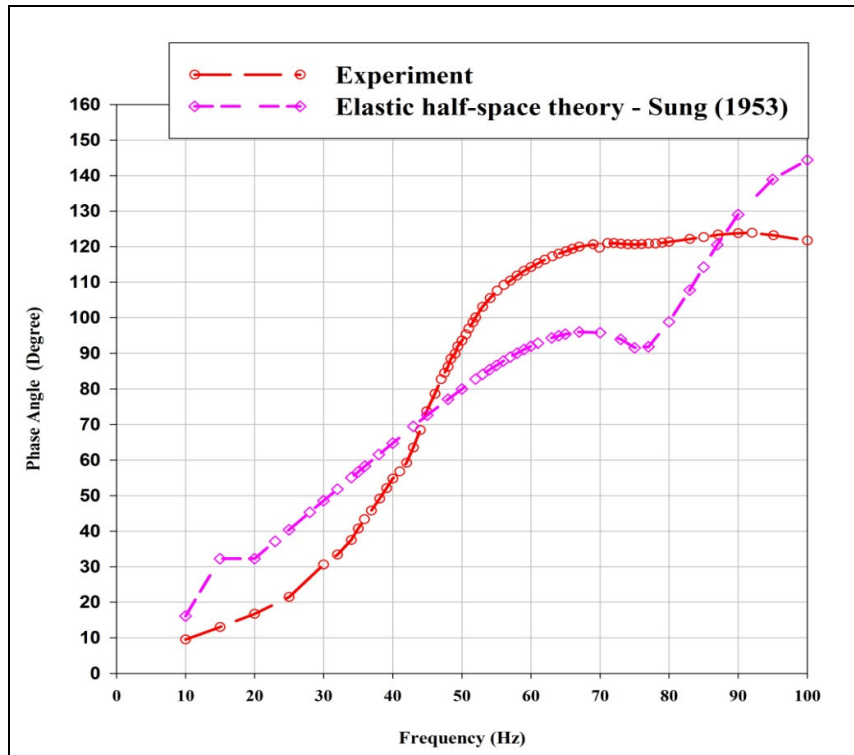
Figure 5.9: Phase angle between displacement and forcing function from field-measured data and Sung (1953)
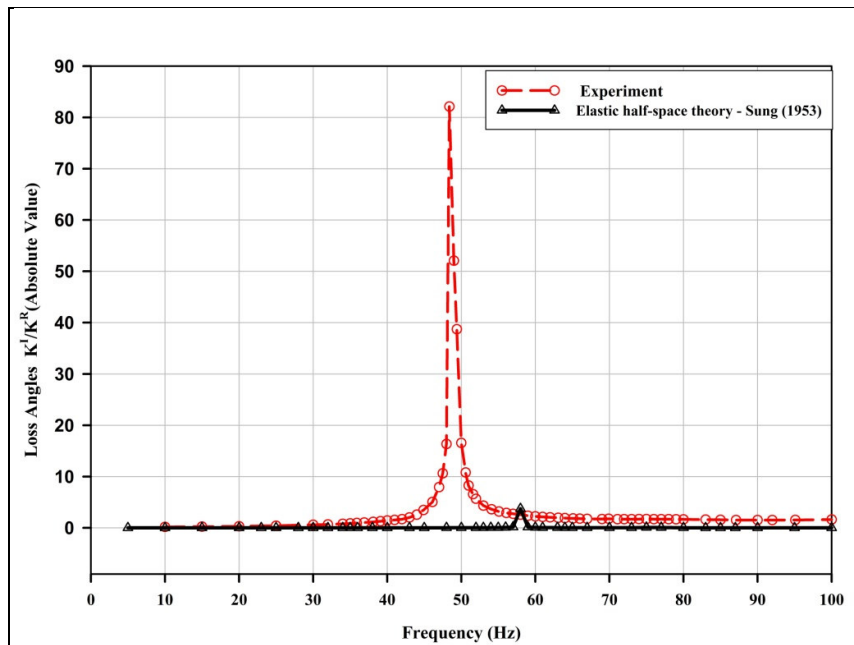
Figure 5.10: Field-measured loss angles and loss angles obtained from Sung (1953)
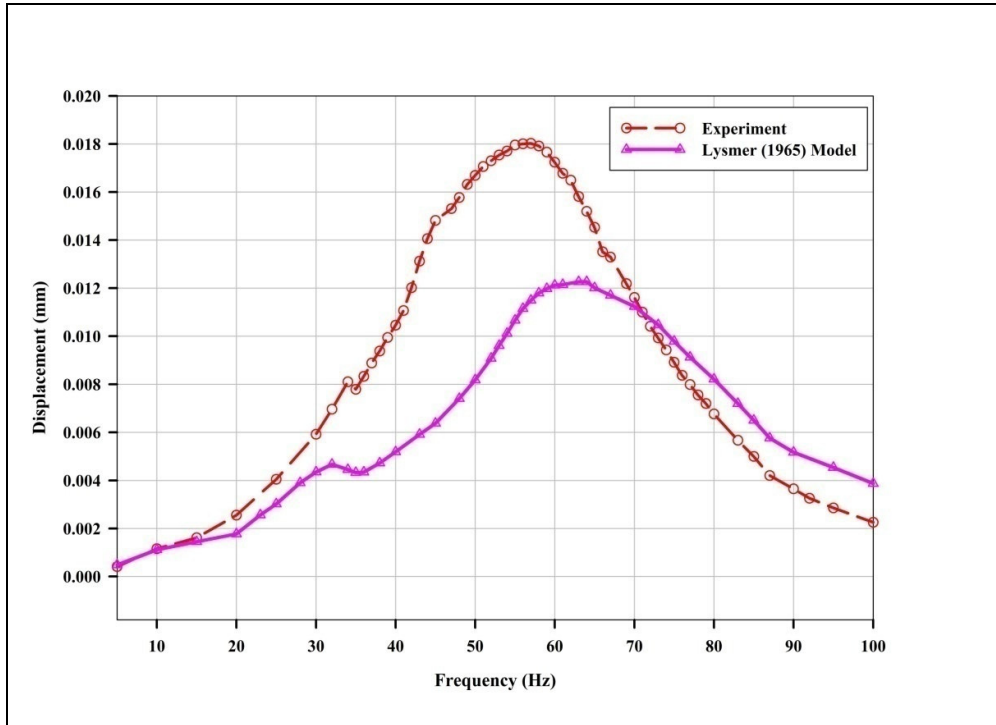
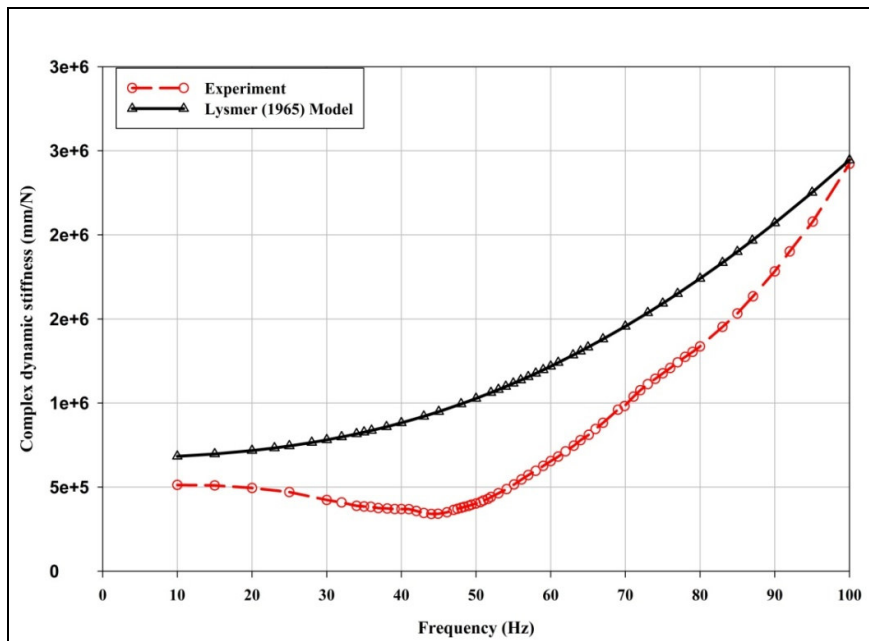Figure 5.11: Vertical displacement response of foundation from field-measured data and Lysmer (1965) Model

Figure 5.12: Vertical complex dynamic stiffness obtained from field-measured data and from Lysmer (1965)
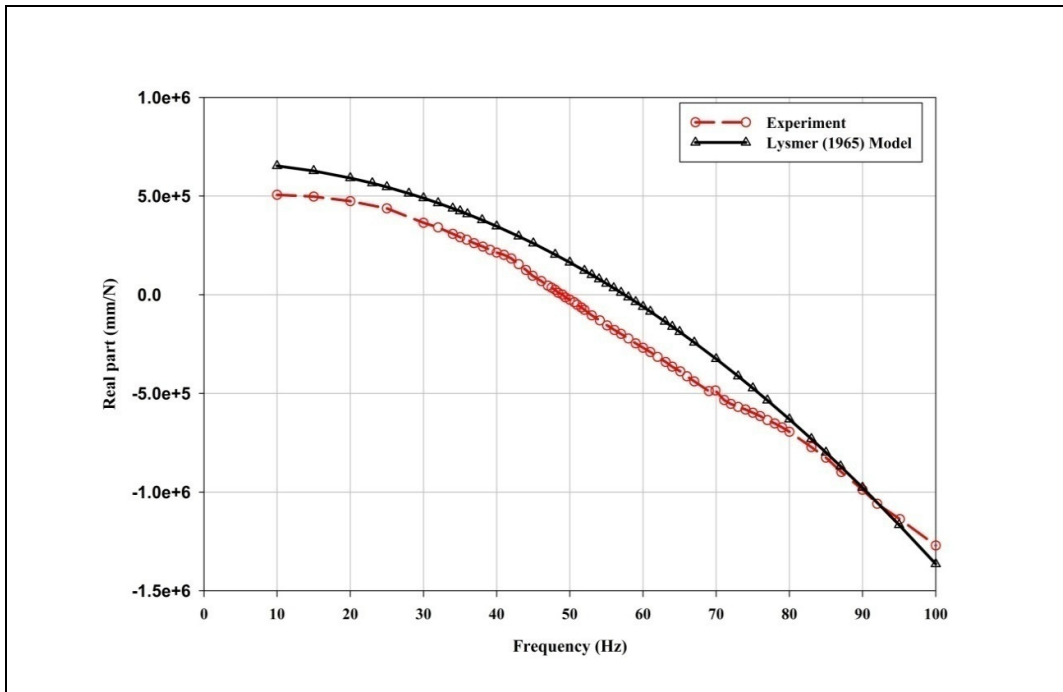
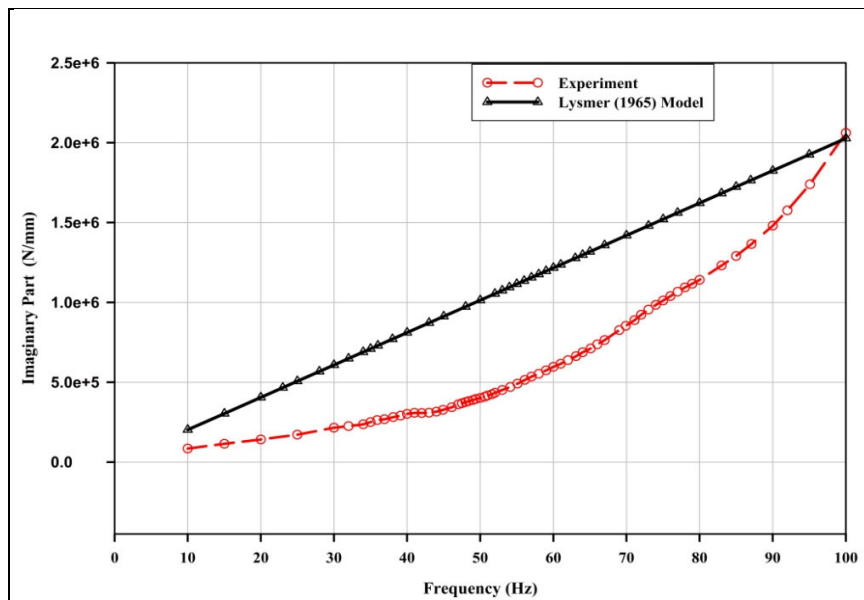Figure 5.13: Effective dynamic stiffness (real part) obtained experimentally and from Lysmer (1965)

Figure 5.14: Imaginary part obtained from field-measured data and from Lysmer (1965) Model
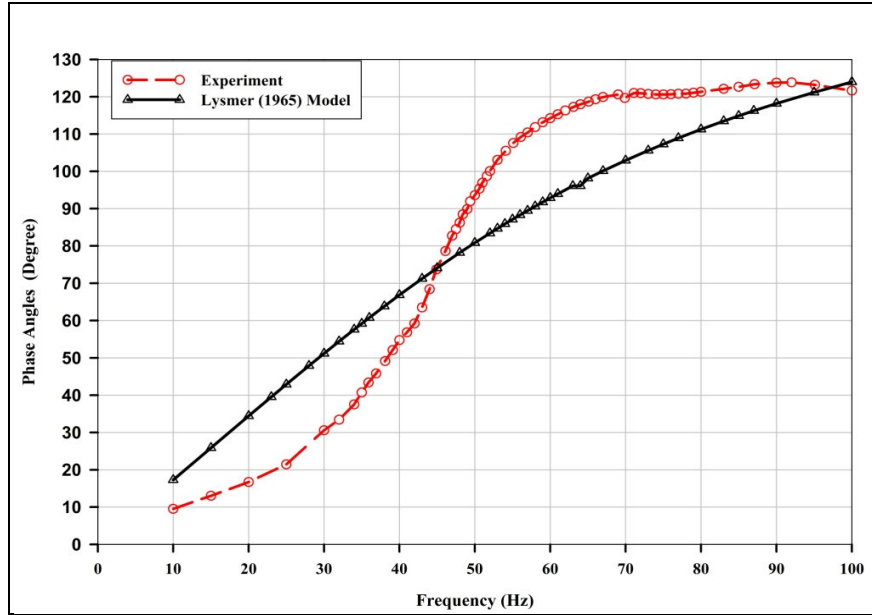
5-40

Figure 5.15: Phase angle between displacement and forcing function from Lysmer (1965) model
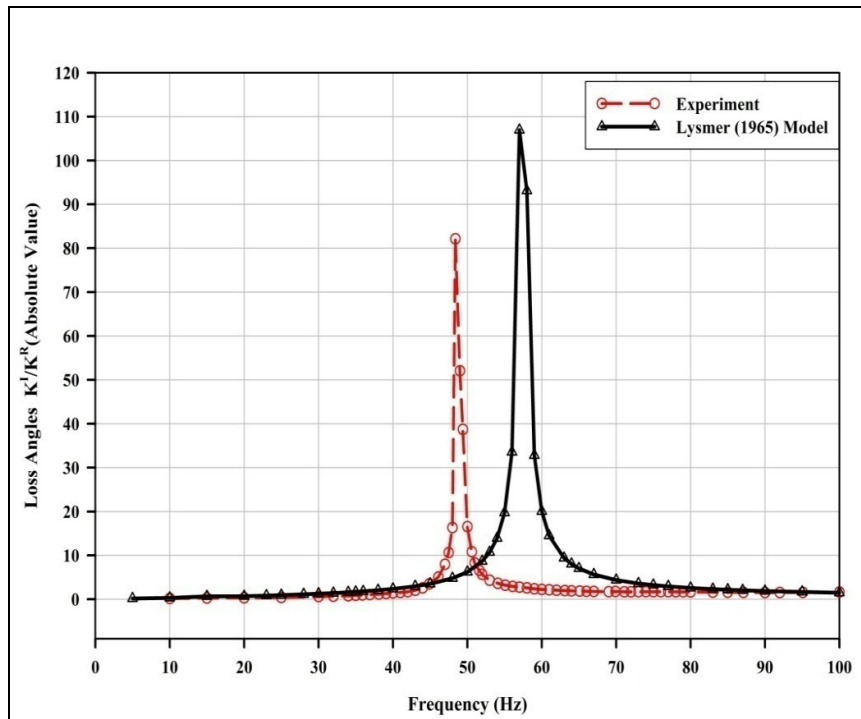

Figure 5.16: Loss angles obtained from field-measured data and from Lysmer (1965)
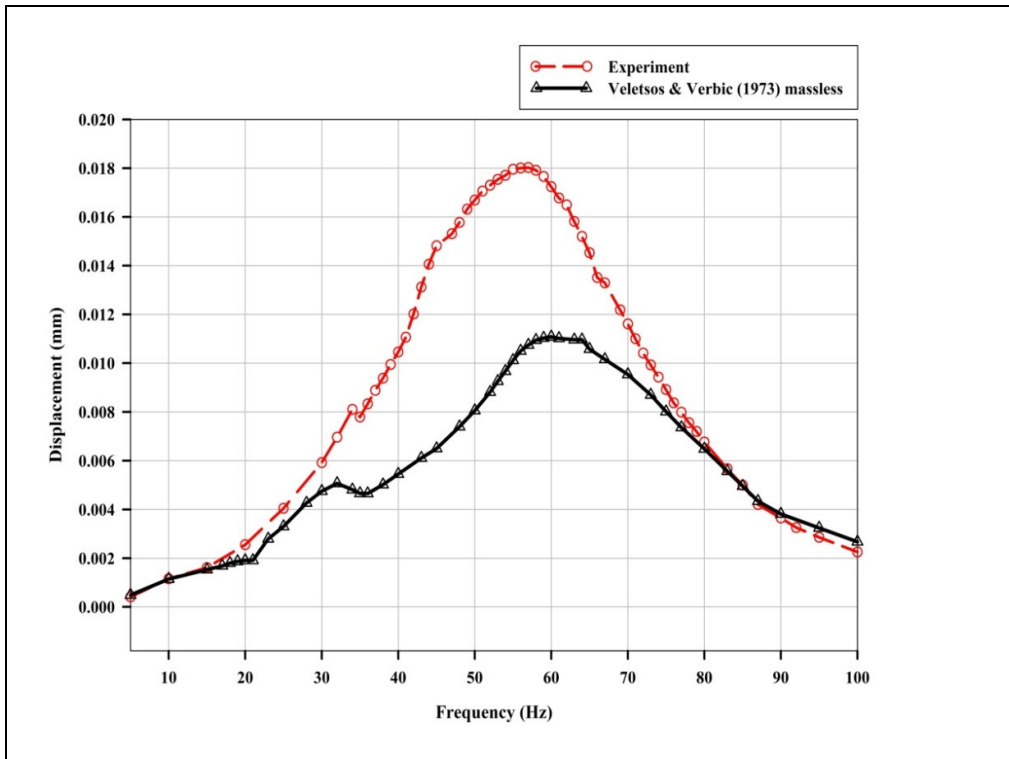
Figure 5.17: Foundation vertical harmonic response obtained from field-measured data and from Veletsos and Verbic (1973) – Massless soil
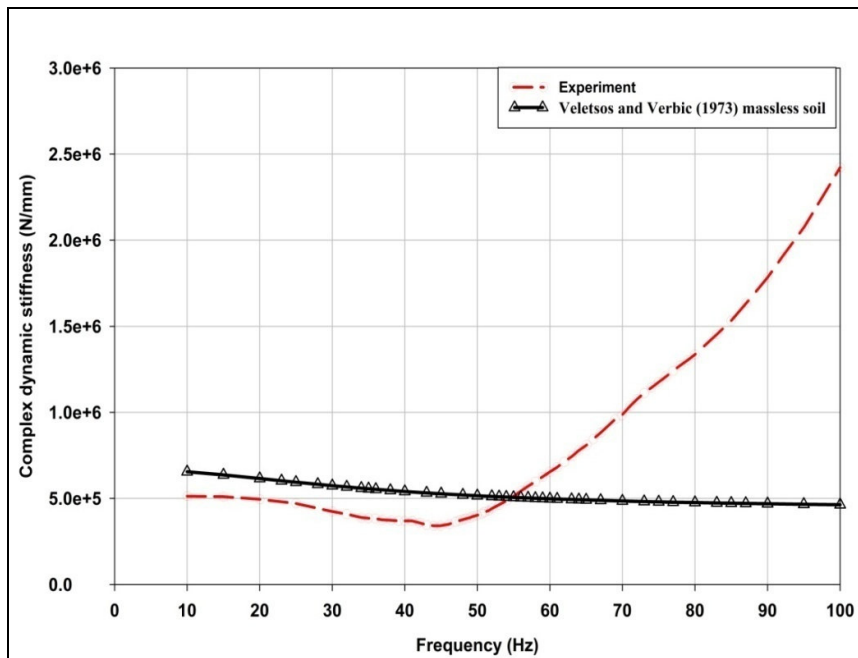

Figure 5.18: Vertical dynamic stiffness impedance function obtained from field-measured data and from Veletsos and Verbic (1973)-massless soil
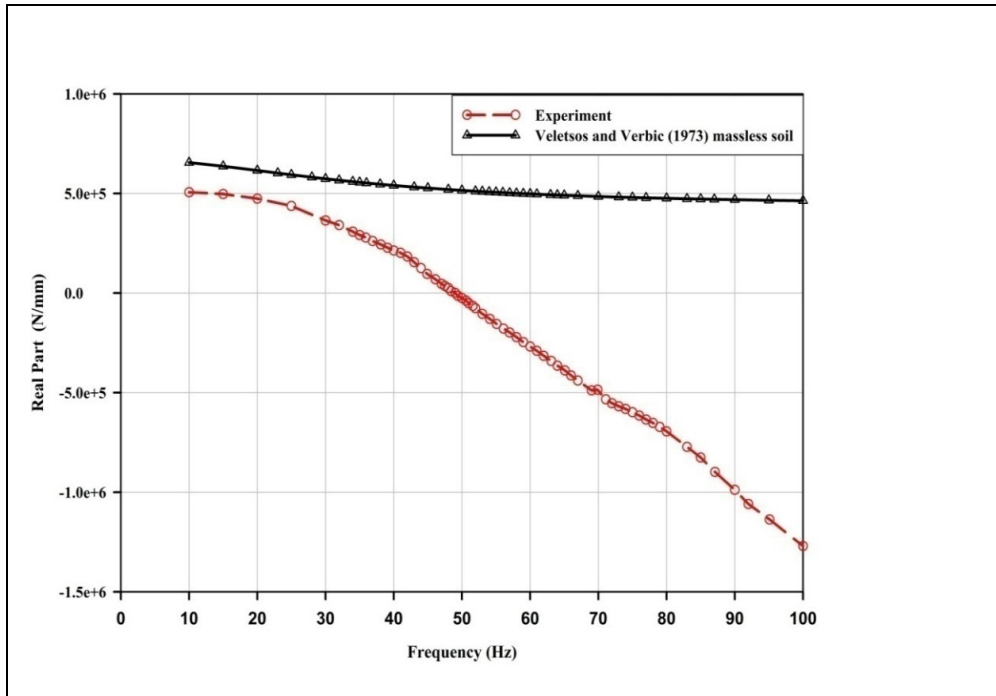
Figure 5.19: Effective dynamic stiffness (real part) obtained experimentally and from Veletsos and Verbic (1973) - massless soil

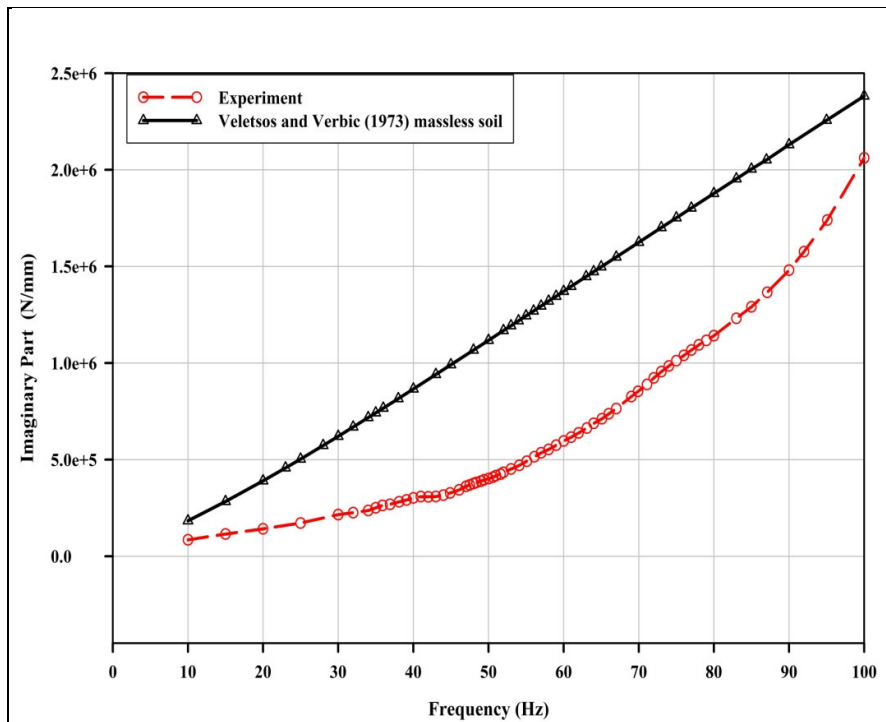
Figure 5.20: Imaginary part obtained from field-measured data and from Veletsos and Verbic (1973)-massless soil

5-43

Figure 5.21: Phase angle between displacement and forcing function from field-measured data and from Veletsos and Verbic (1973)-massless soil
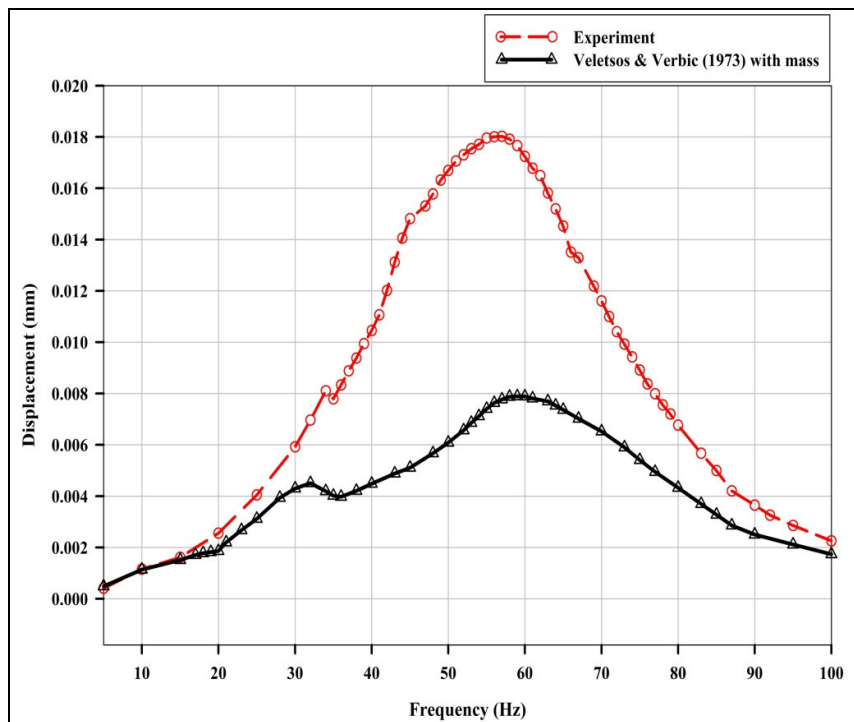
Figure 5.22: Foundation vertical response obtained from field-measured data and from Veletsos and Verbic (1973) soil with mass

5-44
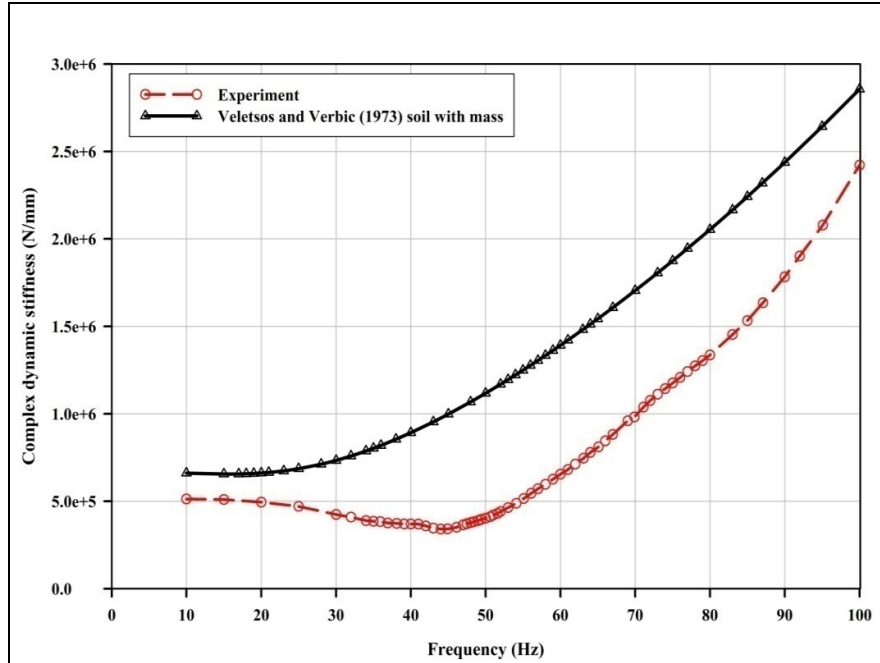
Figure 5.23: Vertical dynamic stiffness impedance function obtained from field-measured data and from Veletsos and Verbic (1973) soil with mass
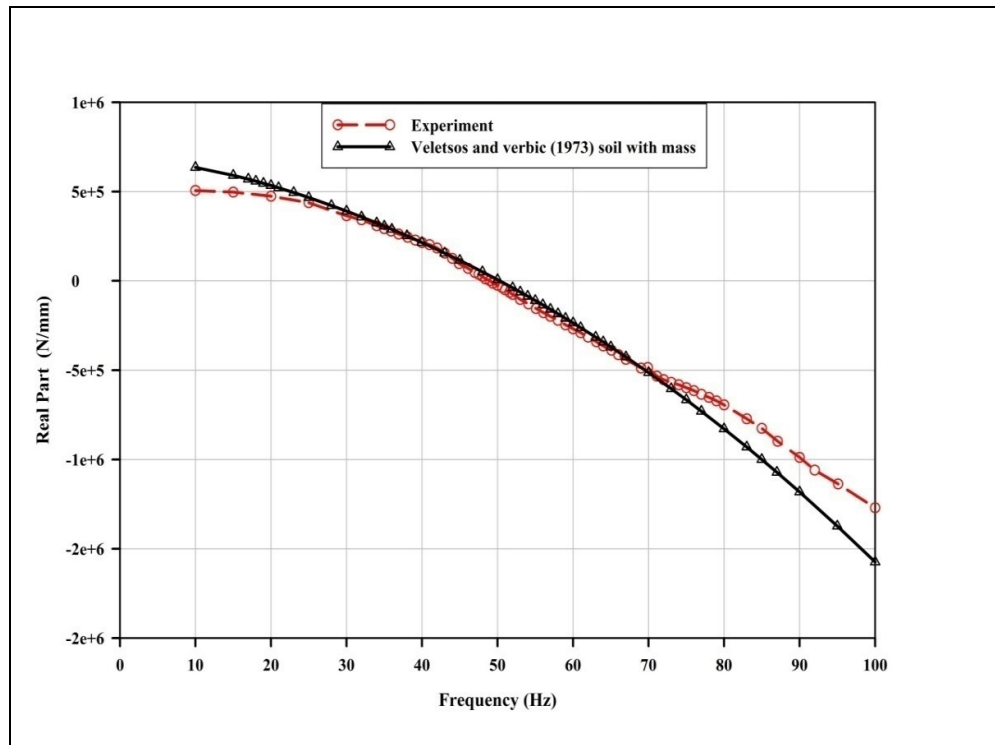
Figure 5.24: Effective dynamic stiffness obtained experimentally and from Veletsos and Verbic (1973) soil with mass

5-45

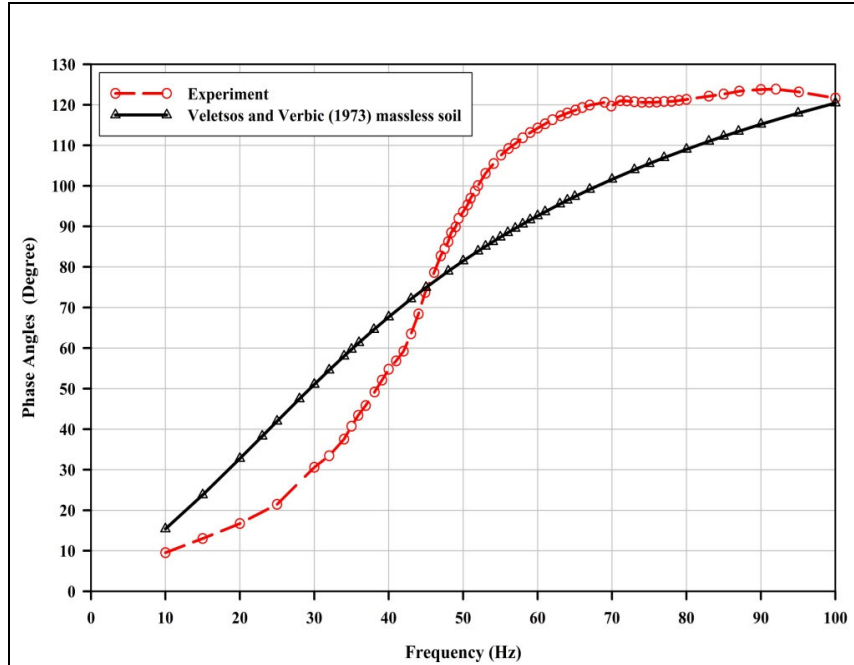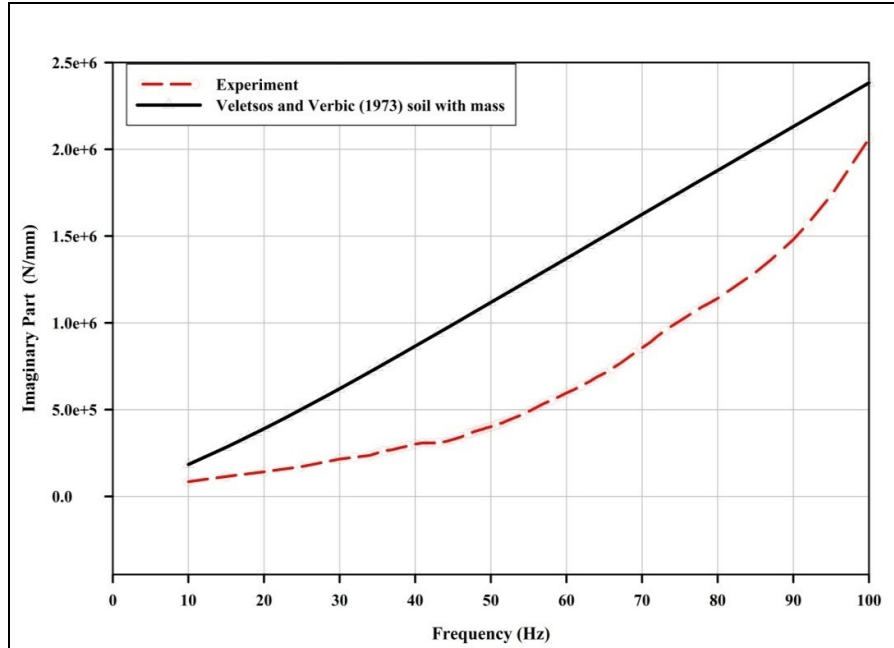Figure 5.25: Imaginary part obtained from field-measured data and from Veletsos and Verbic (1973) soil with mass
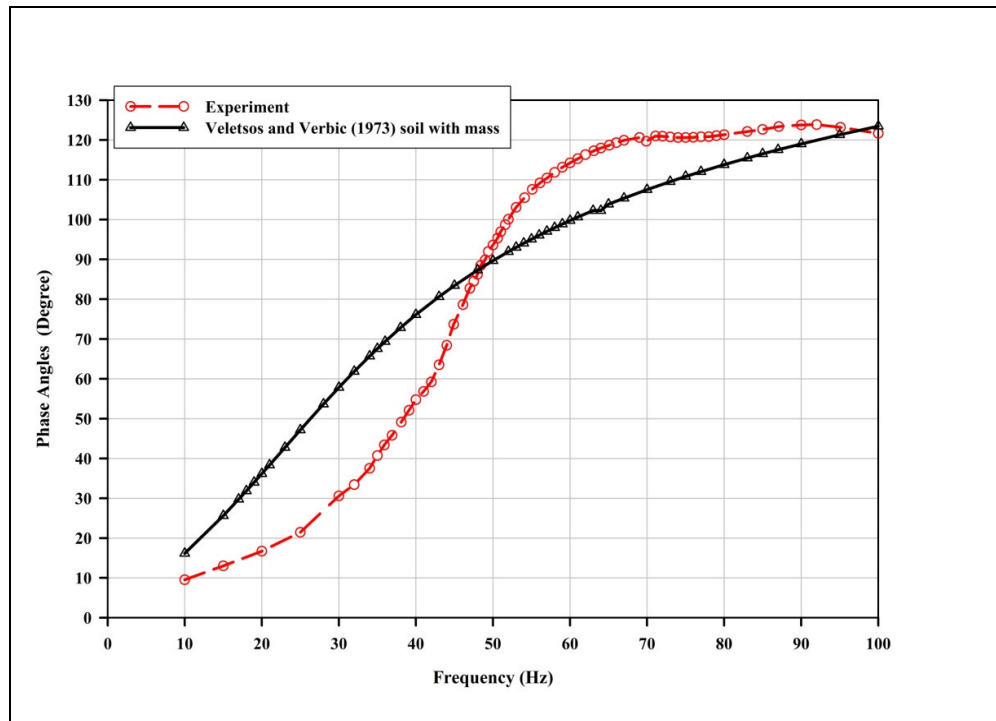
Figure 5.26: Phase angle obtained from field-measured data and from Veletsos and Verbic (1973) soil with mass

5-46
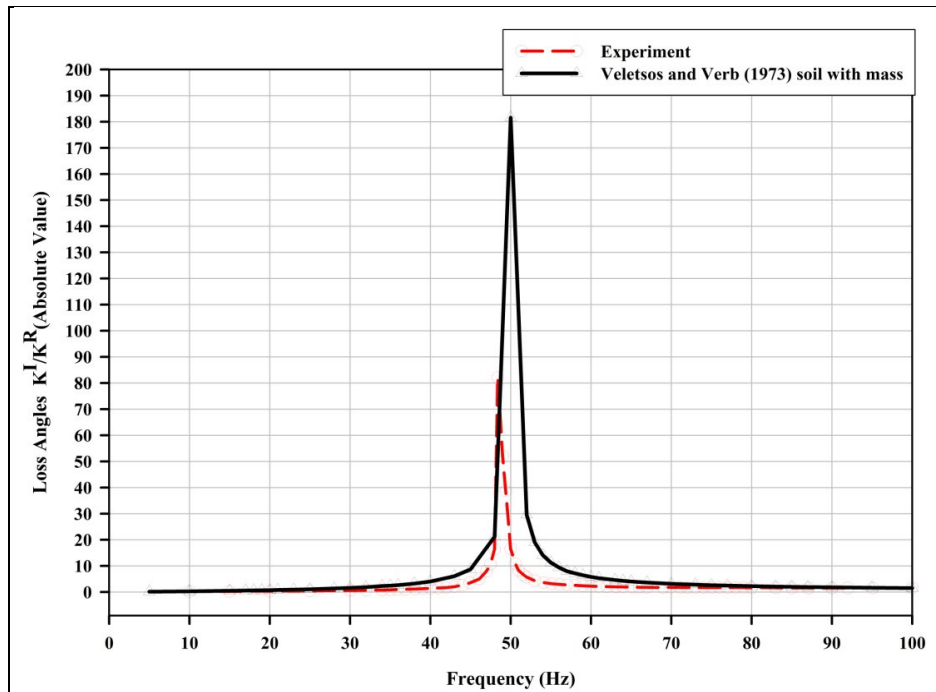
Figure 5.27: Phase angle obtained from field-measured data and from Veletsos and Verbic (1973) soil with mass.
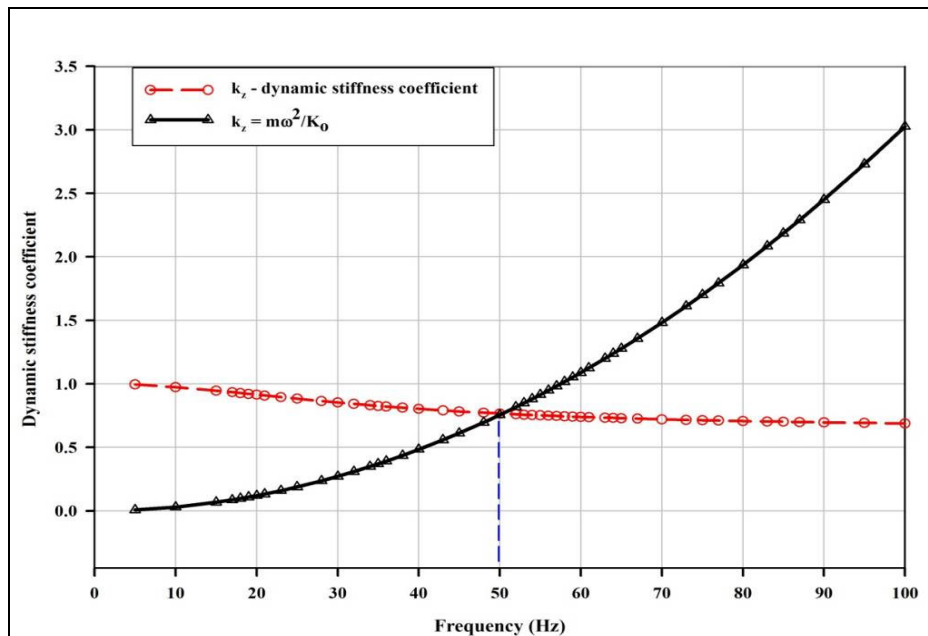
Figure 5.28: Determination of natural frequency using Veletsos and Verbic (1973) soil with mass

5-47
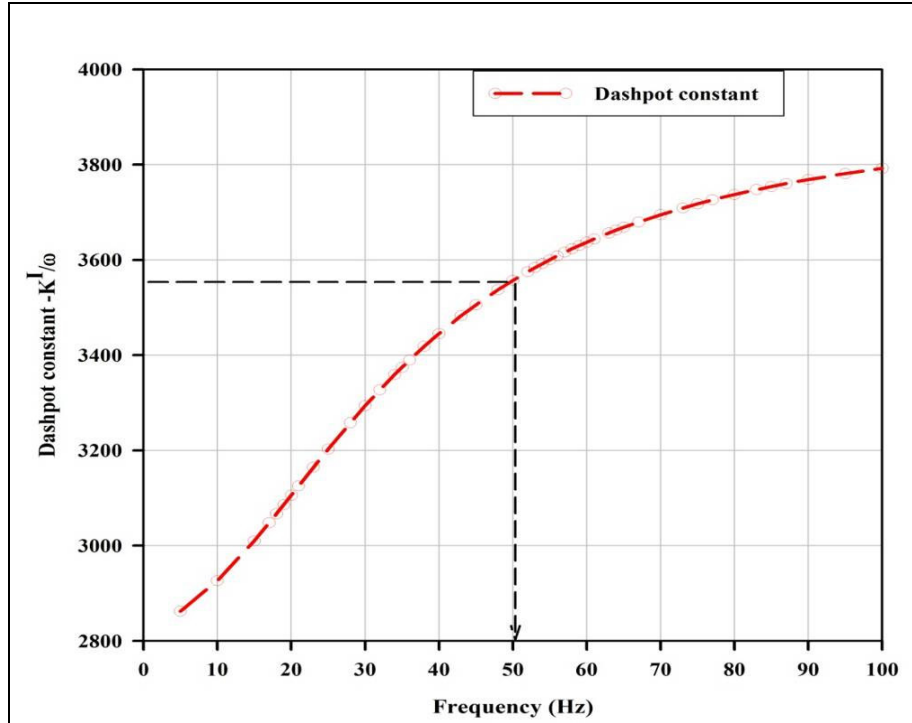
Figure 5.29: Determination of damping constant using Veletsos and Verbic (1973) soil with mass
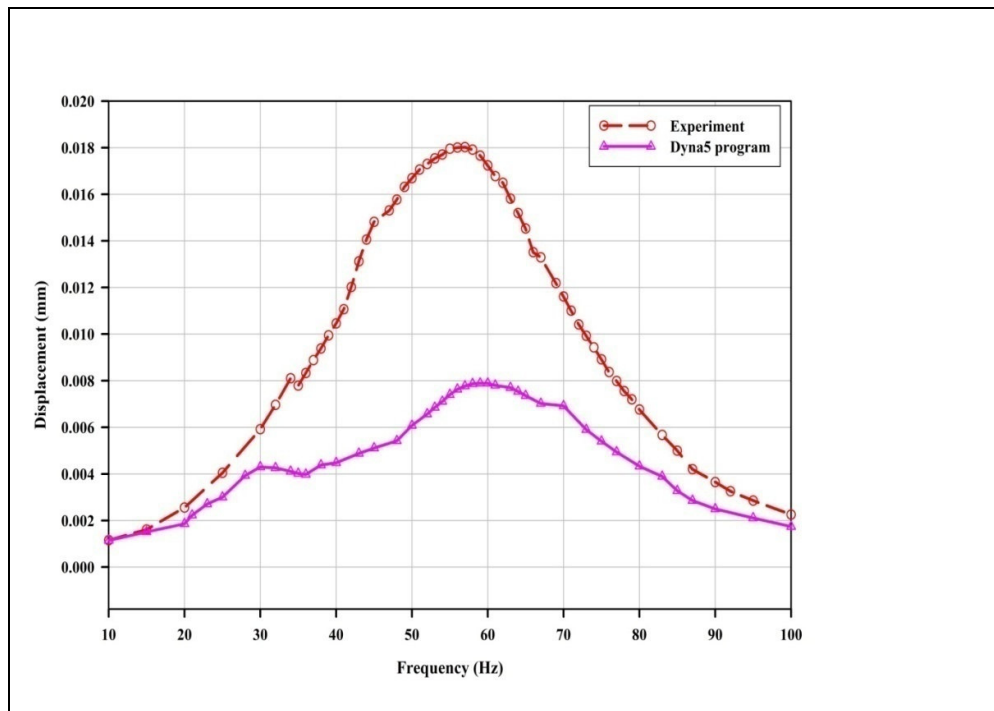
Figure 5.30: Foundation vertical response obtained from field-measured data and Dyna5 program

5-48
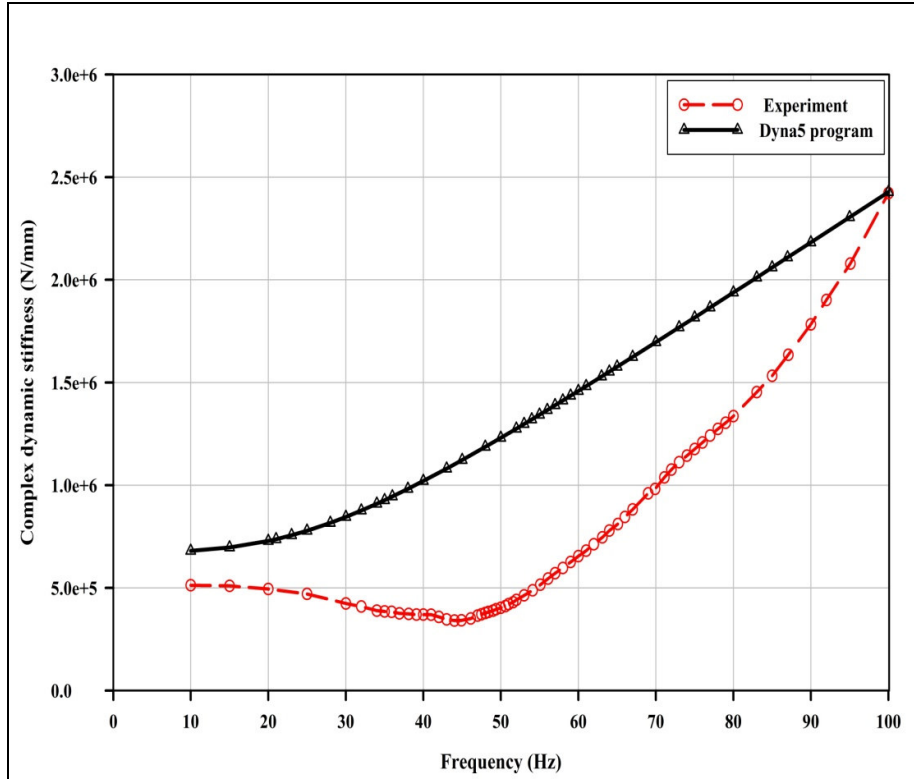
Figure 5.31: Comparison between measured complex dynamic stiffness and Dyna5 program
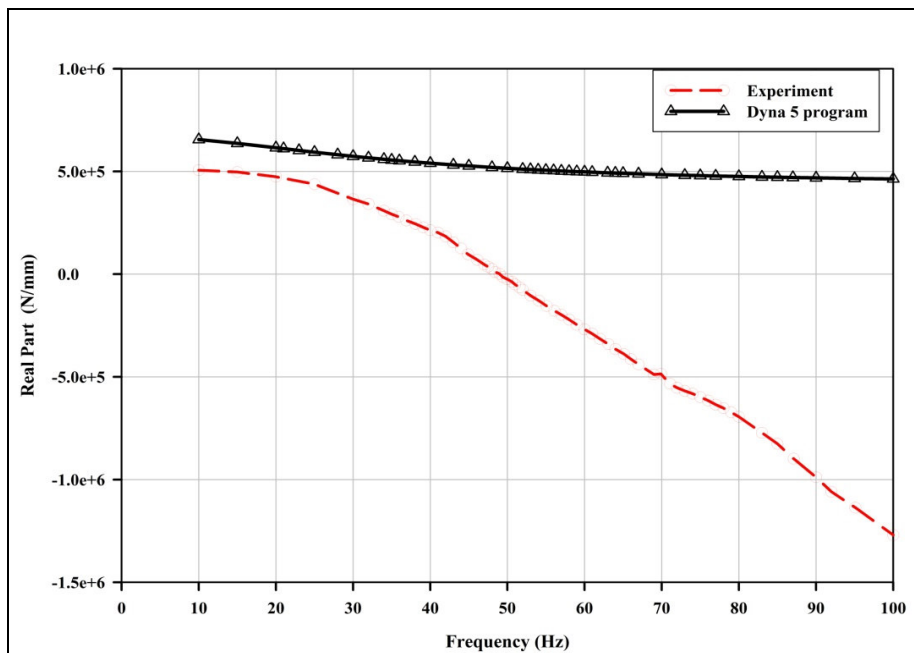
Figure 5.32: Foundation vertical response obtained from field-measured data and Dyna5 program
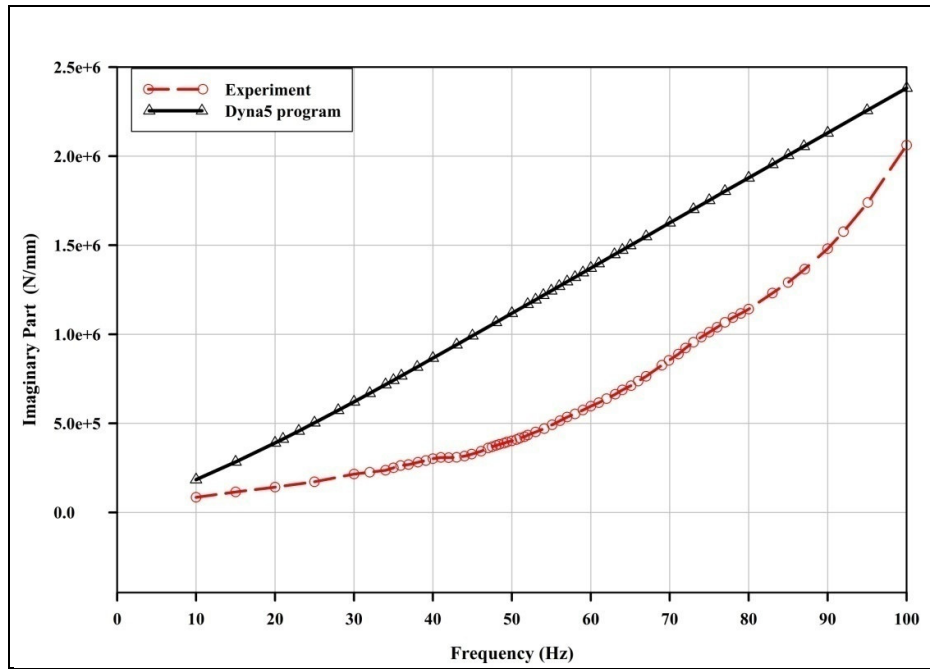
Figure 5.33: Imaginary part obtained from field-measured data and Dyna5 program
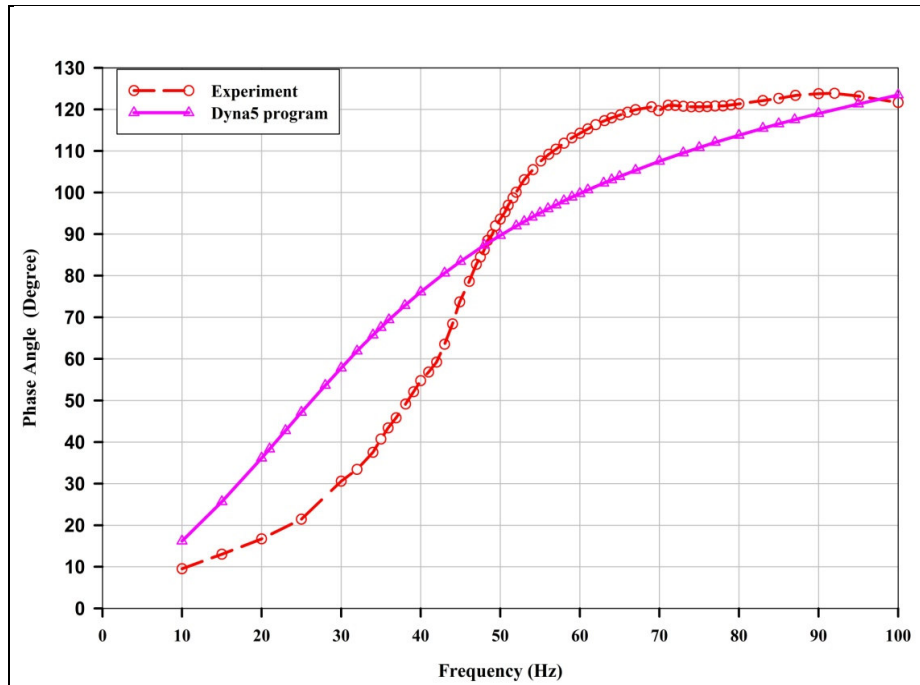
Figure 5.34: Phase angles obtained from field-measured data and Dyna5 program

5-50

1.24 m - Embedment

0.93m - Embedment

0.62 m - Embedment

0.31m - Embedment

0.0m – Embedment

Figure 5.35: Footing embedded at different embedment depths
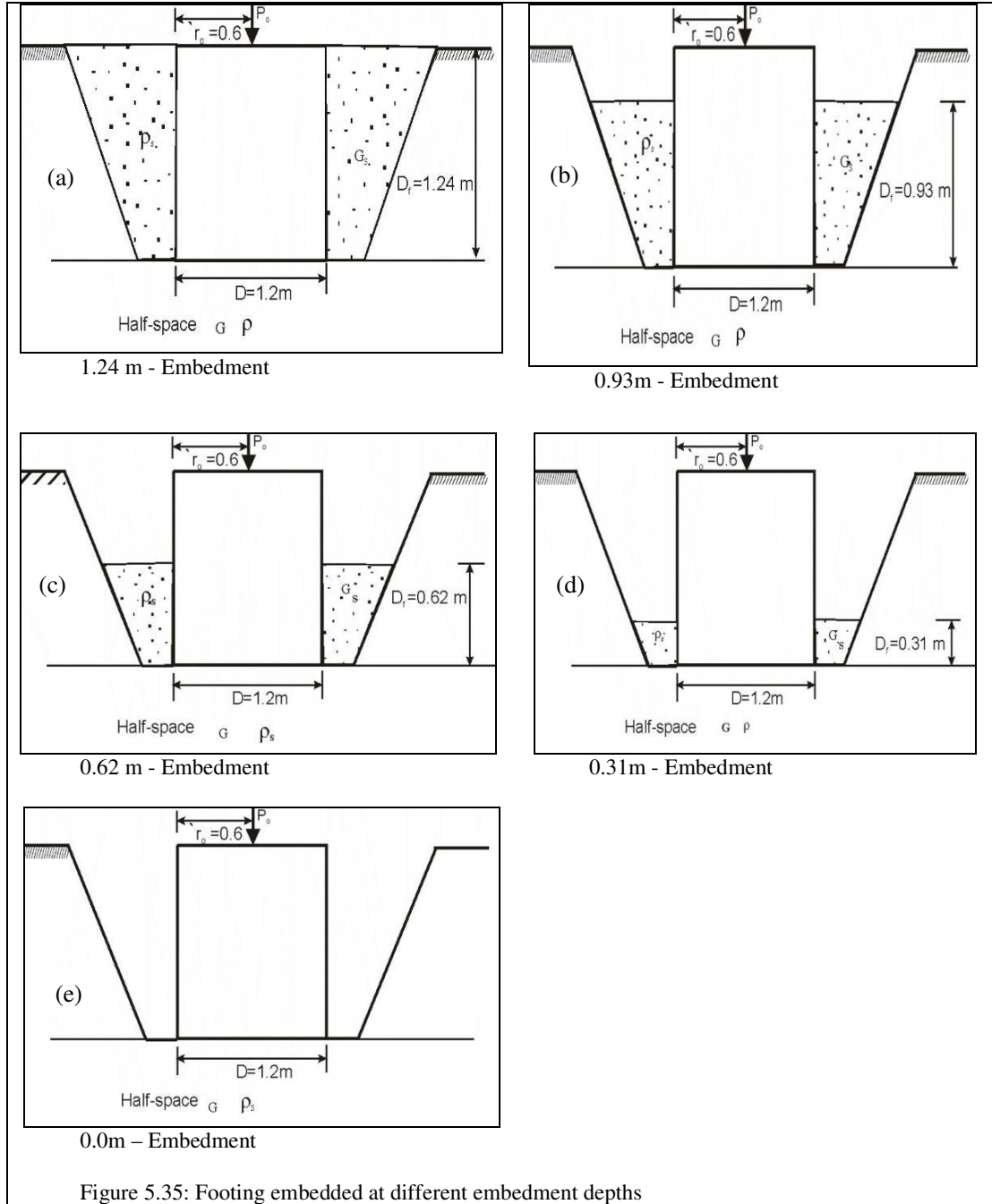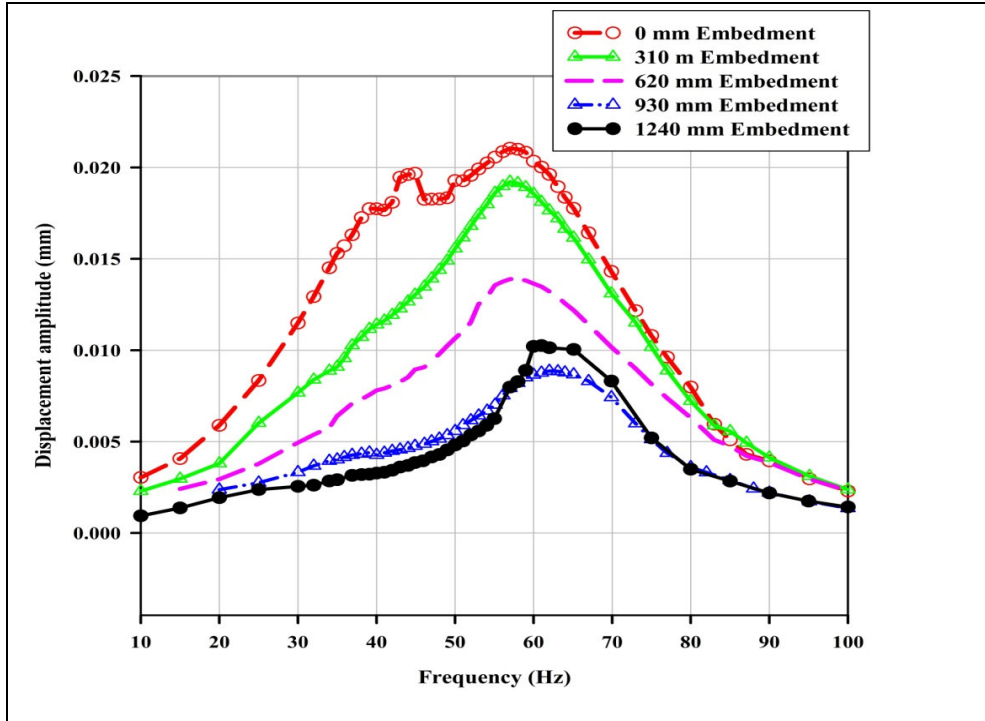
Figure 5.36: Displacement due measured force in the field - Novak and Beredugo (1972)
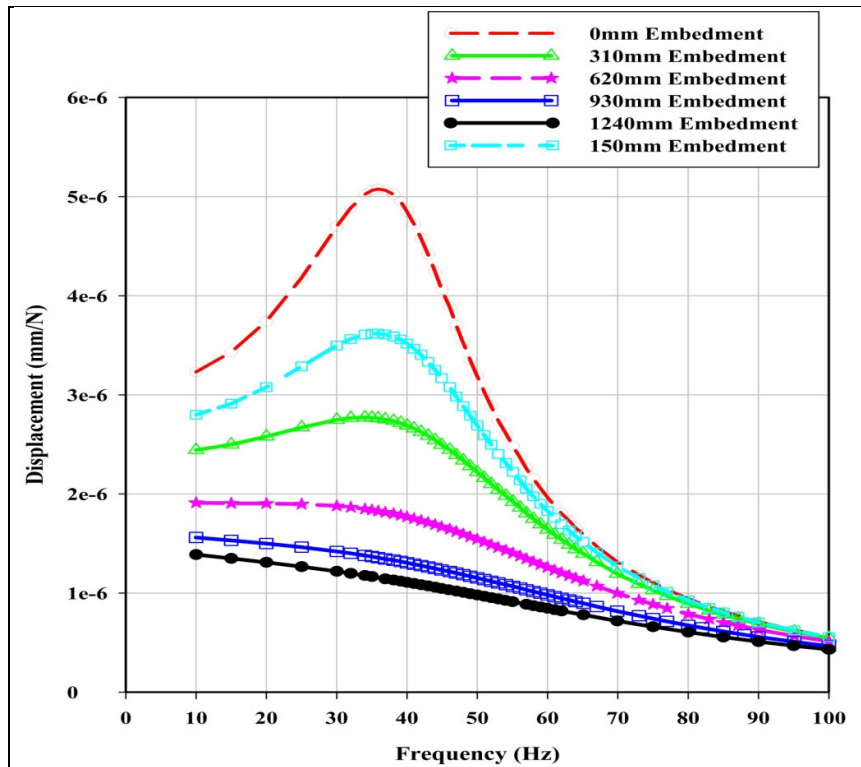
Figure 5.37: Displacement amplitude due to unit load –Novak and Beredugo (1972)
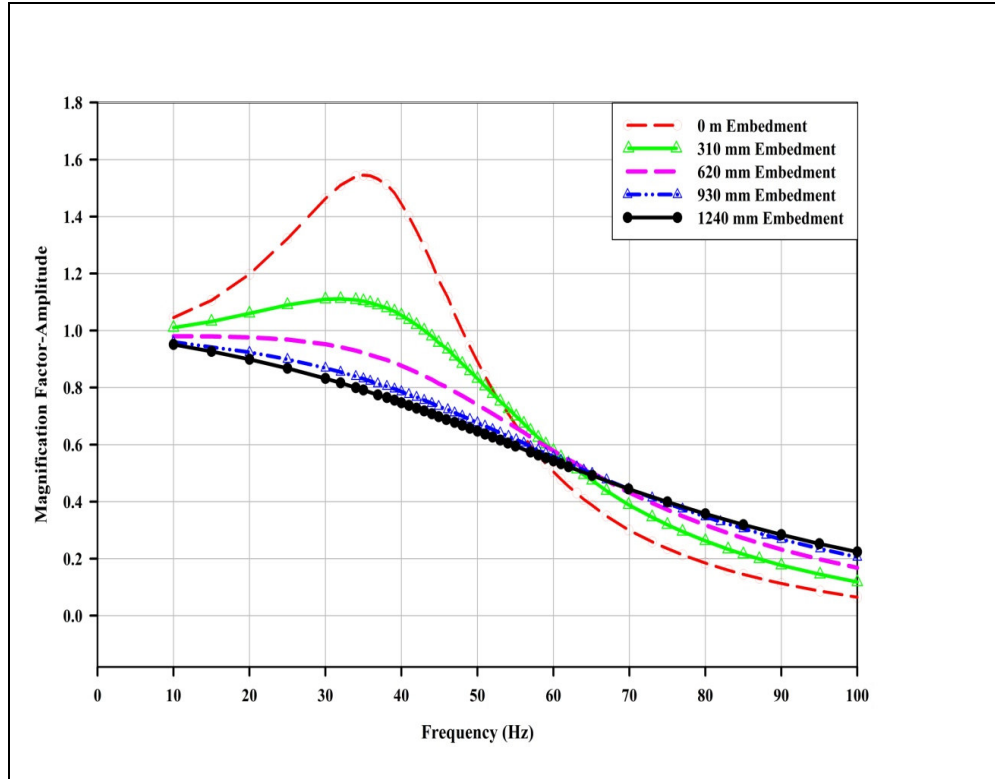
Figure 5.38: Magnification factor – 0, 310, 620, 930 mm, and 1240 mm embedment
Novak and Beredugo (1972)
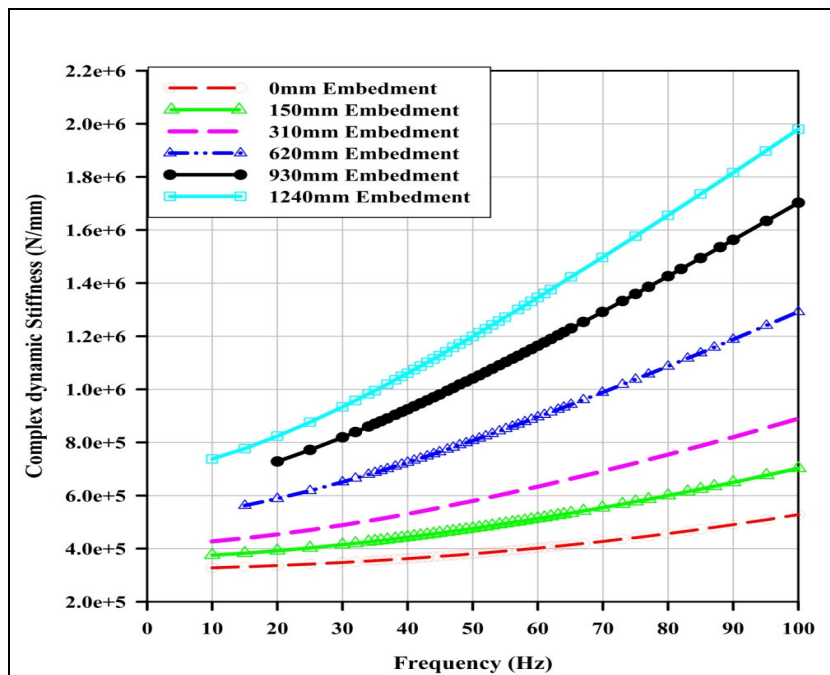
Figure 5.39: Vertical complex dynamic stiffness - Novak and Beredugo (1972)
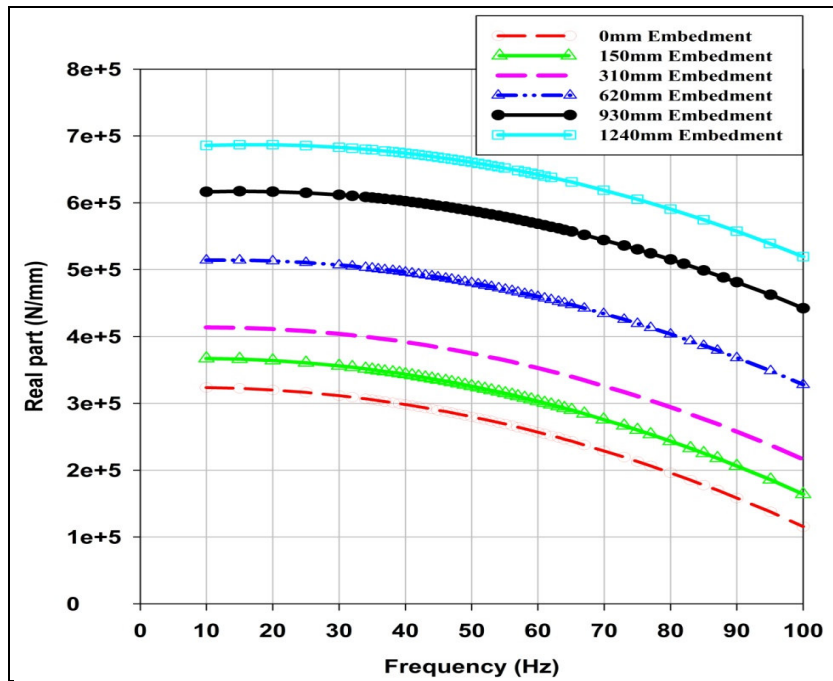
Figure 5.40: Vertical responses- Real part - Novak and Beredugo (1972)
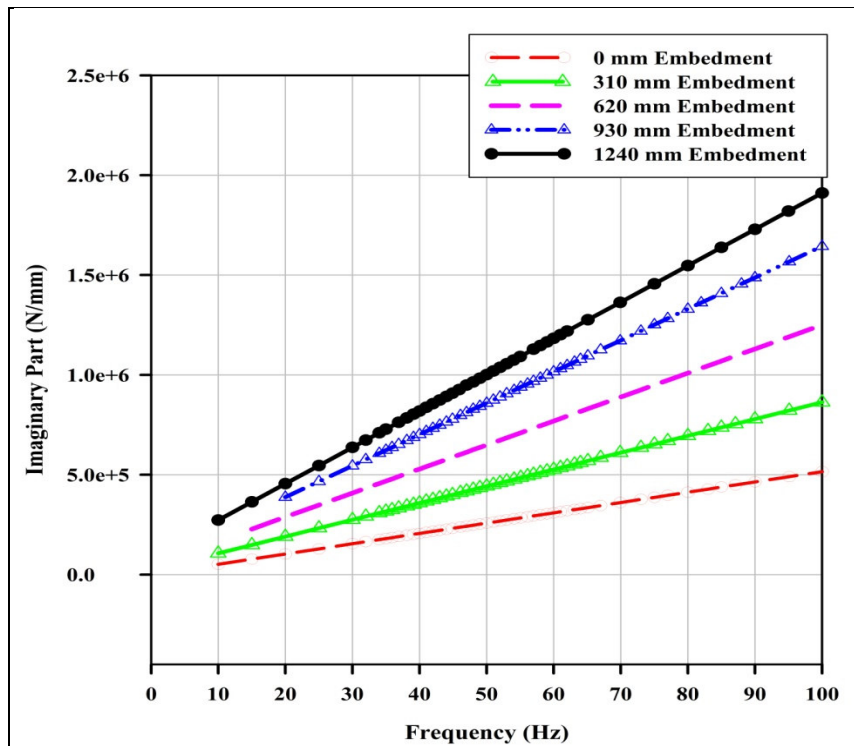
Figure 5.41: Vertical responses- Imaginary part - Novak and Beredugo (1972)

5-54
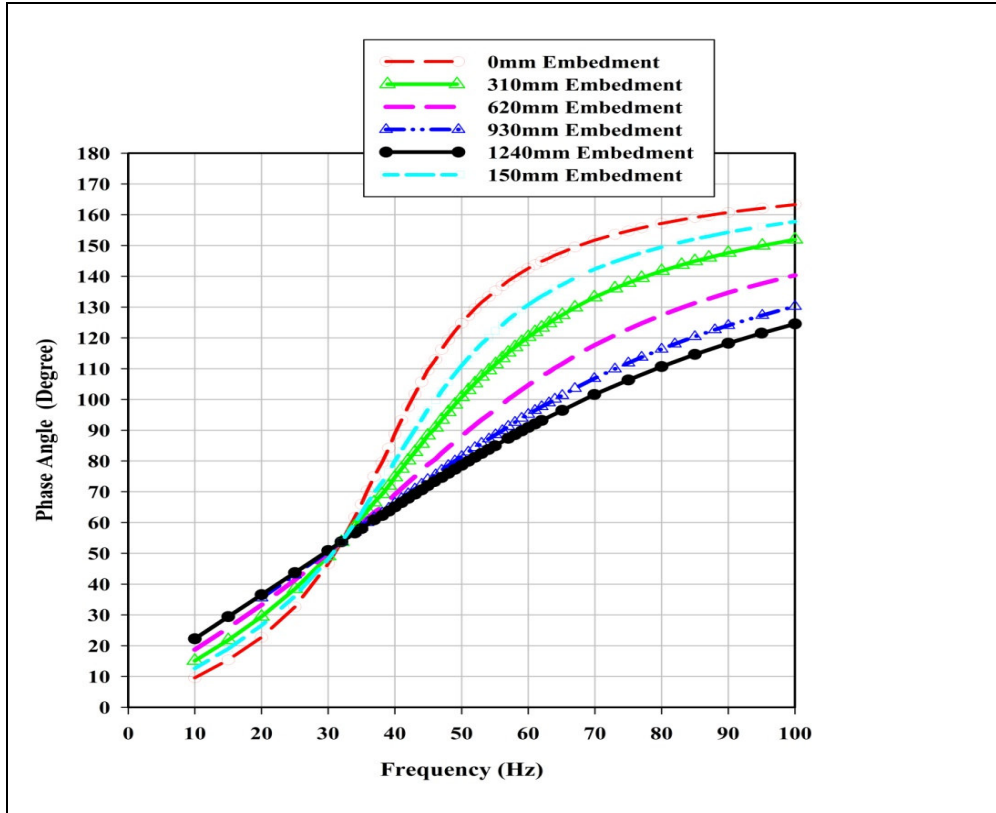
Figure 5.42: Phase angle for different embedment depths - Novak and Beredugo (1972)

5-55
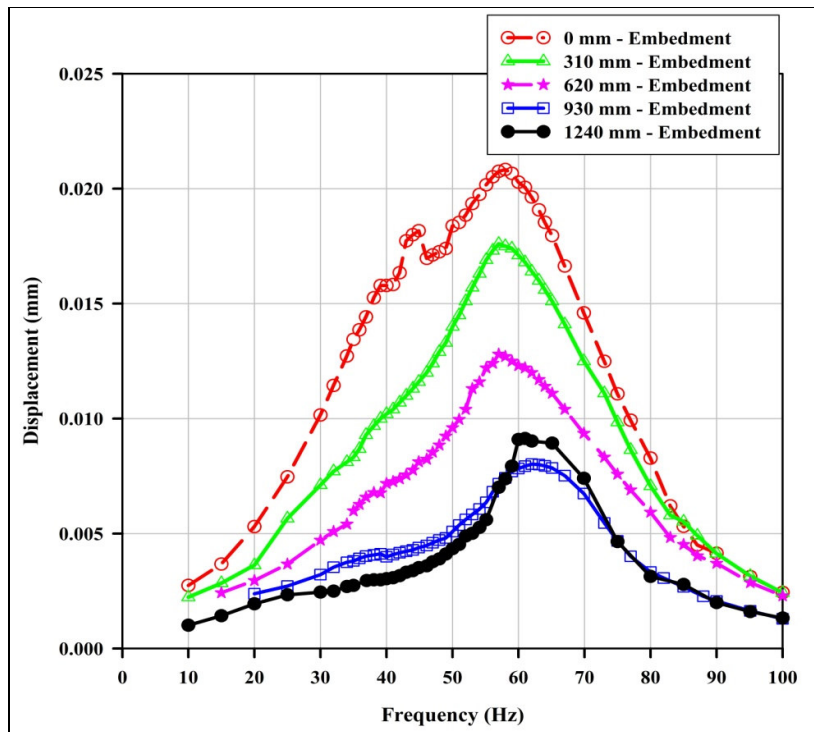
Figure 5.43: Displacement due measured force in the field - Dyna5 program.
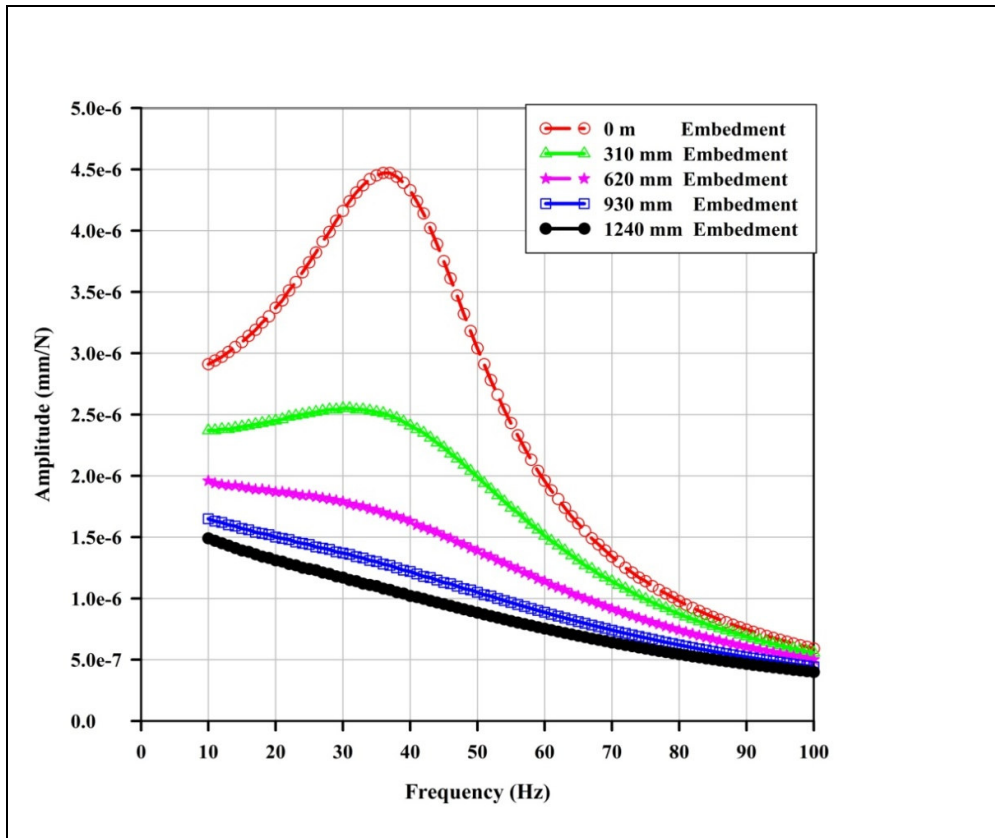
Figure 5.44: Displacement amplitude due to unit load – Dyna5 program
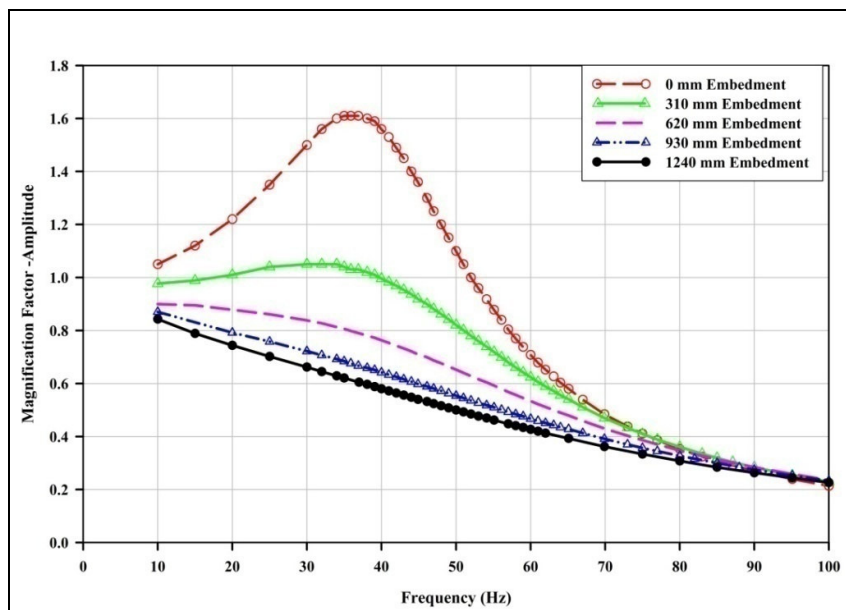
Figure 5.45: Magnification factor – 0, 310, 620, 930 mm, and 1240 mm embedment Dyna5 program
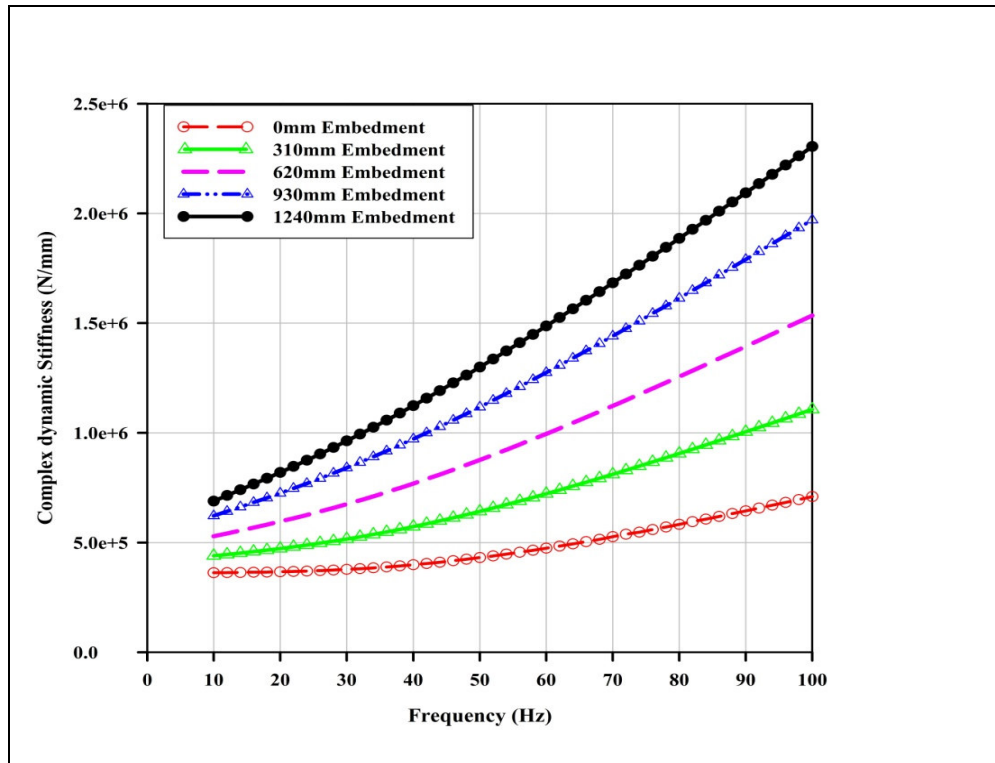
Figure 5.46: Vertical complex dynamic stiffness – Dyna5 program
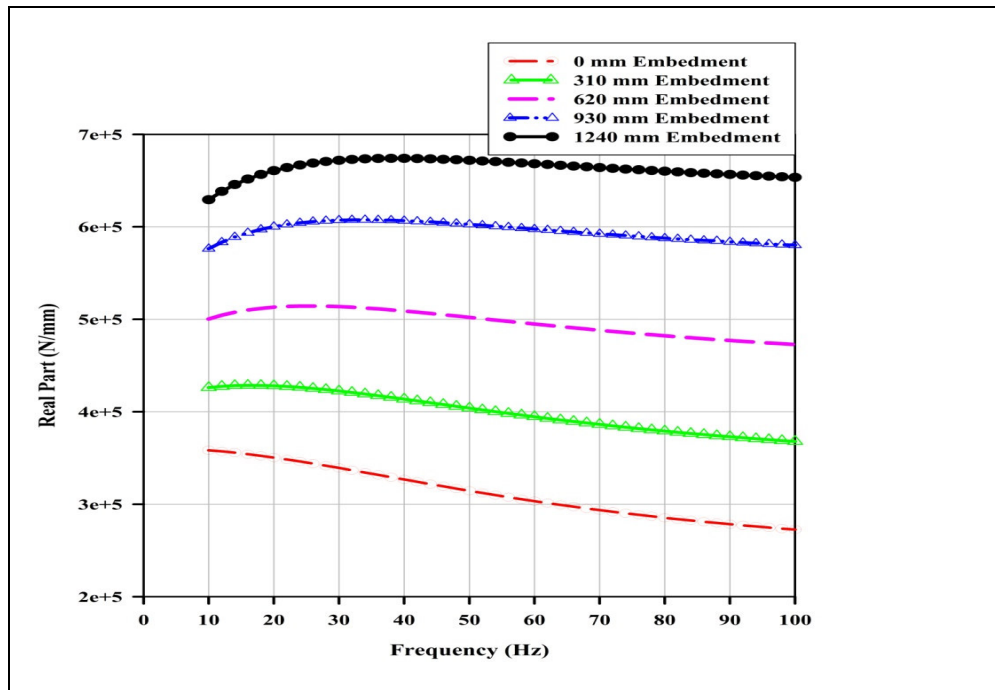
Figure 5.47: Vertical responses- Real part – Dyna5 program

5-57
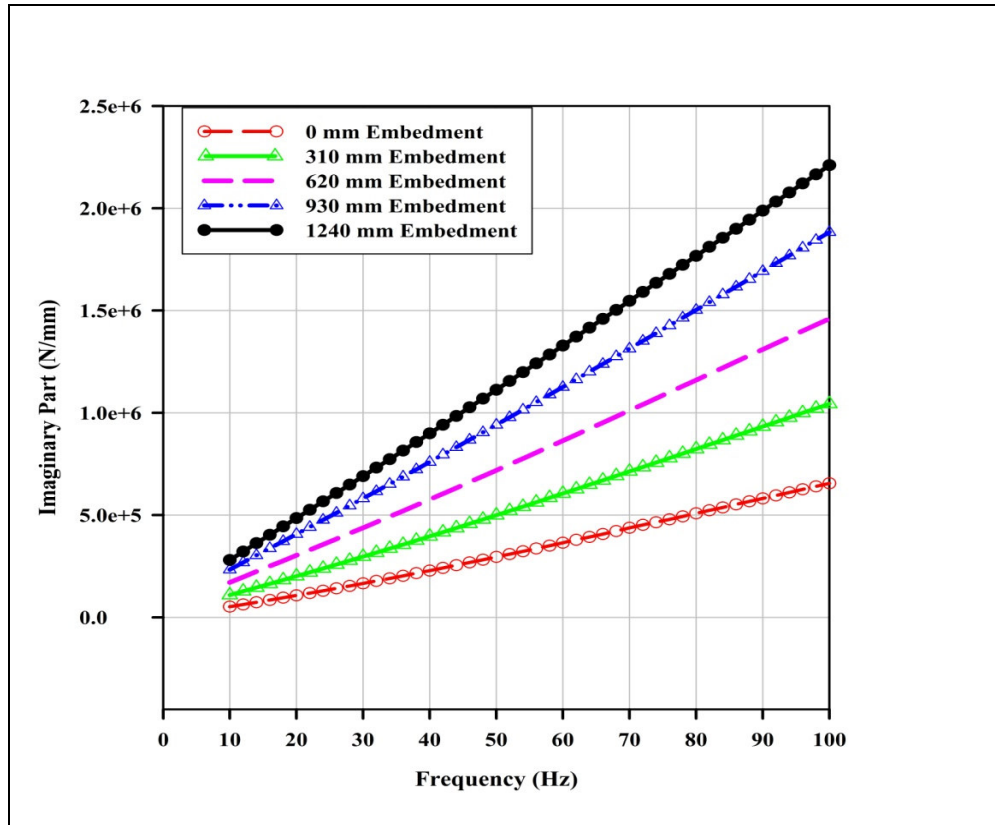
Figure 5.48: Vertical responses- Imaginary part – Dyna5 program
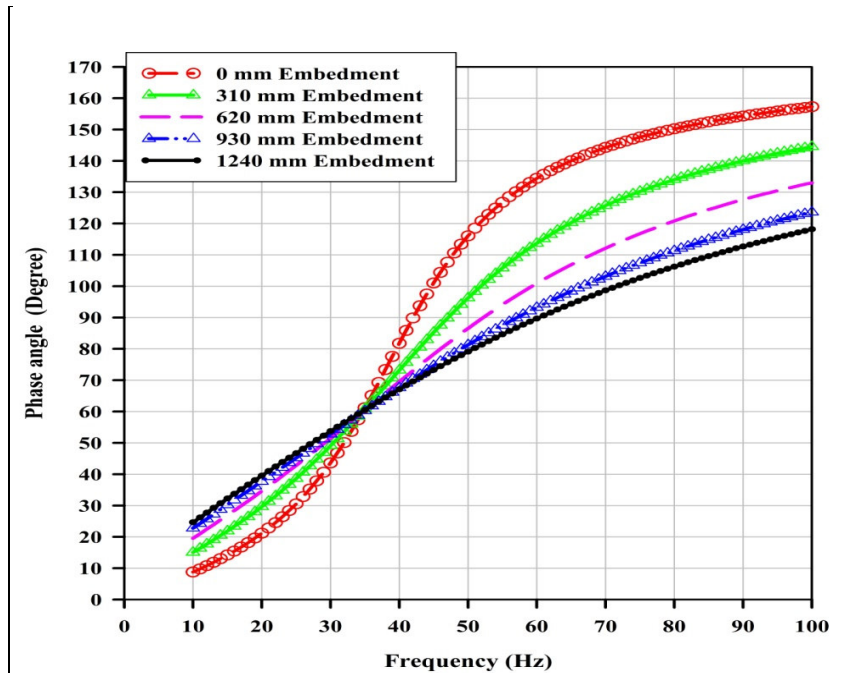
Figure 5.49: Phase angle for different embedment – Dyna5 program
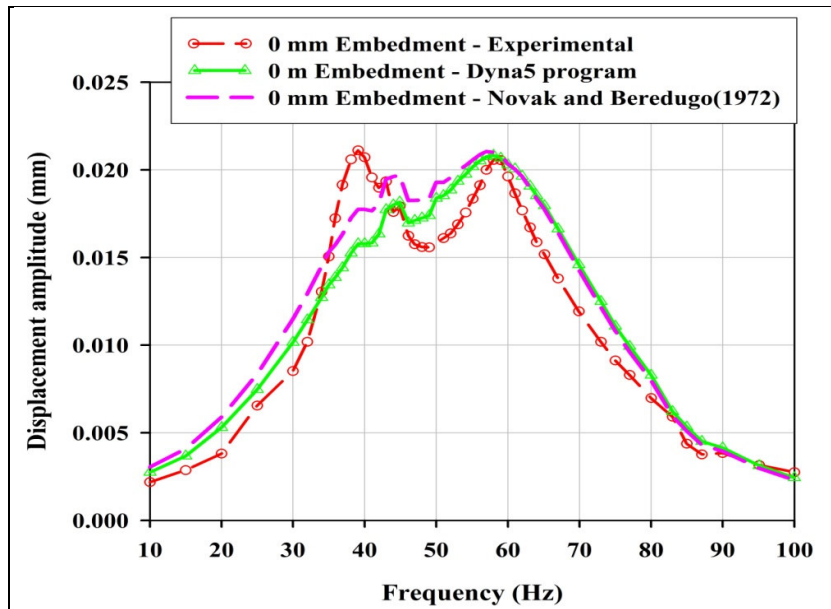
Figure 5.50: Comparison of displacement amplitude for 0mm embedment - Experimental, Dyna5 program and Novak and Beredugo (1972)
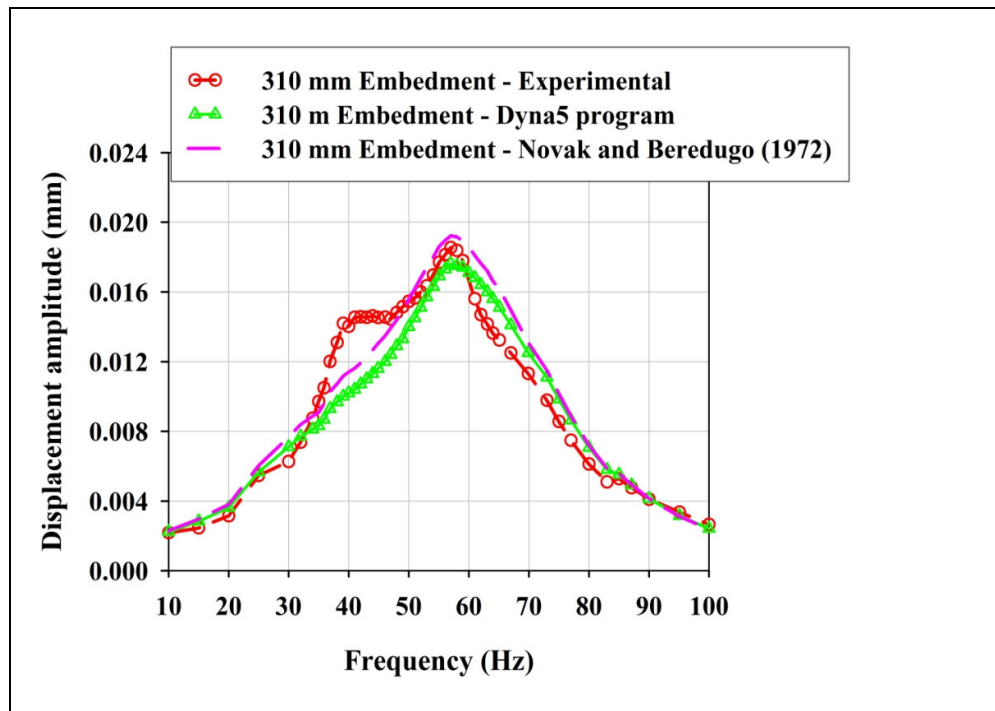
Figure 5.51: Comparison of displacement amplitude for 310mm embedment - Experimental, Dyna5 program and Novak and Beredugo (1972).

5-59
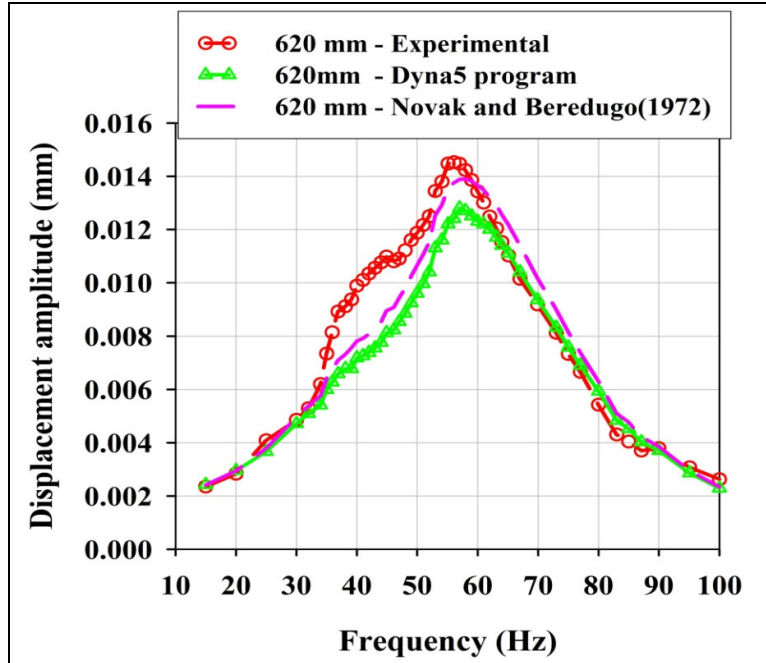
Figure 5.52: Comparison of displacement amplitude for 620mm embedment - Experimental, Dyna5 program and Novak and Beredugo (1972)
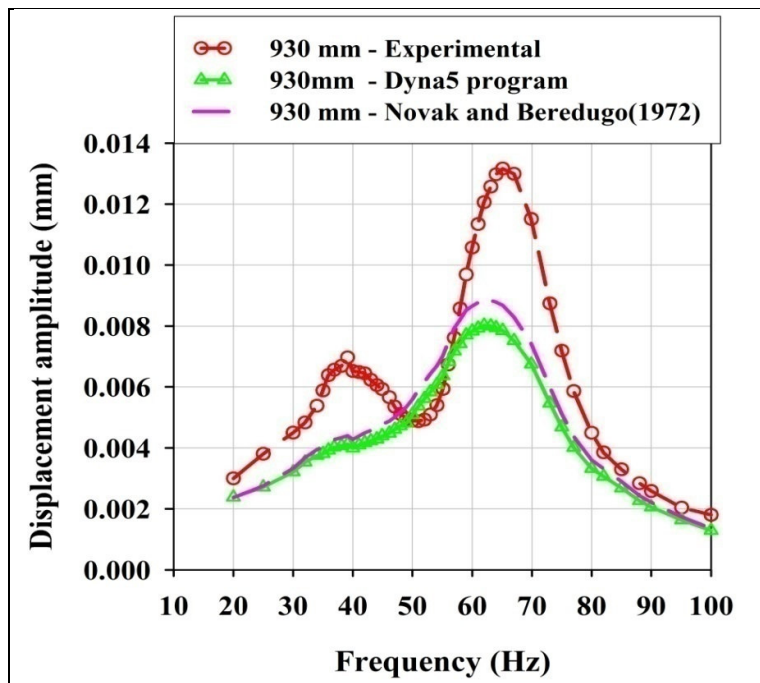
Figure 5.53: Comparison of displacement amplitude for 930mm embedment - Experimental, Dyna5 program and Novak and Beredugo (1972)
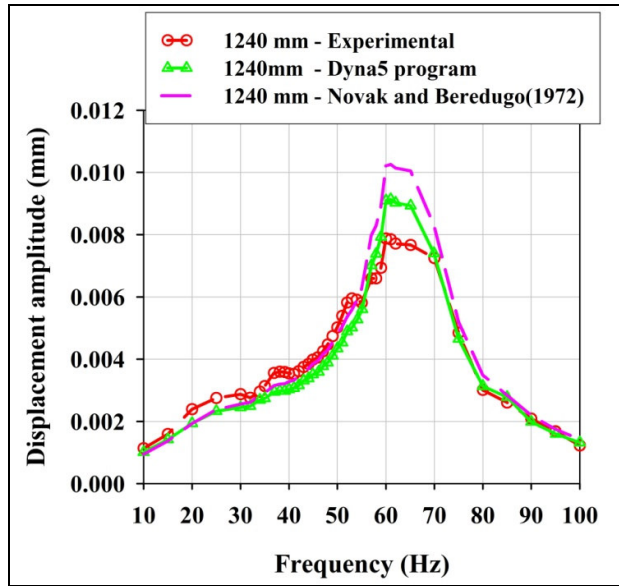
Figure 5.54: Comparison of displacement amplitude for 1240mm embedment - Experimental, Dyna5 program and Novak and Beredugo (1972)
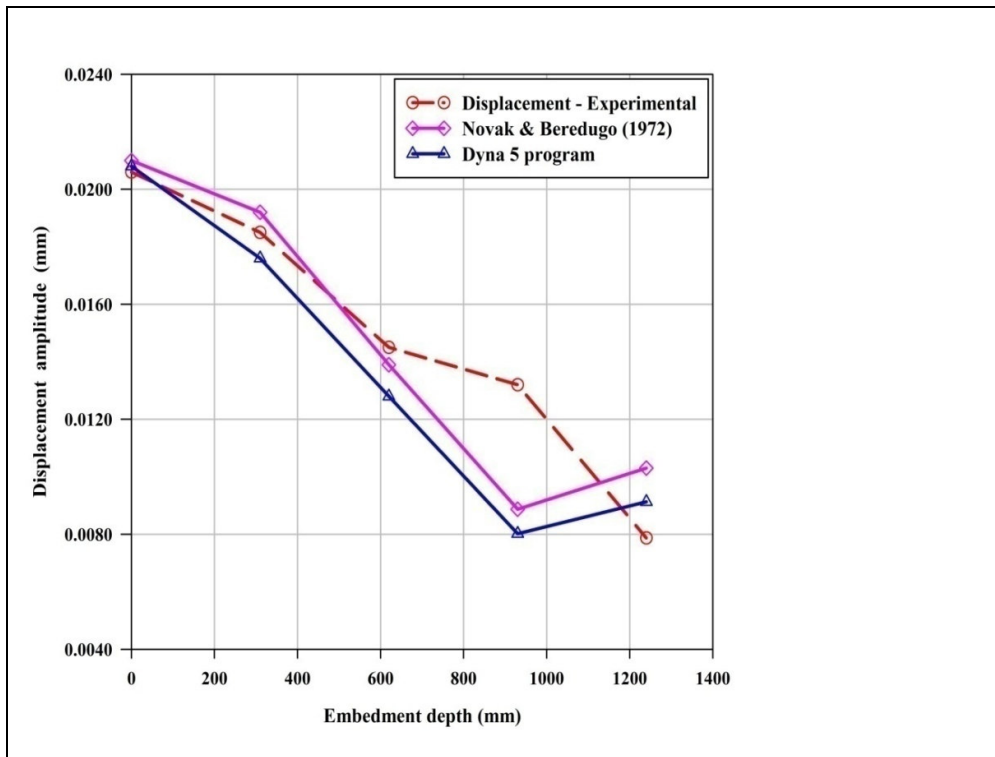
Figure 5.55: Comparison of displacement amplitude at maximum - Experimental, Dyna5 program and Novak and Beredugo (1972)

5-61
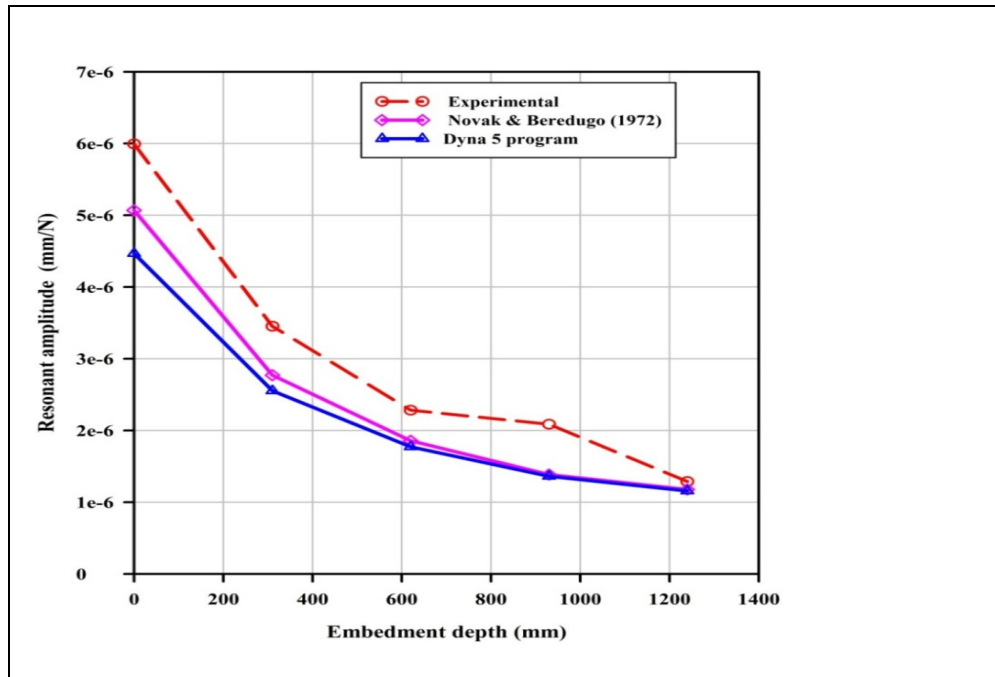
Figure 5.56: Comparison of resonant amplitude - Experimental, Dyna5 program and Novak and Beredugo (1972)
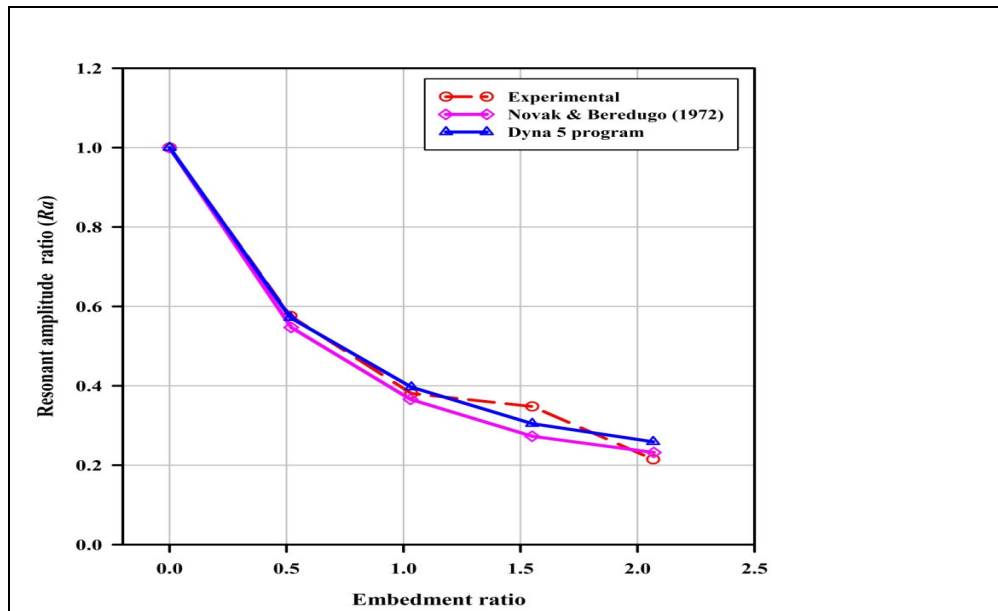
Figure 5.57: Comparison of resonant amplitude ratio - Experimental, Dyna5 program and Novak and Beredugo (1972) – 0, 310, 620, 930 mm, and 1240 mm embedment depths
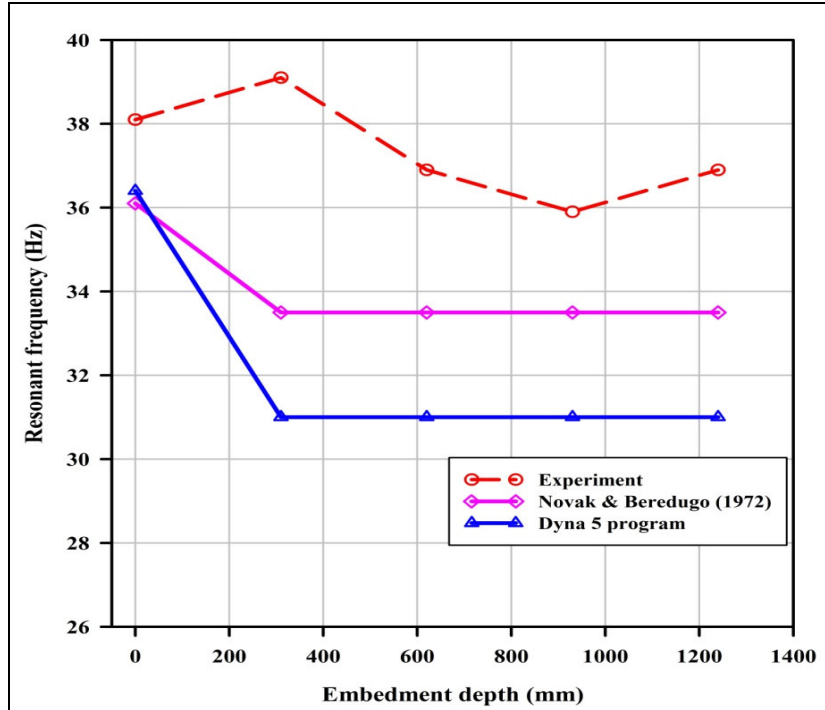
Figure 5.58: Comparison of resonant frequency obtained from - Experimental, Dyna5 program and Novak and Beredugo (1972) – 0, 310, 620, 930 mm, and 1240 mm embedment depth
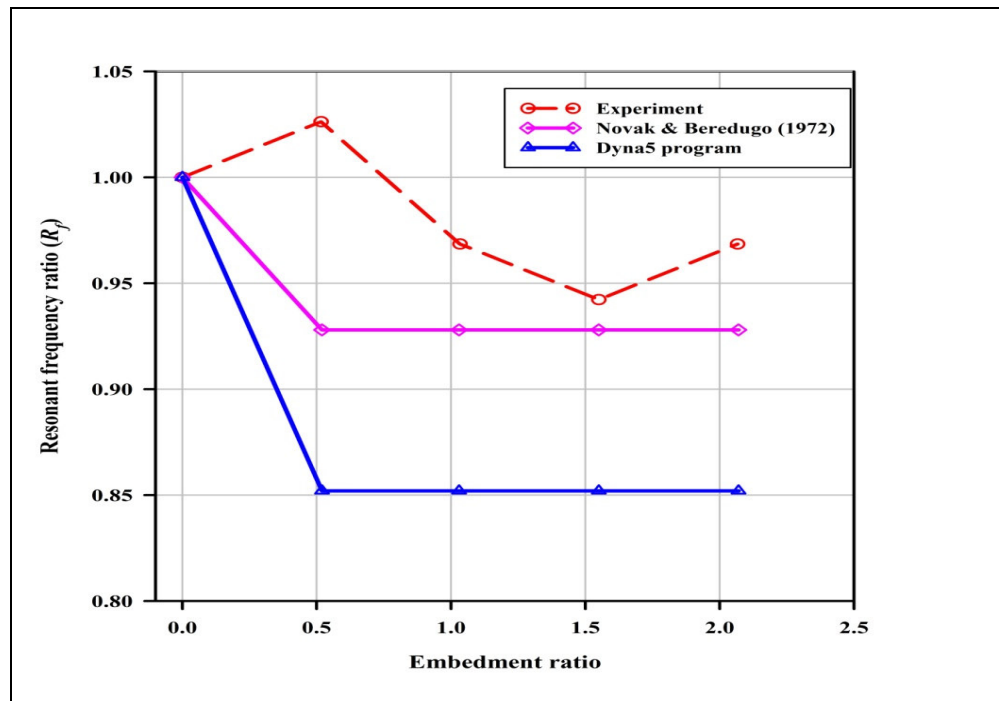
Figure 5.59: Comparison of resonant frequency ratio - Experimental, Dyna5 program and Novak and Beredugo (1972) – 0, 310, 620, 930 mm, and 1240 mm embedment depth

5-63
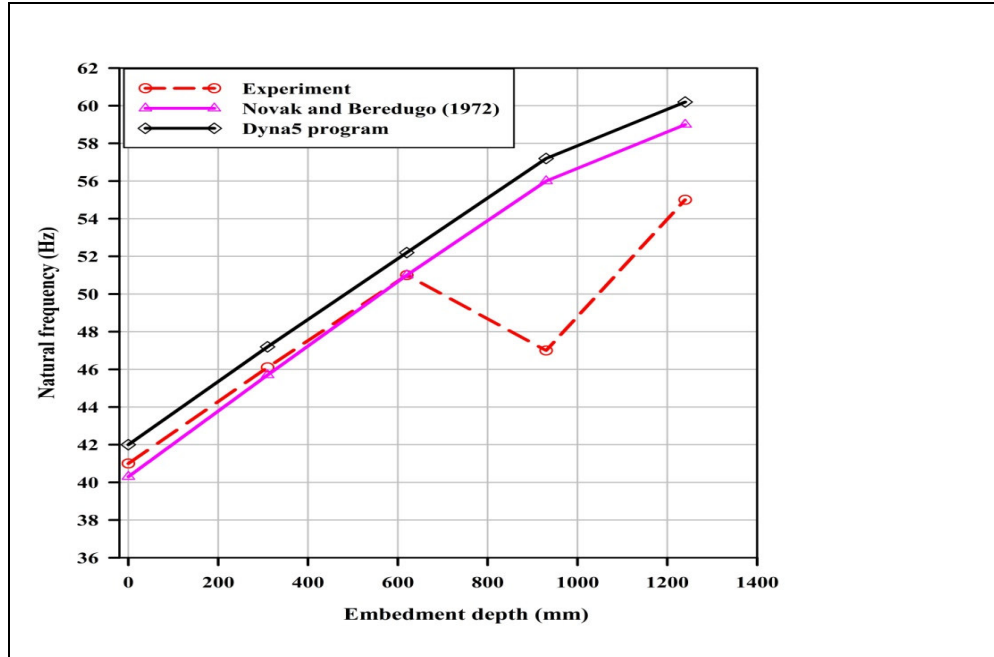
Figure 5.60: Comparison of natural frequency – Experimental, Dyna5 program and Novak and Beredugo (1972) for 0, 310, 620, 930 and 1240 mm embedment
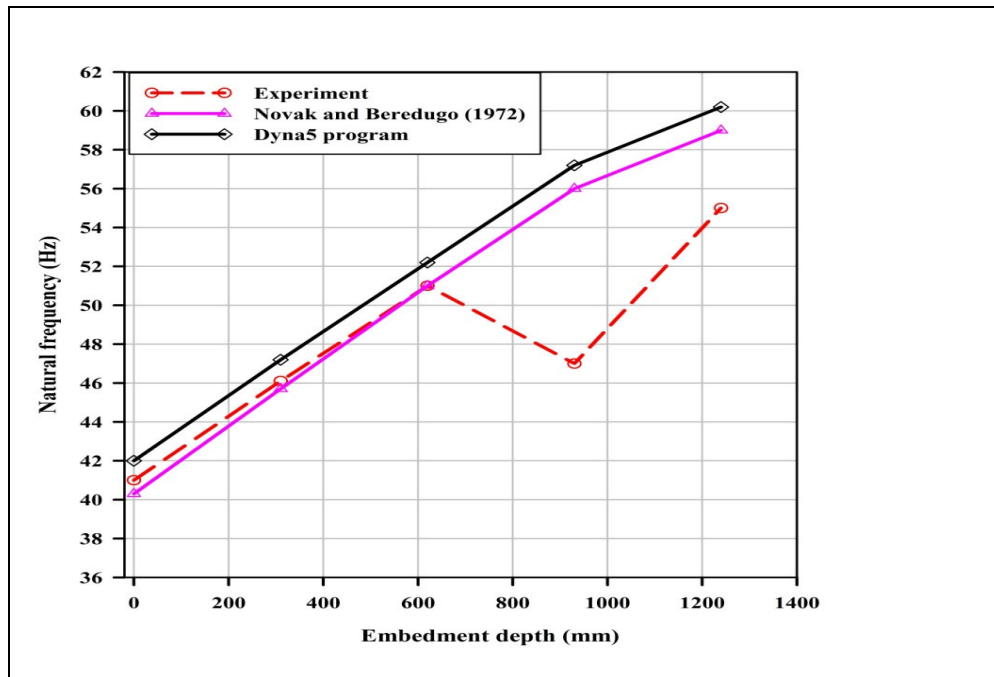
Figure 5.61: Comparison of natural frequency incremental coefficient – Experimental, Dyna5 program and Novak and Beredugo (1972) for 0, 310m, 620, 930 and 1240 mm embedment

CHAPTER 6

6 FINITE ELEMENT METHOD

6.1 Introduction

Numerical analysis of finite element was used to predict the vertical dynamic behaviour of the surface and embedded foundation systems. The surface and embedded foundations described in Chapter 3, Sections 3.5 and 3.7 respectively, were simulated using a three-dimensional finite element method. The Abaqus software was used to analyse the vertical dynamic behaviour of these foundation systems. A major challenge, when analysing wave propagation problems or machine foundation, is the treatment of the model boundaries and it was important to verify the capacity of Abaqus to analyse these. First, a two-dimensional finite element model with non-reflecting boundaries was created to analyse wave propagation in the ground. The model was created to simulate the Continuous Surface Wave test with the main objective being to verify the efficiency of infinite elements in Abaqus to absorb incident waves.

Two models were created to predict vertical dynamic behaviour of the surface foundation system. The first model assumed that the footing is resting on the homogenous, isotropic, elastic half-space soil (here will be referred as Homogenous soil), while the second model presumed that the footing is placed on Gibson soil. In additional, the vertical dynamic behaviour of the embedded foundation systems was determined by considering that the footing is placed on Homogenous and Gibson soil.

6.2 Simulation of the Continuous Surface Wave test using the finite element method

A major challenge when modelling wave propagation problems using the finite element method is defining non-reflecting boundaries. Abaqus/Explicit was used to simulate the wave propagation problem in the ground. The calculations are based on the equations presented in section 2.7. The Continuous Surface Wave (CSW) test was simulated in Abaqus/Explicit by determining the dispersion of a homogenous, isotropic, elastic half-space soil medium. Abaqus/Explicit is a special-purpose analysis module that is part of the Abaqus products and uses an explicit dynamic finite element formulation.

The modelling procedures assumed that the ground is a homogeneous isotropic, elastic half-space medium with soil properties shown in Table 4.1. The domain size of the finite element model used to simulate the wave propagation in the ground is shown in Figure 6.1. The main parts of the model were created in Abaqus/CAE as a visualization tool. Because the soil is loaded axially symmetrically about its central axis, an axisymmetric analysis performed. The finite sections comprise 4-node, linear, axisymmetric, solid continuum and reduced integration elements (CAX4R). The infinite section comprises 4-node linear, one-way axisymmetric solid continuum infinite elements (CINAX4) as seen in Figure 6.1. The domain is comprised of 63,000 elements. The infinite elements were included in the model by editing the created input file manually.

The performance of non-reflecting boundaries was checked by the introduction of fixed boundaries on the right and at the bottom of the model. Thus, the infinite elements were replaced with finite elements. In all cases, a vertical harmonic force excited the model along the axis of symmetry. The time history of vertical dynamic displacement was observed at point A which is located 4.0 m from the source of excitation, as illustrated in Figure 6.1.

Figure 6.2 illustrates the ground displacement response of the finite element model with non-reflecting boundaries and fixed boundaries. The plots show that between 0.3 and 0.55 sec, the displacement response of the model with the fixed boundary is higher than the wave displacement for the model with non-reflecting boundaries by about 85 %. This confirms the importance of introducing non-reflecting boundaries when dealing with wave propagation problems in finite element analysis.

Wave propagation along the surface ground was analysed by simulating a force vibration tests, from which the dispersion of the soil profile illustrated in Figure 6.1 was assessed. Since homogenous soil was modelled, the results were expected to be non-dispersive.The vertical response in the time domain were observed at intervals of 1 m, starting at 1 m away from the applied load. The dominating frequency and phase angle at each observation point was determined by calculating the Fourier transform of the displacement by means of the fast Fourier transform (FFT) algorithm. The phase angles for frequencies between 10 Hz and 95 Hz were calculated using Equation 4.1. Consequently, the phase angles were used to estimate the Rayleigh wave velocity using Equation 4.3.

Figure 6.3 reflects the plots of phase angles versus distance for the frequencies ranging from 10 Hz to 95 Hz. The straight lines indicate that the phase velocity remained constant

within the domain at a particular frequency. The Rayleigh wave velocity remained almost constant at all frequencies ranging between 193 m/s and 204 m/s. The non-dispersion reflects the behaviour of the assumed soil medium of homogeneous, isotropic, elastic half-space. Mbawala et al., (2011) showed that, for an elastic half-space, the Rayleigh wave velocity obtained numerically compared favourably with the one measured experimentally.

From the above, it may be concluded that the Abaqus program is suitable for solving problems of wave propagation using the finite element method.

6.3 Three-dimensional finite element modelling of surface foundation

The vertical dynamic behaviour of the surface foundation systems described in Chapter 3 Section 3.5 was analysed using the finite element method. The calculations are based on the equations presented in section 2.8. This modelling involved the creation of finite elements and infinite elements as shown in Figure 6.4. The problem was modelled in three-dimensions as shown in Figures 6.5 and 6.6. For a vertical displacement, the symmetry boundary condition was applied to the xy (i.e., z = 0) plane and zy (i.e. x=0) plane. The size of the model was 20.0 m x 20.0 m in plan and 10.0 m in depth. Taking advantage of symmetry, only one quarter of the model was used for analysis.

The modelling involved creating two parts consisting of the footing and the soil half-space and these were created in Abaqus/CEA as a visualization tool. The footing comprised of finite elements while the soil half-space comprised of finite elements and infinite elements as shown in Figure 6.4. The finite element section comprised 8-node, linear brick, solid continuum reduced integration elements (C3D8R). The infinite sections comprised 8-node, linear, solid continuum infinite element (CIN3D8). The domain comprised 9,240 elements. The infinite elements were included in the model by editing the created input file manually.

6.3.1 Material properties

The elastic material properties of the soil and footing used for the analysis are presented in Table 4-1. For dynamic finite element analysis it is usual to introduce damping of the system using Rayleigh damping. In this analysis, the material damping was not considered as it was assumed that the foundation system response is linear with a very small strain level.

6.3.2 Three-dimensional linear elastic half-space finite element model

A vertical harmonic pressure excited the footing at the centre as shown in Figure 6.5. To check the efficiency of the non-reflecting boundaries in 3D, the Abaqus/explicit step analysis was used to determine the vertical dynamic displacement response of the foundation in the time domain. Figure 6.7 shows the plot of vertical dynamic displacement response of the footing versus time for a three-dimensional model with infinite elements at the boundaries. The plot shows that displacement amplitude is constant indicating that the infinite elements placed at the boundaries are capable of absorbing incident waves.

To determine the steady state response of the foundation system in the frequency domain, the analysis procedure was changed to Abaqus/Standard. The linear steady state dynamic response of a system due to harmonic excitation was calculated using a direct solution for steady-state dynamic analysis as described in section 2.8. In Abaqus/standard, the method calculates the response of the system directly in terms of the physical degrees of freedom of the model using the mass, damping, and stiffness matrices of the system, which depends on the frequency. Essentially, the output is a frequency response function in terms of recceptance.

The steady state dynamic analysis provides the steady-state amplitude and phase response of the system due to harmonic excitation at the given frequency. The response is determined by the inverse of Equation 2.26. The analysis is carried out as a frequency sweep by applying the loading at a series of different frequencies and recording the responses. In this case, the frequency interval was specified as 1.0 Hz. The minimum frequency was set at 10.0 Hz and maximum frequency set to 100 Hz. The vertical response was measured at the top of the footing.

6.3.3 Three- dimensional finite element of Gibson soil

Gibson soil is characterised by its shear modulus increasing linearly with depth (Gibson 1967). The Gibson soil was modelled in Abaqus/standard by dividing the soil profile into layers to simulate an increase in shear modulus as the depth increases (Motamed et al. 2009) as shown in Figure 6–8 and 6-9. In this study, soil profile was divided into five layers, each layer being 1.0 m thick as shown in Figure 6.10. The Young's moduli for different layers are shown in Figure 6.10. In the next sections, the vertical dynamic responses of foundation systems obtained from the numerical solutions of the finite

element methods (Abaqus) are presented. The results obtained numerically are compared with the results obtained experimentally.

6.4 Results for three-dimensional finite element models on isotropic and Gibson soil

The vertical dynamic behaviour of the surface and embedded foundation systems determined using numerical analysis is compared with the results obtained from the field measurements. The vertical dynamic behaviour of the foundation systems discussed in this section are displacement amplitude, resonant amplitude, resonant frequency, complex dynamic stiffness, real and imaginary part of complex dynamic stiffness, phase angle between force and displacement and loss angles. The effect of footing embedment is described by the dimensionless quantities of resonant amplitude ratio, resonant frequency ratio and natural frequency ratio. For the embedded foundation systems, the analyses are carried out for embedments of 0, 300, 600, 900 and 1200 mm.

6.4.1 The results for three-dimensional finite element model - Surface foundation

Displacement amplitude

The predicted displacement amplitude for the surface footing placed on homogenous half-space and Gibson soil is shown in Figure 6.11. From the plot, it is shown that the footing placed on homogenous half-space underestimated displacement amplitude by about 52.4 % and the surface footing placed on Gibson soil underestimated displacement amplitude by about 51.3 %. The result indicates that the amplitude response of the footing placed on Gibson soil is almost the same in comparison to the footing placed on homogenous soil.

Resonant amplitude

The predicted resonant amplitude for the surface footing placed on homogenous half-space and Gibson soil is shown in Figure 6.12. From the plot, it is shown that the numerical solution predicted resonant frequency of 32 Hz while the resonant frequency measured in the field is about 44.5 Hz. Therefore, numerical analysis underestimated resonant frequency by about 28.1%. The result indicates that the resonant amplitude response of the footing placed on Gibson soil is almost the same in comparison to the footing placed on homogenous soil. From Figure 6.12, it is shown that the response of footing placed on homogenous soil has the second peak at about 50 Hz and the footing placed on Gibson soil has the second peak at about 52 Hz. The experimental measured displacement amplitude at

6-5

resonance is higher than the amplitude for the footing placed on Gibson soil and homogenous soil as shown in Figure 6.12. At the resonant frequency, the measured resonant amplitude is higher than the resonant amplitude obtained from numerical analysis by 50.9 %.

Complex dynamic stiffness

Figure 6.13 shows the plot of the complex dynamic stiffness versus forcing frequency for the surface footing placed on homogenous half-space soil and Gibson soil. The complex dynamic stiffness obtained from the numerical analysis is compared with the complex dynamic stiffness measured experimentally. The responses show that the complex dynamic stiffness obtained from the numerical analysis is higher than the one measured experimentally. At low frequency, the complex dynamic stiffness for the homogenous half-space soil, and Gibson soil decreases as the forcing frequency increases up to about 32 Hz, and starts increasing thereafter. The trend of the plots of curves from experimental measured complex dynamic stiffness is similar to the one obtained from surface footing placed on homogenous half-space soil and Gibson soil. However, for complex dynamic stiffness obtained experimentally at low frequency decreases up to about 44.5 Hz and then starts to increase as the forcing frequency increases as shown in Figure 6.13.

Real part of complex dynamic stiffness

The plot of the predicted and measured real part versus frequency of excitation is shown in Figure 6.14. The finite element calculates the responses in terms of compliances functions. For comparison purposes, the real part obtained from compliance function was converted to impedance function using Equation 2.77. The shape of the curves shows good similarity between the measured and predicted responses. The real part of the complex dynamic stiffness for the footing placed on the homogenous half-space soil and Gibson soil decreases as the forcing frequency increases. The real part obtained numerically crosses zero at the forcing frequency of 52.3 Hz and 53.6 Hz for the footing placed on the homogenous soil and Gibson soil respectively. Therefore, finite element method overestimated the natural frequency compared to the one obtained from field-measured data. The measured real part crosses zero at the forcing frequency of 49 Hz.

Imaginary part of complex dynamic stiffness

Figure 6.15 is the plot of the imaginary part versus forcing frequency for the surface footing placed on half-space and Gibson soil as well as the experimental results. The

imaginary part obtained from the compliances function was converted to impedance function using Equation 2.78. The plots show that, at low frequencies, the measured imaginary part is lower than the imaginary part obtained from numerical analyses.

Phase and loss angles

The plot of phase angle between force and displacement versus frequency of excitation for the surface footing placed on homogenous half-space soil, Gibson soil and experimental results are shown in Figure 6.16. The plot of loss angle versus the frequency of excitation for the surface footing placed on half-space soil, and Gibson soil and the experimental results are shown in Figure 6.17. The footing on half-space soil predicted the natural frequency of 52.3 Hz, while on Gibson soil it predicted natural frequency of 53.6 Hz. The natural frequency obtained experimentally is 49 Hz. Therefore, the footing placed on homogenous half-space soil overestimated natural frequency by 6.7 % while Gibson soil overestimated natural frequency by 9.4 %.

6.5 Three-dimensional – Finite element method - Embedded footing

The embedded footing of size of 1200 mm x 1200 mm in the plan and 1240 mm depth described in Chapter 3 Section 3.8 was simulated using finite element method. The footing was assumed to be placed on homogeneous, isotropic and elastic half-space soil. The same modelling strategy used to model surface foundation was used to model the embedded foundation. The elastic properties of soil and footing are shown in Table 4-1. Taking advantage of symmetry, only one quarter of the model was used for analysis. In this section, the vertical dynamic responses of the embedded footing placed on homogenous half-space soil and Gibson soil will be discussed.

6.5.1 Results of three-dimensional finite element analysis of embedded footing placed on linear elastic half-space soil

The domain sizes of the models for different embedments placed on homogenous half-space soil are shown in Table 6-1. Figures 6.18 to 6.27 show the unmeshed and meshed models of foundation system embedded at depths of 0, 300, 600, 900 and 1200 mm. These embedment depths were chosen to accommodate the mesh size of the finite element model. The embedment was simulated by adding an embedment layer of 300 mm on top of each other as illustrated in Figures 6.18 to 6.27. The embedment of 0 mm assumed that the footing is placed on homogenous, isotropic elastic half-space soil. The vertical harmonic load that excited the model is shown in Figure 6.18.

6-7

The field-measured mass density of the soil for each layer was used as input in Abaqus to simulate the field condition. The elastic soil properties for each layer are shown in Table 6.2. The shear modulus of the compacted layers (G_S) was calculated from Equation 2.58 using the shear modulus of the half-space (G) and mass density of the compacted layers measured in the field. The calculated shear modulus and shear wave velocities of the compacted side layers adjacent to the footing used as input in Abaqus software are described in Table 6-2. The analysis was carried out to assess the vertical dynamic responses of foundation systems with an embedment of 300 mm. The same analysis procedures were employed for 600, 900 and 1200 mm embedment.

Table 6-1: Domain size and number of elements for different embedment depths

Embedment depth (mm)	Model Domain size		Number of elements	Number of nodes
	Plan (m)	Depth (m)		
0	19.2 x 19.2	8.40	27,264	30,099
300	19.2 x 19.2	8.71	29,408	23,375
600	19.2 x 19.2	9.00	31,552	34,651
900	19.2 x 19.2	9.30	31,696	36,927
1200	19.2 x 19.2	9.60	35,840	39,203

Table 6-2: Input parameters for numerical solution

Embedment depth (mm)	Density of soil (ρ_s= kg/m^3)	Unit weight of soil (γ_s = N/m^3)	Shear modulus (G_s = MPa)	Shear wave velocity (V_s = m/s)
0	2028	19895	100	222
300	2040	20042	102	224
600	2078	20385	108	228
900	2095	20552	110	229
1200	2043	20042	102	224

The modelling of the embedded footing assumed that there is perfect connection between the sides of the footing and the soil. The tangential interaction between the surface of the footing and soil was assumed to be frictionless while the normal interaction between footing and soil was assumed to be a hard contact. In other word the soil could slide relative to side of the embedded footing but could not separate from side of the embedded footing.

Displacement amplitude

The vertical displacement response of the embedded footing placed on homogenous half-space soil with embedment of 0 mm, 310 mm, 620 mm, 930 mm and 1240 mm was determined using numerical solution (FEM - Abaqus Homogeneous). The vertical harmonic unit pressure excited the footing at the centre of the footing and the response was recorded at the top of the footing. The field measurement was simulated by multiplying the field-measured forces and the dynamic response obtained from a unit force excitation. The vertical displacement amplitude of the foundation system is shown in Figure 6.28. From the plots, it is shown that as the embedment increases, the displacement amplitudes decreases.

In addition, the displacement of the numerical solution at the frequency of $1.25 \times fmax$ and $0.75 \times fmax$ for embedment of 0 mm, 310 mm, 620 mm, 930 mm and 1240 mm is compared with the one obtained experimentally as shown in Table 6.3 to Table 6.7, where *fmax* is the frequency at the maximum displacement amplitude.

The displacement percentage error in comparison to the experimental results at maximum displacement at 0 mm, 310 mm and 620 mm embedment is 58.3 %, 62.3 % and 64.6 % respectively. At embedment of 930 mm and 1240 mm the error is 76.7 % and 56.7 % respectively. The prediction model underestimated displacement for all embedments.

Table 6-3: Predicted displacement for 0mm Embedment - FEM (Abaqus - Homogeneous)

Method	Displacement (mm)			Estimated frequency (Hz)	% Error		
	0.75*fmax*	*fmax*	+1.25*fmax*	*fmax*	0.75*fmax*	*fmax*	+1.25*fmax*
Experimental results	0.0177	0.0206	0.0101	58.8	69.5	58.3	41.6
FEM (Abaqus) - Homogeneous	0.0054	0.00859	0.0059	57.0			

Table 6-4: Predicted displacement for 310mm Embedment - FEM (Abaqus)

Method	Displacement (mm)			Estimated frequency (Hz)	% Error		
	0.75*fmax*	*fmax*	+1.25*fmax*	*fmax*	0.75*fmax*	*fmax*	+1.25*fmax*
Experimental results	0.0146	0.0185	0.0106	57.6	76.6	62.3	54.0
FEM (Abaqus) - Homogeneous	0.00342	0.006974	0.00488	56.1			

6-9

Table 6-5: Predicted displacement - 620mm Embedment - FEM (Abaqus)

Method	Displacement (mm)			Estimated frequency (Hz)	% Error		
	0.75f_{max}	f_{max}	+1.25f_{max}	f_{max}	0.75f_{max}	f_{max}	+1.25f_{max}
Experimental results	0.0103	0.0145	0.0093	56.0	75.4	64.6	63.1
FEM (Abaqus) - Homogeneous	0.00253	0.00513	0.00343	58.0			

Table 6-6: Predicted displacement - 930mm Embedment - FEM (Abaqus)

Method	Displacement (mm)			Estimated frequency (Hz)	% Error		
	0.75f_{max}	f_{max}	+1.25f_{max}	f_{max}	0.75f_{max}	f_{max}	+1.25f_{max}
Experimental results	0.0051	0.0132	0.0039	65.8	69.7	76.7	55.8
FEM (Abaqus) - Homogeneous	0.001544	0.00307	0.001722	62.0			

Table 6-7: Predicted displacement - 1240mm Embedment - FEM (Abaqus)

Method	Displacement (mm)			Estimated frequency (Hz)	% Error		
	0.75f_{max}	f_{max}	+1.25f_{max}	f_{max}	0.75f_{max}	f_{max}	+1.25f_{max}
Experimental results	0.0040	0.0079	0.0050	58.8	70.0	56.7	71.1
FEM (Abaqus) - Homogeneous	0.0012	0.003423	0.001447	61.0			

Displacement amplitude at resonance

The vertical dynamic resonant amplitudes due to unit loads taken from the finite element analysis are presented in Table 6-8. The vertical resonant amplitude due to unit load measured experimentally is shown in Table 6-9.

Table 6-8: Resonant amplitude due to unit load – Finite element method

Embedment depth (mm)	Embedment ratio	Resonant amplitude (mm/N)	Resonant amplitude ratio
0	0.0	1.5418×10^{-6}	1
300	0.5	9.8416×10^{-7}	0.638
600	1.0	7.3681×10^{-7}	0.478
900	1.5	5.7925×10^{-7}	0.376
1200	2.0	4.8957×10^{-7}	0.318

6-10

Table 6-9: Resonant amplitude due to unit load - Experimental

Embedment depth (mm)	Embedment ratio	Resonant amplitude (mm/N)	Resonant amplitude ratio
0.0	0.0	5.9926×10^{-6}	1
310	0.52	3.4514×10^{-6}	0.5759
620	1.03	2.2808×10^{-6}	0.3806
930	1.55	2.0849×10^{-6}	0.3479
1240	2.07	1.2874×10^{-6}	0.2148

The plots of resonant amplitudes predicted numerically for different embedments against forcing frequency are shown in Figure 6.29. From this, it is shown that the resonant amplitude decreases as the embedment increases. In addition, Figure 6.29 shows that there is a second peak between 50 Hz and 60 Hz. These results show that on average, full embedment reduced the resonant displacement by about 68.3 %. The resonant displacement response for zero embedment for the field measurement and from the numerical solution can be seen in Figure 6.30. The numerical solution under predicted the resonant amplitude by about 74.2% compared to the resonant amplitude measured experimentally. The resonant amplitudes obtained from the numerical solution for different embedments are plotted together with the experimental measured resonant amplitudes as shown in Figure 6.31. These conclude that resonant amplitudes obtained from field-measured data are higher compared to those predicted by the numerical method.

Resonant amplitude ratio

The resonant amplitude ratio was determined using Equation 2.47. The resonant amplitude ratios from different embedments are shown in Table 6-8. The relationship between the resonant amplitude ratio and embedment ratio obtained numerically is plotted together with those obtained experimentally as shown in Figure 6.32. From Figure 6.32, it can be seen that the resonant amplitude ratio decreases as embedment ratio increases. The plot shows that the resonant amplitude ratio predicted by the numerical solution is in good agreement with experimental results up to about embedment ratio of 0.5. Beyond this point, the resonant amplitude ratio obtained experimentally is lower compared to that obtained from the numerical solution.

Resonant frequency

A resonant frequency is defined as the forcing frequency at which the largest amplitude occurs in the frequency response curve. The resonant frequencies predicted by the numerical solution are presented in Table 6-10. The plot of the resonant frequency versus

embedment depths obtained from the finite element method is shown in Figure 6.33. From the plot, it can be seen that the predicted resonant frequency slightly decreases as the embedment increases. Comparing the results from predicted and measured resonant frequency it is shown that, in both cases, the embedment has insignificant effect on resonant frequency.

Resonant frequency ratio

The effect of embedment on the resonant frequency of the foundation system can be described using a dimensionless parameter referred as the resonant frequency ratio. This may be calculated using Equation 2.48. The resonant frequency ratios predicted by the numerical solution are presented in Table 6-10. The plots of the resonant frequency ratio versus embedment ratio obtained from the field-measured data and finite element method are shown in Figure 6.34. The results show that the embedment has insignificant effect on the resonant frequency ratio.

Table 6-10: Resonant frequency and resonant frequency ratio - FEM (Abaqus)

Embedment depth (m)	Embedment ratio	Resonant frequency (Hz)	Resonant frequency ratio
0	0	35	1
300	0.5	33.9	0.969
600	1.0	33.3	0.951
900	1.5	33.3	0.951
1200	2.0	33.3	0.951

Complex dynamic stiffness

Figure 6.35 shows the plot of the complex dynamic stiffness versus forcing frequency for the footing embedded at 0, 300, 600, 900, and 1200 mm. This shows that for different embedments, at low frequencies, the complex dynamic stiffness decreases as the forcing frequency increases. At about 35 Hz, the complex dynamic stiffness starts to increase as the forcing frequency increases. Also, the complex dynamic stiffness increases as the embedment increases.

Real part of complex dynamic stiffness

The relationship between the real part and forcing frequency is shown in Figure 6.36. For comparison purposes, the real part was converted to impedance function using Equation 2.77. This plot shows that the real part increases as the embedment increases. The natural frequency can be estimated from the plot of the real part versus frequency of

6-12

excitation. Here the natural frequency increases as embedment increases. The predicted natural frequency ranges between 47.6 Hz and 60.9.0 Hz.

Imaginary part of complex dynamic stiffness

Figure 6.37 is the plot of the imaginary part versus forcing frequency. For comparison purposes, the imaginary part of compliances was converted to impedance function using Equation 2.78. From Figure 6.37, it can be seen that as the embedment increases, the imaginary part increases.

Phase and loss angles

The natural frequency of the foundation system can be obtained from the plot of phase angle between force and displacement versus frequency of excitation. Figure 6.38 considers the plot of phase angle versus frequency of excitation for different embedment depths. The natural frequencies predicted by numerical solutions are presented in Table 6-11. The natural frequency of the foundation system can also be taken from the plot of loss angle versus frequency of excitation as shown in Figure 6.39. From Figures 6.38 and 6.39 it is clear that the natural frequency of the foundation system increases as the embedment increases.

Natural frequency

Figure 6.40 show the plot of natural frequency versus embedment depth for the foundation system for different embedment obtained numerically and experimentally. This shows that the numerical solution overestimates the natural frequency compared to the natural frequency measured in the field. The natural frequencies for different embedments are presented in Table 6-11. From Figure 6.40, it is shown that the natural frequency increases as the embedment increases.

Natural frequency ratio

The effect of foundation embedment can be shown by the dimensionless quantity known as the natural frequency ratio which is calculated using Equation 4.18. The natural frequency ratios obtained numerically are presented in Table 6-11. The plots of the natural frequency ratio versus embedment ratio obtained from field measurements and that obtained from the finite element solution are shown in Figure 6.41. This illustrates that as the embedment increases, the natural frequency ratio increases. The general trend of the plots shows that the rate of increase of natural frequency ratio is higher at small embedment. From

6-13

Figure 6.41, it is shown that at low frequencies up to embedment ratio of 0.5 there is a good agreement between measured and predicted natural frequency ratio. The plots show that above the embedment ratio of 0.5, the natural frequency ratio obtained from measured field data is slightly higher, in comparison to the natural frequency ratio obtained from the finite element method.

Table 6-11: Natural frequency and natural frequency ratio FEM (Abaqus) for different embedment depths - Half-space soil medium

Embedment depth (mm)	Embedment ratio	Natural frequency (Hz)	Natural frequency ratio
0.0	0	47.6	1
300	0.5	53.6	1.126
600	1.0	56.6	1.189
900	1.5	59.1	1.242
1200	2.0	60.9	1.279

6.5.2 Results for three- dimensional finite element analysis for embedded footing placed on Gibson soil

The same modelling strategy used to model embedded foundation placed on the homogenous, isotropic elastic half-space soil was used to model footings placed on Gibson soil. The change was made by introducing Gibson soil below the footing. The increase of shear stiffness was modelled by dividing an elastic half-space soil into five layers of 1m thick each to simulate an increase in the shear modulus as the depth increases. The fully-embedded foundation model with different layers is shown in Figure 6.42. The increase of shear modulus as the depth increases was simulated in Abaqus/Standard by specifying Young's modulus for each layer as shown in Figure 6.43. The fully embedded foundation is shown in Figure 6.44.

Displacement amplitude

The vertical displacement response of the embedded footing placed on Gibson soil with embedment of 0 mm, 300 mm, 600 mm, 900 mm and 1200 mm was determined using numerical solution (FEM - Abaqus Gibson soil). The vertical displacement amplitude of the foundation system is shown in Figure 6.45. From the plots, it is shown that as the embedment increases, the displacement amplitudes decreases.

In addition, the displacement of the numerical solution at the frequency of $1.25 \times fmax$ and $0.75 \times fmax$ for embedment of 0 mm, 300 mm, 600 mm, 900 mm and 1200 mm is

6-14

compared with the one obtained experimentally as shown in Table 6.12 to Table 6.16, where *fmax* is the frequency at the maximum displacement amplitude.

The displacement percentage error in comparison to the experimental results at maximum displacement at 0 mm, 300 mm and 600 mm embedment is 58.6 %, 61.0 % and 64.4 % respectively. At embedment of 900 mm and 1200 mm the error is 76.6 % and 56.7 % respectively. The prediction model underestimated displacement for all embedments.

Table 6-12: Predicted displacement for 0mm Embedment - FEM (Abaqus - Gibson soil)

Method	Displacement (mm)			Estimated frequency (Hz)	% Error		
	0.75*fmax*	*fmax*	+1.25*fmax*	*fmax*	0.75*fmax*	*fmax*	+1.25*fmax*
Experimental results	0.0177	0.0206	0.0101	58.8	67.8	56.8	41.1
FEM (Abaqus) - Gibson soil	0.0057	0.0089	0.00595	57.0			

Table 6-13: Predicted displacement for 310mm Embedment - FEM (Abaqus - Gibson soil)

Method	Displacement (mm)			Estimated frequency (Hz)	% Error		
	0.75*fmax*	*fmax*	+1.25*fmax*	*fmax*	0.75*fmax*	*fmax*	+1.25*fmax*
Experimental results	0.0146	0.0185	0.0106	57.6	74.7	61.0	58.5
FEM (Abaqus) - Gibson soil	0.0037	0.00721	0.0044	58.0			

Table 6-14: Predicted displacement for 620mm Embedment - FEM (Abaqus - Gibson soil)

Method	Displacement (mm)			Estimated frequency (Hz)	% Error		
	0.75*fmax*	*fmax*	+1.25*fmax*	*fmax*	0.75*fmax*	*fmax*	+1.25*fmax*
Experimental results	0.0103	0.0145	0.0093	56.0	74.8	64.4	64.5
FEM (Abaqus) - Gibson soil	0.00259	0.00516	0.0033	58.0			

Table 6-15: Predicted displacement for 930mm Embedment - FEM (Abaqus - Gibson soil)

Method	Displacement (mm)			Estimated frequency (Hz)	% Error		
	0.75*fmax*	*fmax*	+1.25*fmax*	*fmax*	0.75*fmax*	*fmax*	+1.25*fmax*
Experimental results	0.0051	0.0132	0.0039	65.8	69.6	76.6	66.2
FEM (Abaqus) - Gibson soil	0.00155	0.00309	0.00132	62.0			

6-15

Table 6-16: Predicted displacement for 1240mm Embedment - FEM (Abaqus - Gibson soil)

Method	Displacement (mm)			Estimated frequency (Hz)	% Error		
	0.75*fmax*	*fmax*	+1.25*fmax*	*fmax*	0.75*fmax*	*fmax*	+1.25*fmax*
Experimental results	0.0040	0.0079	0.0050	58.8	70.0	56.7	71.1
FEM (Abaqus) - Gibson soil	0.00153	0.00299	0.00184	62.0			

Displacement amplitude at resonance

The vertical resonant amplitude for Gibson soil obtained numerically is shown in Figure 6.46 and the resonant amplitude decreases as the embedment increases. The resonant amplitude values are presented in Table 6-17. The results for embedded footing resting on Gibson soil reflect that, on average, full embedment reduces the resonant displacement by about 56.7 %.

Phase and loss angles

The plot of phase angle between force and displacement versus frequency of excitation for the embedded foundation resting on Gibson soil is shown in Figure 6.47. From the plot, it is shown that the natural frequency of foundation system increases as the embedment increases and that this can also be obtained from the plot of loss angle versus frequency of excitation as shown in Figure 6.48. Natural frequencies for different embedment are presented in Table 6.18.

Table 6-17: Resonant amplitude and resonant amplitude ratio FEM (Abaqus-Gibson soil) for different embedment depths

Embedment depth (m)	Embedment ratio	Resonant amplitude (mm/N)	Resonant amplitude ratio
0	0	1.5748×10^{-6}	1
300	0.5	9.9350×10^{-7}	0.631
600	1.0	7.4340×10^{-7}	0.472
900	1.5	5.8870×10^{-7}	0.374
1200	2.0	4.9382×10^{-7}	0.314

Table 6-18:Natural frequency ratio FEM (Abaqus-Gibson soil) for different embedment depths

Embedment depth (m)	Embedment ratio	Natural frequency (Hz)	Natural frequency ratio
0.0	0	47.8	1
0.30	0.5	54.3	1.1360
0.60	1.0	57.2	1.1967
0.90	1.5	59.6	1.2469
1.20	2.0	61.4	1.2845

6-16

Resonant amplitude ratio

The resonant amplitude ratios are determined using Equation 2.47 and the results from the different embedments are shown in Table 6-17. From Table 6-17, it is shown that as the embedment increase the resonant amplitude ratio decreases.

6.6 Comparison between experimental and numerical responses for three-dimensional – Finite element method - Embedded footing

In this section, the vertical dynamic responses of embedded footings placed on a homogeneous isotropic soil profile and Gibson soil obtained numerically and the experimental results are compared. The dynamic responses to be discussed, are the displacement amplitude, resonant frequency and natural frequency. In addition, the dimensionless quantities of resonant amplitude ratio, resonant frequency ratio and natural frequency ratio are considered.

Displacement amplitude

For comparison purposes, the plots of displacement amplitude versus frequency for the footing placed on homogenous soil and Gibson soil obtained numerically are plotted together with the experimental results. Figure 6.49 show the plot of measured and predicted displacement amplitude for zero embedment. This figure indicates that the numerical solution underestimated displacement amplitude in the range of 58.3% and 64.4%. The comparison between predicted and measured displacement amplitude for 310 mm and 1240 mm embedment is shown in Figure 6-50 and Figure 6-51 respectively. The plot of predicted maximum displacement amplitude for all embedment is plotted together with measured maximum displacement amplitude and are shown in Figure 6-52. From the plot, it is shown that numerical solution underestimated maximum displacement amplitude for all embedments.

Resonant amplitude ratio

The resonant amplitude ratio was determined using Equation 2.47. The relationship between the resonant amplitude ratio and embedment ratio obtained numerically is plotted together with the resonant amplitude ratio experimentally as shown in Figure 6.53. From Figure 6.53, it can be seen that the resonant amplitude ratio decreases as embedment ratio increases. The plot shows that the resonant amplitude ratio predicted by the numerical

solution is in good agreement with experimental results up to about embedment ratio of 0.5. Beyond this point, the resonant amplitude ratio obtained experimentally is lower compared to that obtained from the numerical solution.

Resonant frequency

The comparison between measured resonant frequencies and predicted resonant frequency by the finite element is shown in Figure 6.54. This illustrates that the resonant frequency obtained from homogenous soil and Gibson soil decreases as the embedment increases, while the measured resonant frequencies increases as the embedment increases to the depth of 310 mm, then starts decreasing as the embedment increases.

Table 6-19: Resonant frequency and resonant frequency ratio FEM (Abaqus-Gibson soil) for different embedment depths

Embedment depth (m)	Embedment ratio	Resonant frequency (Hz)	Resonant frequency ratio
0.0	0	36.2	1
0.30	0.5	35.0	1.0343
0.60	1.0	34.8	1.0402
0.90	1.5	34.2	1.0585
1.20	2.0	35.5	1.0197

Resonant frequency ratio

The effect of embedment of the foundation system can be explained using a dimensionless parameter which is referred to as the resonant frequency ratio. The plots of the resonant frequency ratio versus embedment ratio obtained from the field-measured data and finite element methods are shown in Figure 6.55. Here it is evident that the resonant frequency ratio for Gibson soil increases as the embedment increases up to an embedment ratio of 1.5, then, decreases as the embedment ratio increases. From the plot, it shows that the resonant frequency ratio for homogeneous soil decreases as embedment ratio increases. It is shown that the resonant frequency ratio has an insignificant effect on the foundation embedment.

Natural frequency

Figure 6.56 shows the plot of measured and predicted natural frequencies plotted against embedment depth. From this, it is explained that the natural frequency increases as the embedment increases. The plots show that the natural frequencies of the embedded foundation obtained from finite element (Abaqus) for footing placed on homogenous and Gibson soil are higher when compared to the natural frequencies obtained from the field-measured data.

Natural frequency ratio

Figure 6.57 show the plots of measured and predicted natural frequency ratio versus embedment ratio, which reveal that as the embedment increases, natural frequency ratio increases. From Figure 6.57, it is shown that there is a good agreement between the natural frequency ratios predicted by finite element method and the one from the field-measured data at low frequencies up to embedment ratio of 0.7.

6.7   Summary

Finite element analysis was used to study the vertical dynamic behaviour of surface and embedded foundations. The results obtained from numerical analysis of finite element method (Abaqus) were compared with the results measured in the field. From this study, it is shown that the Abaqus software is capable of analysing machine foundation and wave propagation problems.

6.7.1   Surface foundation

The dynamic responses summarised here are the resonant amplitude, resonant frequency, dynamic stiffness, and the natural frequency. From the numerical analysis, the following is established:

- The finite element method underestimates the displacement amplitude compared to the resonant amplitude obtained from the field-measured data;
- The finite element method underestimates the resonant amplitude compared to the resonant amplitude obtained from the field-measured data;
- The results show that the finite element method underestimates the resonant frequency compared to the resonant frequency which is obtained from the experimental results;
- At low frequency of about 10 Hz, the finite element method overestimates the complex dynamic stiffness, the real part and imaginary part compared to the stiffness measured in the field, and
- The finite element method overestimates the natural frequency compared to the natural frequency obtained experimentally.

6.7.2 Embedded foundation

The results from numerical analysis were compared with the results obtained from field-measured data. The investigation was carried out on the square footing (1200 mm x 1200 mm) embedded at the depth of 0, 300, 600, 900 and 1200 mm. The design of the machine foundations is aimed at identifying the dynamic behaviour of the machine foundations. These dynamic behaviours are displacement amplitude, resonant amplitude, resonant frequency, dynamic stiffness and natural frequency. The dimensionless quantities used to describe the effect of the embedment include resonant amplitude ratio, resonant frequency ratio, damping ratio and the natural frequency ratio. From the study, the following were observed.

- The numerical analysis underpredicted displacement amplitudes and displacement amplitudes decrease as the embedment increases. The same behaviour was observed from experimental results

- The numerical analysis predicted resonant amplitudes which decrease as the embedment increases. The rate of decreases of resonant amplitude is more pronounced at the low values of embedment depth than at higher embedment. As the embedment increases, the rate of increase of resonant amplitude is insignificant. The same behaviour was observed from experimental results.

- The dimensionless resonant amplitude ratio was used to describe the effect of the foundation embedment. The results from the numerical solution showed that as the embedment increases the resonant amplitude ratio decreases. The observed and predicted resonant amplitude ratios are in agreement especially at the small embedment.

- Gibson soil and homogenous soil give vitually identical results.

- The resonant frequency predicted by finite element decreases as the embedment increases up to the embedment depth of 600 mm. The resonant frequency predicted by finite element is constant for embedment depth higher than 600 mm. This is contrary to what was observed in the field measurement. The measured resonant frequency increased as the embedment increased to an embedment of about 310 mm, then decreased as the embedment continued to increase. The error between predicted and observed are in an acceptable range showing that resonant frequencies of the embedded foundation systems can be predicted by finite element method (Abaqus).

6-20

- The response shows that numerical analysis underestimated the resonant frequency compared to the resonant frequency measured experimentally.
- Resonant frequency ratio obtained numerically decreases as the embedment ratio increases up to the embedment ratio of 1.0. Beyond the embedment ratio of 1.0 the resonant frequency ratio remains constant. The measured resonant frequency ratio increases as embedment increases up to an embedment ratio of about 0.5, then decreased as embedment increases. Finite element method (Abaqus – homogenenous) underestimates resonant frequency ratio while Gibson soil overestimated resonant frequency ratio compared to the measured resonant frequency ratio.
- The measured and predicted complex dynamic stiffness are almost constant at the low frequencies; the complex dynamic stiffness tends to decrease when is close to the resonant frequency of the foundation system. The complex dynamic stiffness then increases as the forcing frequency increases. The same response is observed for the imaginary part of complex dynamic stiffness. This observation indicates that the resonant frequency can be obtained from the plot of complex dynamic stiffness against forcing frequency. It is also observed that at the low frequencies the numerical analysis overestimates the stiffness of embedded foundation systems.
- The numerical solution for embedded foundations shows that embedment increases the natural frequency of the foundation system. The numerical analysis overestimated the natural frequency compared to the natural frequency obtained from field-measured data. Embedment has a much bigger effect on natural frequency than on resonant frequency.

The new dimensionless quantities, referred as the natural frequency ratio, were introduced to describe the effect of embedment on the natural frequency of the machine foundations.

- The dynamic response of the embedded foundation determined numerically showed that the natural frequency ratio increases as the embedment ratio increases.
- The comparison between the natural frequency ratio obtained from numerical analysis, and the one obtained experimentally was found to be remarkable similar.
- The natural frequency ratio obtained numerically is similar to the one obtained from field-measured data up to the embedment ratio of 0.7. Beyond 0.7, the natural frequency ratio obtained from numerical analysis is lower than the natural frequency ratio measured in the field with a maximum error of 4.7 %.
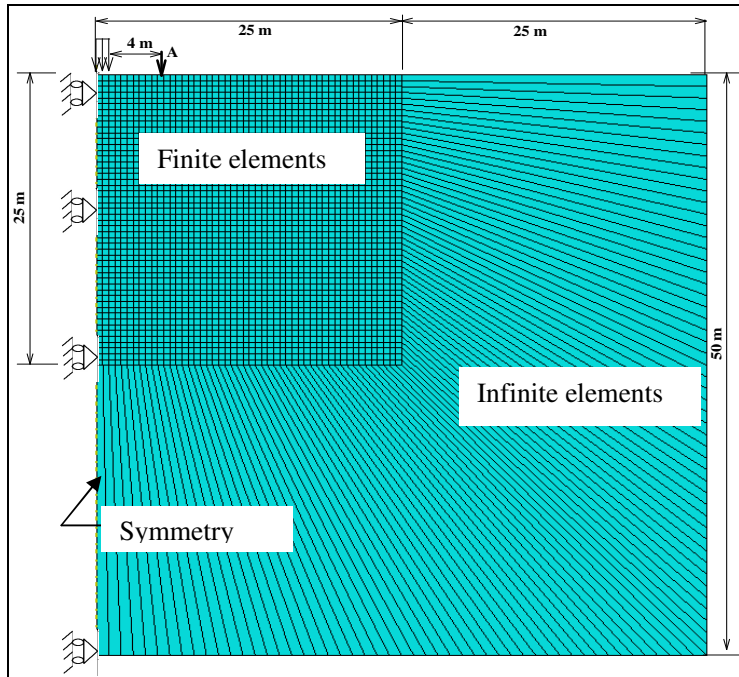
Figure 6.1: Domain for wave propagation model
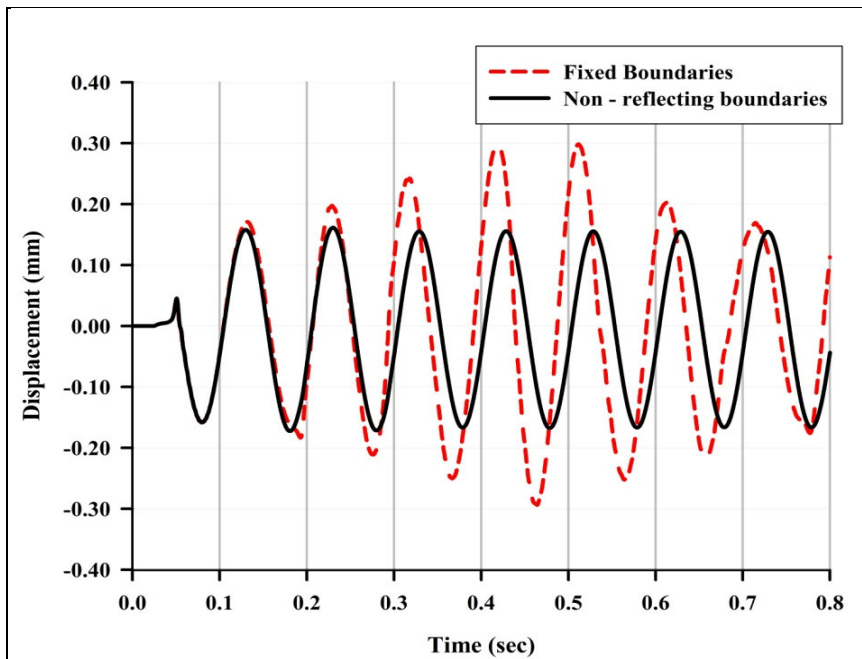
Figure 6.2. Results from fixed boundaries and non – reflecting boundaries -Vertical Harmonic Load
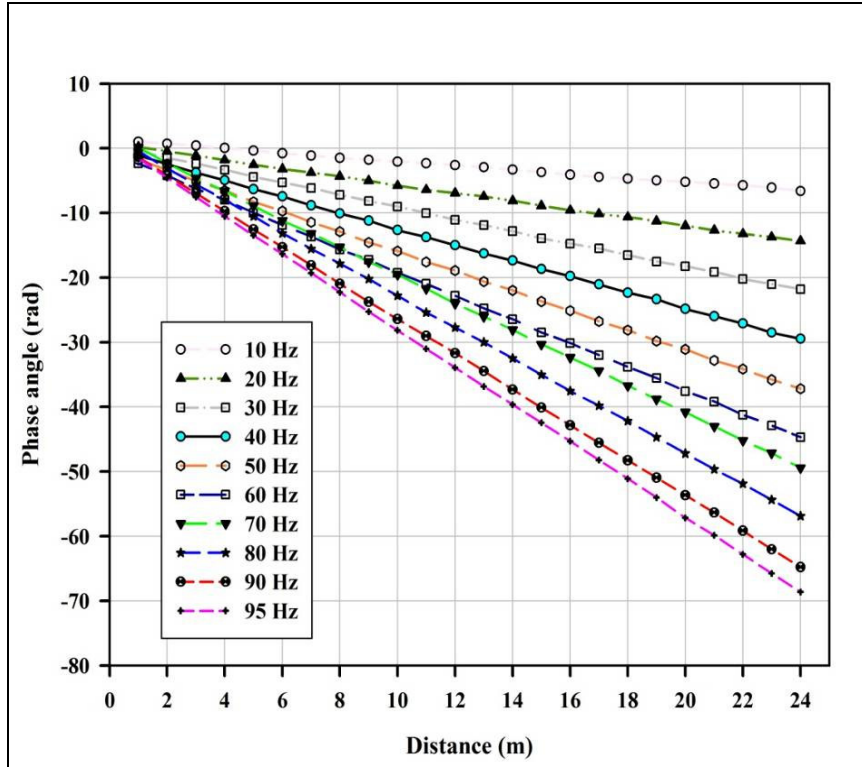
Figure 6.3: Illustration of homogenous soil profile (half-space-Non-dispersive)

Finite elements-Soil medium

Infinite elements-Soil medium

Footing-Finite elements
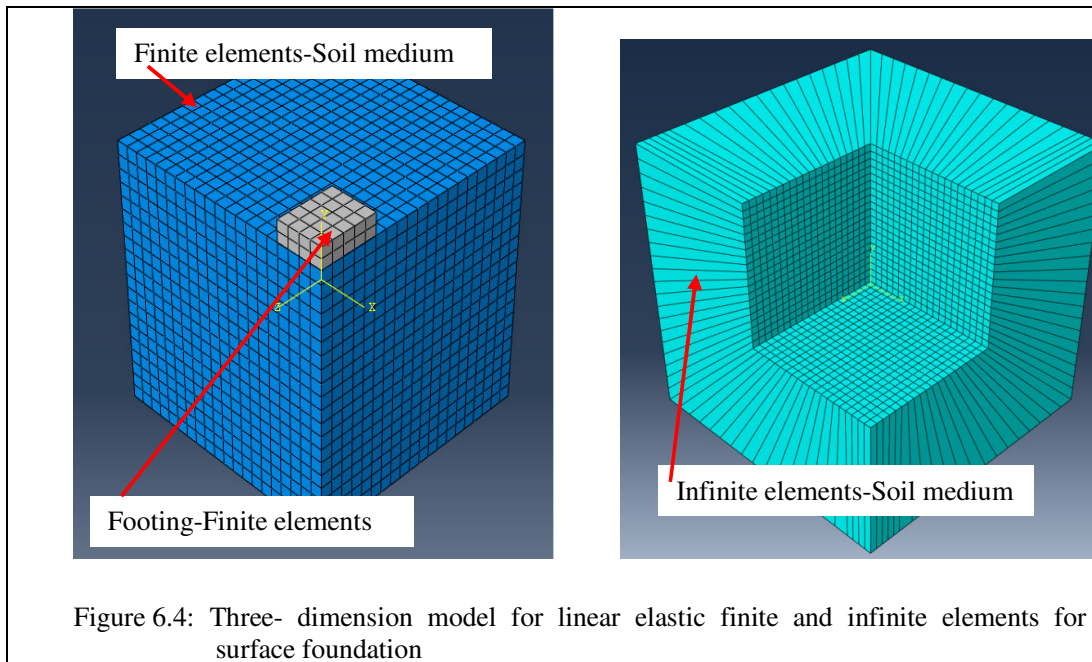
Figure 6.4: Three- dimension model for linear elastic finite and infinite elements for surface foundation
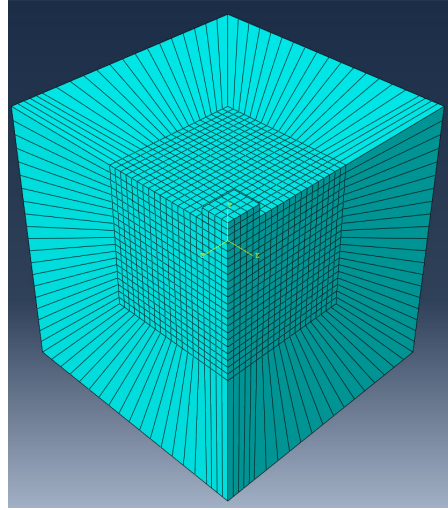
6-23
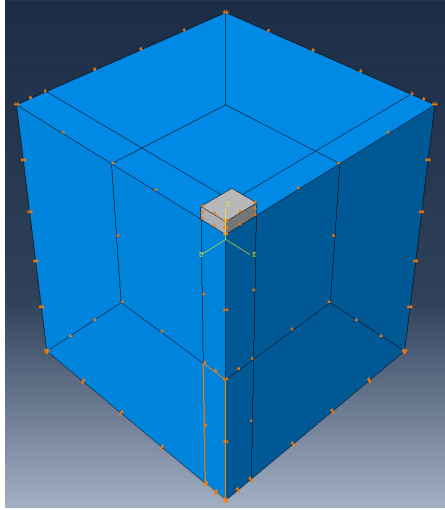
Figure 6.5: Partitioned three - dimensional model

Figure 6.6: Three- dimensional model with finite and infinite elements
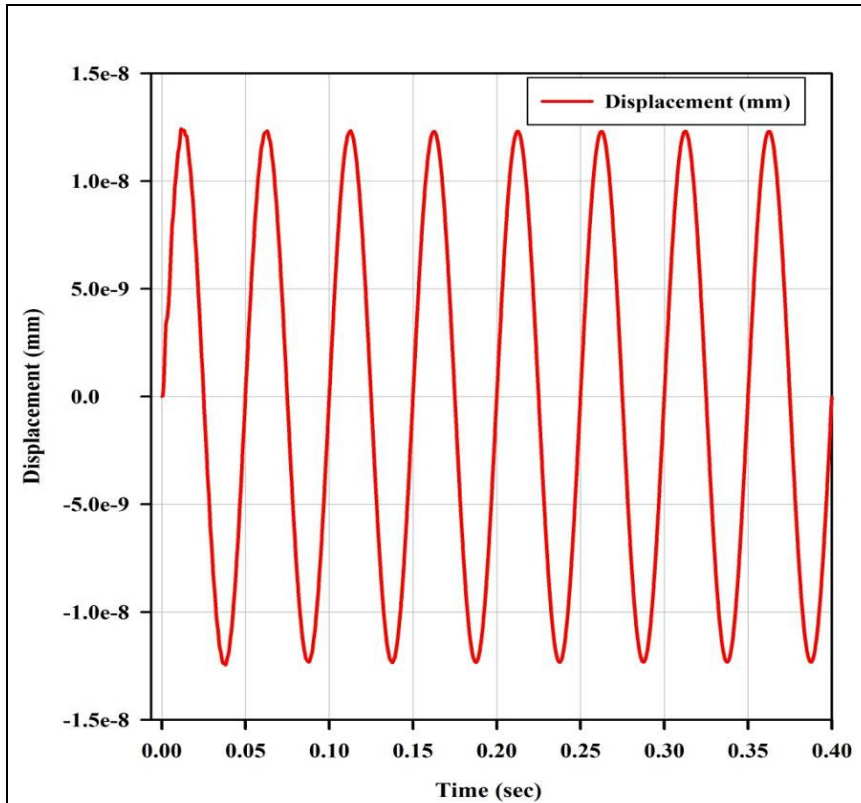
Figure 6.7: Vertical displacement for three-dimension model with infinite elements

6-24
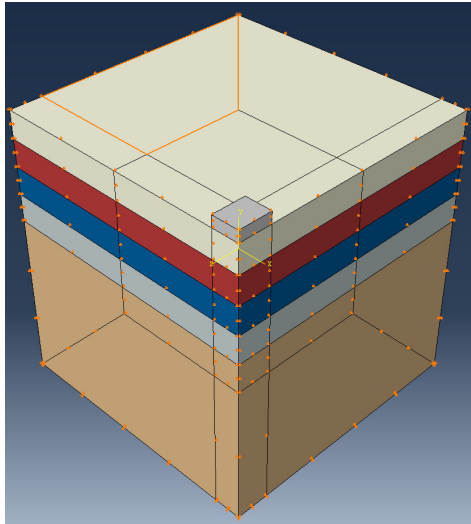
Figure 6.8:Three- dimensional model -
Gibson soil
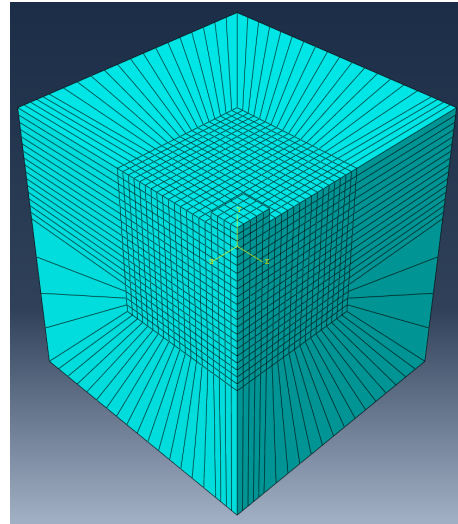
Figure 6.9: Three-dimensional- Gibson soil
with finite and infinite
elements.
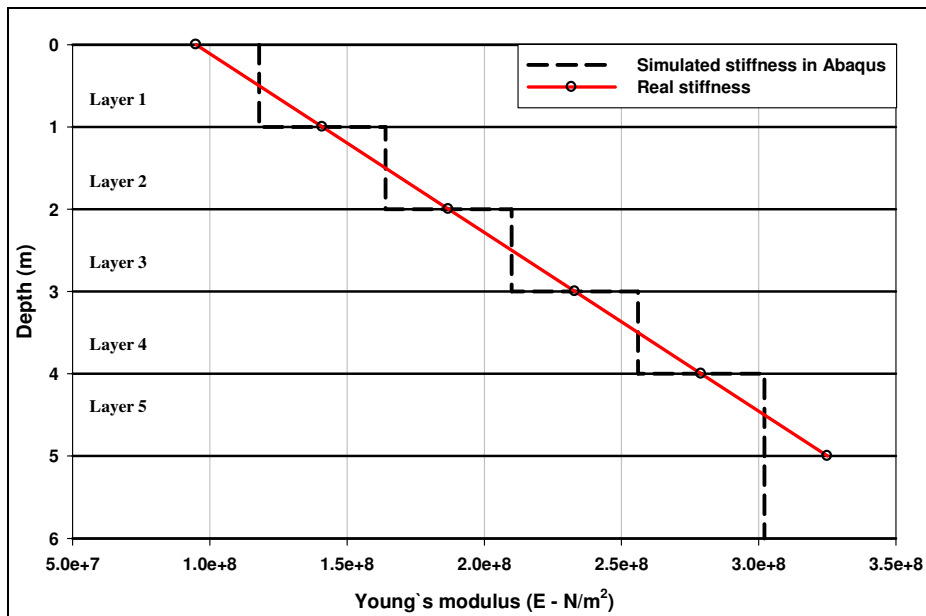
Figure 6.10: Simulated Young's modulus (E) in Abaqus
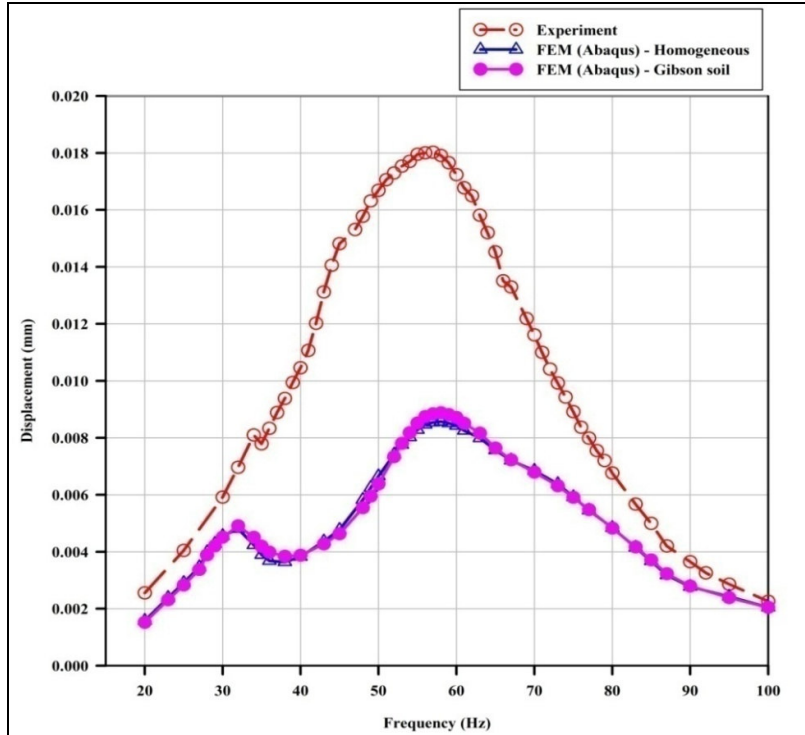
Figure 6.11: Comparison of displacement amplitude for homogeneous, Gibson soil (FEM-Abaqus) and experimental results for surface foundation
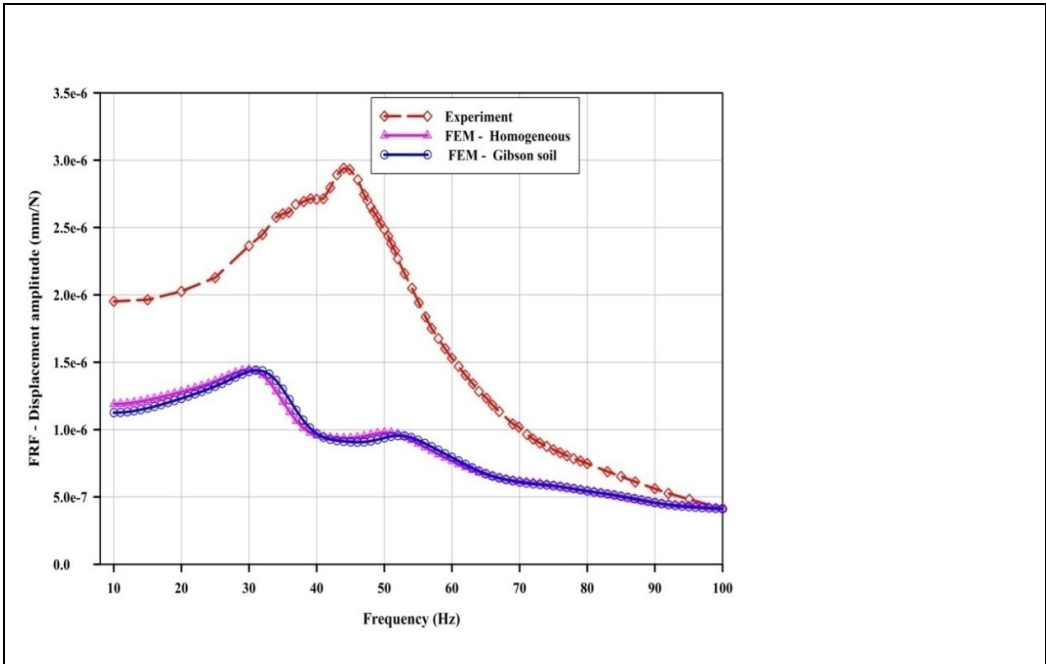
Figure 6.12: Comparison of resonant amplitude for homogeneous, Gibson soil (FEM-Abaqus) and experimental results for surface foundation
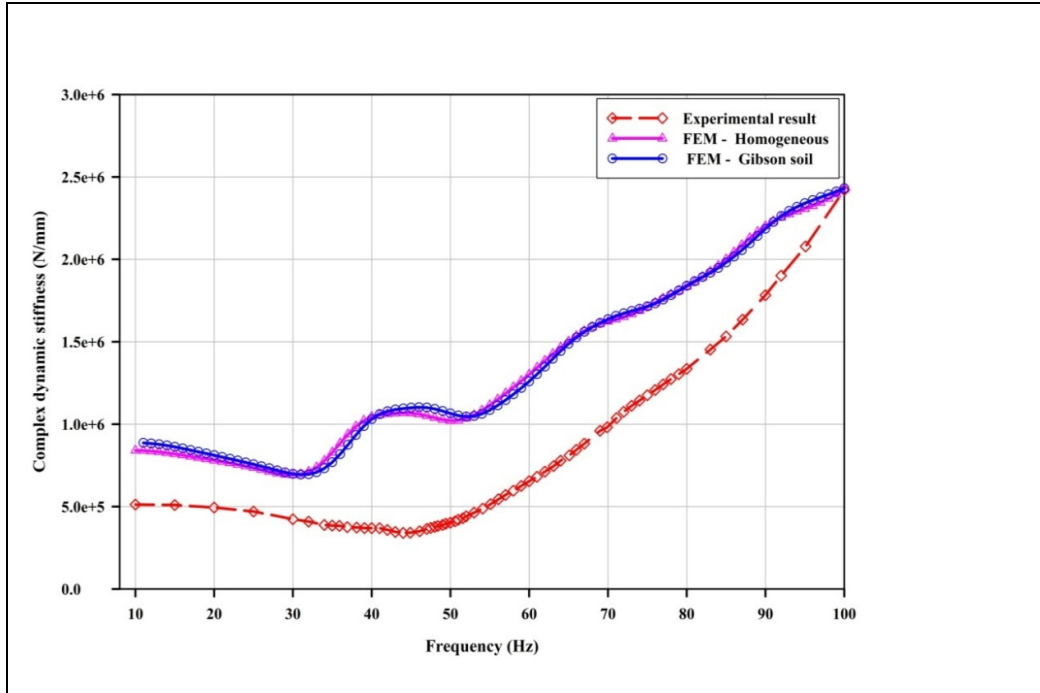
Figure 6.13: Comparison between complex dynamic stiffness for homogeneous, Gibson soil (FEM-Abaqus) and experimental results for surface foundation
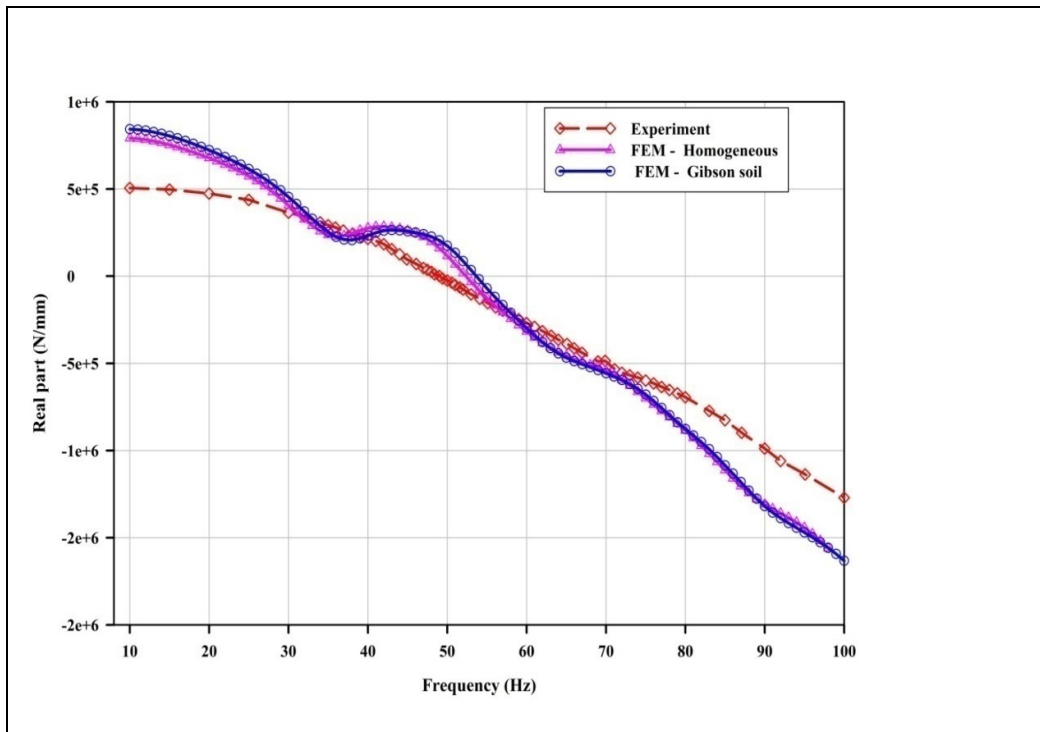
Figure 6.14: Comparison between real part for homogenous and Gibson soil (FEM-Abaqus) and Experimental results for surface foundation

6-27
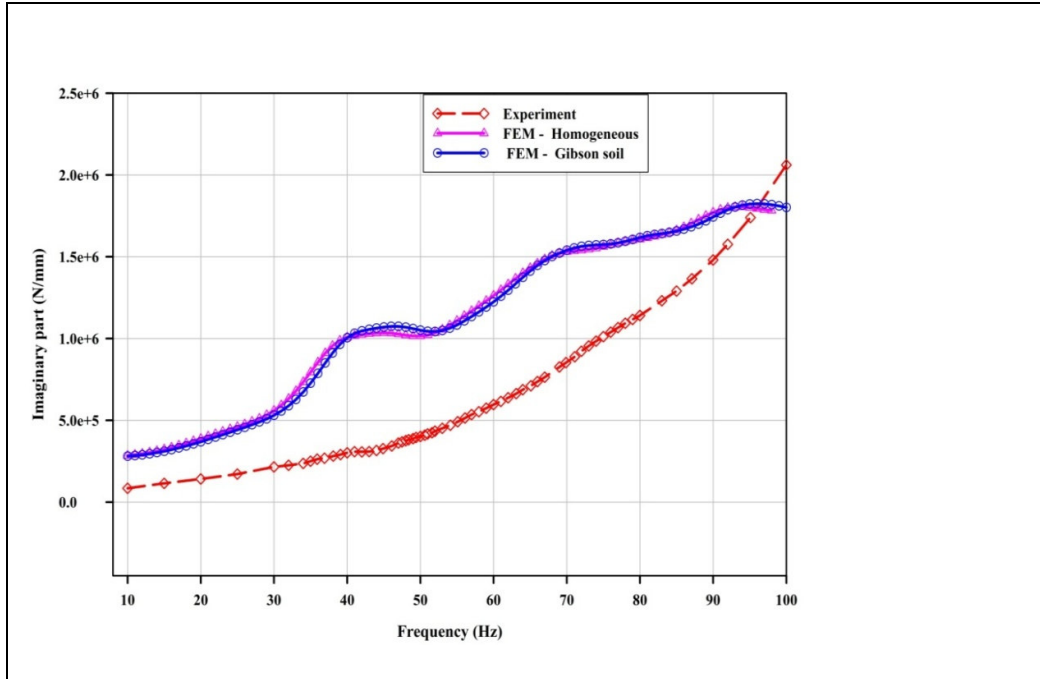
Figure 6.15: Comparison between imaginary part and homogeneous, Gibson soil (FEM-Abaqus) and Experimental results for surface foundation
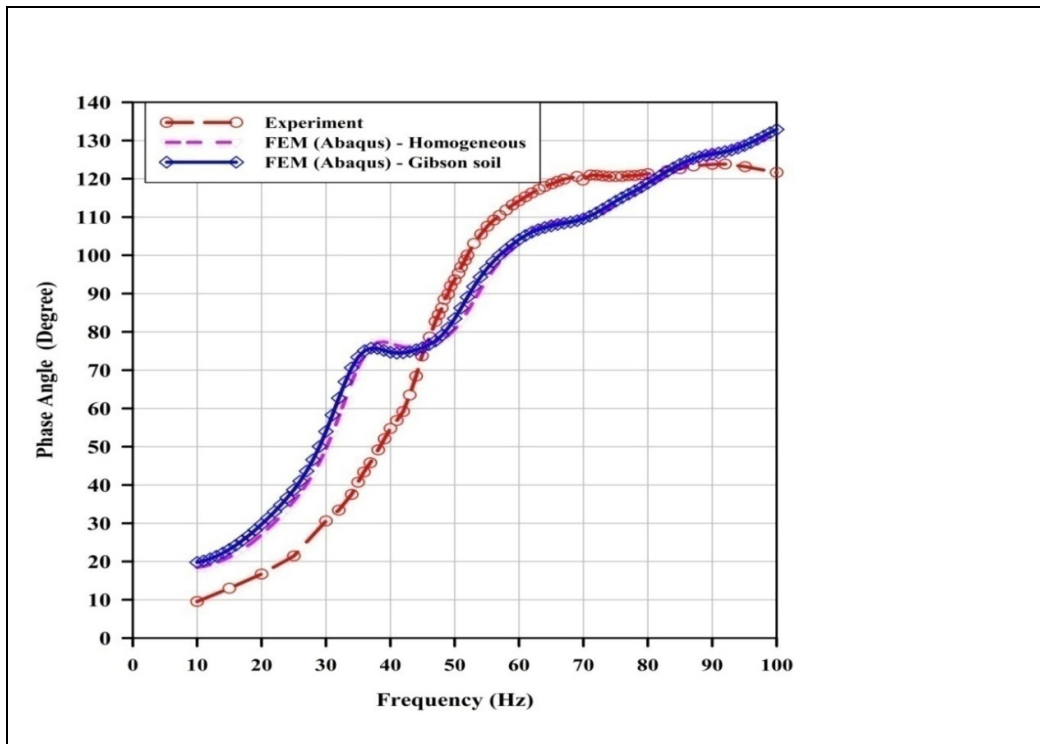
Figure 6.16: Phase angle between force and displacement for homogeneous and Gibson soil - (FEM-Abaqus) and experimental results for surface foundation
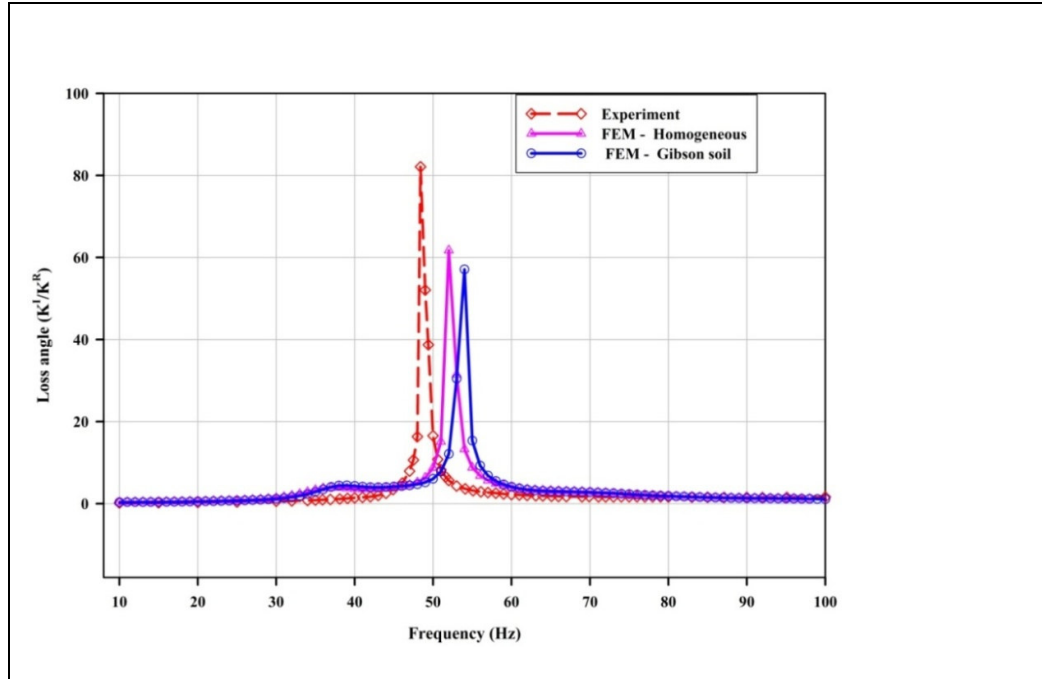
Figure 6.17: Comparison between loss angle and homogeneous, Gibson soil (FEM-Abaqus) and experimental results surface foundation
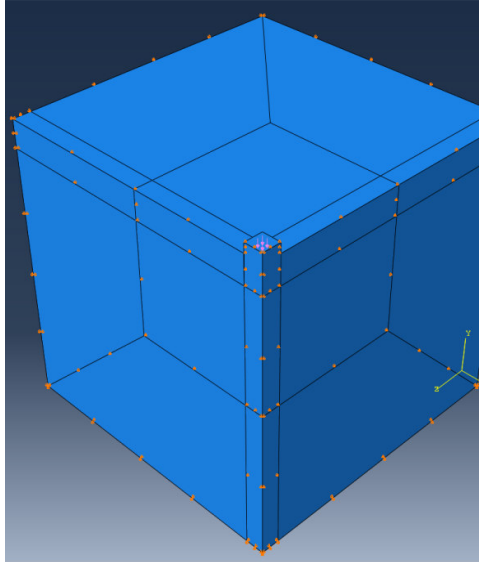

Figure 6.18: Three - dimensional model for 0 mm embedment

Figure 6.19: Three- dimensional model for 0 mm embedment with finite and infinite elements

6-29
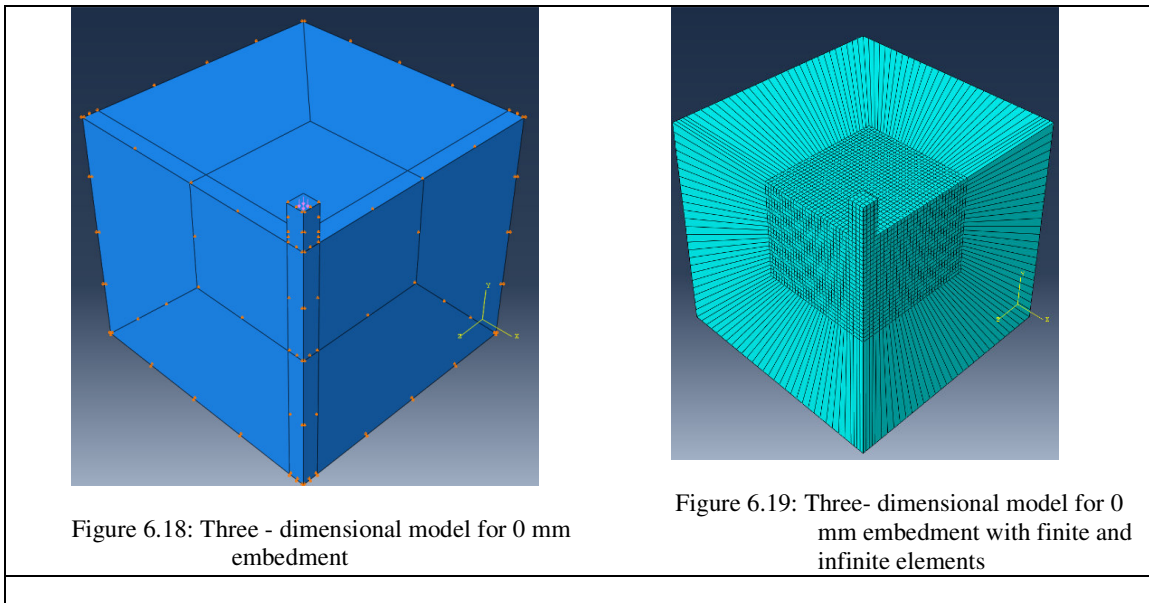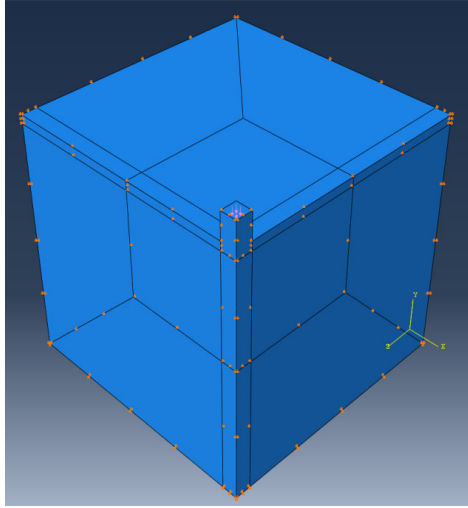
Figure 6.20 :Three – dimensional model for 300 mm embedment
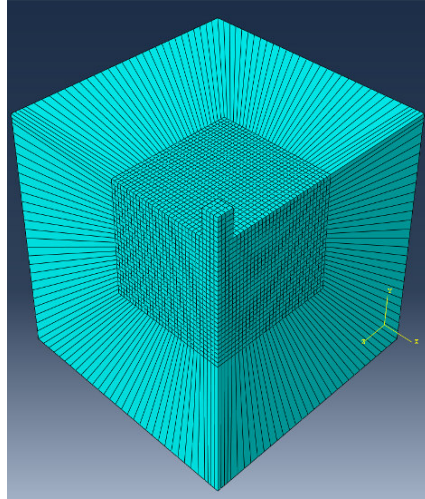
Figure 6.21: Three – dimensional model for 300 mm Embedment with finite and infinite elements
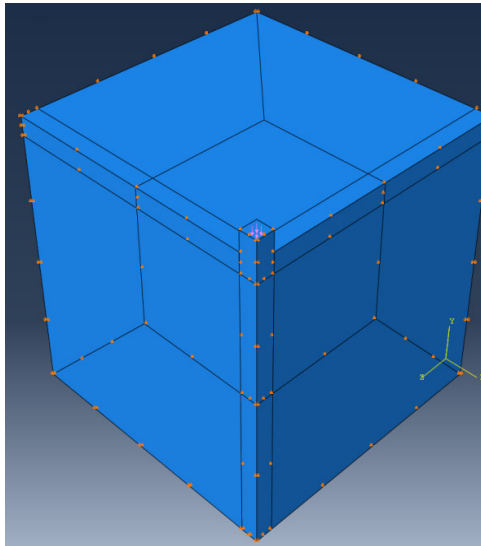
Figure 6.22 :Three - dimensional model for 600 mm embedment
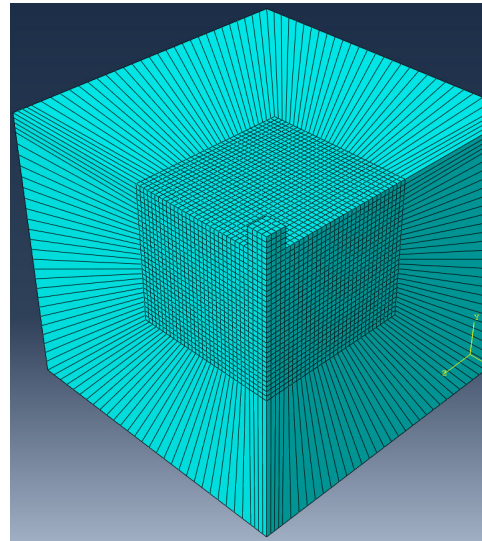
Figure 6.23: Three- dimensional model for 600 mm embedment with finite and infinite elements

6-30

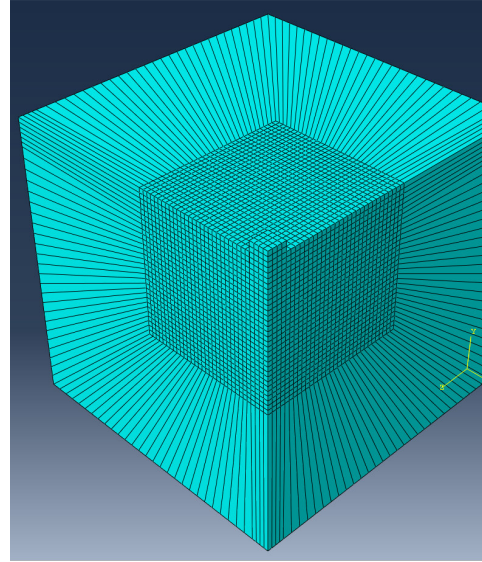Figure 6.24: Three - dimensional model for 900 mm embedment

Figure 6.25: Three- dimensional model for 900 mm embedment with finite and infinite elements
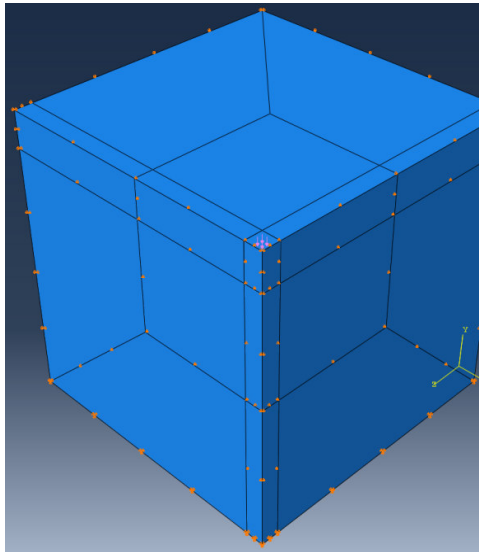

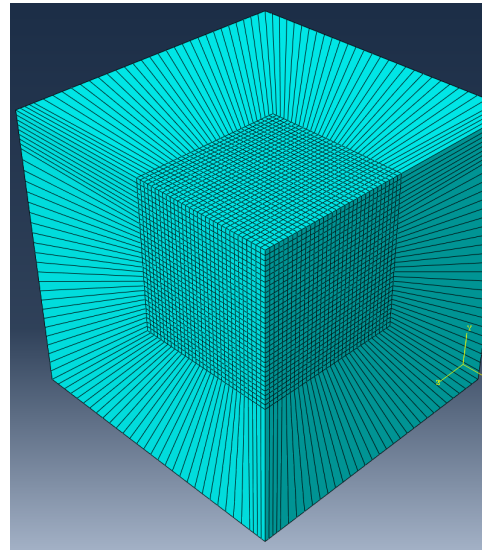Figure 6.26: Three - dimensional model for 1200 mm embedment

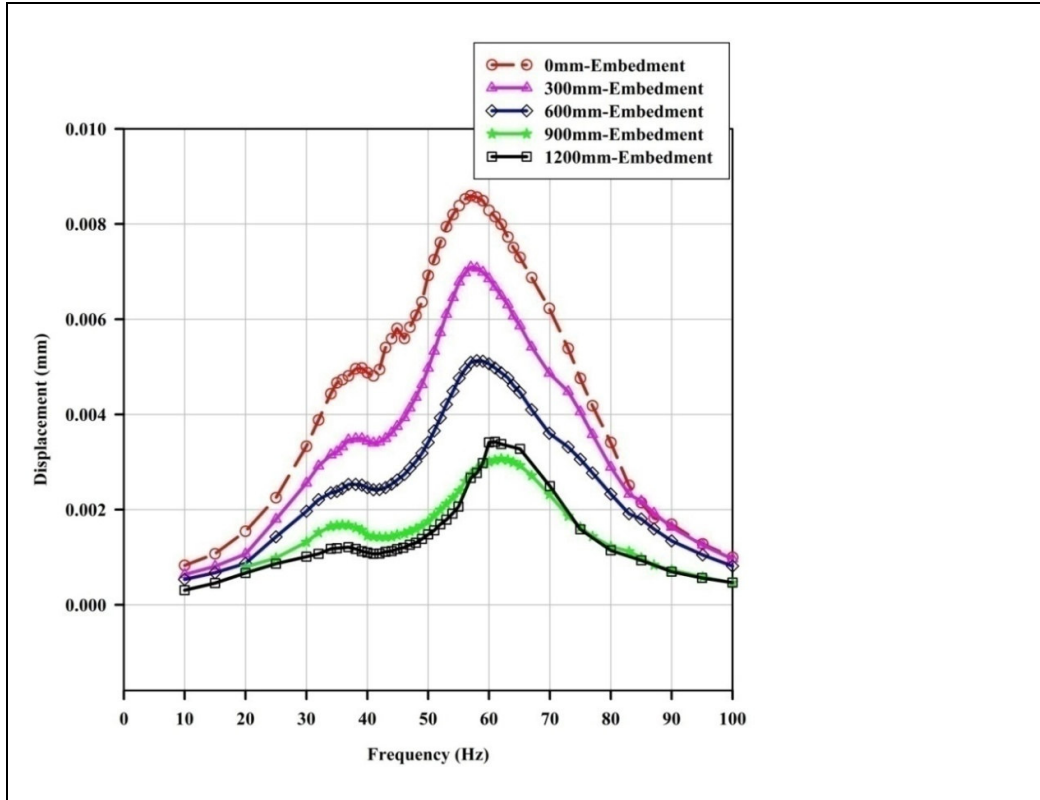Figure 6.27: Three - dimensional model for 1200 mm embedment with finite and infinite elements

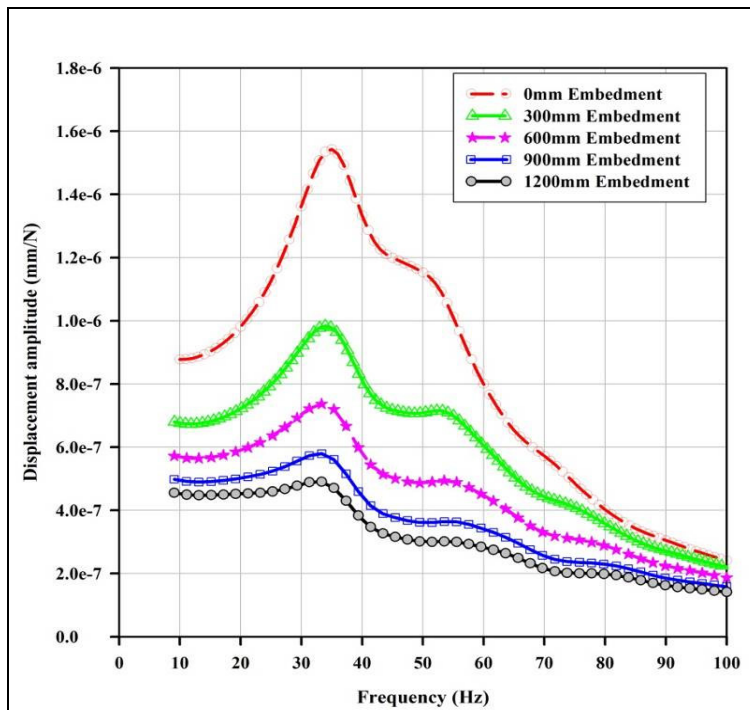Figure 6.28: Displacement amplitude due to measured force – FEM-Homogeneous

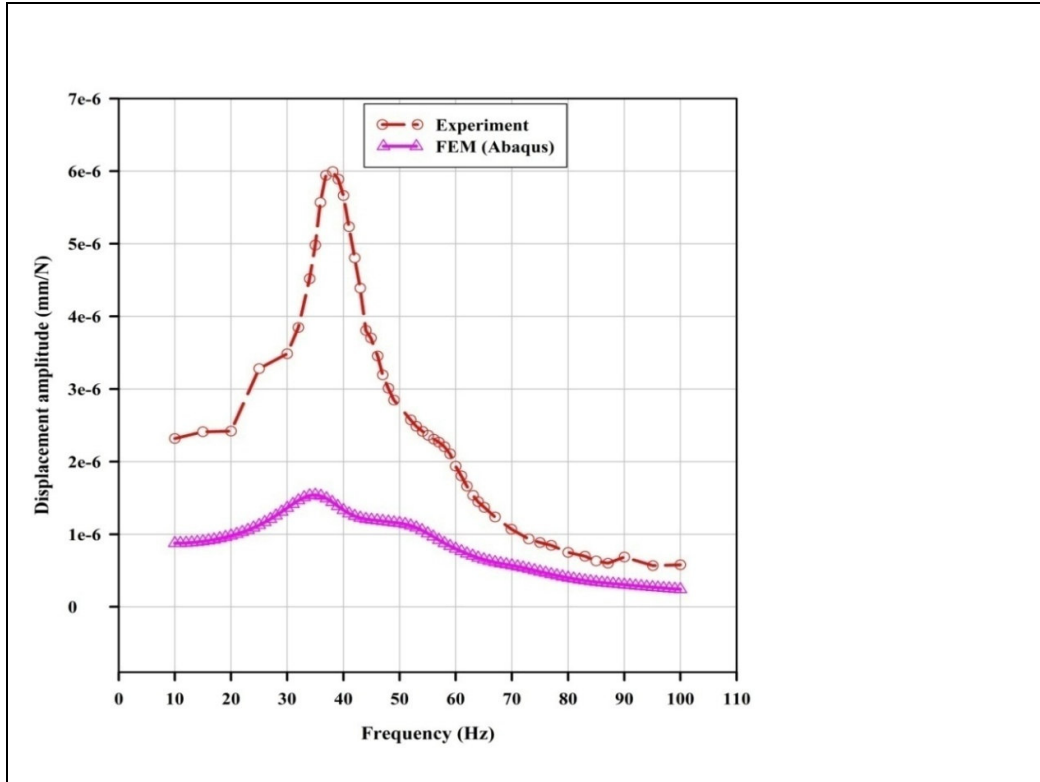Figure 6.29: Resonant amplitude – FEM (Abaqus)

6-32

Figure 6.30: Comparison between resonant amplitude (FEM - Abaqus) and experimental results at 0 mm embedment
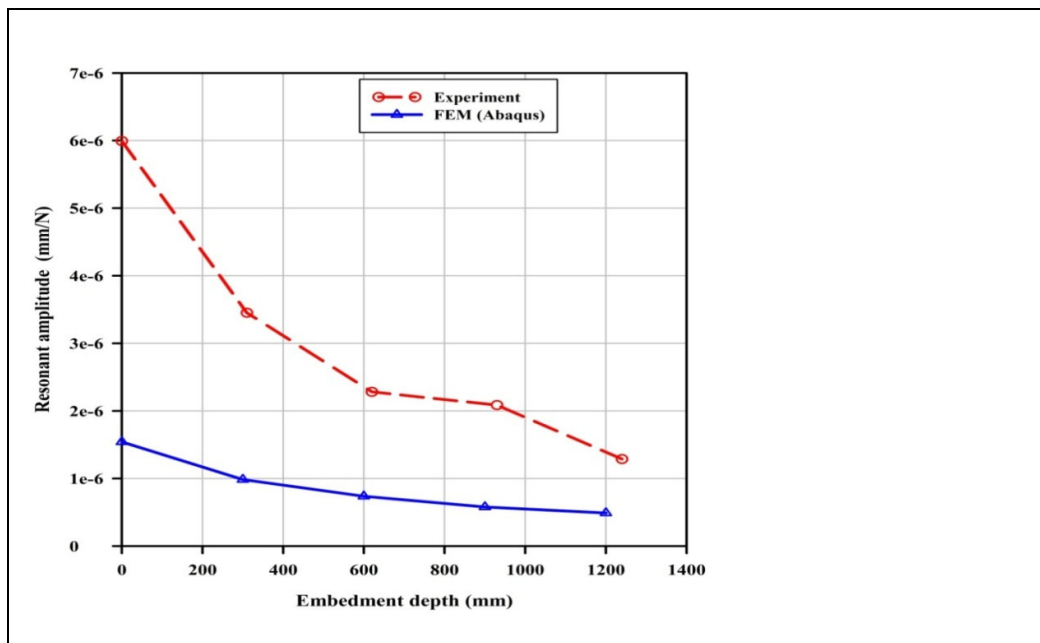

Figure 6.31: Comparison between predicted resonant amplitude (FEM) and experimental results
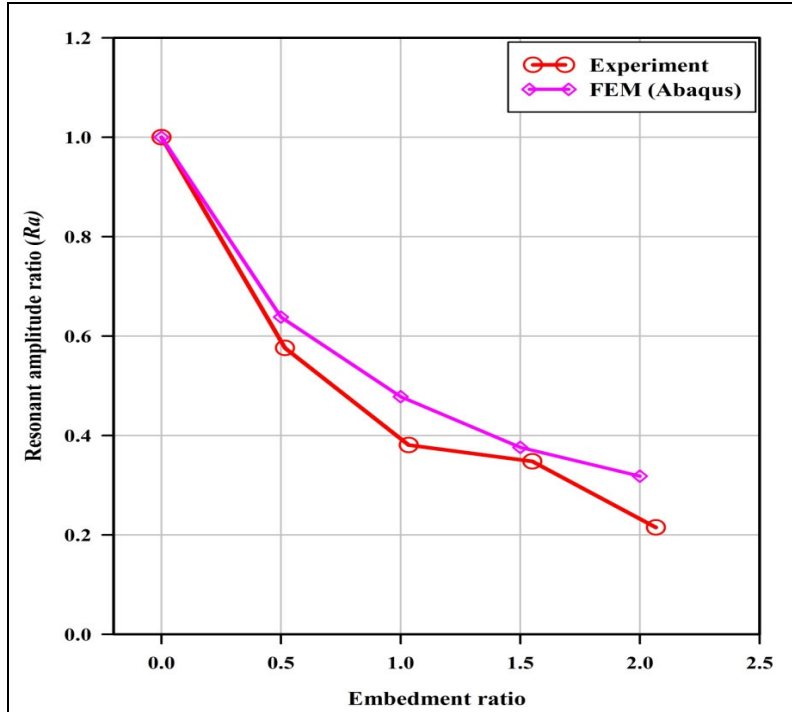
Figure 6.32: Comparison between resonant amplitude ratio from FEM and experiment
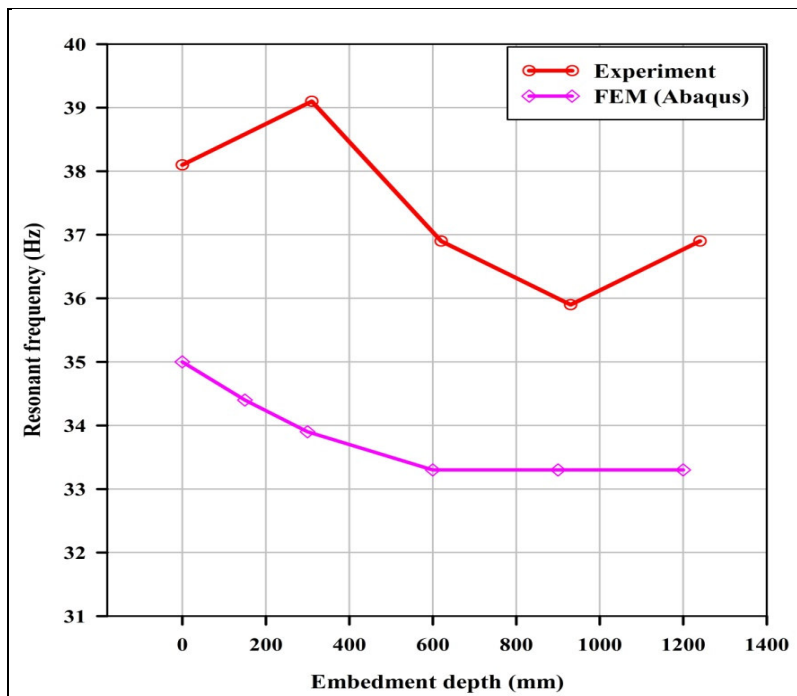
Figure 6.33: Comparison between resonant frequency predicted by FEM (Abaqus - Homogeneous soil) and experiment results

6-34
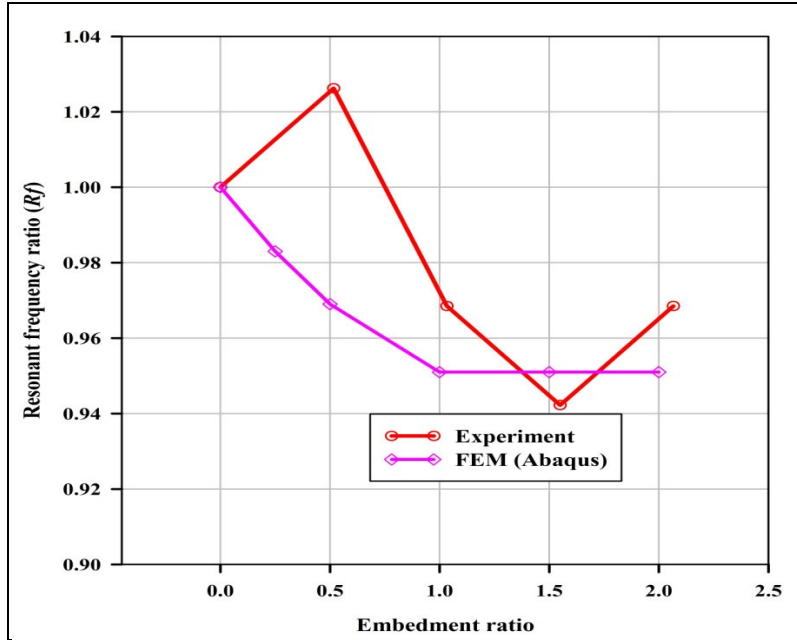
Figure 6.34: Resonant frequency ratio from FEM (Abaqus - Homogeneous soil) and experiment
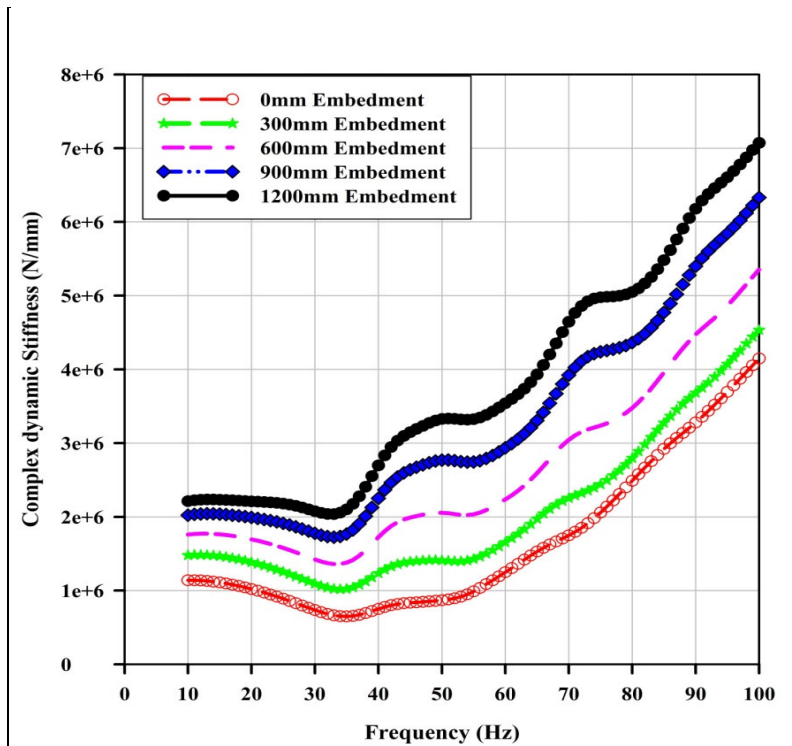
Figure 6.35: Complex dynamic stiffness – FEM (Abaqus - Homogeneous soil)
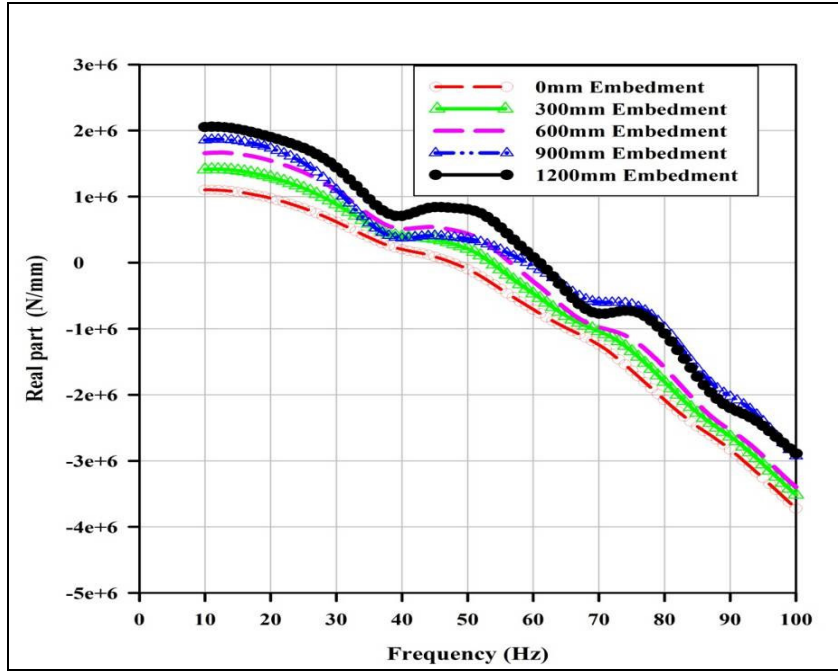
Figure 6.36: Real part - FEM (Abaqus - Homogeneous soil)
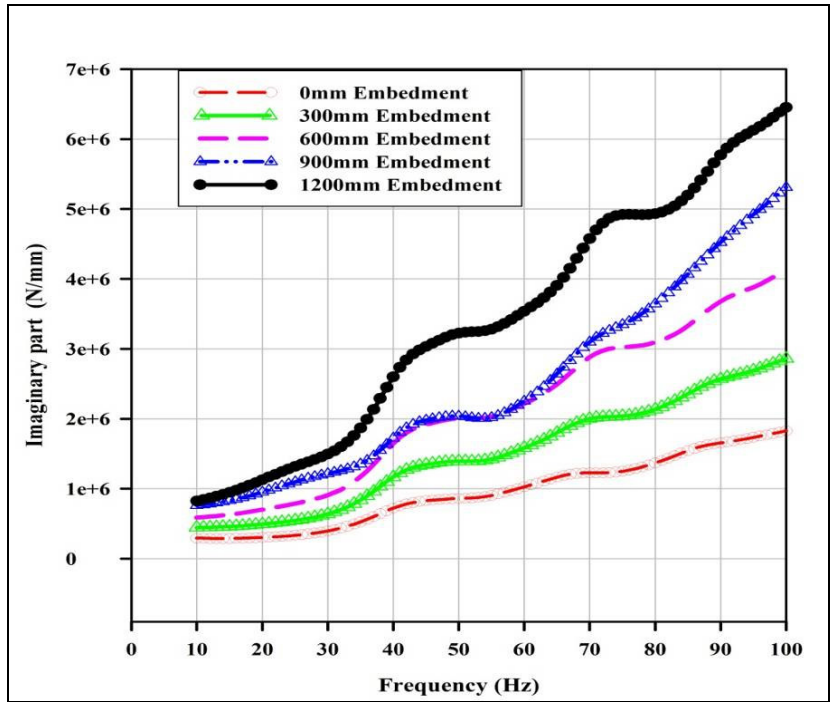
Figure 6.37: Imaginary part – FEM (Abaqus - Homogeneous soil)
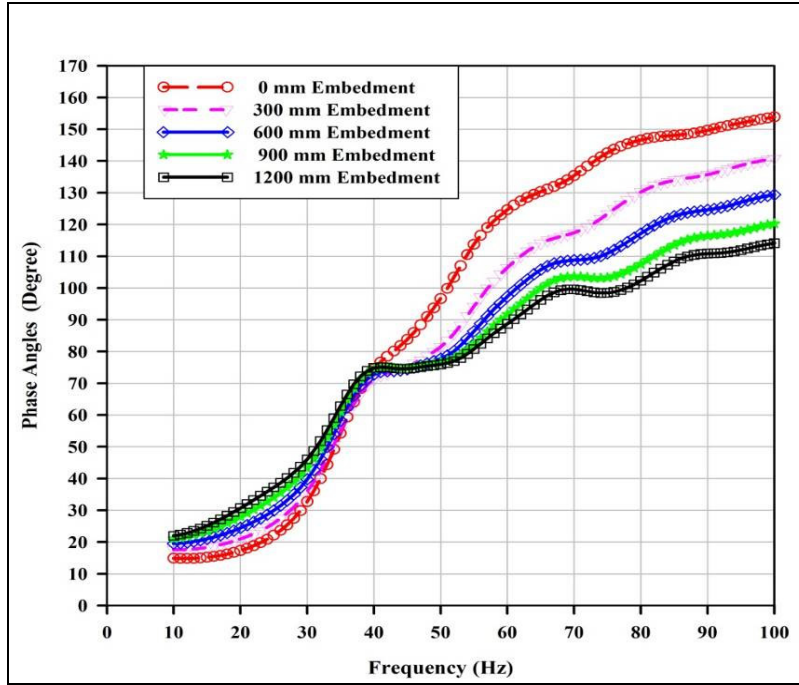
Figure 6.38: Phase angles for different embedment depths
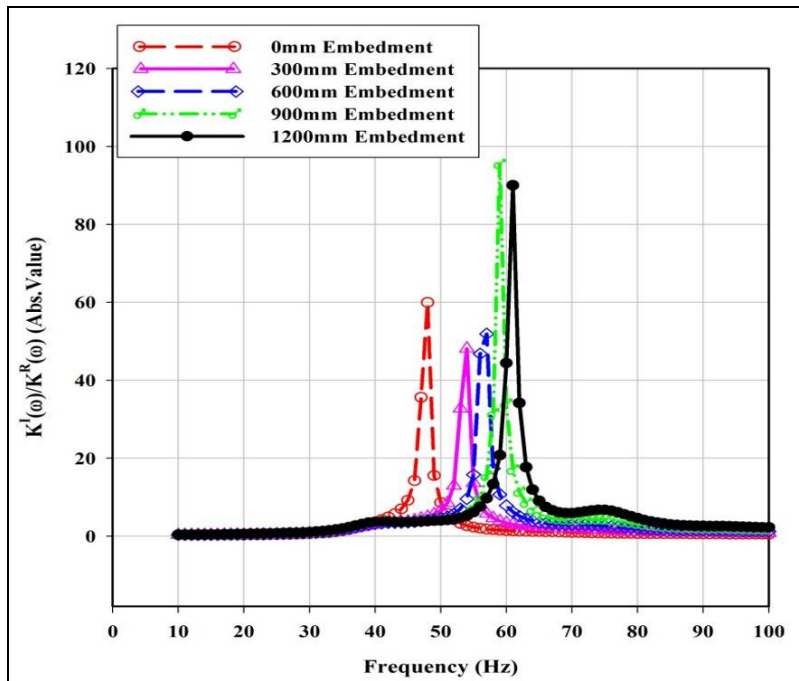
Figure 6.39: Loss angle – FEM (Abaqus)
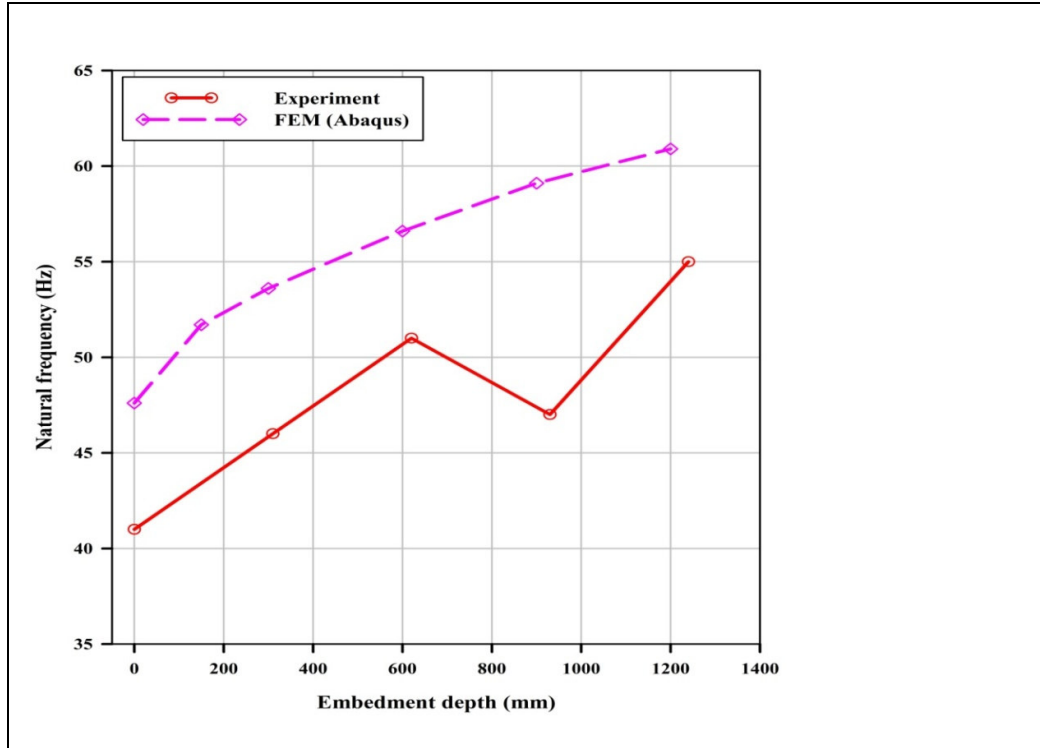
Figure 6.40: Comparison between natural frequency predicted by FEM and experiment
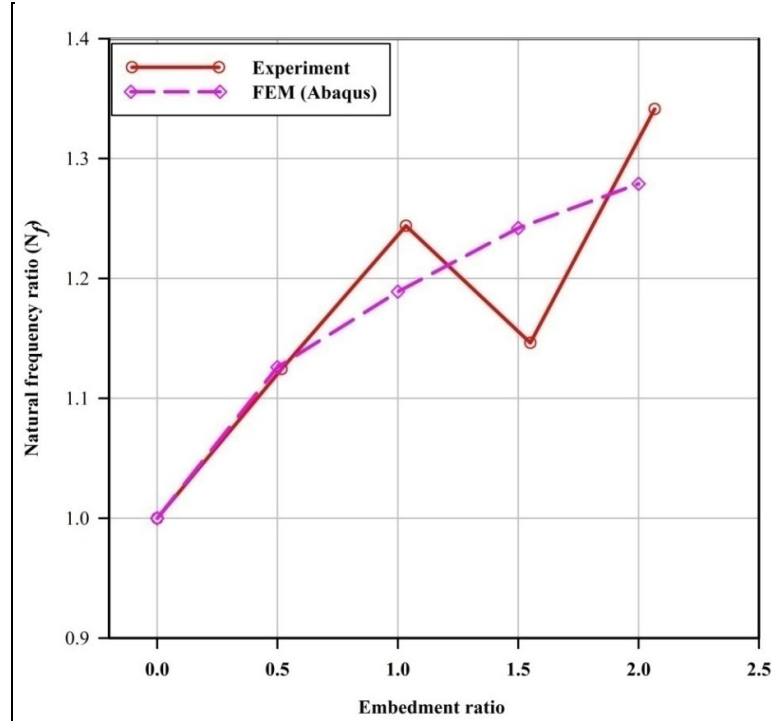
Figure 6.41: Comparison between natural frequency ratio from FEM and experiment

6-38
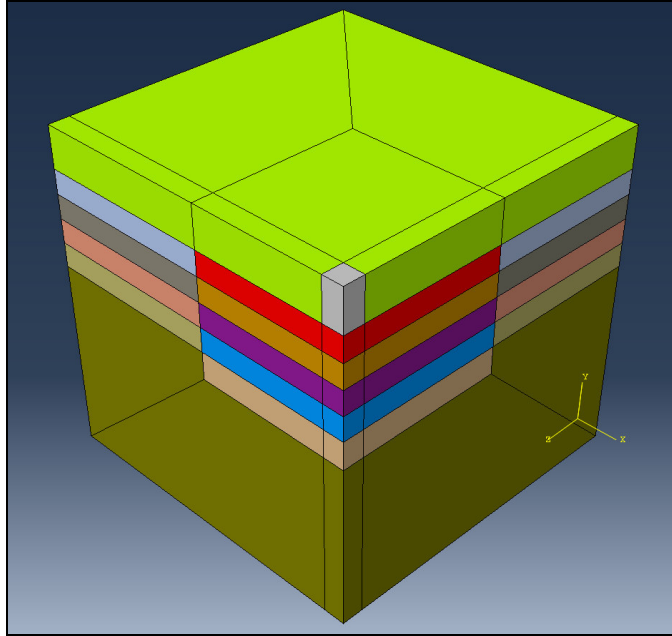
Figure 6.42: Fully embedded three-dimensional finite element model for Gibson soil
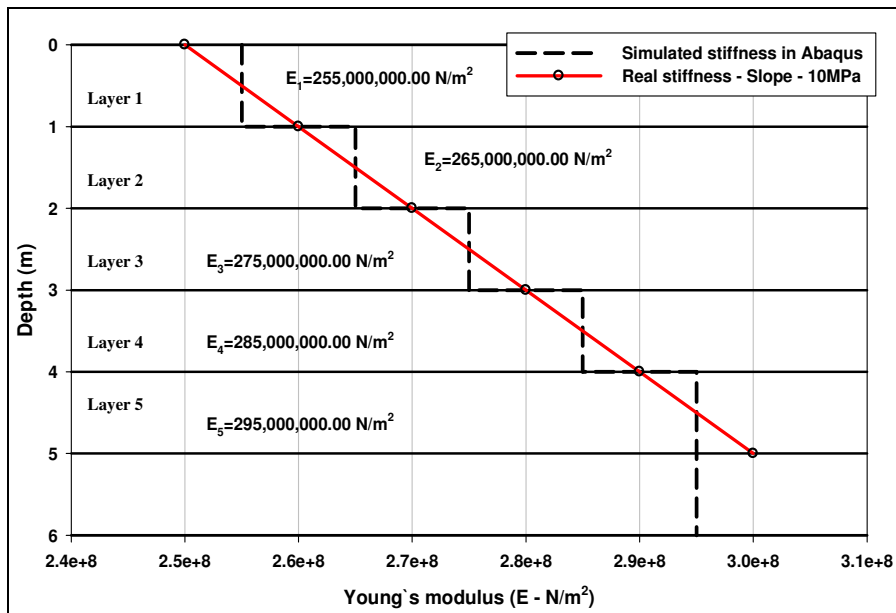
Figure 6.43: Simulated Young's modulus (E) in Abaqus for Gibson soil
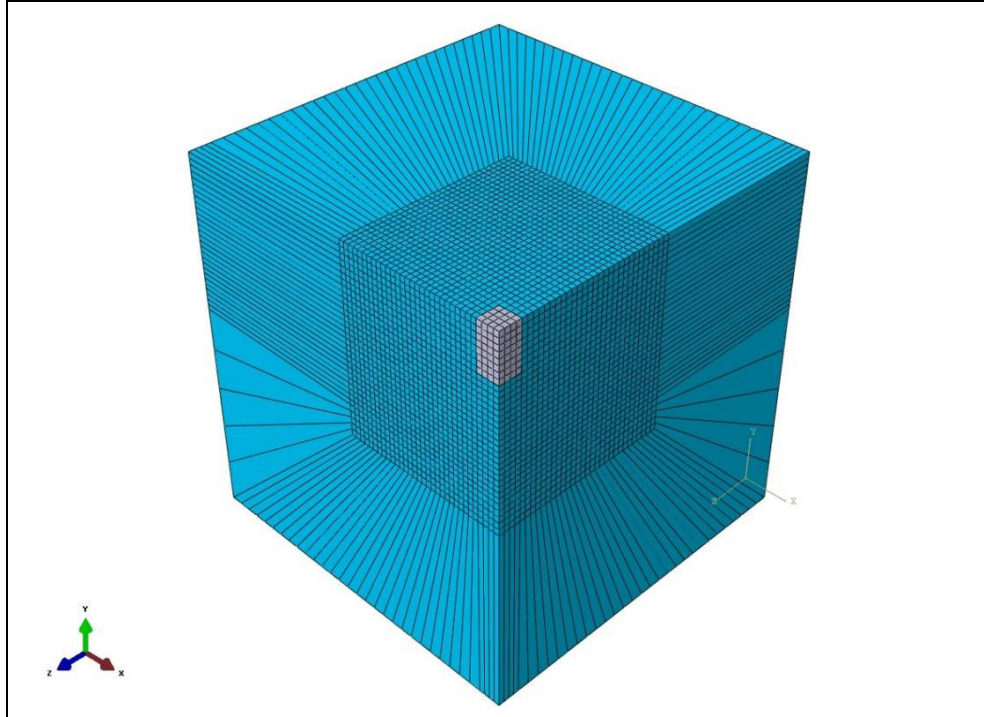
Figure 6.44: Three-dimensional model - Gibson soil - 1200 mm embedment
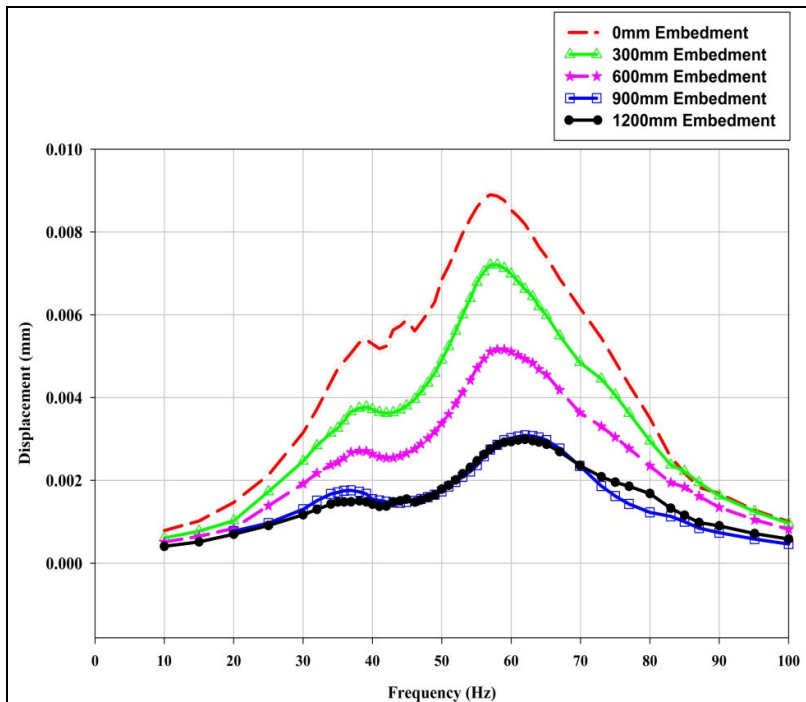
Figure 6.45: Displacement amplitude due to force– FEM (Abaqus-Gibson soil)
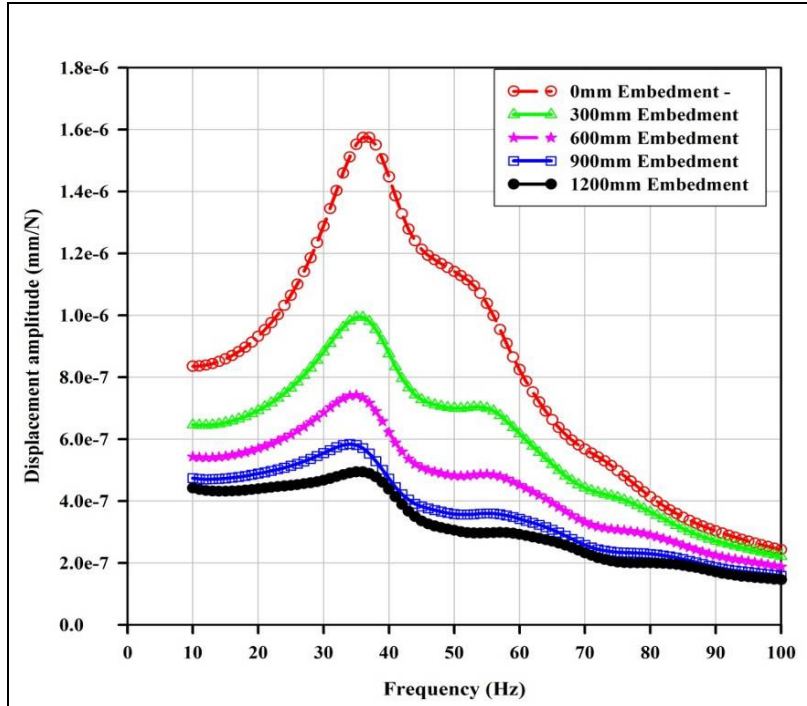
Figure 6.46: FRF -Displacement amplitude – FEM (Abaqus-Gibson soil)
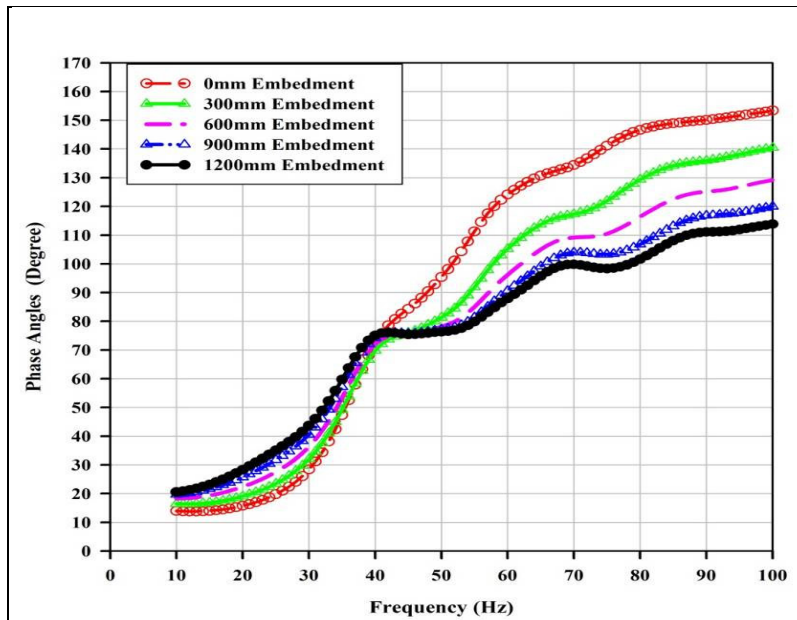
Figure 6.47: Plot of phase angle - FEM (Abaqus - Gibson soil)
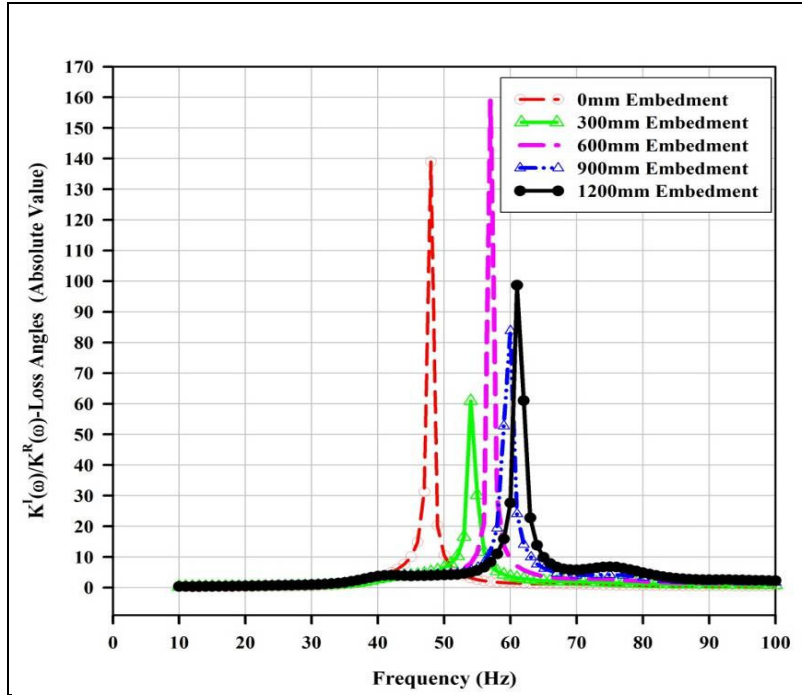
Figure 6.48: Loss angle – FEM (Abaqus - Gibson soil)
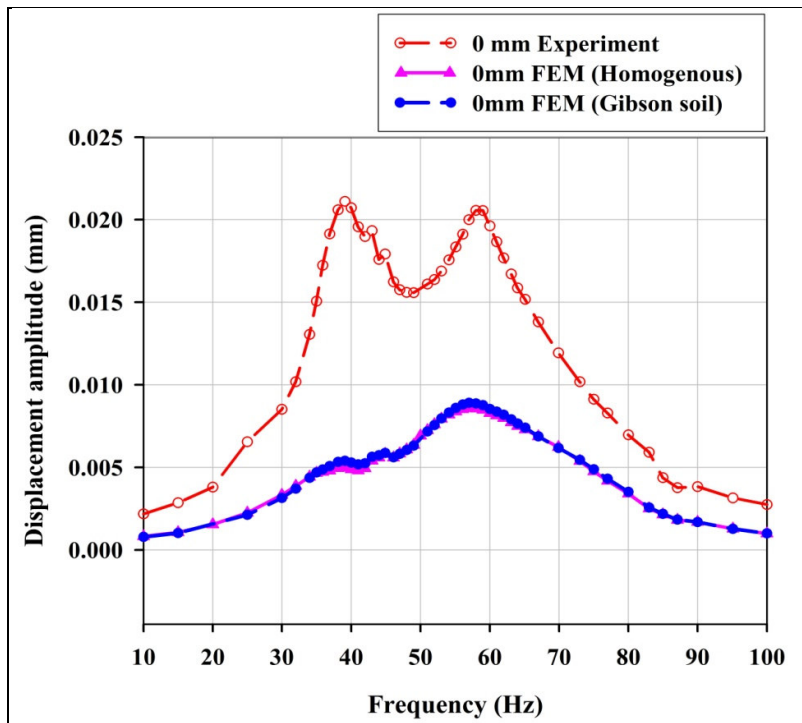
Figure 6.49: Comparison betwen measured displacement amplitude – FEM (Abaqus-Homogeneous and Gibson soil) and experimental results.

6-42
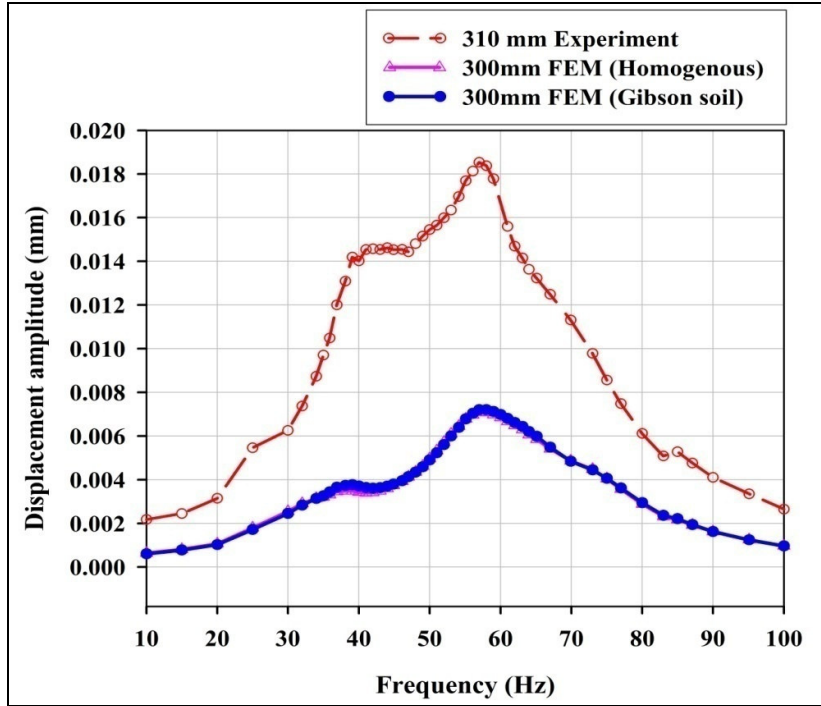
Figure 6.50:Comparison betwen measured displacement amplitude – FEM (Abaqus-Homogeneous and Gibson soil) and experimental results.
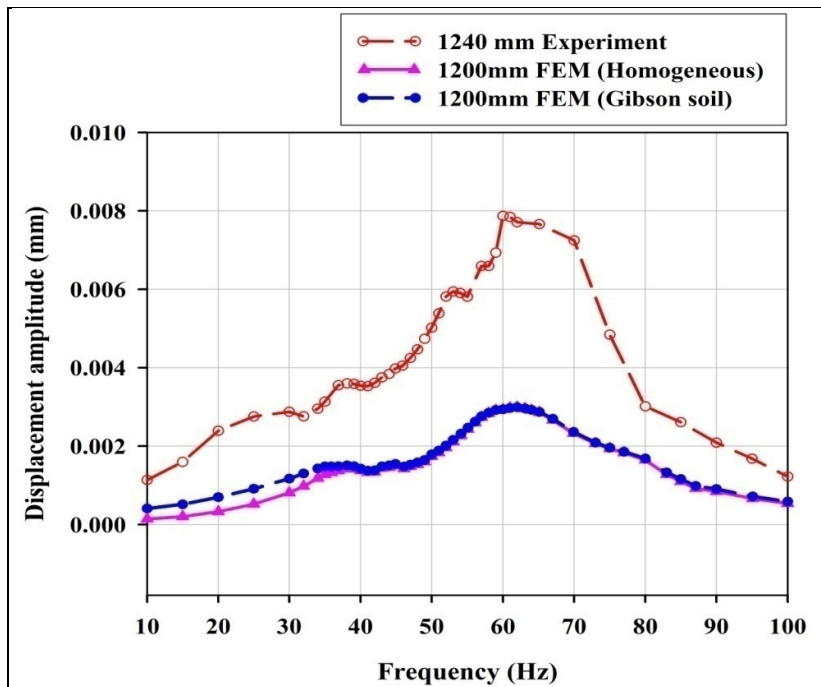
Figure 6.51: Comparison between measured displacement amplitude - FEM (Gibson soil and homogeneous) and experimental results.

6-43
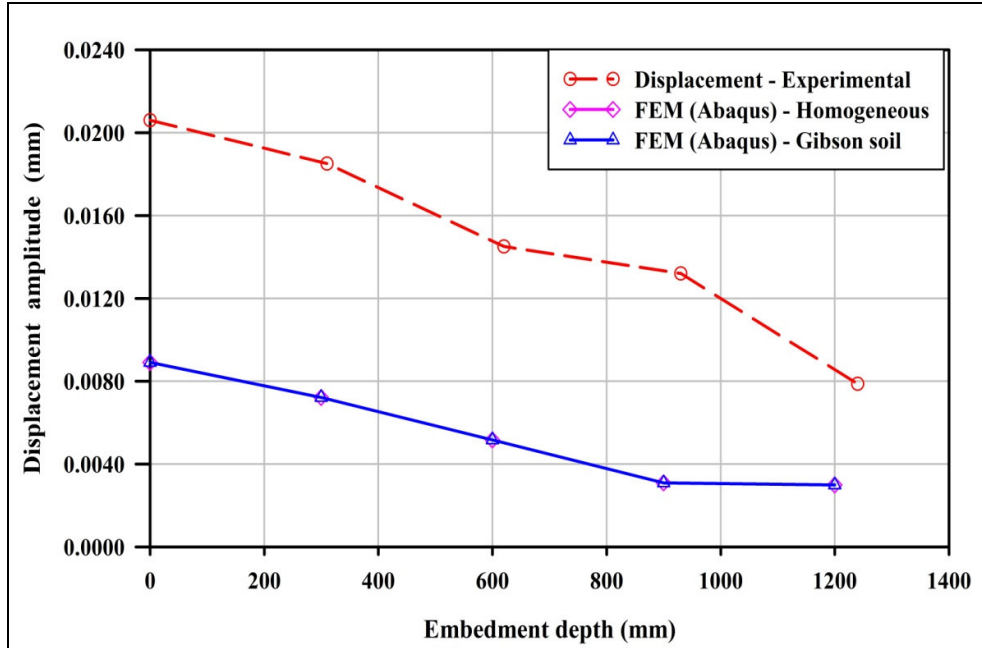
Figure 6.52: Comparison between maximum displacement amplitude - FEM (Gibson soil and homogeneous) and experimental results.
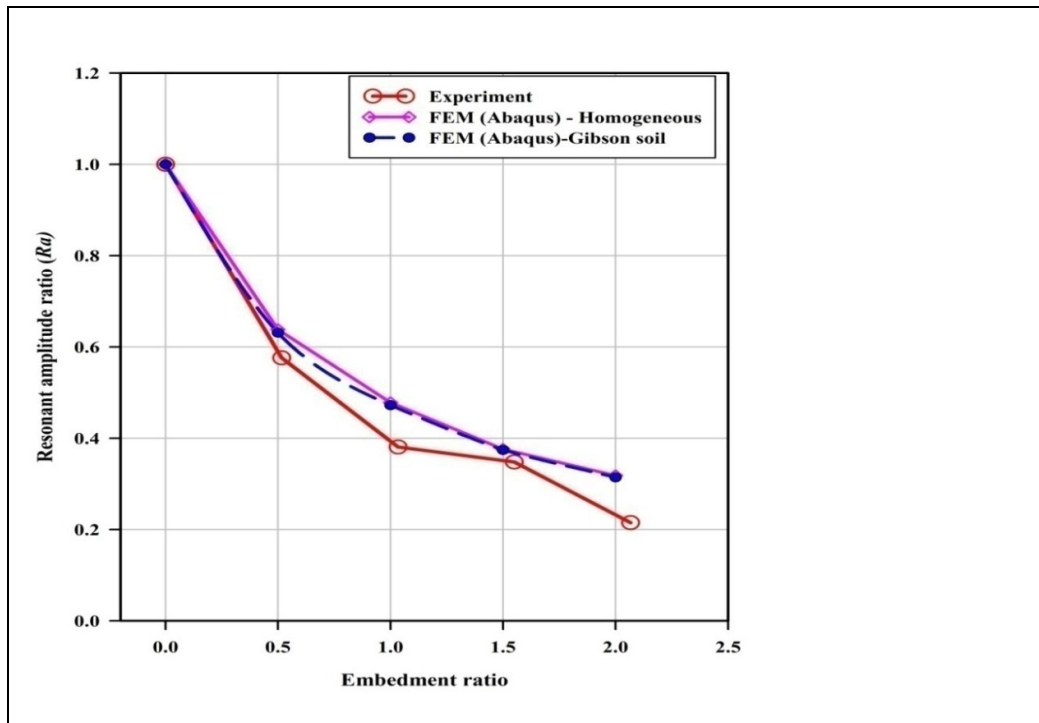
Figure 6.53: Comparison between resonant amplitude ratio FEM (Gibson soil and homogeneous) and experimental results

6-44
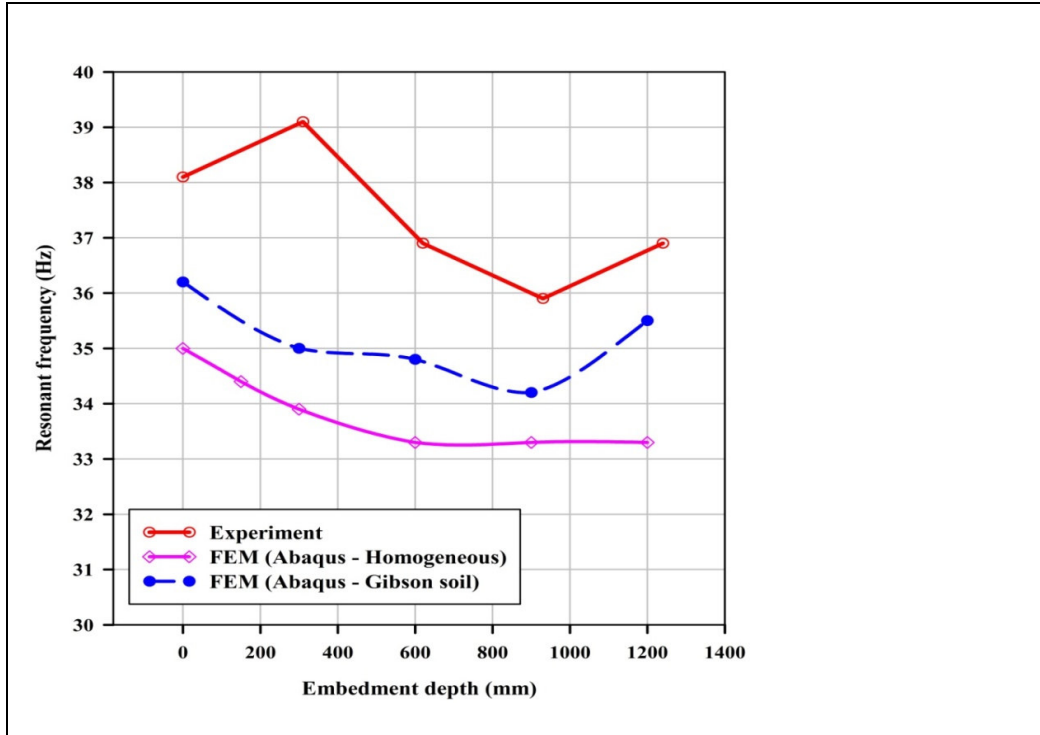
Figure 6.54: Comparison between resonant frequency FEM (Gibson soil and homogeneous) and experimental results
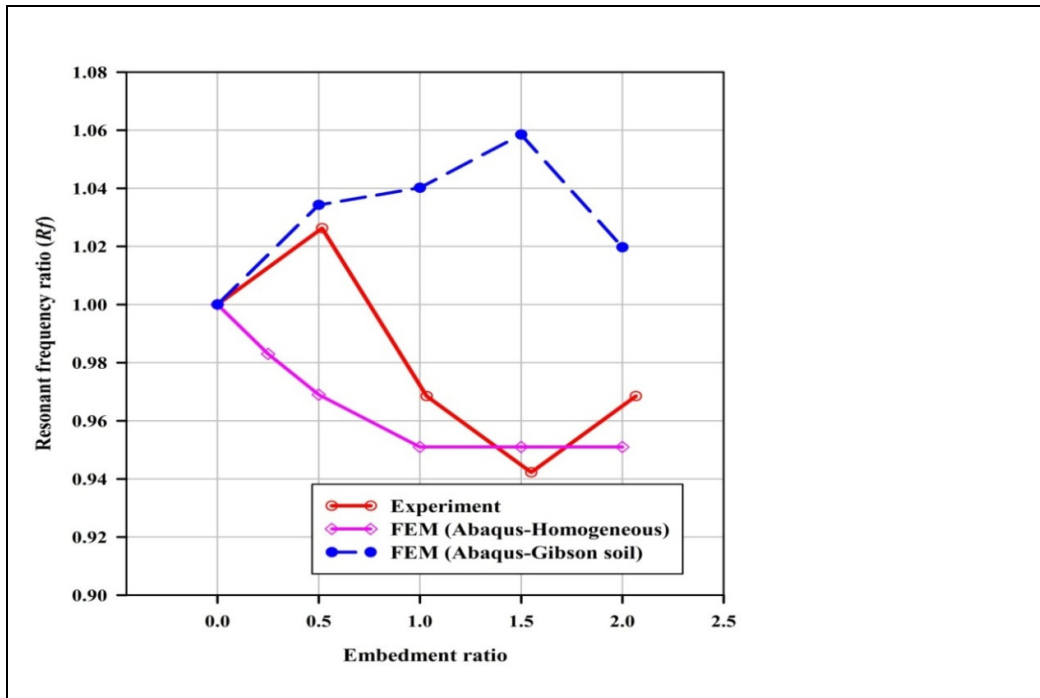
Figure 6.55: Comparison between obtained - Resonant frequency ratios

6-45
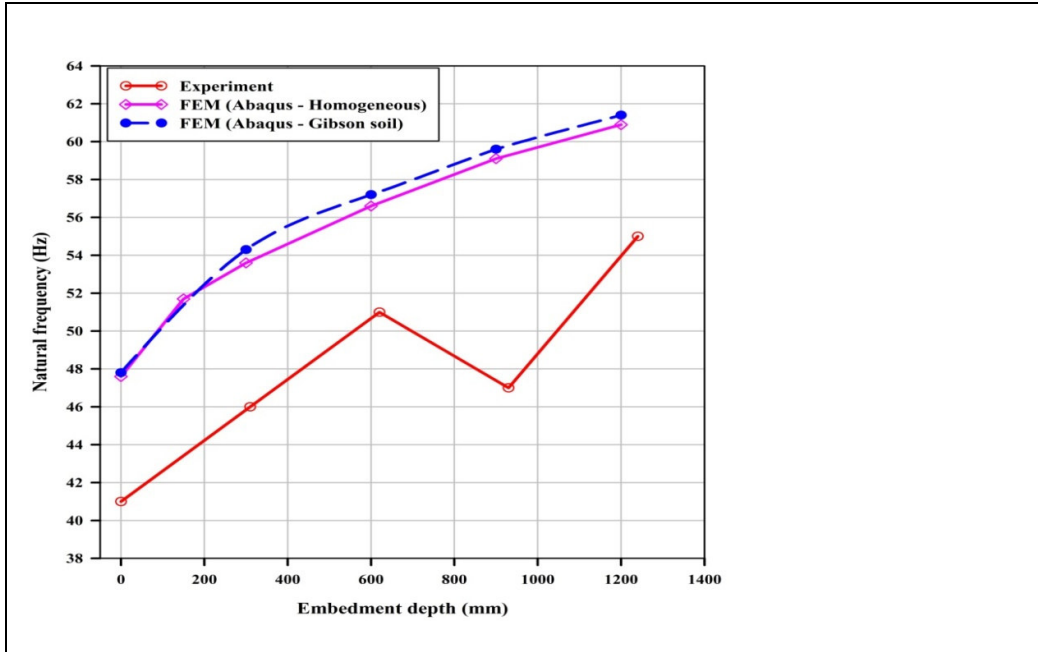
Figure 6.56: Comparison between natural frequency obtained numerically (FEM - Homogeneous and Gibson soil) and experimentally
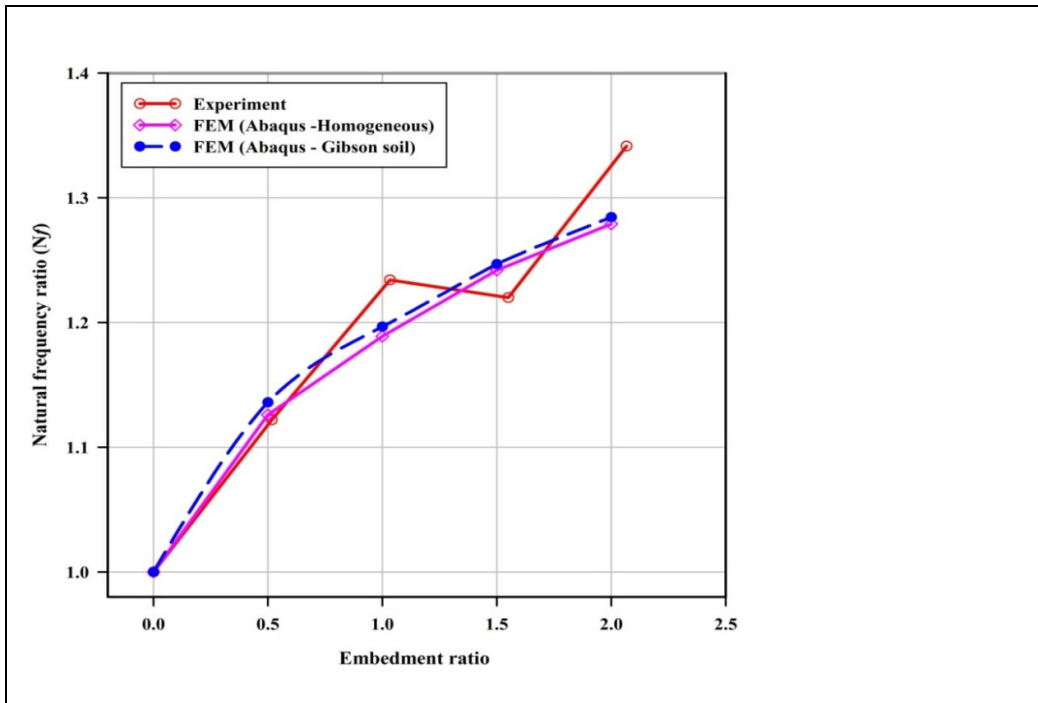
Figure 6.57: Comparison between natural frequency ratio obtained numerically (FEM - Homogeneous and Gibson soil) and experimentally

CHAPTER 7

7 DISCUSSION

7.1 Introduction

This chapter discusses the results of the vertical dynamic behaviour of surface and embedded foundations subjected to vertical harmonic loading. In the field, a hydraulic shaker was used to excite the footings by applying a harmonic vertical force at frequencies ranging from 10 to 100 Hz. The shaker was fixed at the centre of the footings and the measured displacements were analysed to calculate measured impedance functions. The field-measured vertical dynamic behaviour was predicted using analytical solution, numerical solution of the finite element method and the Dyna5 program. The discussion is based on the comparison of the measured and predicted responses obtained from the analytical solution and numerical analysis. The field measurements were carried out on the surface and embedded foundations. The field measured vertical dynamic responses are plotted together with the predicted responses for easy discussion and evaluation.

For the surface foundation, the results from the following numerical and analytical models were compared with the results obtained from field measurements.

- Elastic half-space theory (Sung 1953);
- Simplified model of Veletsos and Verbic (1973) massless soil;
- Simplified model of Lysmer (1965);
- Simplified model of Veletsos and Verbic (1973) soil with mass;
- Dyna5 program
- Finite element method – homogeneous soil, and
- Finite element method – Gibson soil

The comparison is based on the following vertical dynamic responses plotted against forcing frequency.

- The displacement amplitude;
- The resonant frequency;
- The complex dynamic stiffness;
- The real part of the complex dynamic stiffness;

- The imaginary part of the complex dynamic stiffness, and
- The phase and loss angles.

For the embedment foundation, the measured vertical dynamic responses were compared with the predicted responses obtained from the following analytical and numerical solution.

- The analytical model suggested by Novak and Beredugo (1972);
- Dyna5 program;
- The numerical solution of finite element method (Abaqus) with the assumption that the footing is placed underneath the homogeneous soil, and
- The numerical solution of the finite element method with the assumption that the footing is placed on Gibson soil.

The comparison was based on the following measured dynamic responses:

- Displacement amplitude;
- Amplitude at resonance;
- Resonant frequency, and
- Natural frequency.

The effects of embedment were evaluated using the following dimensionless quantities:

- Resonant amplitude ratio;
- The resonant frequency ratio;
- Natural frequency ratio, and
- Damping ratio.

7.2 Surface foundation

7.2.1 Vertical dynamic displacement

Figure 7.1 shows the measured vertical dynamic displacement amplitudes plotted together with predicted vertical dynamic displacements amplitudes. The forces measured in the field were used to simulate the actual forces exerted on the footing for analytical and numerical analysis. From Figure 7.1, it is shown that at maximum displacement both numerical and analytical solutions underestimated the vertical dynamic responses. It is shown that Dyna5 and Veletsos and Verbic (1973) soil with mass predicted the lowest displacement compared to Lysmer (1965) model and Sung's (1953) solution. Dyna5 and Veletsos and Verbic (1973) with mass underestimated the displacement by 56.2 %. Lysmer (1965) model predicted the highest vertical displacement but still underestimated displacement by about 31.9 %. Therefore, the analytical and numerical models under predicted the displacement in the range of 31.9 % and 56.2 %. This indicates that the design engineer should expect an

error in this range when predicting displacement of the machine foundation by using the listed analytical and numerical models under the described conditions. The performance of the models was fairly similar. All models predicting peak displacement amplitudes between 0.008mm and 0.012mm. In contrast, the computational effort to use the models is very different. Some are quite easy and others are very difficult to use.

The numerical and analytical models predicted the first peak at about 32 Hz, which was also observed from the measured responses. It is interesting to note from the plots in Figure 7.1 that there is good agreement between the results obtained from the finite element method and the analytical solution by Verbic (1973) with mass of footing.

7.2.2   Resonant resonant amplitude and frequency

Figure 7.2 shows the measured frequency response function plotted together with predicted frequency response function. From the plot, it is shown that analytical models could not predict the resonant frequency close to what was measured experimentally. The finite element method (Abaqus) underpredicted the resonant frequency for about 28.9 %.

7.2.3   Complex dynamic stiffness

The predicted and measured complex dynamic stiffness are plotted together and shown in Figure 7.3. The response shows that, at low frequencies, the prediction models overestimated the complex dynamic stiffness. It is observed that, at low frequency, the analytical solutions converged to a single point, which is lower than the complex dynamic stiffness obtained from finite element method. The prediction models overestimated the complex dynamic stiffness except Sung's (1953) and Veletsos and Verbic (1973) massless model could not predict the trend of the measured complex dynamic stiffness at the higher frequencies. The general responses of the predicted complex dynamic stiffness at low frequency is reasonably similar to the one obtained from field-measured data.

The complex dynamic stiffness tends to be constant at the low frequencies then increases as the forcing frequency increases. It is also shown that there is a good agreement between the evaluated numerical and analytical models. For instance, Figure 7.3 shows that from about 25 Hz to 100 Hz, the finite element solution and analytical solution of Veletsos and Verbic (1973) with mass, Lysmer (1965) model and Dyna5 program plots are very similar. The similarity of these measured responses and the predicted responses by finite element method shows that Abaqus software is suitable for predicting complex dynamic stiffness of machine foundations. Moreover, the observation from Figure 7.3 shows that the shapes of

the response curves predicted by finite element are similar to those measured, although the finite element overestimated the complex dynamic stiffness.

7.2.4 Real part of complex dynamic stiffness

The field-measured and predicted real parts of complex dynamic stiffness are plotted together in Figure 7.4. The real part is sometimes referred to as effective dynamic stiffness. Essentially, the real part is the solution of Equation 2.31. The solution depends on the assumptions made in relation to the inertia force. It is common to assume that the footing and soil is massless or has mass. If the model assumes that footing and the soil underneath the footing is massless, in Equation 2.31, the mass of vibrating footing mechanism becomes zero. This reflects that the dynamic response is frequency independent. From Figure 7.4, it is shown that the measured real part is frequency dependent except for the solution by Veletsos and Verbic (1973) massless soil and Dyna5 program. The plot shows that, as the forcing frequency increases the real part decreases. From the plot, it is shown that at a low frequency, the analytical and numerical solution overestimated the real part of the complex dynamic stiffness. The frequency dependence of the response is only influenced by the presence of the inertia forces because the soil properties are essentially frequency independent.

An advantage in plotting the frequency dependency of the real part is that the natural frequency of the foundation systems can be estimated when the real part crosses zero. The real part for field-measured data crosses zero at the frequency of 49.5 Hz. The responses predicted by Veletsos and Verbic (1973) massless soil and Dyna5 program did not cross zero at the real part as it assumes the footing and soil is massless. The other numerical and analytical solution estimated the natural frequency ranging between 50 and 59.4 Hz. It was observed that the analytical solution by Veletsos and Verbic (1973) which assumes that the footing and soil have mass predicted more accurately the natural frequency with an error of 2 %. The general responses of the numerical and analytical solution show a remarkable similarity except for Dyna5 program and Veletsos and Verbic (1973) with massless soil. The results show the importance of considering the mass of the footing and the soil medium where the machine foundations are placed in relation to wave propagation.

7.2.5 Imaginary part of complex dynamic stiffness

Figure 7.5 show the imaginary part of complex dynamic stiffness and the responses reflect the solution of the Equation 2.32. The plots show that analytical and numerical solution overestimated the imaginary part, except for elastic half-space theory where at around

78 Hz the imaginary part becomes small. The same trend is observed from the finite element method. The general responses show that the imaginary part increases as the forcing frequency increases. This shows that the radiation damping is frequency dependent. The result from field measurements describe that at the low frequency of up to about 45 Hz, the dependence of the frequency is very low indicating that material damping moderated the responses.

7.2.6 Phase and loss angles

Figure 7.6 shows the plot of phase angle between force and displacement against forcing frequency. The natural frequency of the foundation can be estimated from the plot of phase angles versus forcing frequency. From the plot, it is shown that analytical and numerical solution compared favourably with the measured responses and that the analytical and numerical solutions overestimated natural frequency. The predicted natural frequencies range between 50 Hz and 59.4 Hz. The analytical solution by Veletsos and Verbic (1973) with mass predicted natural frequency close to the one measured in the field. The prediction percentage error of the natural frequency is within the range of 2 % and 18.4 %.

Figure 7.7 shows the plots of the measured and predicted loss angles. The loss angle in radians is almost constant at the low frequency when the forcing function is in phase with displacement. The sudden rise in loss angles indicates that the forcing function goes out of phase with displacement. The natural frequency is the frequency at the peak point as shown in Figure 7.7. It is also seen from the plot of loss angles versus forcing frequency that analytical and numerical solution overestimated natural frequency. The prediction models, which assumed that the footing is massless, cannot predict natural frequency from the loss angle versus forcing frequency.

7.3 Embedded foundation

7.3.1 Displacement amplitudes

The measurements of the embedded foundation were carried out for the embedment depths of 0, 310, 620, 930 and 1240 mm. Figure 7.8 shows the measured and predicted displacement amplitudes for zero embedment plotted against forcing frequency. From the plot it is shown that at low frequencies up to about 33 Hz the analytical solutions overestimated the amplitude displacements. The analytical solution by Novak and Beredugo (1972) overestimated amplitude displacement at maximum peak by 2%. Dyna5 program also overestimated amplitude displacement for about 1%. The finite element

method with homogeneous and Gibson soil soil medium underestimated the amplitude displacement at maximum peak by 58.2 %.

Figure 7.9 shows the measured and predicted displacement amplitude for 310 mm embedment plotted against forcing frequency. From the plot, it is shown that the analytical solution by Novak and Beredugo (1972) overestimated amplitude displacement at maximum peak by 3.8%. Dyna5 program also underestimated amplitude displacement for about 4.9%. The finite element method with homogeneous and Gibson soil medium underestimated the amplitude displacement at maximum peak by 61.6 %. Figures 7.10, 7.11 and 7.12 show the displacement amplitude for embedment 620, 930 and 1240 mm respectively.

Figure 7.13 show the plots of measured and predicted maximum displacement amplitude against embedment depth. From this, it is shown that the measured and predicted resonant amplitude decreases as the embedment increases. The rate of decrease is very pronounced at the small embedment. As the embedment increases, the benefit of this embedment is insignificant. From the plot, it is shown that Dyna5 program and Numerical solutions under estimated displacement amplitude. The analytical solution by Novak and Beredugo (1972) overestimated displacement for embedment of 0 and 310 mm and underestimsted displacement amplitude for embedment of 620, 930 and 1240 mm.

The responses conclude that analytical solutions predict the displacement amplitude of machine foundations close to what measured in the field. The error between measured and prediction by analytical solution is between 1 % and 39 % for all embedments. The finite element method with homogeneous and Gibson soil medium underestimated the amplitude displacement in the range of 58.3% and 61.6 % for all embedments.

7.3.2 Resonant amplitudes and resonant frequency

The frequency response function of the embedded foundation were determined for the embedment depths of 0, 310, 620, 930 and 1240 mm. Figure 7.14 shows the measured and predicted displacement amplitudes for zero embedments plotted against forcing frequency. From the plot it is shown that the analytical solution by Novak and Beredugo (1972) and Dyna 5 program underestimated the resonant amplitude by about 18.2 %. Dyna5 program also underestimated resonant amplitude for about 34.2%. The finite element method with homogeneous soil medium underestimated the resonant amplitude for about 288.7 %. The finite element with Gibson soil underestimated resonant amplitude for about 280.5 %.

Figures 7.15 and 7.16 show the frequency response function for embedment of 310 and 620 mm respectively. From the plot, it is seen that in both cases the analytical solution under predicted the resonant amplitude at resonant frequency. The analytical solution by Novak and Beredugo (1972) underestimated the resonant frequency within the range of 5.3% and 14.3% for all embedments. Dyna5 program under predicted resonant frequency in the range of 4.5% and 20.7% for all embedments.

Figure 7.17 show the plot of resonant amplitude against embedment depth. From this, it is shown that the measured and predicted resonant amplitude decreases as the embedment increases. The rate of decrease is very pronounced at the small embedment. As the embedment increases, the benefit of this embedment is insignificant.

7.3.3   Resonant amplitude ratio

The resonant amplitude ratio is the ratio of the peak amplitude for an embedment footing to the peak amplitude for zero embedment. Figure 7.18 shows the plot of resonant amplitude ratio versus embedment ratio and this presents that the resonant amplitude ratio decreases as the embedment ratio increases. The rate of decrease is noticeable at the lower values of embedment ratio. This suggests that even small embedment can significantly reduce the resonant amplitude. In all cases, the plots show that, at higher embedment ratios, the effect of embedment is insignificant. The response indicates that the Dyna 5 program predicted resonant amplitude ratio close to what was measured in the field. The results from resonant amplitude ratio indicate that for a given dimension of square footing, the reduction in displacement can be predicted.

7.3.4   Resonant frequency

The predicted and measured resonant frequencies are plotted against embedment depth as shown in Figure 7.19. The prediction models underestimated resonant frequencies. The predicted resonant frequencies decrease as the embedment increases up to 310 mm embedment, after this it remains mostly constant. The error between predicted and measured resonant frequency at zero embedment ranges between 5.0 % and 8.1 %.

7.3.5   Resonant frequency ratio

Figure 7.20 show the predicted and measured resonant frequencies ratio plotted against embedment ratio. The resonant frequency ratios predicted by analytical solution and finite element method with the assumed homogenous soil decrease as the embedment increases

up to embedment ratio of about 0.52. Beyond embedment ratio of 0.52, resonant frequency ratios remain constant. The finite element method with assumed Gibson soil predicted resonant frequency ratio almost similar to that measured in the field up to embedment ratio of 0.5. The error between measured and predicted resonant frequency ratio for embedment ratio of 0.5 and 2.07 is between 0.8 % and 17 %. The general responses show that there is a good conformity between measured and predicted resonant frequency ratio.

7.3.6   Natural frequency

The predicted and measured natural frequencies of embedded foundations are shown in Figure 7.21. This reflects that the predicted and measured natural frequency increases as the embedment depth increases. The variation in the natural frequency obtained from the field-measured data and finite element method is between 10.4 % and 14.2 %. The finite element method overestimated natural frequencies for all embedment depths as per Figure 7.21. At the embedment, between 0 and 600 mm the analytical solution by Novak and Beredugo (1972) predicted natural frequency very close to the measured natural frequencies. For analytical solutions, the error between predicted and measured natural frequency for all embedment ranges is between 0.0 % and 6.8 %. The variation in the natural frequency obtained from the field-measured data and Dyna5 are between 2.4 % and 8.9 %.

7.3.7   Natural frequency ratio

The predicted and measured natural frequency ratios are shown in Figure 7.22. This describes that the predicted and measured natural frequency ratio increase as the embedment ratio increases. There is a favourable agreement between predicted and measured natural frequency ratio up to embedment ratio of 0.7. At full embedment, the predicted error ranges between 4.7 % and 9.1 %. The finite element method underestimated natural frequency ratio between embedment ratio of 0.7 and at full embedment. The analytical solution by Novak and Beredugo (1972) and Dyna5 program overestimated natural frequency ratio between embedment ratio of 0.7 and at full embedment.

7.3.8   Damping ratio

The measured and predicted damping ratios plotted against embedment ratio are shown in Figure 7.23. From the plots in both cases the damping ratio increases as the embedment increases. From Figure 7.23, all prediction models overestimated damping ratio. In all cases, the rate of increases of damping ratio is pronounced at low values of embedment

ratio. As the embedment increases, the rate of increases of damping ratio is insignificant. The shapes of the curves indicate that dynamic responses of machine foundations are very sensitive to damping ratio. The error between observed and predicted damping ratio at zero and fully embedment is 84.4% and 15.8% respectively. In all cases, the minimum error occurs at full embedment and ranges between 11.0 % and 15.8%.

Figure 7.1: Comparison between measured and predicted displacement amplitudes
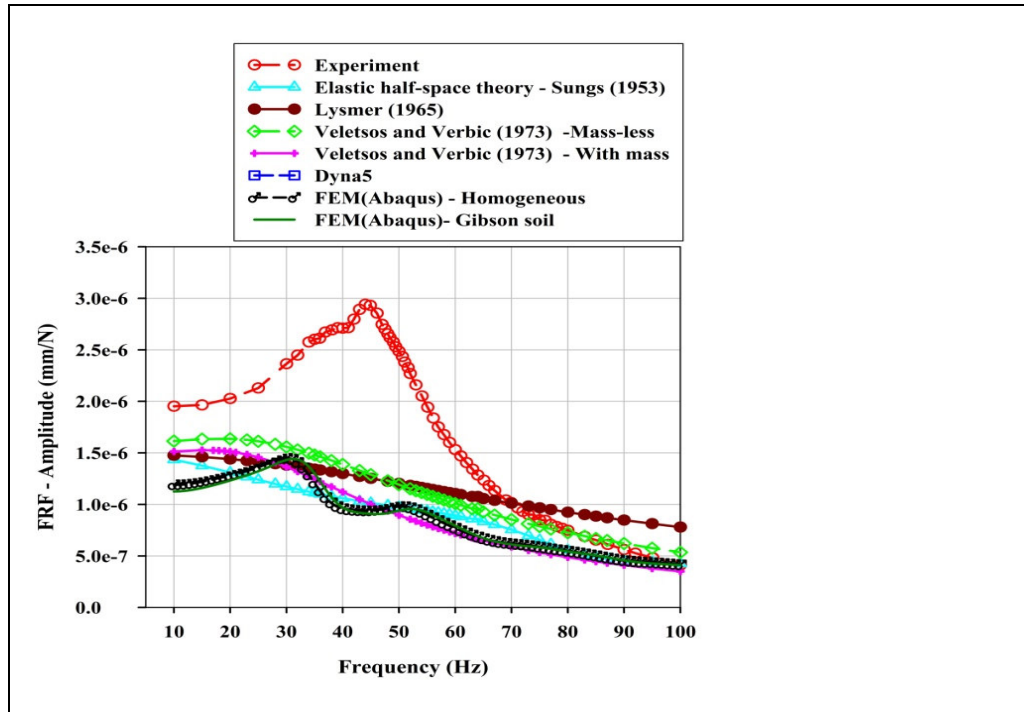
Figure 7.2: Comparison between measured and predicted frequency response function
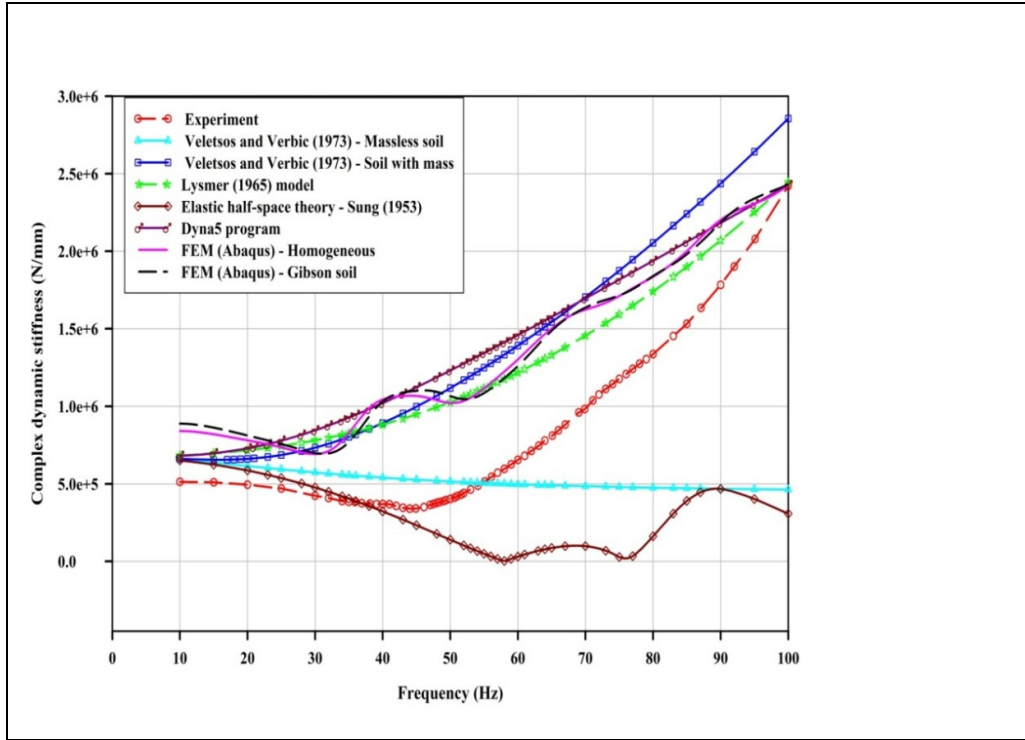
Figure 7.3: Comparison between measured and predicted complex dynamic stiffness
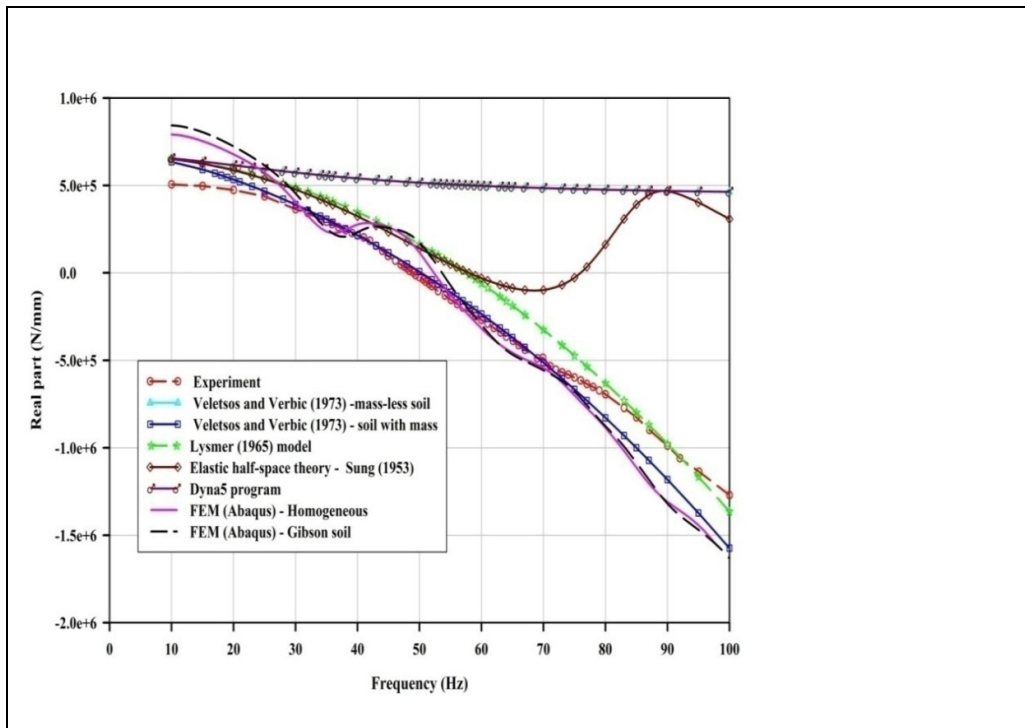
Figure 7.4: Comparison between measured and predicted real part of complex dynamic stiffness

7-11
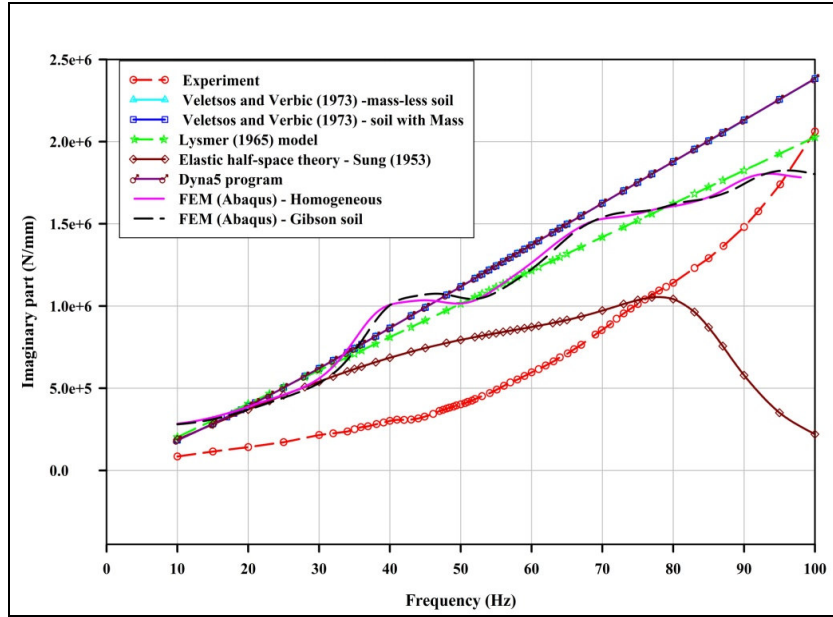
Figure 7.5: Comparison between measured and predicted imaginary complex dynamic stiffness
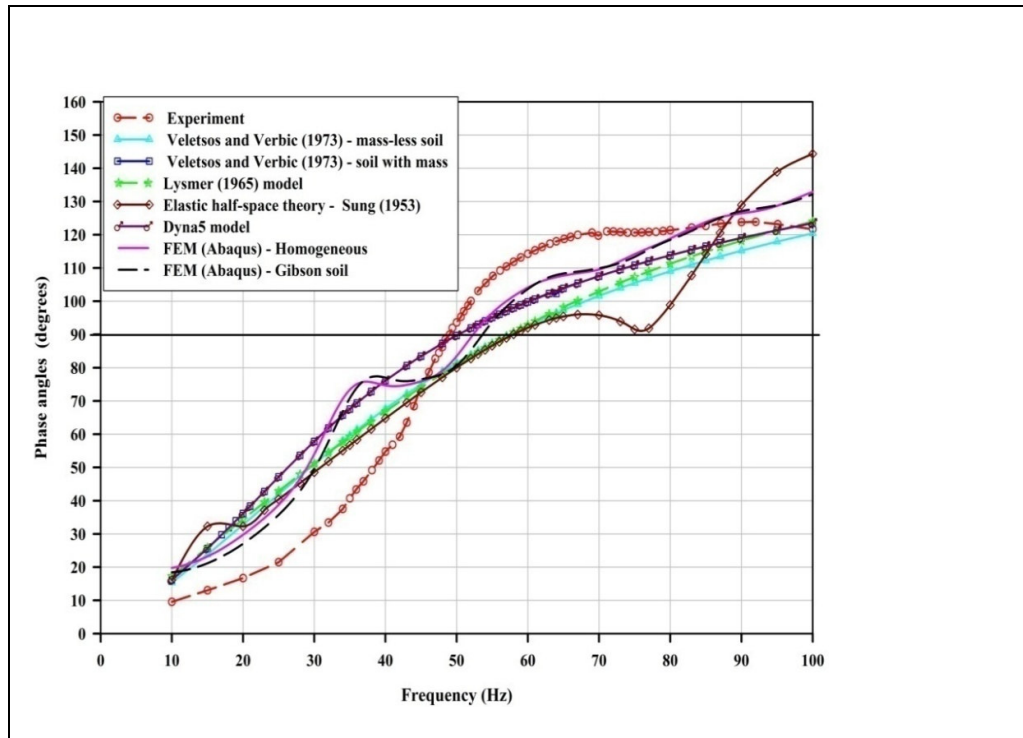
Figure 7.6: Comparison between measured and predicted phase angles

7-12
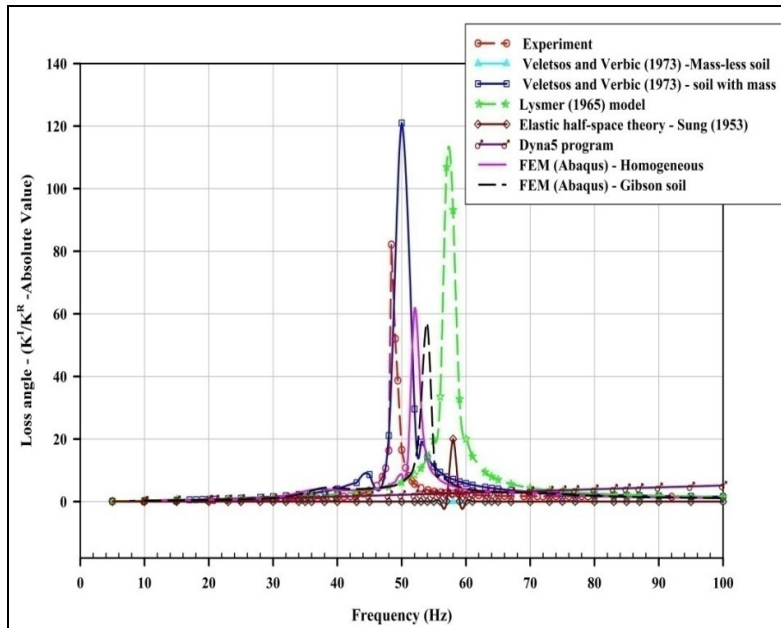
Figure 7.7: Comparison between measured and predicted loss angles
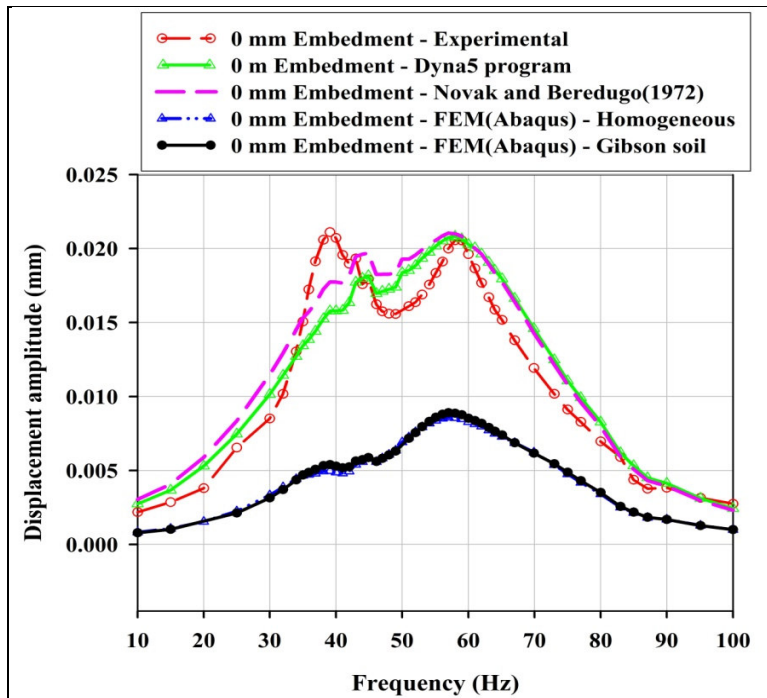
Figure 7.8: Comparison between measured and predicted displacement - 0mm

7-13
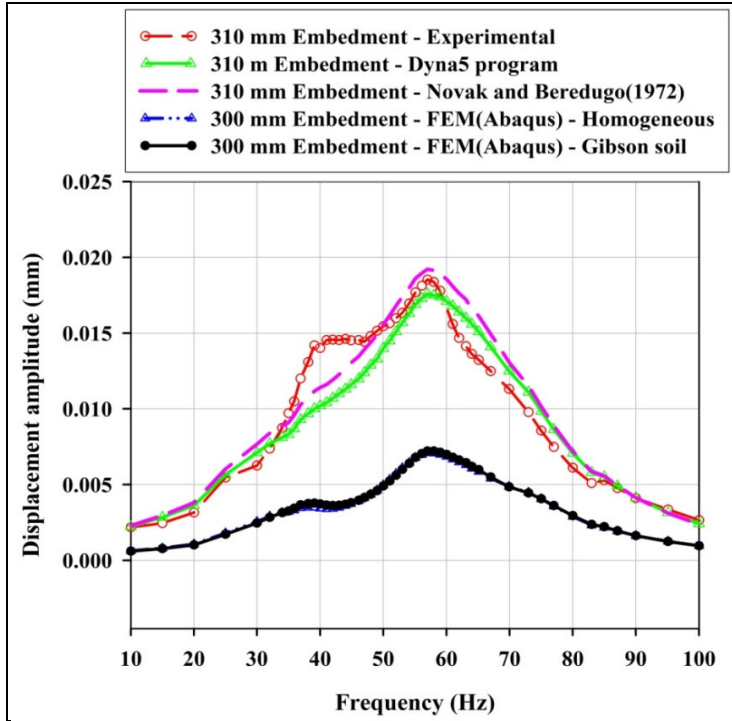
Figure 7.9: Comparison between measured and predicted displacement - 310mm

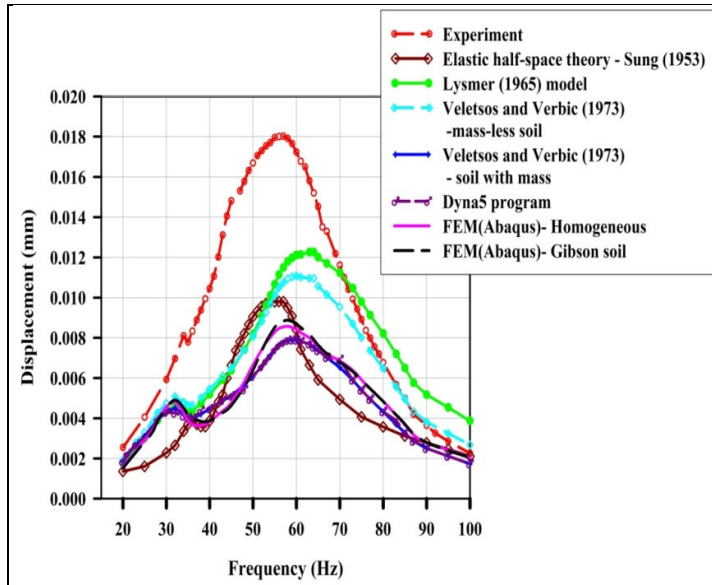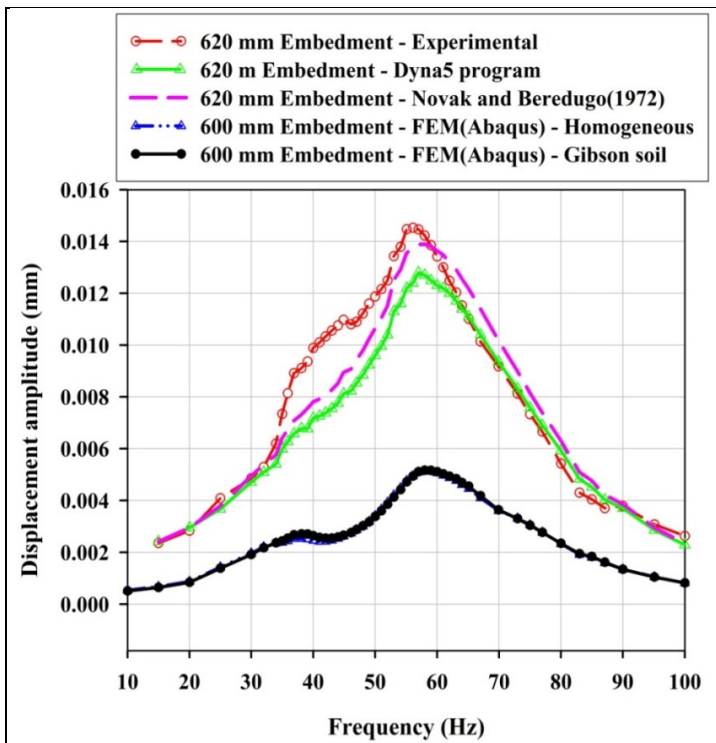Figure 7.10: Comparison between measured and predicted displacement - 620mm
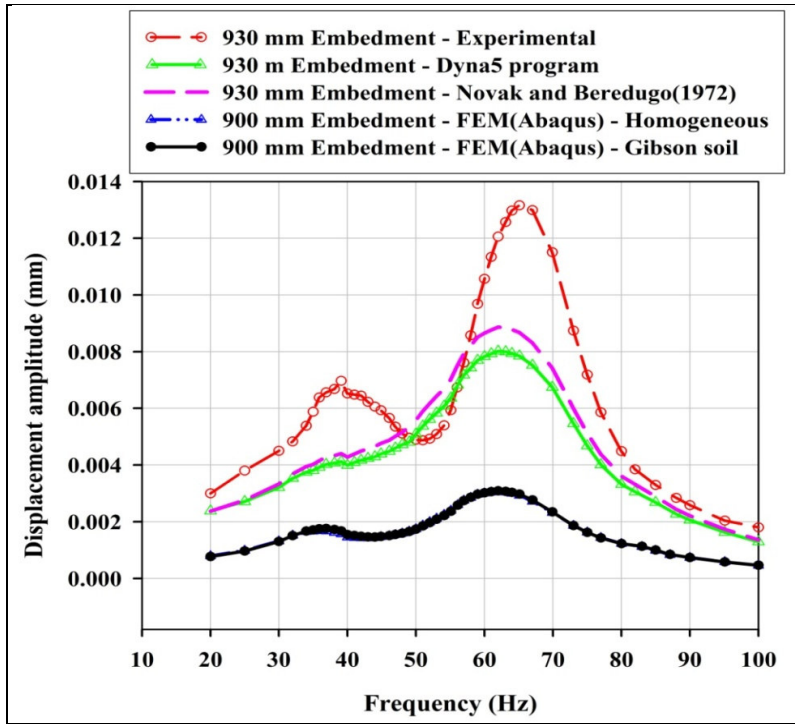
Figure 7.11: Comparison between measured and predicted displacement - 930mm
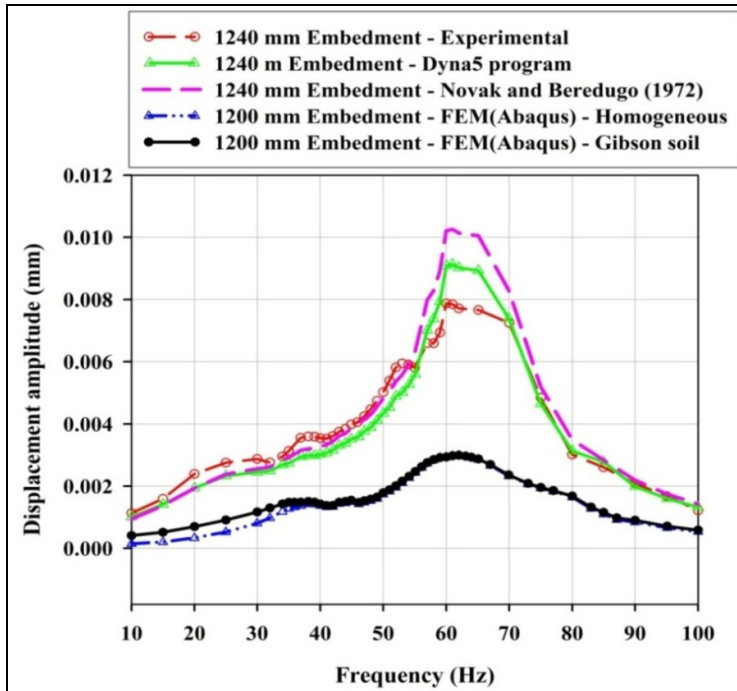
Figure 7.12: Comparison between measured and predicted displacement - 1240mm

7-15
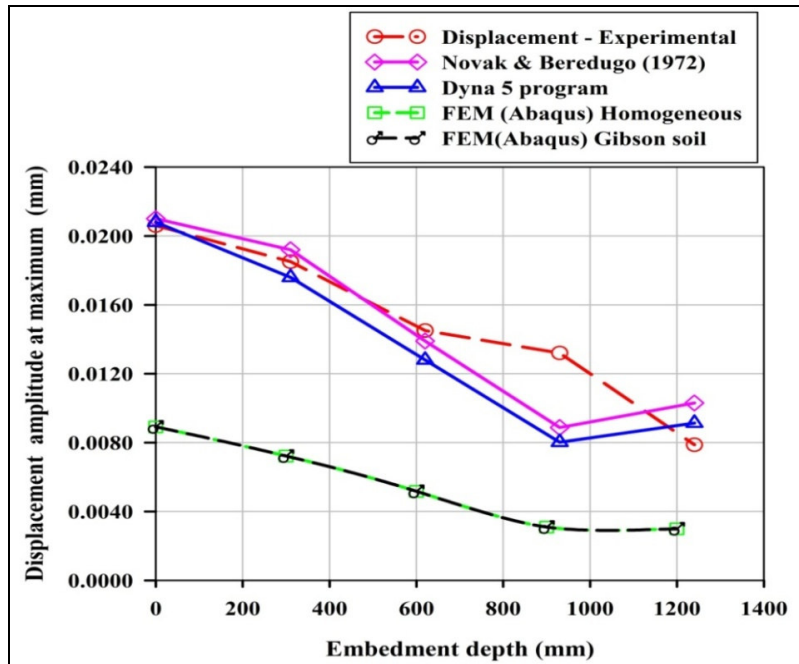
Figure 7.13: Comparison between measured and predicted displacement at the peak
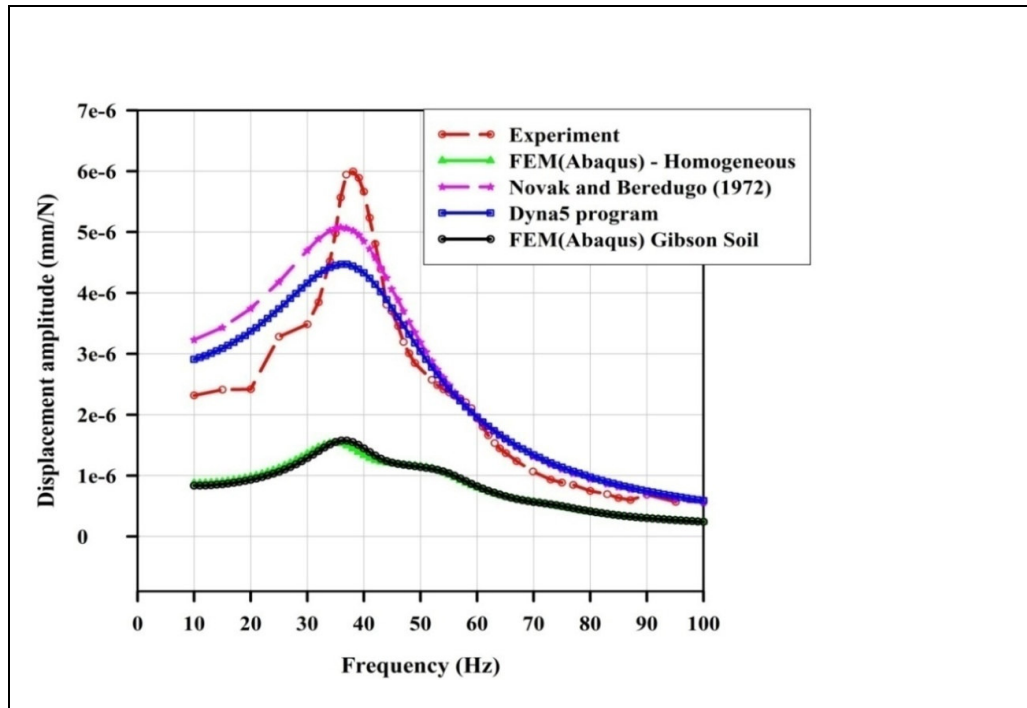
Figure 7.14: Comparison between measured and predicted displacement amplitudes (FRF) - 0 mm embedment

7-16
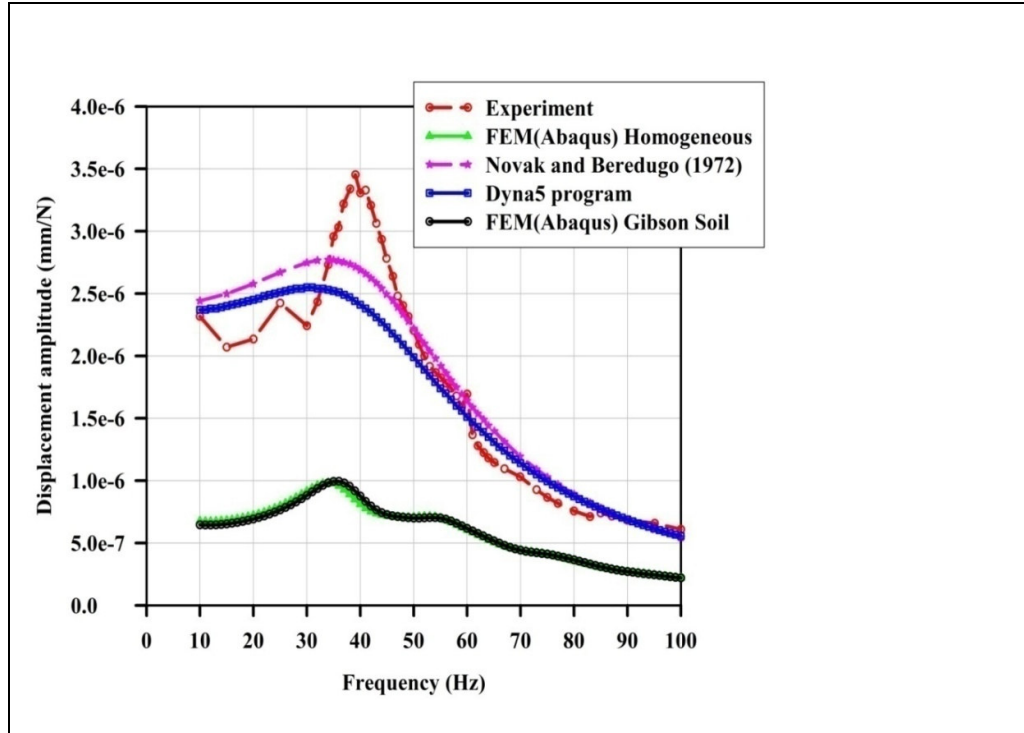
Figure 7.15: Comparison between measured and predicted displacement amplitudes (FRF) - 310 mm embedment
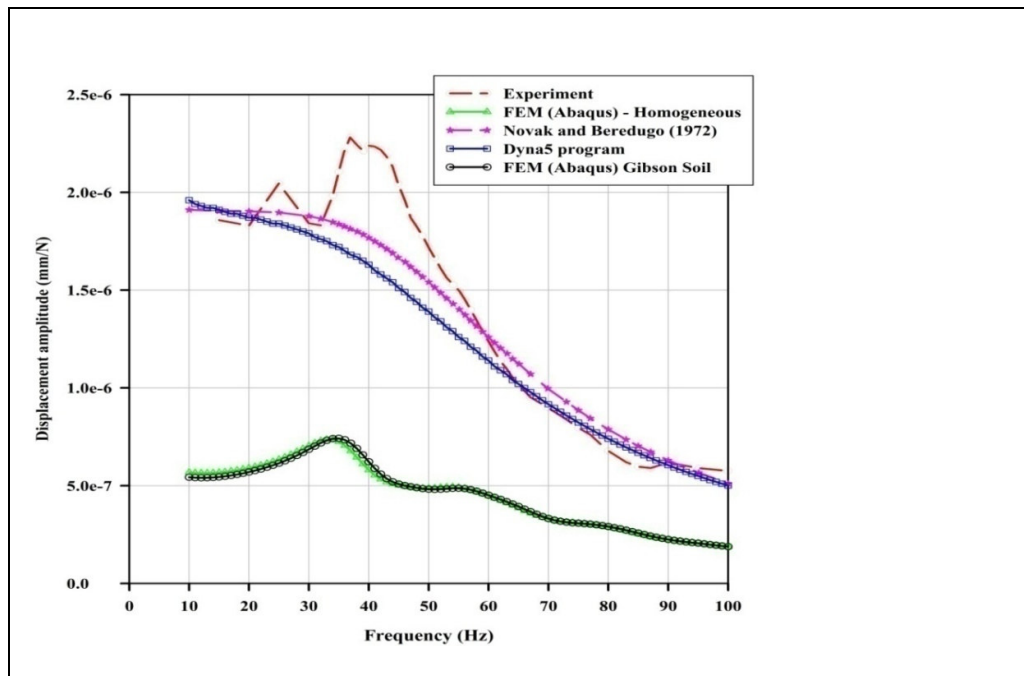
Figure 7.16: Comparison between measured and predicted displacement amplitudes (FRF) - 620 mm embedment

7-17
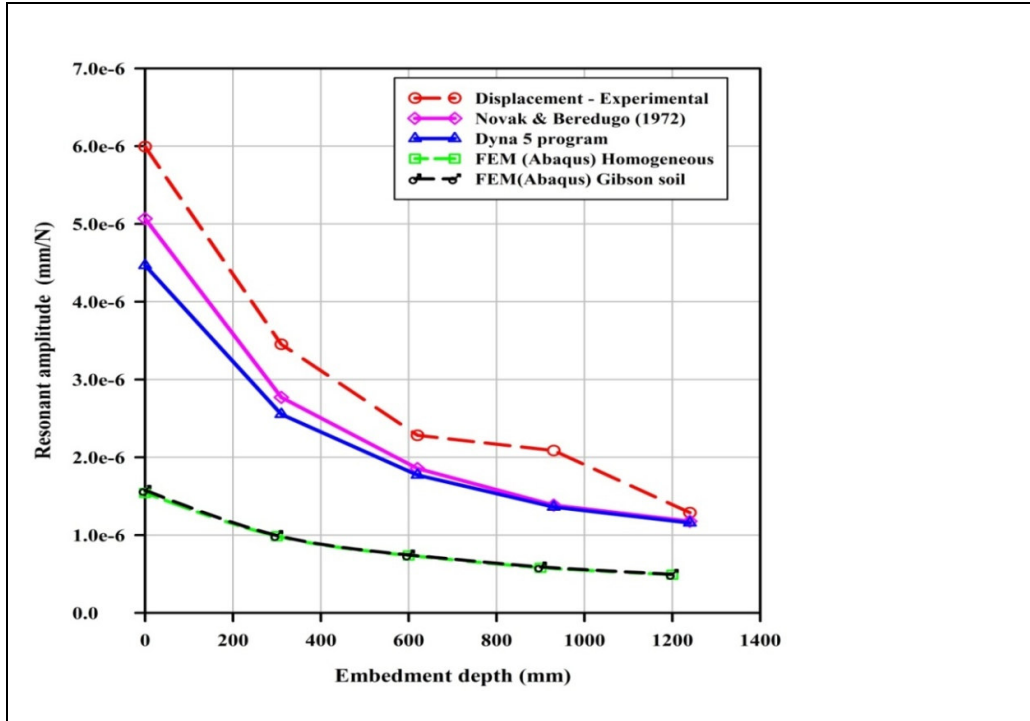
Figure 7.17: Measured and predicted resonant amplitudes
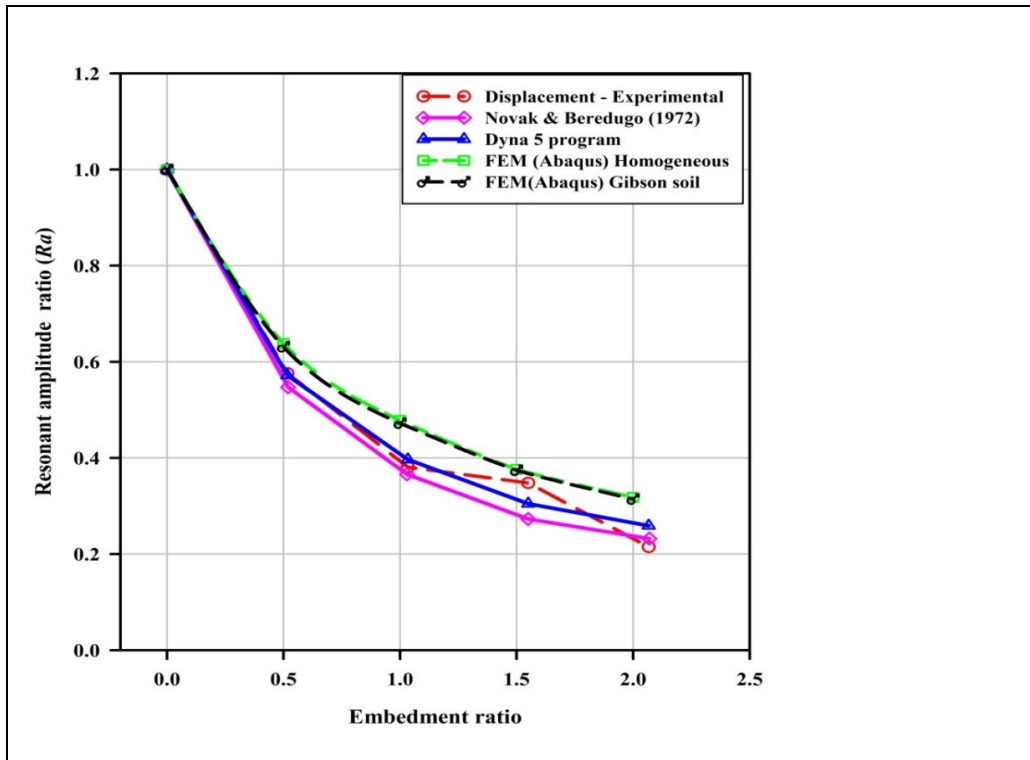
Figure 7.18: Comparison between measured and predicted resonant amplitude ratio
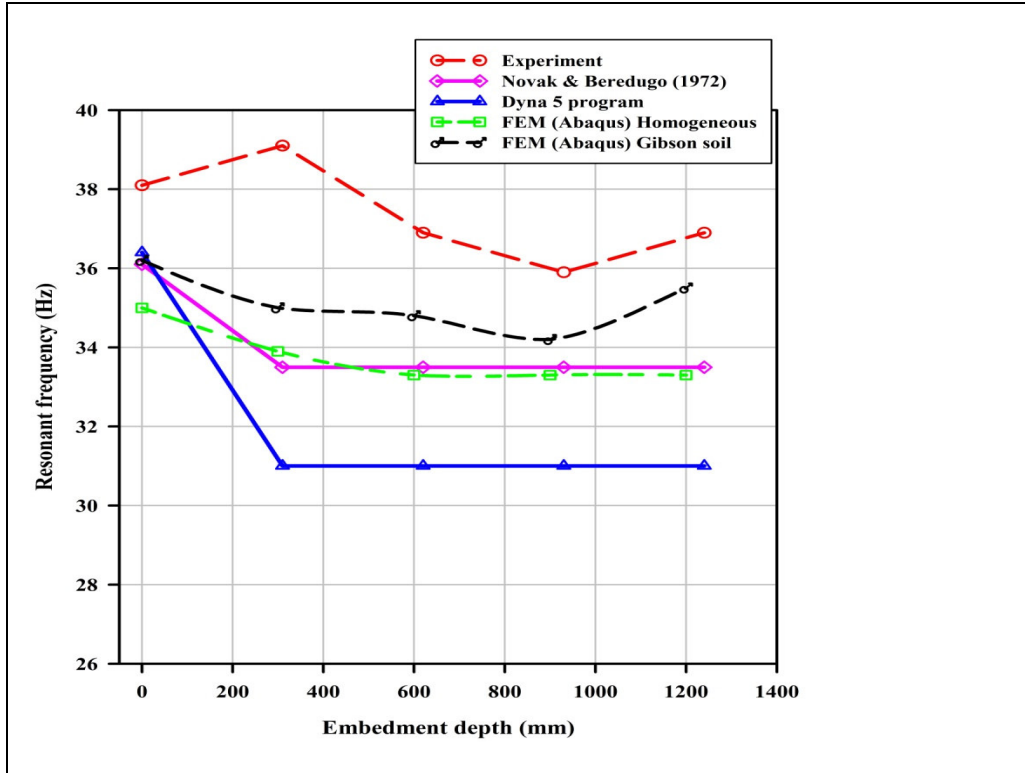
Figure 7.19: Comparison between measured and predicted resonant frequency
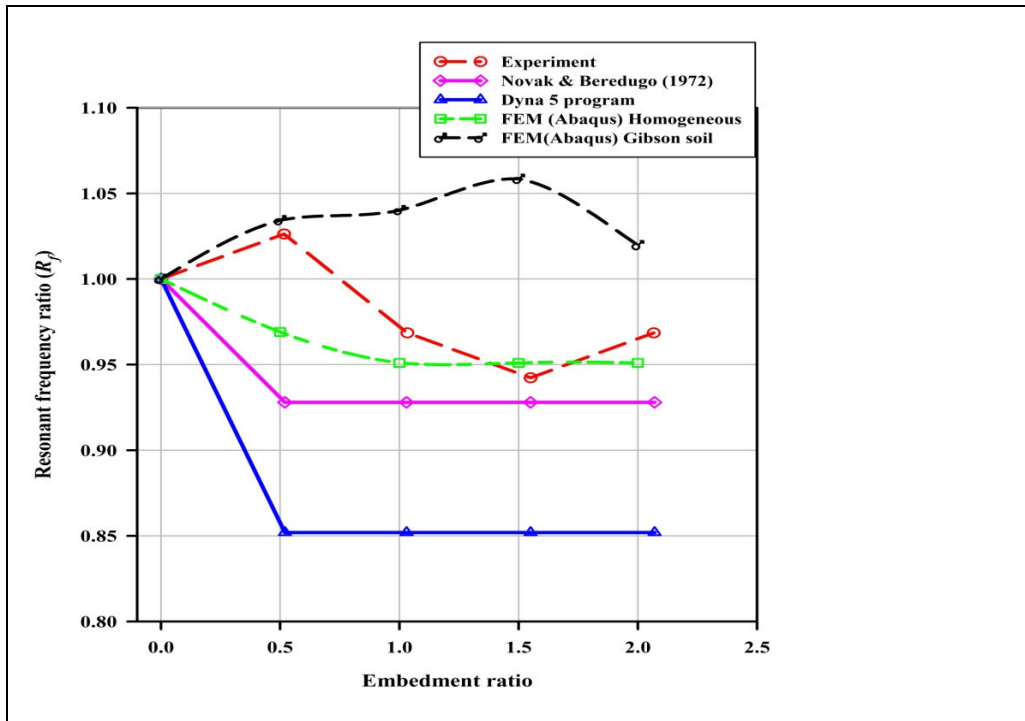
Figure 7.20: Comparison between measured and predicted resonant frequency ratio

7-19
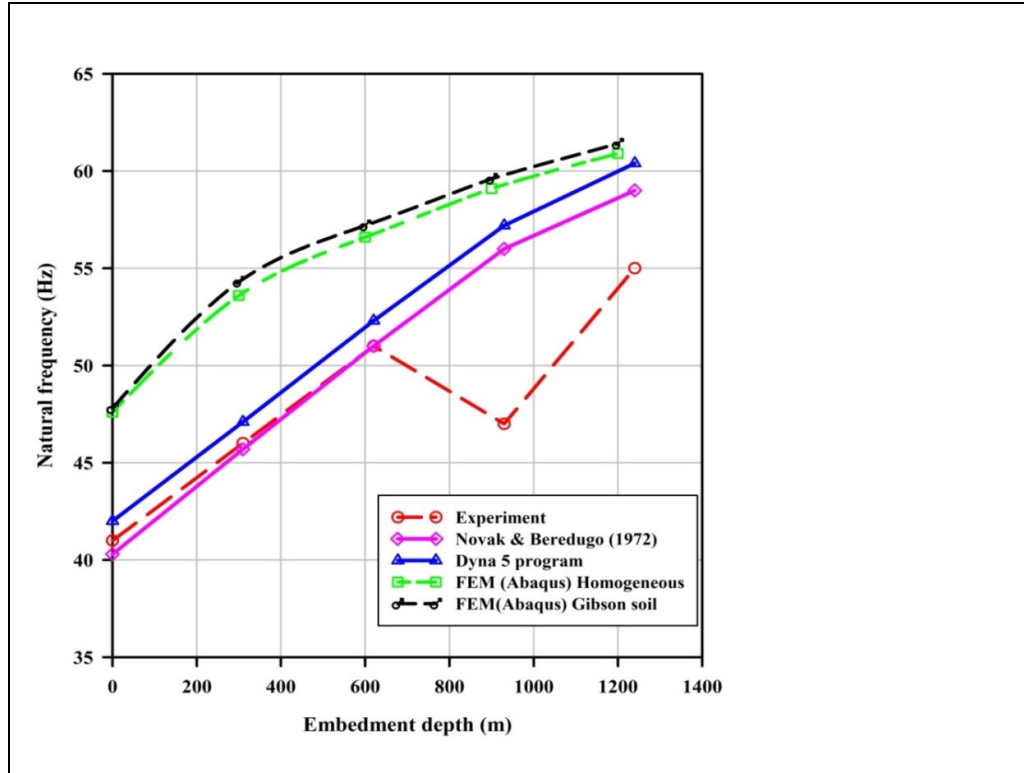
Figure 7.21: Comparison between measured and predicted natural frequency
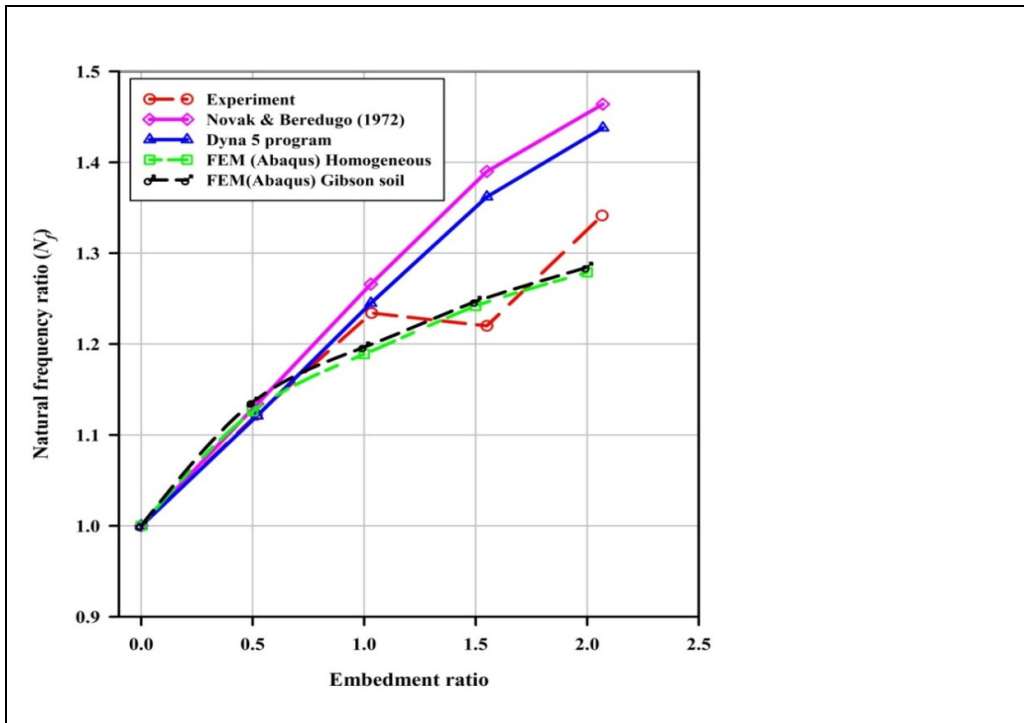
Figure 7.22: Comparison between measured and predicted natural frequency ratio
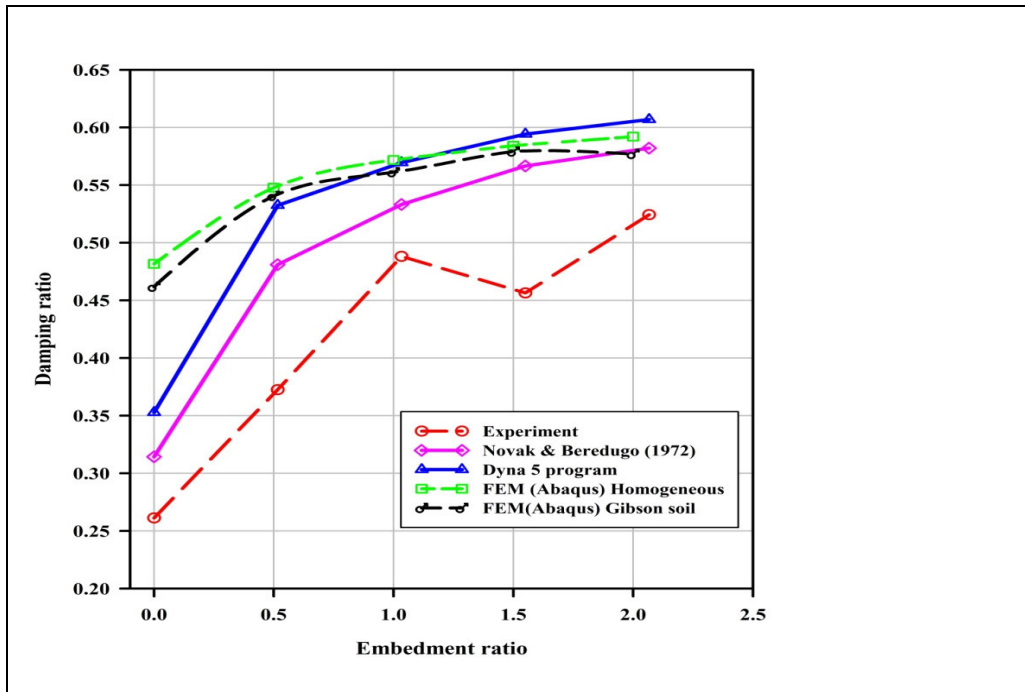
Figure 7.23: Comparison between measured and predicted damping ratio

CHAPTER 8

8 SUMMARY AND CONCLUSIONS

In this study, the vertical dynamic behaviour of machine foundations subjected to vertical loading was investigated for the surface and embedded foundations. The hypothesis states that the **appropriate analytical and numerical models are required to accurately predict the vertical response of machine foundations subjected to dynamic loads.** Two typical concrete foundations were tested to investigate the accuracy of existing chosen analytical and numerical models of the finite element methods in comparison to field-measured experimental results. The first was the rectangular footing of 2000 mm x 2500 mm in the plan with a depth of 400 mm placed on the surface of the ground. The second was the square footing of 1200 mm x 1200 mm embedded at the depth of 0, 310, 620, 930, and 1240 mm. The site is located at the University of Pretoria experimental station. The site was characterised to determine the shear wave velocity.

A hydraulic shaker was used to excite the footings by applying a harmonic vertical force at frequencies ranging from 10 to 100 Hz. The shaker was fixed at the centre of the footings. The measured displacements were analysed to calculate measured impedance functions by back-calculation.

8.1 Experimental results for surface foundation

The concern of this study was to evaluate the chosen existing analytical models and select the most accurate analytical model for the prediction of dynamic behaviour of surface machine foundations. The responses measured on the surface foundation included the foundation displacement amplitude, resonant amplitude, resonant frequency, natural frequency, and dynamic stiffness. The field experimental investigation was carried out to obtain the measured impedance functions and these results were compared with impedance functions obtained from analytical and numerical solution. From the experimental results, the following conclusions were made:

- It is common to determine the resonant frequency of the foundation system from the frequency response functions. The experimental results show that the resonant frequency may be estimated from the plot of complex dynamic stiffness against forcing frequency. It is shown from the plot of the complex dynamic stiffness

versus forcing frequency that the resonant frequency is the frequency at the point when the response is minimum;

- The measured dynamic responses of the foundation systems showed a strong frequency dependency;

- The damping ratio could be estimated from the measured resonant frequency and natural frequency of the machine foundations;

- The natural frequency of the machine foundations system can be obtained from the plot of the phase angle between displacement and force against forcing frequency. Also, the natural frequency can be obtained from the plot of the real part of complex dynamic stiffness and from the plot of loss angle versus forcing frequency, and;

- Negative foundation dynamic stiffness (real part) was found to occur when forcing function is out of phase with displacement by 90 to 180 degrees.

8.2   The results for surface foundation prediction models

The field-measured dynamic responses were compared with predicted responses obtained from Mass-Spring Dashpot (MSD or Winkler model, elastic half-space theory - Sung (1953), simplified models of Lysmer (1965) model and Veletsos and Verbic (1973). Two analytical models proposed by Veletsos and Verbic (1973) were evaluated. One assumes that the footing and soil medium are massless, and the other assumes the footing and soil medium have mass. Furthermore, the numerical solution by Dyna5 program was evaluated and compared with the measured responses. The general responses between measured and predicted responses show remarkable similarities. The evaluation of the analytical methods shows that:

- If the damping constant is properly chosen, the damped Winkler model can be used at the preliminary design stage to predict natural and resonant frequency of the machine foundations.

- The small strain shear stiffness obtained from Continuous Surface Wave tests with properly selected damping ratios, can be used to predict resonant frequency of the machine foundation systems using the Winkler model.

8-2

- Both analytical and numerical analysis was not able to predict the displacement amplitude, resonant amplitude and resonant frequency accurately.

- Analytical and FEM (Abaqus) models predicted natural frequency in the range of 2 % to 20 % error.

- The analytical model proposed by Veletsos and Verbic (1973) with the mass of footing and the soil medium rated as the most accurate analytical model among the evaluated analytical models.

8.3   Experimental results for embedded foundation

For the embedded foundation, the measured vertical dynamic responses included the foundation displacement amplitude, resonant amplitude, resonant frequency, natural frequency, damping ratio and dynamic stiffness. The effect of embedment of the foundation was explained by the dimensionless quantities known as resonant amplitude ratio, resonant frequency ratio and newly introduced quantity referred as the natural frequency ratio. From the experimental results, the following were observed:

- The displacement amplitude decreases as embedment increases. The rate of reduction of the resonant amplitude ratio was higher at the lower values of embedment ratio. This suggests that even small levels of embedment can significantly reduce the maximum vibration amplitude. The results also indicate that the added benefit of embedment diminishes at high embedment depths;

- The resonant amplitude decreases as embedment increases. The rate of reduction of the resonant amplitude ratio was higher at the lower values of embedment ratio;

- The resonant frequency changes very slightly as the embedment increases. At the low embedment, the resonant frequency increases as the embedment increases;

- The resonant frequency ratio obtained experimentally increases up to the embedment ratio of 0.5 then decreases as embedment increases;

- The natural frequency increases as the embedment increases. The rate of increase of the natural frequency becomes smaller as the embedment increases;

- From measured resonant frequency and natural frequency of machine foundations, the damping ratio could be determined. The measured damping ratio increases as the embedment increases, and

- The natural frequency ratio increases as the embedment increases.

8.4   The results for embedded foundation prediction models

The field-measured dynamic responses were compared with the predicted responses obtained from numerical analysis of finite element method (Abaqus) and the Dyna5 program. Furthermore, the measured responses were compared with the analytical method suggested by Novak and Beredugo (1972). This comparison between measured and predicted responses shows that:

- Novak and Beredugo (1972) and Dyna5 program predicted displacement amplitude for all embedment within the range of 1 % and 39.2 % of the observed displacement;

- FEM – Abaqus predicted the similar shape of observed displacement amplitude curve plotted against forcing frequency but underestimated displacement amplitude.

- Novak and Beredugo (1972), Dyna5 program and FEM – (Abaqus) predicted observed resonant frequency reasonably;

- The measured and predicted displacement amplitude decreases as embedment increases. In all cases, the rate of reduction of the displacement amplitude is higher at the low values of embedment ratio. At full embedment, the observed reduction in displacement amplitude was 61.8 %, and the predicted reduction in displacement amplitude ranged between 8.6 and 66.4 %. It was found that the currently available analytical techniques predicted the vibration amplitude of embedded foundations favourably.

- The measured and predicted resonant amplitude decreases as embedment increases. In all cases, the rate of reduction of the resonant amplitude is higher at the low values of embedment ratio. At full embedment, the observed reduction in resonant amplitude was 82.2%, and the predicted reduction in resonant amplitude for all embedments ranged between 36.2 % and 81.4 %. It was found that the best analytical and numerical techniques currently available do not accurately predict the resonant amplitude for embedded foundations, even for the simplest case of vertical vibration.

- The measured and predicted resonant amplitude ratio decreases as the embedment increases. In all cases, the rate of decreasing of resonant amplitude ratio is more pronounced up to the embedment ratio of about 0.5.

- The numerical solution by Dyna5 program is more accurate than analytical solution by Novak & Beredugo (1972) and finite element method when predicting the resonant amplitude ratio for embedded foundations. However, the accuracy of the analytical impedance method suggested by Novak & Beredugo (1972) and finite element method is reasonable and are within 48% of the observed resonant amplitude ratio at all embedment ratios. This is encouraging for industrial applications since the computational effort required for Dyna5 program is reasonable compared to the finite element method.

- The effect of embedment on the measured and predicted resonant frequency changes very slightly as the embedment increases. At a low embedment, the resonant frequency measured experimentally increases as the forcing frequencies increase. The resonant frequency for the numerical and analytical solution at low embedment decreases as the embedment increases then remain constant as the embedment increases. The resonant frequencies obtained from numerical and analytical solutions are low compared to the one measured experimentally in the range of 4.7 and 20.7 %.

- The resonant frequency ratio obtained experimentally increases up to the embedment ratio of 0.5 then decreases as the embedment increases. The resonant frequencies ratio obtained from numerical and analytical solution decreases as the embedment ratio increases up to the embedment ratio of 0.52 then remain constant as embedment increases.

- The predicted and measured natural frequency increases as the embedment increases. The rate of increase of the natural frequency becomes smaller as the embedment increases. Both the finite element and analytical methods were able to model an increase in natural frequency with increased embedment. At the small embedment, the predicted natural frequencies are very close to the observed natural frequencies.

- The predicted and observed damping ratio increases as the embedment increases. From the study, it is shown that numerical and analytical solutions overestimated damping ratio in comparison with experimental results.

- The measured and predicted natural frequency ratio increases as the embedment increases. A comparison between observed and predicted natural frequency ratio show that there is a good agreement at shallow embedment and that as embedment increases, the different can be noticed.

In conclusion, it is indicated that for the surface foundation, the analytical solution proposed by Veletsos and Verbic (1973) soil with mass predicted the natural frequency accurately among the evaluated analytical models.
The finite element method (Abaqus) predicted the similar shape of measured response curve for both surface and embedded foundation. The analytical solution by Novak & Beredugo (1972) and Dyna 5 program predicted favourable dynamic responses of embedded foundation when comparing to what measured in the field.

Based on the conclusions presented in Chapter 8, it is indicated that the hypothesis: **Appropriate analytical and numerical models are required to accurately predict the vertical response of machine foundations subjected to dynamic loads is accepted.**

9 References

Abaqus/Explicit User's Manual, Vol. I-II, Version 9.10, 2010, Hibbitt, Karlsson & Sorensen, Inc.

Alheid, H.J. 1994. Seismic response of deep underground openings. *Interaction: Numerical analysis and modelling*, Chapter 1, J.W. Bull (eds), E and FN Spon, pp 1 – 36.

Al-Homoud A. S. and Al-Maaitah O. N. 1996. An experimental investigation of vertical vibration of model footings on sand. *Journal of Soil Dynamics and Earthquake Engineering*, Vol. 15, No. 7, pp 431–445.

Ahn, J. 2007. *In situ determination of dynamic soil properties under an excited surface foundation*, PhD Dissertation. Texas A&M University.

Ahn, J., Biscontin, G and Roesset, J. 2011. Natural frequency and damping ratio of a vertically vibrated surface foundation. *Soil Dynamic and earthquake engineering*, Vol. 31, No.4, May, pp 674-681.

Asik, M. S. 1993. *Vertical vibration analysis of rigid footings on a soil layer with a rigid base*. PhD Thesis, Graduate Faculty of Texas Tech University.

Barkan, D. D. 1962. *Dynamics of bases and foundations*. McGraw-Hill Book Company, New York.

Bhatia, K.G. 2008. *Foundations for industrial machines: Handbook for practising engineers*, First edition, D-CAD Publisher, New Delhi.

Bycroft, G.N. 1956. Forced vibrations of a rigid circular plate on a semi-infinite elastic space and on an elastic stratum. *Philosophical Transactions of the Royal Society*, London Series A, Vol.248, No. 948, January, pp 327 - 368.

Bycroft, G.N. 1959. Machine foundation vibration. *Proceedings of the Institute of Mechanical Engineers*, Vol. 173. No. 18, June, pp 469 – 473.

Chopra, A.K. 2007. *Dynamics of Structures: Theory and Applications to Earthquake Engineering.* 3rd Edition, Prentice hall. Canada.

Chae, Y.S. 1971. Dynamic Behaviour of Embedded Foundation-soil Systems. *Highway research record*, No. 323, pp 49 – 59.

Chowdhury, I and Dasgupta, S. 1998. Computation of Rayleigh damping coefficients for large systems, *Electronic Journal of Geotechnical engineering*, Vol.8, Bundle 8C,

Chowdhury, I and Dasgupta, P.S. 2009a. *Dynamic of structure and foundation - A unified approach. Volume 1. Fundamentals*. CRC Press/Balkema.

Chowdhury, I and Dasgupta, P.S. 2009b. *Dynamic of structure and foundation - A unified approach. Volume 2. Applications*. CRC Press/Balkema.

Clayton, C.R.I. Heymann, and Matthews, M.C. 2012. The value of stiffness measured in field seismic surveys. *International Journal of Geo-Engineering*, Vol.4, No. 2, pp 17 – 36.

Cook, R.D. Malkus, D.S. Plesha, M.E and Witt, R.J. 2002. *Concept and Applications of Finite Element Analysis*. Fourth Edition. John Wiley & Sons, USA.

Crockett, J.H.A and Hammond, R.E.R. 1949. The Dynamic Principles of Machine Foundations and Ground. *Proceedings of the Institute of Mechanical Engineers*, Vol. 160. April, pp 512 – 531.

Crouse, C.B. Hushmand, B., Luco, E. and Wong, H.L. 1990. Foundation impedance functions: Theory versus experiment. *Journal of Geotechnical Engineering*, Vol. 116, No.3, March, pp 432 – 449.

Crouse, C.B, Liang C.G and Martin, R.G. 1984. Experimental study of soil – structure interaction at an accelerograph station. *Bulletin of the seismological of America*. Vol.74, No. 5, pp 1995-2013.

Das, B.M and Ramana, G.V. 2011. Principles of Soil Dynamics. 2ed. Cengage learning, US.

De Barros, F.C.P and Luco, J. E. 1995. Identification of foundation impedance functions and soil properties from vibration tests of the Hualien containment model. *Soil Dynamics and Earthquake Engineering,* Vol. 14, pp 229-248.

Deolalkar, S.P. 2009. *Handbook for Designing Cement Plants*. BS Publication, Kundlia, Haryana.

Di Mino, G, Giunta, M and Di Liberto, M. 2009. Assessing the open trenches in screening railway ground-born vibrations by means of artificial neural network, Advances in acoustics and vibration, Hindawi Publishing Corporation.

Dunn, P.W. 2010. *Comparison of cone model and measured dynamic impedance functions of shallow foundations*. PhD Dissertation. University of Florida.

Dunn, P.W, Hiltunen, D.R and Woods, R.D. 2009. In situ determination of dynamic impedance functions of shallow foundations. *Proceedings of the 17th International conference on soil mechanics and geotechnical engineering*, M. Hamza (Eds), Cairo, Egypt, pp 2084 – 2087.

Dutta, S.C and Roy, A. 2002. A critical review on idealization and modelling for interaction among soil-foundation-structure system. *Computer & Structures*, Vol. 80 pp 1579 – 1594.

El Naggar, M.H. 2003. Performance evaluation of vibration-sensitive equipment foundations underground-transmitted excitation. *Canadian Geotechnical journal*, Vol. 40, pp 598 - 615

El Naggar, M.H. 2009. Design of foundations for dynamic loads. Short course notes 8 - 10 June, SAICE House, Midrand.

El Naggar, M. H. 2001. Dynamics of Foundations. *Geotechnical and Geoenvironmental Engineering Handbook*, Chapter 12, R.K. Rowe, Kluwer Academic Publisher, Boston Dordrecht London. pp 337-359.

Ewins, D.J. 1991. *Modal Testing: Theory and practice*. Research studies press Ltd, England.

Filonenko-Borodich 1954. A very simple model of an elastic foundation capable of spreading the load. Sb. Tr. Mosk, eletrot. Inst.inzh. *Trans. 53*. Tran-Zheldorizdat (in Russian).

Gazetas, G. Dobry, R and Tassoulas, A.M. 1985. Vertical Response of Arbitrarily-Shaped Embedded Foundations. *Journal of Geotechnical Engineering*, Vol. 111, No.6, June, pp 750 - 771.

Gazetas, G. 1991a. Foundation engineering. *Foundation engineering handbook*, Chapter 15,Ed. H.Y. Fang, 2nd Edition ,Van Nostrand Reinhold, New York, pp 553-593.

Gazetas, G. 1991b. Formulas and Charts for impedances of surface and embedded foundations. *Journal of Geotechnical Engineering*, Vol. 117, No.9, September, pp 1363-1381.

Gazetas, G.M and Stokoe, H.K. 1991. Free Vibration of embedded foundations: Theory versus experiment. *Journal of Geotechnical Engineering*. Vol.117, No.9, September, pp 1382 - 1401.

Gazetas, G. 1983. Analysis of machine foundation vibrations: State of the art. *Soil dynamics and earthquake engineering,* Vol.2, No.1, pp 2 – 42.

Gibson, R.E. 1967. Some results concerning displacements and stresses in a non-homogeneous elastic half-space, *Geotechnique*, Vol.17, pp 58-67.

Hadjian, A.H. Luco, J.E and Tsai, N.C. 1974. Soil-structure interaction: Continuum or finite element? *Nuclear engineering and design*, Vol.31, pp 151 – 167.

Hall, L and Bodare, A. 2000. Analyses of the cross-hole method for determining shear wave velocities and damping ratios. *Soil dynamics and Earthquake Engineering*, Vol.20, pp 167 – 175.

Hall, J.R and Kissenpfennig J.F 1976. Special topics on soil-structure interaction. *Nuclear Engineering Design*, Vol.38, pp 273 – 287.

He, J and Fu, Z. 2001. *Modal Analysis*. Butterworth– Heinemann, England.

Heymann, G. 2007. Ground stiffness measurement by the continuous surface wave Test. *Journal of South Africa Institution of Civil Engineering*, V.49, No.1, March, pp 25-31.

Hetenyi, M. 1946: Beams on elastic foundation theory with applications in the fields of civil and mechanical engineering. The University of Michigan Press. London: Geoffrey Cumberlege, Oxford University Press.

Hushmand, B. 1983. *Experimental Studies of dynamic response of foundations*. PhD Thesis, California Institute of Technology.

Hsieh, T.K. 1962, 'Foundation Vibrations', *Proc. of Inst. of Civil Engineers*, Vol. 22, No. 2, June, pp 211–226.

Janghai, X, Richard, D.M, Park, C.B and Ivanov, J. 2002. Utilization of high frequency Rayleigh waves in near-surface geophysics. *Near-surface problems and solutions*, SEGs Annual meeting.

Inci, G. 2008. Numerical modelling of wave propagation in elastic-half space with imperfections, *21st SAGEEP*, *Symposium on application of geophysics to engineering and environmental problems*, New partnerships, New discoveries. Marriott Philadelphia Downtown Pennsylvania.

Inukai, T and Imazawa, T. 1992. Dynamic behaviour of embedded structure on hard rock site. *Earthquake Engineering*. Tenth World conference. Balkem, Rotterdam, pp 1695-1700.

Irish, K. and Walker, W.P. 1969. *Foundations for reciprocating machines*. Concrete Publications, London.

Jafarzadeh, F and Asadinik, A. 2008. Dynamic Response and Impedance Functions of foundation resting on sandy soil using physical model tests. *The 14th World conference on Earthquake Engineering*. October 12-17, Beijing, China.

Jesmani, M and Kamalzare M. 2010. Comparison between numerical and analytical solution of dynamic response of circular shallow footing. *Electronic Journal of Geotechnical Engineering*, Vol.15, Bundle.P, pp 1768 – 1781.

Ju, S.H and Ni, S.H. 2007. Determining Rayleigh damping parameters of soils for finite element analysis. *International Journal for Numerical and Analytical Methods in Geomechanics*, Vol.31, January, pp 1239 – 1255.

Kaldjian, J.M. 1969. Discussion of ''Design Procedure for Dynamic Loaded Foundations'' by Whitman, R.V and Richart, F.E. *Journal of the soil Mechanics and Foundation Division*, ASCE, Vol. 95, No.1, January, pp 364 – 366.

Kameswara Rao, N.S.V. 1998. *Vibration Analysis and Foundation Dynamics*. Wheeler.

Kameswara Rao, N.S.V. 2011. *Foundation design: Theory and practice*. John Wiley and Son (Asia) Pte Ltd.

Kausel, E. 2010. Early history of soil-structure interaction. *Soil dynamics and earthquake engineering*, Vol.30, No. 9, September, pp 822 – 832.

Kerr, A.D. 1964. Elastic and Viscoelastic Foundation Models. *Journal of Applied Mechanics*. 31:491-498.

Kramer, S.L. 1996. *Geotechnical Earthquake Engineering*. Prentice – Hall, USA

Kruijtzer, G.FJ. 2001. A comparative treatise on the vertical vibration of rigid bodies on deep elastic strata, Heron, Vol.46, No. 1, pp 27 – 48.

Lamb, H. 1904. On the Propagation of tremors over the surface of an elastic solid. *Philosophical Transaction of the Royal Society*, London Series A, Vol.203 No. 1, pp 1-42.

Lin, A.N. Jennings, P.C. 1984. Effect of embedment on foundation-soil impedances. *Journal of Engineering Mechanics*, Vol. 110, No. 7, July, pp 1060 – 1075.

Liu, G.R and Jerry, S.S. 2003. A non-reflecting boundary for analyzing wave propagation using the finite element method. *Finite Elements in Analysis and Design,* Vol.39 pp 403–417.

Liu, G.R and Achenbach, J.D. 1994. A strip element method for stress analysis of anisotropic linearly elastic solids, *Journal of Applied Mechanics*, Vol. 61, June, pp 270–277.

Luco, J.E and Hadjian, A.H. 1974. Two-dimensional approximations to the three-dimensional soil-structure interaction problem. *Nuclear engineering and design*, Vol. 31, December, pp 195 – 203.

Lysmer, J and Kuhlemeyer, R.L. 1969. Finite dynamic model for infinite media. *Journal of the Engineering Mechanics Division of the ASCE, American Society of Civil Engineers,* Vol. 95, No. EM4, August, pp 859–877.

Lysmer, J. 1965. *Vertical Motion of rigid footings*. U.S Army Engineers Waterways Experiment Station. Contract No.DA-22-079 – eng – 340: Report No. 3 – 115. Department of Civil Engineering, University of Michigan. USA.

Lysmer, J and Richart, F.E. 1966. Dynamic response of footings to vertical loading. *Journal of the Soil Mechanics and Foundation Division, Proceeding of ASCE*, Vol. 92, No. SM1, January, pp 65 – 91.

Matthews, M.C, Hope, V.S and Clayton, C.R.I. 1995. The geotechnical Value of Ground Stiffness Determined Using Seismic Methods. *30th Annual Conference of Engineering Geophysics Geology Society*, Modern Geophysics in Engineering Geology Liege.

Matthews, M.C, Hope, V.S and Clayton, C.R.I. 1996. The use of surface waves in the determination of ground stiffness profiles. Proceedings of the Institution of Civil Engineers*, Geotechnical engineering*. Vo.119, pp 85 – 95.

Mbawala, S.J, Heymann, G. Roth, C.P and Heyns, P.S. 2011. Numerical Modelling of Wave Propagation in Ground Using Non-Reflecting Boundaries. *Proceedings*. *The 15th African Regional Conference on Soil Mechanics and Geotechnical Engineering*. (Eds.)
C. Quadros and S.W. Jacobsz, July, pp 644-652.

Meimaris, C. 2002. Design of very large mill installation: Mill design specification and audits. The Australasian Institute of Mining and Metallurgy. *Metallurgical Plant Design and Operating Strategies Conference*, Sydney- April 15-16.

Meimaris, C and Cox, L. 2001. Remedial design of the world`s largest SAG mill gearless drive. *SAG Conference*. The Third international conference on autogenous and semi-autogenous grinding technology, Vancouver, Canada, pp 74- 83.

Melersiki, S.E. 2000. *Design analysis of beams, circular plates and cylindrical tanks on elastic foundation*. 2nd Edition, Taylor & Francis group, London.

Mercer, C. 2006. Acceleration, Velocity, and Displacement Spectra – *Omega Arithmetical*. Prosig signal processing tutorial.

Motamed, R, Itoh, K, Hirose, S, Takahashi, A and Osamu, K. 2009. Evaluation of wave barriers on ground vibration reduction through numerical modelling in Abaqus. *SIMULIA Customer Conference,* pp 1-19.

Nayfeh, A.H and Serhan, S.J. 1989. Vertical vibration of machine foundations. *Journal of Geotechnical Engineering*. Vol.115, No.1, January, pp 56 - 74.

Nielsen, A.H. 2006. Absorbing boundary conditions for seismic analysis in Abaqus. *ABAQUS User's conference*.

Nii, Y. 1987. Experimental half-space dynamic stiffness. *Journal of Geotechnical Engineering*, Vol.113, No.11. November. pp 1359 - p.1373.

Novak, M. 1970. Prediction of Footing Vibrations. *Journal of the Soil Mechanics and Foundation Division, Proceeding of ASCE*, Vol. 96, No. SM3, May, pp 837 – 861.

Novak, M and Beredugo, Y.O. 1972. Vertical vibration of embedded footings. *Journal of the Soil Mechanics and Foundation Division*, ASCE, Vol. 98, No. SM12, December, pp 1291 – 1310.

Novak, M. 1974. The Effect of Embedment on Vibration of Footings and Structures. Proceeding of the Fifth World conference on Earthquake Engineering. Rome. Vol. 1, pp 2658-2661.

Novak, M, Nogami, T and Aboul-Ella, F. 1978. Dynamic soil reactions for plane strain case. *Journal of the Engineering Mechanics Division, Proceedings ASCE*, Vol. 104, No. EM4, August, pp 953 – 959.

Novak, M and Han, Y.C. 1990. Impedance of Soil Layer with Boundary Zone. *Journal of Geotechnical Engineering*, Vol.116, No.6, June, pp1008- 1014

Orser, T, Svalbonas, V and Van de Vijfeijke, M. 2011. Conga: The World's first 42 foot diameter 28 MW gearless SAG Mill. In: Major, et al. (Eds.), *Proceedings International Autogenous Grinding, Semi-autogenous Grinding and High Pressure Grinding Roll Technology*, vol. II. September 25–28, pp 38–57.

Pak, R.Y.S and Guzina, B.B. 1995. Dynamic Characterization of Vertically-Loaded Foundations on Granular Soils. *Journal of Geotechnical Engineering*. Vol.121, No.3, March pp 274 - 286.

Pais, A and Kausel, E. 1988. Approximate formulas for dynamic stiffnesses of rigid foundations. *Soil Dynamics and Earthquake Engineering*. Vol.7, No.4, pp 213 – 227.

Pasternak, P.L. 1954. On a new method of analysis of an elastic foundation by means of two foundation constants.

Prakash, S. 1981. *Soil Dynamic*. McGraw-Hill Book Company.

Prakash, S and Puri, V. 2006. *Foundation for vibrating machines. Special issue of the Journal of Structural Engineering*, SERC, Madras, India, April-May, pp 1-39.

Quinlan, P.M. 1953. Elastic theory of Soil Dynamics. *Symposium on dynamic testing of soils*, American Society for Testing and Materials, Special technical publication, No. 156, July, pp 3-34.

Reese, P. 2000. Innovation in mineral processing technology. *Proceeding*. New Zealand Minerals & Mining Conference, October, pp 29-31.

Richart, F.E., Hall, J.R and Woods, R.D. 1970. *Vibrations of soils and foundations*. Prentice-Hall, USA.

Seed, H.B and Hwang, R. 1975. Soil-structure interaction analyses for seismic response. *Journal of the Geotechnical Engineering Division*. Vol. 101, No. GT5, May, pp 439 – 457.

Seed, H.B and Lysmer, J. 1978. Soil-structure interaction analyses for by finite elements – State of the art. *Nuclear Engineering and Design*, Vol. 46, pp 349 – 365.

Shah, P. M. 1968. *On the Dynamic Response of Foundation Systems*. PhD Thesis, Rice University, Houston, TX.

Srinivasan, M. G. Kot, C.A. and Hsieh, B. J. 1991. Determination of soil impedance functions from vibration-test response of a circular foundation. *Soil Dynamic and Earthquake Engineering*, Vol. 10, No.4, May, pp 212-227.

Stokoe, K.H and Richart, F.E. 1974. Dynamic response of embedded machine foundations. *Journal of the Geotechnical Engineering Division*. Vol. 100, No. GT4, April, pp 427-447.

Sung, T.Y. 1953. Vibrations in semi infinite solids due to Periodic surface loading, ASTM, Special Technical Publication, *Symposium on soil dynamics*, Vol. 156, July, pp 35–64.

Tileylioglu, S. Stewart, P.J and Nigbor, L.R. 2011. Dynamic stiffness and Damping of a shallow foundation from forced vibration of a field-test structure. *Journal of Geotechnical Engineering and Geoenvironmental Engineering*, Vol.137, No. 4 April.

Tileylioglu, S. 2008. *Evaluation of soil-structure interaction effect from field performance*. PhD Thesis, University of California Los Angeles.

Terzaghi, K. 1955. Evaluation of Coefficient of Subgrade Reaction. *Geotechnique*, No. 5, pp 297-326.

Veletsos, A.S and Verbic, B. 1973. Vibration of Viscoelastic Foundation. *Earthquake Engineering and Structural Dynamics*, Vol. 2, pp 87-102.

Veletsos, A.S and Verbic, B. 1974. Basic response functions for elastic Foundations. *Journal of the Engineering Mechanics Division*, ASCE, Vol.100, No. EM2, pp 189–202.

Veletsos, A and Tang, Y. 1986. Vertical vibration of ring foundations with mass. *Journal of Engineering Mechanics*, Vol. 112, No. 10, October, pp 1090 – 1098.

Verbic, B. 1972. *Analysis of certain structure-foundation interaction systems*. PhD Thesis. Texas A&M University.

Verruijt, A. 2003. *Soil Dynamics*. TU Delft, Delft, The Netherlands.

Gong, W. Xie, H. and Wang, Y. 2006. Semi-analytical and semi-numerical method for dynamic analysis of foundation, Applied Mathematics and Mechanics (English edition), Vol.27, No. 5, pp 607-615.

Whitman, R.V and Richart, F.T. 1967. Design Procedures for dynamically loaded foundations. *Journal of the Soil Mechanics and Foundation Division*, ASCE, Vol. 93, No. SM 6, November, pp 169 – 193.

Wolf, J.P. 1994. *Foundation vibration analysis using simple physical models*. Englewood Cliffs, NJ: Prentice-Hall.

Wolf, J.P and Deeks, A.J. 2004. *Foundation vibration analysis*: *A strength-of-materials approach*, Elsevier Linacre House, Jordan Hill, Oxford OX2 8DP, 200 Wheeler Road, Burlingto, MA 01803.

Wong, H.H. and Trifunac, M.D. 1988. A comparison of soil-structure interaction calculation with results of full-scale force vibration. *Soil Dynamic and Earthquake Engineering,* Vol.7 No.1, pp 22-31

Zerwer, A, Polak, M.A and Santamarina, J.C. 2003. Rayleigh Wave Propagation for the Detection of Near Surface Discontinuities: Finite element Modelling, *Journal of non-destructive evaluation*, Vol. 22, No.2, June, pp 39 -51.

Zerwer, A, Cascante, G and Hutchinson, J. 2002. Parameter Estimation in finite element simulations for Rayleigh waves. *Journal of Geotechnical and Geoenvironmental Engineering*, American Society of Civil Engineers, Vol.128, No. 3, March, pp 250-261.

Zhang, J and Yuchuan, T. 2007. Radiation damping of shallow foundations on nonlinear soil medium. *4ᵗʰ International Conference on Earthquake Geotechnical Engineering*. Greece, No. 1150, June, 2007.

Zhao, C 2009. *Dynamic and Transient Infinite Elements theory and Geophysical, Geotechnical and Geoenvironmental Applications*. Springer Berlin.

10 APPENDICES

Appendix A: Calibration information for accelerometer 1

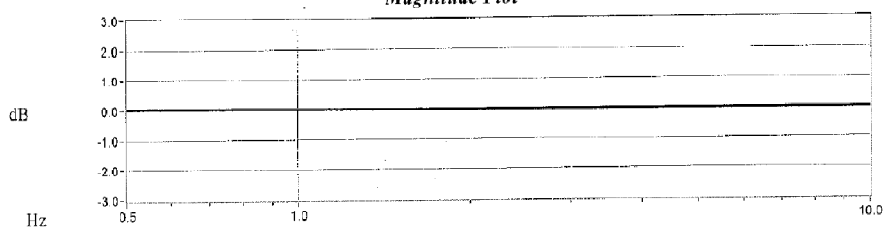~ *Calibration Certificate* ~
Per ISO 16063-21

Model Number: 393C

Serial Number: 22590

Description: ICP® Accelerometer   Method: Back-to-Back Comparison Calibration
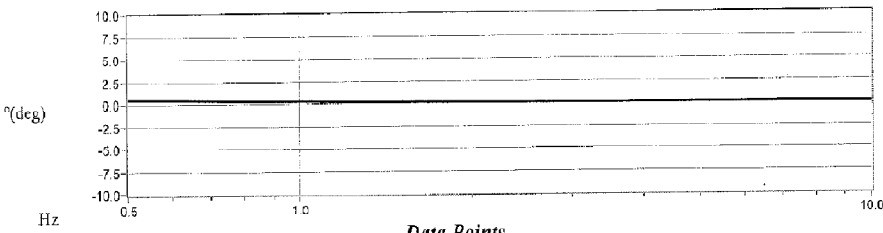
Manufacturer: PCB

Calibration Data

Sensitivity @ 100.0 Hz   1048   mV/g   Output Bias   3.4   VDC

(106.9   mV/m/s²)   Transverse Sensitivity   3.4   %

Resonant Frequency   5523   Hz

Sensitivity Plot

Temperature: 76 °F (24 °C)   Relative Humidity: 36 %

Data Points

Frequency (Hz)	Dev. (%)	Frequency (Hz)	Dev. (%)
10.0	0.1	300.0	0.4
15.0	-0.0	500.0	1.0
30.0	0.3	800.0	2.6
50.0	0.0		
REF. FREQ.	0.0		

Mounting Surface: Stainless Steel w/Silicone Grease Coating   Fastener: Stud Mount   Fixture Orientation: Vertical
Acceleration Level (rms)¹: 1.00 g (9.81 m/s²)²
¹The acceleration level may be limited by shaker displacement at low frequencies. If the listed level cannot be obtained, the calibration system uses the following formula to set the vibration amplitude; Acceleration Level (g) = 0.010 x (freq)².   ²The gravitational constant used for calculations by the calibration system is; 1 g = 9.80665 m/s².

Condition of Unit

As Found: n/a

As Left: New Unit, In Tolerance

Notes

1. Calibration is NIST Traceable thru Project 822/274086 and PTB Traceable thru Project 1060.
2. This certificate shall not be reproduced, except in full, without written approval from PCB Piezotronics, Inc.
3. Calibration is performed in compliance with ISO 9001, ISO 10012-1, ANSI/NCSL Z540-1-1994 and ISO 17025.
4. See Manufacturer's Specification Sheet for a detailed listing of performance specifications.
5. Measurement uncertainty (95% confidence level with coverage factor of 2) for frequency ranges tested during calibration are as follows: 5-9 Hz; +/- 2.0%, 10-99 Hz; +/- 1.5%, 100-1999 Hz; +/- 1.0%, 2-10 kHz; +/- 2.5%.

Technician: Thomas Witnauer   Date: 04/26/07

PCB PIEZOTRONICS INC.
VIBRATION DIVISION

ACCREDITED
CALIBRATION CERT #1862.01
PAGE 1 of 2

3425 Walden Avenue   ·   Depew, NY 14043
TEL: 888-684-0013   ·   FAX: 716-685-3886   ·   www.pcb.com   CAL43 - 3260434155.67

Appendix B : Calibration information for accelerometer 2